

University of New Hampshire

University of New Hampshire Scholars' Repository

Doctoral Dissertations

Student Scholarship

Spring 2013

Development of unsaturated flow functions for low impact development stormwater management systems filter media and flow routines for hydrological modeling of permeable pavement systems

Iulia Aurelia Barbu

Follow this and additional works at: <https://scholars.unh.edu/dissertation>

Recommended Citation

Barbu, Iulia Aurelia, "Development of unsaturated flow functions for low impact development stormwater management systems filter media and flow routines for hydrological modeling of permeable pavement systems" (2013). *Doctoral Dissertations*. 730.

<https://scholars.unh.edu/dissertation/730>

This Dissertation is brought to you for free and open access by the Student Scholarship at University of New Hampshire Scholars' Repository. It has been accepted for inclusion in Doctoral Dissertations by an authorized administrator of University of New Hampshire Scholars' Repository. For more information, please contact Scholarly.Communication@unh.edu.

**DEVELOPMENT OF UNSATURATED FLOW FUNCTIONS FOR LOW IMPACT
DEVELOPMENT STORMWATER MANAGEMENT SYSTEMS FILTER
MEDIA AND FLOW ROUTINES FOR HYDROLOGICAL
MODELING OF PERMEABLE PAVEMENT SYSTEMS**

BY

**IULIA AURELIA BARBU
B.S., Technical University of Civil Engineering Bucharest, 2005**

DISSERTATION

**Submitted to the University of New Hampshire
in Partial Fulfillment of
the Requirements for the Degree of**

**Doctor of Philosophy
In
Civil Engineering**

May, 2013

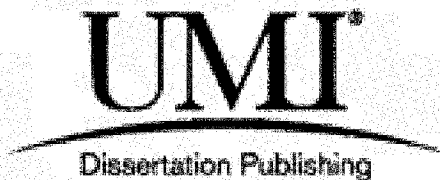
UMI Number: 3572949

All rights reserved

INFORMATION TO ALL USERS

The quality of this reproduction is dependent upon the quality of the copy submitted.

In the unlikely event that the author did not send a complete manuscript and there are missing pages, these will be noted. Also, if material had to be removed, a note will indicate the deletion.

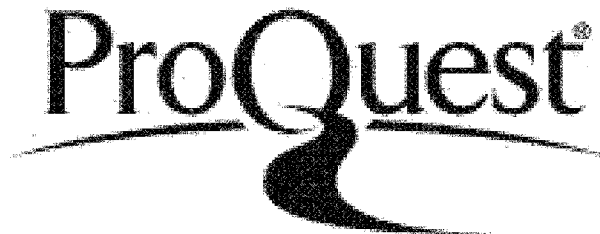


UMI 3572949

Published by ProQuest LLC 2013. Copyright in the Dissertation held by the Author.

Microform Edition © ProQuest LLC.

All rights reserved. This work is protected against unauthorized copying under Title 17, United States Code.

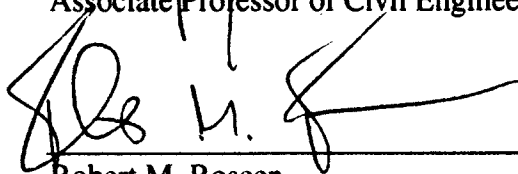


ProQuest LLC
789 East Eisenhower Parkway
P.O. Box 1346
Ann Arbor, MI 48106-1346

This dissertation has been examined and approved.



Dissertation Director, Thomas P. Ballestero
Associate Professor of Civil Engineering



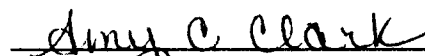
Robert M. Roseen
Adjunct Professor of Civil Engineering



Alison Watts
Assistant Research Professor of Civil Engineering



Mark E. Lyon
Assistant Professor of Mathematics and Statistics



Amy Clark
Professional Civil Engineer



Date

ALL RIGHTS RESERVED

© 2013

Iulia Aurelia Barbu

Dedication

To my Mom, for her sacrificial love.

Acknowledgements

I would like to thank the members of the UNH Stormwater Center group for the continuous help with this project. Particularly, I would like to thank my advisor Dr. Thomas Ballestero for providing guidance and expertise with this project, his mentorship in navigating the academic world, encouragement for my adventurous academic activities while at UNH, and brightening my days with his good humor and colorful Hawaiian shirts. I would like to thank also the members of my doctoral committee who made positive contributions to shape the final version of this dissertation.

Special thanks to my fellow graduate students: Pedro Avellaneda, George Fowler, Kris Houle, Josh Briggs, Nicholas DiGennaro, Ann Scholz, Robin Stone and Viktor Hlas with whom I shared the challenges and joys of graduate school. Many thanks to Ann and Robin for last minute proofreading, and to Tim for always being willing to help with instrument calibration and gathering data, no matter the weather conditions. I would like to thank my many friends at UNH, the Graduate Christian Fellowship group and the Seacoast Calvary Chapel community for being my second family, my home away from home during graduate school. Finally, I would like to thank my family for their support and their encouragement to pursue my dreams.

Funding for this project was provided by the Cooperative Institute for Coastal and Estuarine Environmental Technology (CICEET), the National Oceanic and Atmospheric Administration (NOAA) and the Great Bay National Estuary Research Reserve (GBNERR).

List of Tables

Table 1 – The particle size distribution for the sandy gravel used as filter media in the PP system.	13
Table 2 – The time difference from the beginning of precipitation event to the VMC response at different levels in the PP system.	21
Table 3 – Seasonal variation in volumetric moisture content in the PP system’s sublayers	25
Table 4 – Temperature variation in the PP system sublayers	25
Table 5 – Comparison of the porosity of the filter media soil and the observed VMC....	28
Table 6 – Average values of the initial, maximum and the change in the VMC during precipitation events	30
Table 7 – Van Genuchten fitting parameters	52
Table 8 – The goodness of fit of the interpolated and Van Genuchten curves to the measured data: the coefficient of determination (r^2) and root mean square error (RMSE).	55
Table 9 – Extended $\theta - \psi$ data points for the fine and coarse gravel soil fractions	61
Table 10 – Soil properties for the four types of filter media	61
Table 11 – Arya-Paris model sensitivity analysis with respect to the number of intervals	64
Table 12 – Arya-Paris model scaling parameters	64
Table 13 – Segments of flow identified in the PP system, recommended equations and data input needed	86
Table 14 – The “goodness of fit” analysis for routing stormwater through the filter media of the Alumni lot with Richard’s Equation and Barbu framework for obtaining the $\theta-\psi-K_r$ curves (Barbu and Ballesterio, 2013b), and the initialization parameters.	101
Table 15 – The “goodness of fit” analysis for the flow modeled with Glover Equation, Manning Equation, and flow at the bottom of the filter media layer, compared with the observed flow at the end of the subdrain	104
Table 16 – Total stormwater volumes computed as the cumulative area under hydrographs generated at the bottom of the filter media, and at the end of the pipe (Glover Equation). These are compared with the total volume observed at the end of the subdrain, and total precipitation fallen on the pavement surface.....	110
Table 17 – The power function coefficients for the family of curves presented in Figure 38.....	115

List of Figures

Figure 1 – The cross section of the PP system studied and the location of the four 5 TE Decagon moisture/temperature/conductivity probes (Ports 1 - 4). Duplicate probes are installed at each location.	11
Figure 2 – Installation of the 5TE probes at the bottom and middle of the filter media layer (Port 2 and Port 3). Half cut, stone filled pipe on the right side of the right figure is a positive pressure water sampler.	13
Figure 3 – Soil specific calibration for the 5TE Decagon probes developed for the bulk and fine fraction of the soil used as a filter media in the permeable pavement system....	15
Figure 4 – Nonexceedance probability of daily precipitation for Durham, NH over the entire gage record and for the study location from October 29, 2010 to January 11, 2012.	17
Figure 5 – Volumetric moisture content estimated from probe signals and converted with the original Topp Equation and the soil specific soil equation developed	18
Figure 6 – Peak moisture content at different levels in the PP system, generated by the infiltration of natural precipitation. Saturation in the filter media layer occurs at 29% VMC.	20
Figure 7 – The volumetric moisture content and temperature for Port 2 for below-freezing conditions. Saturation in this layer occurs at 29% VMC.....	24
Figure 8 – Exceedance probability curves for the VMC monitored by the four ports and VMC at saturation in the filter media soil.	27
Figure 9 – The fluctuation of the VMC in the PP system’s sublayers during the largest storm. Saturation occurs at 29% VMC.	29
Figure 10 – The fluctuation of the VMC at the top (Port 1) and middle (Port 2) of the filter media during the most intense storm. Saturation occurs at 29% VMC. VMC data for probes 3 and 4 was not available for this precipitation event due to probe malfunctioning.	30
Figure 11 – Particle size distributions for the filter media in the PP, SF, GW and BS systems.	44
Figure 12 – Similarity principle: transition from a particle size distribution (a) to a moisture retention curve (b), adjustments for gravel content with Bouwer Equation (b), and extension of the MRC beyond Arya-Paris applicability range (b).	49
Figure 13 – The volumetric moisture content with respect to the matric potential for the PP filter media.....	53
Figure 14 – The volumetric moisture content with respect to the matric potential for the SF filter media.....	53
Figure 15 – The volumetric moisture content with respect to the matric potential for the GW filter media.	54

Figure 16 – The volumetric moisture content with respect to the matric potential for the BS filter media.	54
Figure 17 – The fluctuation of the volumetric moisture content (θ) measured at three levels within the filter media of a pervious pavement system under natural precipitation	56
Figure 18 – Unsaturated hydraulic conductivity developed with Mualem’s Equation as applied to the measured and computed volumetric moisture content – matric potential curves.	58
Figure 19 – The particle size distribution for the BS filter media, developed after dry- and wet-sieving, and combustion of wood chips.	63
Figure 20 – The sensitivity analysis of the Arya-Paris model with respect to the number of intervals used for the particle size distribution data	65
Figure 21 – Cross section of the Alumni lot PP system and location of volumetric moisture content (VMC) sensors	75
Figure 22 – The cumulative frequency of the VMC at the top (Port 1), middle (Port 2) and bottom (Port 3) of the filter media layer, and at the top of the stone reservoir (Port 4) for one year of monitoring, compared to the measured VMC at saturation in the filter media soil.	75
Figure 23 – The cross section (a) and plan view (b) of the PP system at West Edge parking lot. The outflow hydrograph is measured at the end of the subdrain.	81
Figure 24 – Particle size distribution of the soils used as filter media in the West Edge and Alumni PP systems	83
Figure 25 – Comparison of the “bucket and stop watch” flow measurements and automated flow measurements recorded by ISCO bubblers coupled with a Thelmar weir and manufacturer’s rating curve	84
Figure 26 – Representation of θ through the filter media layer in space and time	88
Figure 27 – The particle size distribution (a) of the filter media soil in the West Edge lot and the resulting θ (ψ) and K_r (θ) curves (b) as derived after Barbu and Ballestero, 2013b.	91
Figure 28 – The particle size distribution of the filter media soil in the Alumni lot (a), and the θ (ψ) curve obtained by interpolation and fitted with VG Equation to the A-P generated data points (b)	94
Figure 29 – The θ (ψ) and K_r (θ) curves for the Alumni lot filter media as derived with Barbu methodology (Barbu and Ballestero, 2013b)	95
Figure 30 – The VMC in the filter media soil profile in response to the 11/04/2010 precipitation event (total depth of 3 cm). $K_{sat} = 0.75$ cm/min. θ initial was set to observed VMC values at each level	97
Figure 31 – The moisture gradient in the top half and bottom half of the filter media, computed as the difference between the VMC at the upper and lower boundaries of the two halves of the filter media.....	99

Figure 32 – Moisture content fluctuation in the filter media in response to the 07/23/2009 storm event (dt = 1 min, dz = 2.5 cm (1’’)). Saturation occurs at 27%.	107
Figure 33 – Observed outflow hydrograph as compared to the modeled outflow for the West Edge system computed with Glover and Manning Equations for subdrains, and with Richards’ Equation as draining at the bottom of the filter media	108
Figure 34 – The peak moisture content at the bottom of the filter media layer for various thicknesses, in response to a 2.5 cm Type II – SCS design storm.....	112
Figure 35 – Peak flow lag times of as a function of the filter media thicknesses.....	112
Figure 36 – The peak moisture content at the bottom of a 30 cm filter media layer for various filter media saturated hydraulic conductivities, in response to a 2.5 cm Type II – SCS design storm.....	114
Figure 37 – Peak flow lag times for varying filter media K_{sat} in response to a 2.5 cm Type II – SCS design storm	114
Figure 38 – Lag time through the filter media for permeable pavement systems with various thicknesses and hydraulic conductivities	115

Table of Contents

Dedication	iv
Acknowledgements.....	v
Abstract	xiii
CHAPTER I.....	1
CHAPTER II.....	3
II.1 Introduction	4
II.2 Background	5
II.2.1 Water flow in soils	8
II.3 Methods and Materials.....	10
II.3.1 Moisture content measurements with Decagon devices	13
II.3.2 Precipitation data.....	15
II.4 Results and Discussion.....	17
II.4.1 Volumetric moisture content equations for the 5TE Decagon probes	17
II.4.2 Flow through the system and residence time	19
II.4.3 Water residence time in the system.....	22
II.4.4 Seasonal variability of the VMC.....	23
II.4.5 Volumetric moisture content range in the filter media	25
II.5 Conclusions	30
CHAPTER III	33
III.1 Introduction.....	34
III.1.1 Unsaturated flow functions.....	37
III.1.2 The moisture retention curves: $\theta(\psi)$	39
III.1.3 The unsaturated hydraulic conductivity curves: $K_r(\theta)$	40
III.1.4 Applicability of traditional MRC models to SWM filter media.....	42
III.2 Materials and Methods.....	45
III.2.1 Particle size distributions	45
III.2.2 Arya – Paris Model	45
III.2.3 Correction for coarse particles	48
III.2.4 Curve fitting	50
III.2.5 Testing data.....	50

III.3 Results and Discussions	51
III.3.1 The K_r function	58
III.3.2 Gravel content compensation.....	59
III.3.3 A-P Model sensitivity with respect to number of intervals and α computation	63
III.3.4 Model limitations and error	65
III.4 Conclusion	66
CHAPTER IV	69
IV.1 Introduction.....	70
IV.1.1 Pervious pavement types and configurations	72
IV.1.2 Segments of flow and corresponding equations	73
IV.2 Materials and Methods	80
IV.2.1 Site description	80
IV.2.2 Monitoring and data calibration.....	83
IV.2.3 Model development	84
IV.3 Results and Discussions.....	92
IV.3.1 Derivation of the θ - ψ - K_r functions for the Alumni lot.....	92
IV.3.2 Water routing through the filter media – Alumni lot.....	95
IV.3.3 The complete PP system model – West Edge lot	102
IV.3.4 Design variables effects on lag time through the filter media	110
IV.4 Conclusions.....	116
CHAPTER V	117
Summary and Conclusions	117
References.....	121
Appendix A: Storm events inventory analyzed for the Alumni Lot study (Chapter II)	130
Appendix B: Design Precipitation – Durham, NH	132
Appendix C: The Matlab code for obtaining the $\theta - \psi - K_r$ curves for the PP filter media.....	133
Appendix D: The Matlab code for obtaining the $\theta - \psi - K_r$ curves for the SF filter media.....	146

Appendix E: The Matlab code for obtaining the $\theta - \psi - K_r$ curves for the GW filter media.....	155
Appendix F: The Matlab code for obtaining the $\theta - \psi - K_r$ curves for the BS filter media.....	167
Appendix G: The Matlab code for the PP system for the West Edge lot	178
Appendix H: Storms used for the model calibration of the West Edge PP system	183
Appendix I: Storms used for the calibration of the Alumni Lot - filter media model	184
Appendix J: Calibration storms for the filter media of the Alumni Lot	185
Appendix K: Testing storms for the West Edge PP model.....	190

Abstract

**DEVELOPMENT OF UNSATURATED FLOW FUNCTIONS FOR LOW IMPACT
DEVELOPMENT STORMWATER MANAGEMENT SYSTEMS FILTER
MEDIA AND FLOW ROUTINES FOR HYDROLOGICAL
MODELING OF PERMEABLE PAVEMENT SYSTEMS**

By

Iulia Aurelia Barbu

University of New Hampshire, May 2013

Low Impact Development - Stormwater Management (LID-SWM) systems are relatively new technologies that were developed in order to meet the water quality criteria imposed by the Clean Water Act. LID-SWM is also used to replicate the natural hydrology of developed sites. However, the hydrological benefits of LID systems cannot be accurately predicted with the existing simulation models. Currently used software packages represent LID systems as storage units and do not specifically represent water routing through the systems' hydraulically restrictive sublayers. Since the LID's functionality at system level is not fully understood, the relationships of design variables and the systems' hydrological outcome were not yet empirically related.

In this dissertation, the appropriate equations for representing different flow components of LID systems are investigated. Special attention was given to modeling

water routing through the filter media layers of LID systems. The water movement through a permeable pavement system was monitored for over a year and it was found that the system functions under unsaturated conditions. Saturation was never observed at any levels in the system over the period of study. Solving Richards' Equation, which is typically used to represent flow in unsaturated soils, requires knowledge of the moisture characteristic curves, $\theta(\psi)$ and relative hydraulic conductivity, $K_r(\theta)$ functions. These functions are unique for each soil and have not been analyzed for coarse engineered soils used in stormwater treatment systems. A framework for computing the $\theta(\psi)$ and $K_r(\theta)$ functions for soils used as filter media for four LID systems (permeable pavement, sand filter, gravel wetland, and bioretention system) was developed and tested against laboratory measurements. This framework requires information on soils that is easily accessible to stormwater engineers (porosity and particle size distribution), and allows a detailed representation of filter media soils containing gravel and wood chips.

The $\theta(\psi)$ and $K_r(\theta)$ development framework used in conjunction with Richards' Equation performed well when tested against real time moisture profile in the sublayers of a permeable pavement system under natural precipitation. This framework for modeling flow through the filter media was integrated in a full permeable pavement system model.

CHAPTER I

Introduction

Objective of dissertation work

Low Impact Development - Stormwater Management (LID-SWM) systems are relatively new technologies. They were developed out of the need for more advanced treatment systems to address dissolved pollutants found in stormwater runoff, and to reduce volumes and delay peak flows of the stormwater runoff hydrographs generated by increasing urbanization. Quantifying the hydrological benefits of implementing LID-SWM technologies at site- and watershed-scale is typically performed with computer simulation models. Existing hydrological packages used in stormwater management design do not have the capabilities to route stormwater through the lower hydraulic transmissivity layers in LID systems. The few methodologies proposed for modeling LID systems assume that they function under saturated conditions or treat them as storage units, and do not specifically address the water routing through the filter media layers.

The objective of this dissertation work included: investigation of the nature of flow in a permeable pavement system's sublayers; development of a framework for modeling flow routing through the hydraulic control sublayers for four LID-SWM systems – permeable pavement, sand filter, gravel wetland and bioretention system; and testing of the proposed framework with data from two permeable pavement sites located on the University of New Hampshire campus.

Organization of dissertation

This dissertation has four chapters, three of them being stand-alone papers prepared for submissions to peer-reviewed journals. Chapter 1 gives an overview of the topic addressed in the dissertation work and the organization of the dissertation.

Chapter 2, “The investigation of the nature of flow in a permeable pavement system” is the monitoring study of the moisture transport in the Alumni lot permeable pavement installed on the University of New Hampshire campus. The pervious pavement at the Alumni lot does not receive run-on from adjacent impervious surfaces. Data from this site has shown that in the sublayers of permeable pavements water flows under unsaturated conditions.

Chapter 3, “Unsaturated flow functions for filter media used in Low Impact Development - Stormwater Management Systems”, presents a framework for developing the moisture retention curves, $\theta(\phi)$ and unsaturated hydraulic conductivity function, $K_r(\theta)$ for soil materials used as hydraulic controls in four Low Impact Development Stormwater Management systems: permeable pavement, sand filter, gravel wetland and bioretention system.

Chapter 4, “A physical model for stormwater flow simulation through a porous pavement system: relating the design parameters to the outflow hydrographs”, describes a framework for modeling the segments of flow identified in permeable pavement systems and the most appropriate equations to represent them. The sequence of equations proposed in Chapter 3 for the development of the $\theta(\phi)$ and $K_r(\theta)$ for the filter media soil of the PP system was tested.

CHAPTER II

The investigation of the nature of flow in a permeable pavement system

Abstract

Modeling and designing permeable pavement (PP) systems for hydrologic performance first requires the physical understanding of the nature of flow within the several layers that compose the system. The real time moisture flow transport through the sublayers of a permeable pavement parking lot installed at the University of New Hampshire was monitored for 14 months. The real time volumetric moisture content (VMC) data within the most hydraulically restrictive soil layers of the system, which controls the flow through the PP system, demonstrated that saturation was not achieved at any level, during or after natural precipitation events for the length of the study. The values of VMC in the filter media ranged from 4.3% to 20.2%, while the soils' saturation VMC was measured at 29%. Therefore, unsaturated flow equations (Richard's Equation) are more appropriate than saturated flow equations (Green and Ampt, Darcy) for routing stormwater through the filter media of permeable pavement systems. Winter data showed that residual water in the PP's sublayers freezes in extreme cold weather and VMC recorded with 5TE Decagon sensors were typically lower than in the summer months, even when frozen the layers maintained open pores capable of transmitting water. We also discussed calibration needs for VMC data collected with 5TE Decagon sensors for coarse engineered soils used for filter media in stormwater management systems.

II.1 Introduction

It is generally recognized that the strict water quality and quantity standards imposed by the Clean Water Act (CWA) can only be achieved with more advanced stormwater management technologies. These technologies are known as Low Impact Development - Stormwater Management (LID-SWM) systems or Green Infrastructure and consist of pervious pavements, bioretention systems, vegetated rooftops, gravel wetlands etc. (Roseen et al, 2006; UNHSC 2009, 2012). Permeable pavement systems (PP) are one especially valuable technology; they can serve both as traffic infrastructure and stormwater management practice (Schwartz, 2010). Extensive research on several PP systems at the University of New Hampshire Stormwater Center (UNHSC) have shown that PP systems have the capability to improve the water quality of stormwater runoff (Roseen, 2006; UNHSC, 2009b), and reduce the overall quantity of runoff discharged into surrounding water bodies by allowing infiltration in the native soils. In addition, PP systems may require a reduced amount of de-icing products than conventional pavements in cold climates (Houle, 2006). PP systems are recommended especially in low traffic zones like parking lots or highway shoulders (Ferguson, 2005).

Regardless of the water quality benefits provided by this technology, governmental agencies responsible for reviewing and approving stormwater management plans for construction projects that include LID-SWM systems can be reluctant to approve PPs as stormwater management strategies because of the lack of familiarity with the systems (Houle et al, 2013). Some designers struggle to demonstrate the hydrologic benefits of using PP systems as a functional stormwater management technology with currently available modeling tools: for example, representing the “outflow hydrograph”

for the system and showing that post-development peak flow is less than pre-development peak flow. The relationships of the system's design parameters to the final system outcome have not been yet empirically related for PP systems (Fassman and Blackbourne, 2010). Therefore, the understanding of flow through PP systems and its simulation with computer models currently used for designing and sizing of stormwater management systems have not advanced enough to predict how different system configurations and the use of filter media and underdrains alter the hydrographs flowing from a PP system, or other LID-SWM filtration systems for that matter.

II.2 Background

In current practice, the sublayers of PP systems are designed for traffic load, freeze-thaw, and draindown time (Schwartz, 2010). The water quantity and quality benefits of using filter media in PP systems are dependent on the type of media and sub-base configuration, but currently are not part of the main criteria considered in the system's design. The hydrological behavior of PP systems can only be observed by monitoring after the system is built, as there are presently no effective methods of predicting it before construction.

PP systems are very similar to conventional pavements. The difference is that the pavement layer is designed to allow storm water to infiltrate and pass into the sublayer materials instead of letting it run off. Another difference in cold regions is that the sublayer materials are hydrologically disconnected from the native soils below to minimize impacts of freeze-thaw cycles (Roseen et al, 2012). A PP system is represented

by a layer of pervious asphalt, concrete, or interlocking blocks on top of layered permeable materials. The sublayer structure provides both structural and hydrological functions, and its configuration varies depending on the project goals and site conditions. A typical sublayer configuration includes: a structural layer (choker course) – typically crushed stone – below the permeable surface layer; then a layer of coarse sand/fine gravel (bank run gravel) which serves as a filter media to remove pollutants and slow down the stormwater; and below that another layer of crushed stone which acts as a reservoir to hold water, prevent moisture from moving upwards (frost heave inhibition), allow it to move to underdrains, and/or hold it to allow for infiltration into the soil (Figure 1). At sites with very high permeability soils, the lower stone layer and drainage piping may be absent. Underdrains are placed in the stone layer at the base of the system if drainage control is needed in low permeability native soils or where infiltration is undesirable. Some designs might exclude the filter media layer, instead opting for only a crushed stone reservoir. As with any other filtration LID-SWM systems, the filter media provides significant water quality benefits through filtration and biological treatment processes. The use of a filter media layer in PP systems is also recommended to prevent clogging with fines at the interface between the system sublayers and the native soils (ACI, 2006).

A few suggested methodologies for assessing the hydrological response of PP systems include the SCS-Curve Number (CN) (Swartz, 2010), and/or the use of pond routing methodologies (Jackson and Ragan, 1974; Ladd, 2004; Barbu et al, 2009; Swartz, 2010). These approaches to the analysis of PP systems hydraulics are based on the assumption that the sublayers act as a storage unit with a void space equal to the porosity of the material, and therefore is modeled with stage-storage relationships and outlet

controls. This method is similar to modeling conventional stormwater management systems like detention/retention ponds and was adopted mainly because computer models available to stormwater management practitioners do not have the capabilities to model the more advanced processes that take place in PP systems (Elliot, 2006; Dietz, 2007). These methods might seem appropriate for systems with a sublayer composed only of crushed stone where the water flows freely through the stone, but are highly imprecise for systems that have a more complex configuration and include more hydraulically restrictive layers such as sand.

Some stormwater management software packages (EPA SWMM5 and PCSWMM) now include an LID toolkit with explicit tools for modeling PP systems and other filtration systems. The flow through the filter media is modeled with the Green-Ampt Equation which assumes saturated porous media flow. XPSWMM also developed a tool that allows the user to model PP systems as a storage unit, using stage-storage indication methods. Both these modeling approaches assume that the pore space in the soil is completely saturated with water during precipitation events.

The need for more physically-based models to route stormwater through filtration systems is recognized by scientists who go to great lengths in trying to adapt modeling capabilities of available software to mimic the hydrological behavior of filtration systems (Lucas, 2010; Aad et al, 2010). A few methods suggested for modeling the water movement through filter media include Darcy's Law (Lucas, 2010), original Green-Ampt (Dussailant, 2003; Jayasuriya, 2008; Aad, 2010) or modified Green-Ampt (Lee, 2011), and Richard's Equation (Dussailant, 2004; Browne, 2008). While Darcy's Law and

Green-Ampt are valid only for saturated flow, Richard's Equation is the only one that applies to unsaturated flow conditions.

II.2.1 Water flow in soils

The soil matrix is composed of solid particles and pore space which can be filled either with air or water. Some pores are connected to each other in a way that can transmit fluids, while other pores have dead ends and effectively transmit no fluid. The connected pores are known as the effective porosity of the soil. The tortuosity of the connected pores is dependent on soil texture and compaction. More compacted soils have less pore space available to transmit water. Similarly, when the gradation of the soil covers a wide range of particle sizes, the smaller particles fill the void space between the larger particles, decrease the pore space volume and increase the tortuosity of the flow path (Dane and Topp, 2002). Vertical water flow through soils is driven by gravity and can take place both under unsaturated or saturated conditions. When the pore space is only partially filled with water (unsaturated flow), the water moves at slower rates than when the pores are completely filled with water (saturated flow conditions) because permeability is directly related to moisture content. If the water input at the soil surface is greater than the soil's water transmission capacity, saturated conditions occur, and the water builds up (ponds) above the soil. In PP systems with layers of differing soil media, water could back-up (pond) above the least transmissive layer: the filter layer or the native soil at the bottom. An indication of saturation within the soil matrix is when the volumetric moisture content in the soil reaches the effective porosity value and then plateaus.

The most common equation used to represent saturated porous media flow conditions is Darcy's law (Darcy, 1856):

$$q = -K_{sat} \left(\frac{dh}{dz} \right)$$

Equation 1

Where:

q = Darcian flow (L/T); K_{sat} = saturated hydraulic conductivity (L/T); dh = change in energy that drives the flow (L) across dz = the length of porous media layer (L), z being the vertical direction here.

Unsaturated flow is successfully described with Richard's Equation, which is a combination of Darcy's law and the continuity equation for a partially saturated porous media:

$$\frac{\partial \theta}{\partial t} = \frac{\partial \left[D(\theta) \frac{\partial \theta}{\partial z} + K_r(\theta) \right]}{\partial z}$$

Equation 2

Where:

$\partial \theta$ = the change in volumetric moisture content (-); ∂t = the time interval for analysis (T);

∂z = the space interval/depth of layer (L); $\partial \psi$ = the change in matric potential (L⁻¹);

$K_r(\theta)$ = hydraulic conductivity (L/T); and $D(\theta)$ = water diffusivity (L²/T);

Solving Darcy's Equation requires knowing the hydraulic conductivity at saturation (K_{sat}), which is constant for a given soil and compaction degree. Solving Richard's Equation requires knowing the relative hydraulic conductivity (K_r) of the porous media. This changes with moisture content and so does the diffusivity (D) and the matric potential (ψ). As saturation decreases, K_r can decrease by orders of magnitude. In order to solve Richard's Equation, information is needed on how θ , ψ , and K_r relate to each other. The $\theta - \psi - K_r$ relationships are unique for each soil and degree of compaction. For any specific porous media, these relationships are highly nonlinear, non-unique, and difficult to accurately represent with a function for the entire range of values. The complexity of data input needed to solve unsaturated flow equations is the main drawback to employing unsaturated flow equations for modeling flow through PP systems.

The goal of this study is to improve the understanding of water movement through PP systems, investigate the nature of flow through the filter media under natural precipitation, and select the most appropriate equations for modeling the movement of water through the filter media of PP systems. This information will be useful for developing hydrological assessment methodologies for PP systems.

II.3 Methods and Materials

The study was conducted on a porous asphalt pavement parking lot installed on the University of New Hampshire campus in 2010. The PP system consists of a 10 cm (4") porous asphalt layer laid on top of a choker course consisting of 15 cm (6") of 2 cm

(3/4") crushed stone, 30 cm (12") bank run sandy gravel serving as the filter media layer, 10 cm (4") of 1 cm (3/8") crushed stone as a separation layer, and 30 cm (12") of 5 cm (2") crushed stone serving as an infiltration reservoir with 15 cm (6") diameter slotted drains installed at the top of the stone reservoir (Figure 1). The system was built in a native sandy soil, based on the PP systems design specification developed by the UNHSC (UNHSC, 2009a), with seasonally high water table.

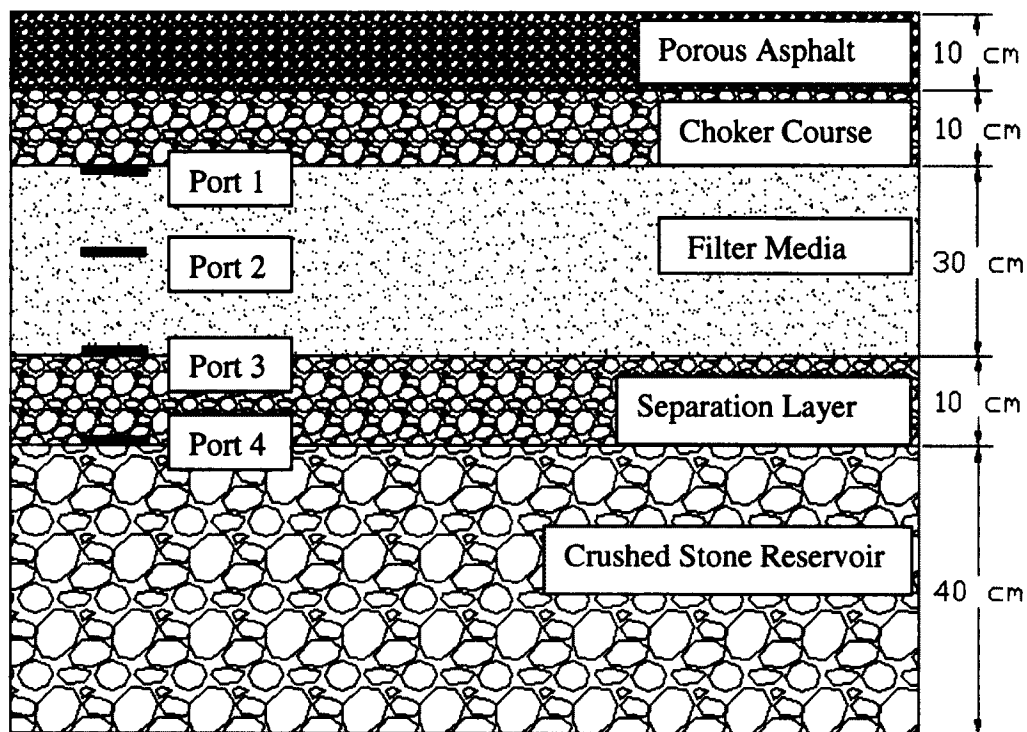


Figure 1 – The cross section of the PP system studied and the location of the four 5 TE Decagon moisture/temperature/conductivity probes (Ports 1 - 4). Duplicate probes are installed at each location.

In order to track the moisture movement through the system, four 5TE Decagon multi-sensor probes were installed at different levels in the PP system. The probes were placed at the top, middle, and bottom of the filter media layer and at the bottom of the crushed stone separation layer placed between the filter media and the infiltration

reservoir. VMC, temperature, and specific conductivity were measured in real time at 5 minute intervals and stored with an Em50 data logger. The setting of two of the 5TE probes is shown in Figure 2. Since the filter media is the most flow restrictive material in the system, special attention was given to the probes installed in this layer. The soil characteristics of the bank run gravel used as filter media are presented in Table 1. The gravel layer was compacted to 92% of maximum density measured with the Modified Procter test. The porosity was computed according to ASTM 7263, and was found to be 32.8% by volume. Using the Vukovic Equation (Vukovic and Soro, 1992), porosity was calculated as 34.4%.

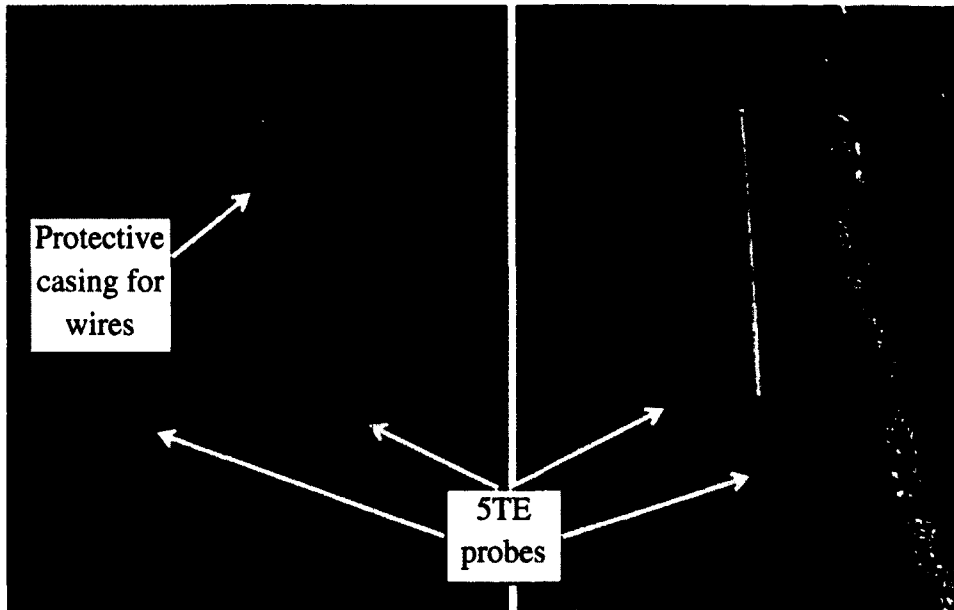


Figure 2 – Installation of the 5TE probes at the bottom and middle of the filter media layer (Port 2 and Port 3). Half cut, stone filled pipe on the right side of the right figure is a positive pressure water sampler.

Table 1 – The particle size distribution for the sandy gravel used as filter media in the PP system.

Sieve Size (mm)	Sieve Size (in)	Percent Finer (%)
38.1	1 1/2"	100.00
19.0	3/4"	96.13
12.5	1/2"	93.93
6.3	1/4"	90.79
4.75	#4	84.41
2	#10	80.86
0.85	#20	66.95
0.425	#40	35.77
0.18	#80	10.98
0.15	#100	2.09
0.075	#200	1.57
<0.075	pan	0.42

II.3.1 Moisture content measurements with Decagon devices

The 5TE Decagon probes measure VMC, temperature, and specific conductivity with three individual probes. The VMC is measured as a dielectric constant, using

capacitance domain technology; temperature is measured with a thermistor; and specific conductivity is measured with a stainless steel electrode array (Decagon, 2011). In order to obtain the actual VMC in the soil, the dielectric constant reading from the probe is automatically converted to VMC through the data management software ECH₂O using the Topp Equation (Topp et. al, 1980):

$$\theta(m^3/m^3) = 3.44 * 10^{-11} * Raw^3 - 2.2 * 10^{-7} * Raw^2 + 5.84 * 10^{-4} * Raw - 5.3 * 10^{-2}$$

Equation 3

Where: *Raw* = the direct output of the 5TE dielectric probe.

Topp's Equation was developed on over 2000 soil samples ranging from clay soils to sandy soils. Literature shows that for improved data accuracy, soil specific calibration and even sensor specific calibration are needed (Rosenbaum et. al, 2010). The filter media in the PP system contains a significant amount of coarse particles and there was a concern that the gravel would influence the readings of these probes. In order to verify the applicability of Equation 3 to the PP filter media and the gravel particle effect on the 5TE probe readings, a soil-specific calibration test was measured in the laboratory. The soil samples were progressively wetted with known volumes of water up to the saturation point, while the probe's dielectric signal was recorded. A soil specific equation was then developed with regression analysis.

Two soil specific equations were developed for the bulk soil and for the fine fraction that remained after removing all particles larger than 2mm, respectively. Calibration data presented in Figure 3 shows that there is no significant difference

between the two equations and that particles larger than 2mm did not influence the moisture content readings of the 5TE probes for this soil. The equation developed on the bulk sample of the soil was further used to convert the raw data to VMC for the filter media:

$$\theta(m^3/m^3) = 0.0004 * Raw - 0.0771$$

Equation 4

Where: Raw = the direct input from each of the 5TE dielectric probes

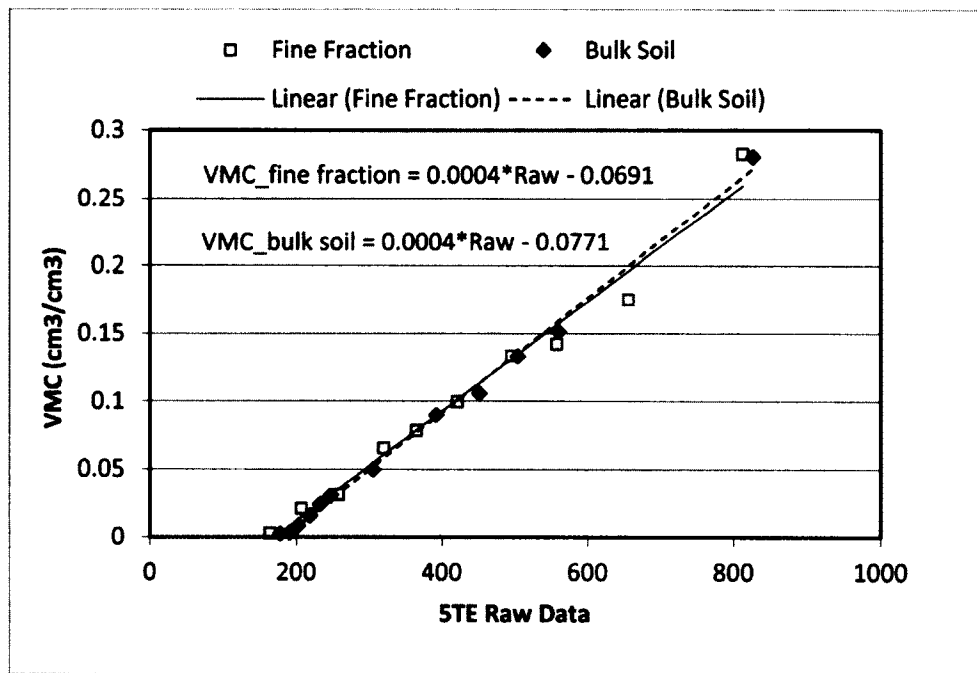


Figure 3 – Soil specific calibration for the 5TE Decagon probes developed for the bulk and fine fraction of the soil used as a filter media in the permeable pavement system

II.3.2 Precipitation data

In order to capture the seasonal variation of climate conditions, precipitation and moisture content data in the PP system’s sub-base was collected from October 29, 2010

to January 11, 2012. Precipitation data was collected with a NOAA rain gage located 2.4 km (1.5 miles) away from the location of the study site. The total amount of precipitation recorded was weighted on an annual basis at 1057 mm (41.6 ") per year. Compared to the annual average for the geographical area of 970 mm (38.2") (NOAA, 2012), this would indicate that the period of study was slightly wetter than normal. However, when comparing the nonexceedance probability distribution of the daily precipitation data for Durham, NH (the NOAA gage) from 1915 to 2007 to that of the precipitation recorded for the period of this study (Figure 4) as developed with Weibull formula (Weibull, 1939), the daily average precipitation during this particular year was lower than in an average year and it was a few extreme events that made the annual amount larger than the long term average annual amount. Over the monitoring period, there were a total of 46 storm events that generated a response in the moisture content in the filter media. Scattered precipitation amounts that did not cause a change in the moisture content or that generated a response for only a very short period of time were not categorized as precipitation events for the purposes of this investigation. The inventory of the 46 storm events is presented in Appendix A.

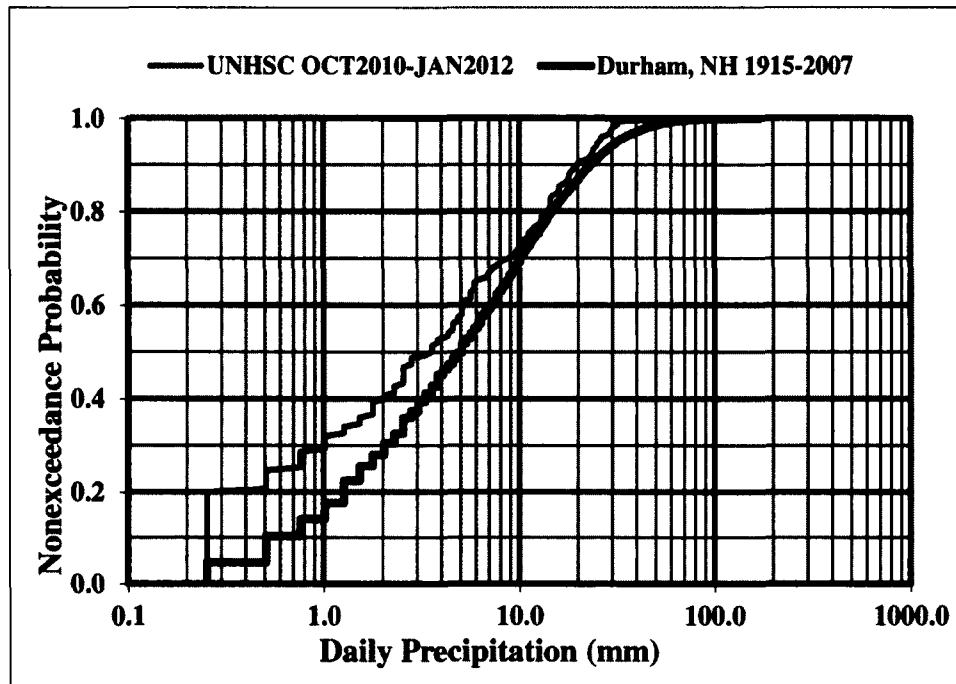


Figure 4 – Nonexceedance probability of daily precipitation for Durham, NH over the entire gage record and for the study location from October 29, 2010 to January 11, 2012.

II.4 Results and Discussion

II.4.1 Volumetric moisture content equations for the 5TE Decagon probes

The VMC at the bottom, middle and the top of the filter media layer were recorded at five minute intervals. Figure 5 shows the VMC data obtained with the Topp Equation (Equation 3) and with the soil specific equation developed for the sandy gravel - filter media in the PP system (Equation 4). It is apparent that Equation 3 consistently overestimated the actual moisture data by approximately 5% of the actual VMC (Figure 5). Given that the range in moisture content through the study period was somewhere between 1.4% and 20.2% (Equation 4), and 6.9% to 24.7% (Equation 3), the actual VMC error introduced by using the Topp Equation for this soil ranges from 24% to 29%. This is the equivalent of 232 to 284 millimeters of rainfall on an annual basis.

The close resemblance of the two soil specific calibration equations developed for the bulk sample and the fine fraction of the sandy gravel suggests that these equations may be used for similar studies of coarse filter media containing various ratios of sand and gravel. Either one of the two developed equations (Figure 3) is recommended as an alternative to the Topp Equation (Equation 3) for disturbed and repacked sandy and gravelly soils used in stormwater management applications.

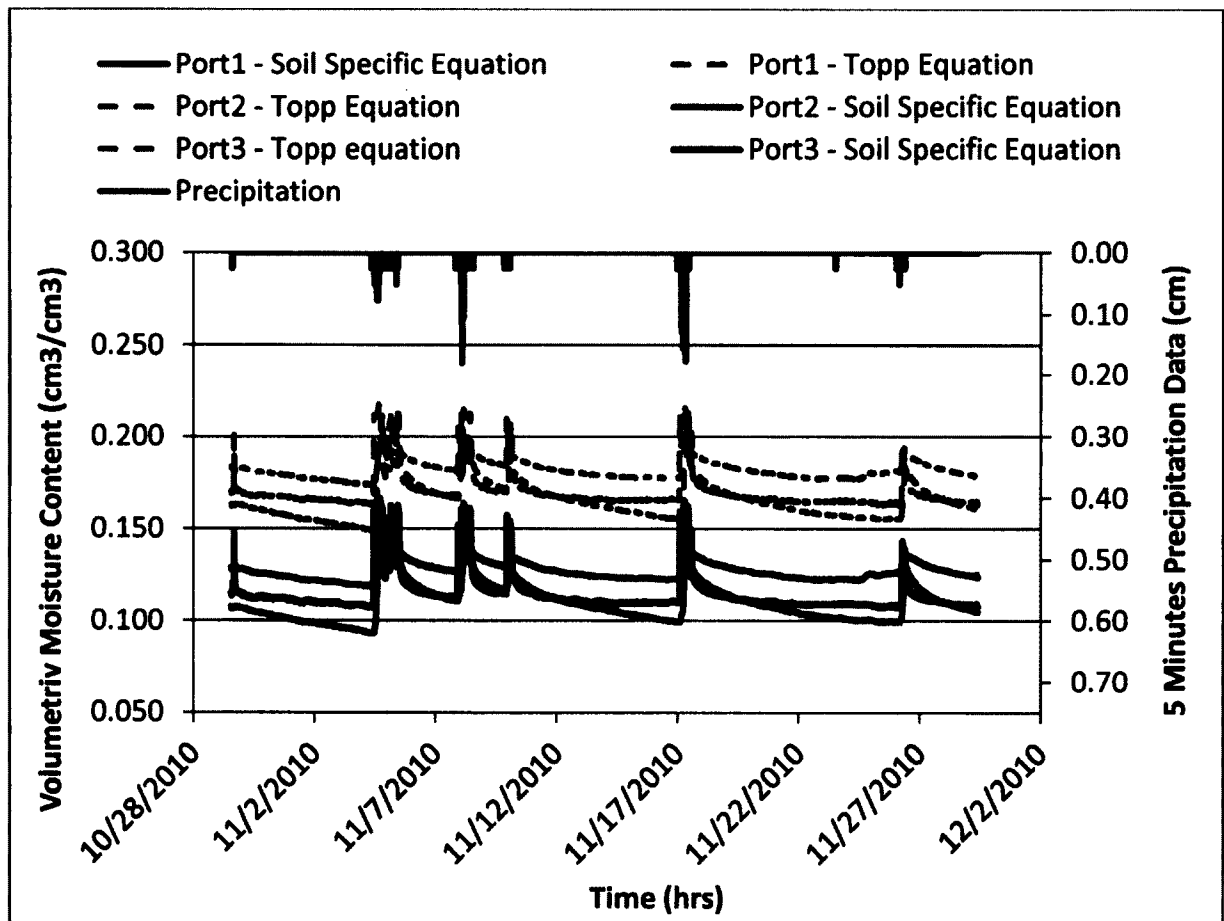


Figure 5 – Volumetric moisture content estimated from probe signals and converted with the original Topp Equation and the soil specific soil equation developed

II.4.2 Flow through the system and residence time

The range of the VMC in the filter media at different levels was somewhat dissimilar (Table 3). The values for the VMC in the middle of the filter media were consistently higher than the VMC at the top and the bottom of that layer. This can be attributed to the fact that the 5TE Ports 1 and 3 were placed in the vicinity of coarser soils layers and the probes readings extended beyond the filter media boundaries. The range of influence of 5TE probes is approximately 0.3 liters which can be illustrated by a cylinder with a radius of 2 centimeters around the probe. Coarser soils have a lower water retention capacity and the mixed signal from the two layers with different porosities would explain why the VMC recorded by Ports 1 and 3 were lower than the VMC recorded in the middle of the filter media layer. Probe 2 which was completely surrounded by the bank run gravel is considered to give a clearer picture on the nature of flow in the filter media than probes 1 and 3. Another case can be made for the fact that engineered soils are not completely homogeneous and uniform densities usually are difficult to obtain in the field and this might have influenced the actual VMC at different locations.

However, the VMC from the four probes gives significant insight in the water movement in the PP system's sub base which can be tracked by means of peak moisture values through the system. The peak moisture content occurrence at the four levels in the system in response to precipitation is exemplified in Figure 6 which shows part of the May 14, 2011 precipitation event.

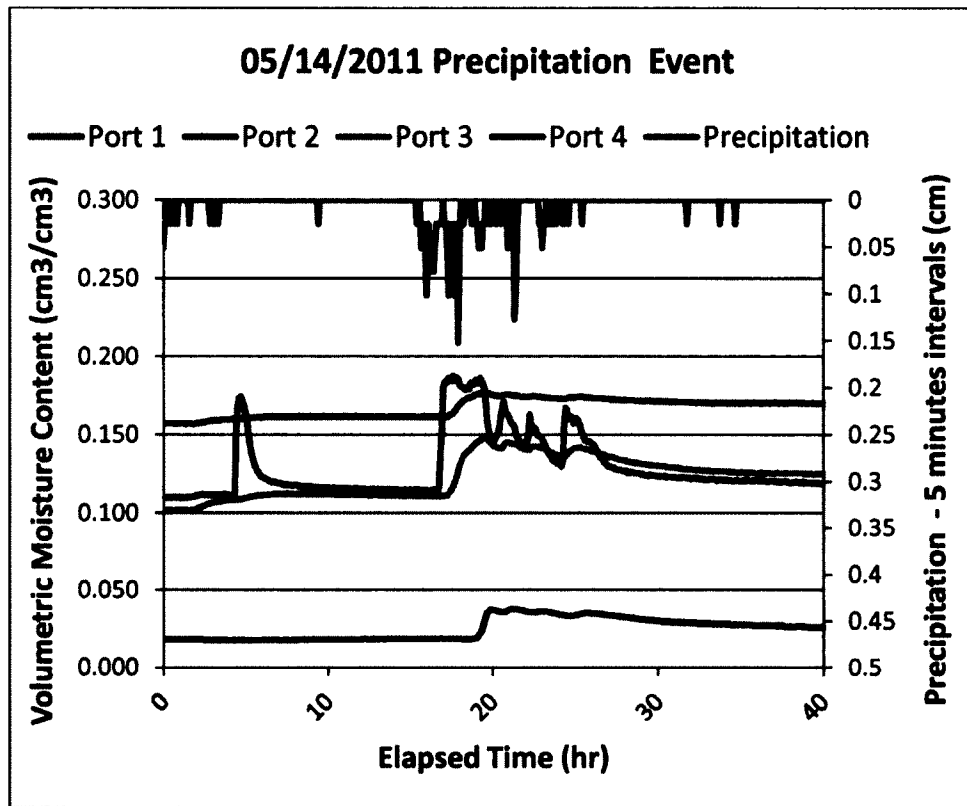


Figure 6 – Peak moisture content at different levels in the PP system, generated by the infiltration of natural precipitation. Saturation in the filter media layer occurs at 29% VMC.

The lag time between the beginning of the precipitation event and the response of the VMC in the system’s sublayers was analyzed for each precipitation event. The average lag time for Port 1, Port 2 and Port 4 were 2.45, 3.48 and 7.61 hours, respectively (Table 2). Port 3 had multiple data gaps due to probe malfunctioning and there were not sufficient storms to generate an unbiased lag time value for this location. If the system were to function under saturated conditions, it would take only 8 minutes for the moisture to travel through the entire filter media layer (Port 1 to Port 3) based on the $K_{sat} = 3.6$ cm/min measured for the bank-run gravel, rather than the observed average of 2 hours.

In order to generate a response in the VMC at Port 1, the precipitation needs to travel through 10 cm of pervious asphalt and 10 cm of 2 cm diameter crushed stone. Infiltration rates for pervious asphalt and pervious concrete pavements are typically in the range of 1,250 to 10,000 cm per hour (UNHSC, 2012) as measured with double ring infiltrometers or other testing methods that create ponding conditions on top of the pavement's surface (Ferguson, 2005). Infiltration rates for crushed stone are around 4,000 cm/hour and generally it is assumed that these two top layers of a PP system can easily absorb the natural occurring precipitation rates which are significantly smaller than their infiltration capacity. In addition, their pore sizes are sufficiently large that there does not appear to be a capillary barrier effect. When modeling PP systems, the travel time through these coarse materials is often assumed insignificant when compared to the travel time through the more hydraulically restrictive layers and is not explicitly modeled. Commonly, when modeled, precipitation is considered to accumulate directly at the bottom of the system or on top of the most impermeable layers without delays (Jackson, 1974; Ferguson, 2005). However, real time data (Table 2) shows that the time to travel through the pavement and chocker course could contribute significantly when evaluating the lag time for the entire system.

Table 2 – The time difference from the beginning of precipitation event to the VMC response at different levels in the PP system.

Lag Time (hours)	Port 1	Port 2	Port 3	Port 4
Average	2.45	3.48	N/A	7.97
Minimum	0.25	0.50	0.58	0.75
Maximum	9.83	14.42	7.92	23.08

The difference in lag time between Port 1 and Port 2 can be used to estimate the average hydraulic conductivity rates in the filter media layer. The design specification for

the filtration layer requires the saturated hydraulic conductivity to be between 3 to 18 meters per day (10 to 60 ft/day) (UNHSC, 2009a). With an average lag time between Port 1 and 2 of 1:09 hours and a distance of 15 cm, the average unsaturated hydraulic conductivity of the soil was 3.35 meters/day (11ft/day). This is the hydraulic conductivity corresponding to a VMC of 17.5% for this soil, based on the measured unsaturated hydraulic conductivity test performed on this soil in a parallel study (Barbu, 2013). This would imply that the actual saturated hydraulic conductivity is above the minimum value required by design standards, but that in practice, if systems are designed at the low end of the required range, the actual unsaturated system performance could easily miss the minimum target. Testing of permeability on each material layer during construction phase is typically performed with inundation tests, which create saturated condition at least at the surface of the soil tested.

II.4.3 Water residence time in the system

Typical PP system design standards require that the system completely drains down in 1 to 5 days (Leming et al, 2007), which represents the mean time between precipitation events in most geographical areas in the U.S. The more frequent design standard is for the system to drain down the 10-year 24-h design storm in less than 72 hours (Schwartz, 2010). The residence time in the PP system in our study was analyzed for each storm, by tracking the time it took for the VMC in the filter media to return to the initial moisture content of the soils recorded at the beginning of the storm. The average time was 3.04 days, with a minimum and maximum value of 0.39 and 7.52 days, respectively. For some storm events, the VMC did not return to the initial value before the next precipitation event.

II.4.4 Seasonal variability of the VMC

Freeze-thaw phenomenon is a concern in PP systems as well as in conventional pavements. During extreme cold weather, as water infiltrates into the sub-base of pavements and freezes, its volume expands and could potentially cause damage in the pavement layer as well as disturb the sub-base materials. Because of the free draining nature of PP system's sublayers as well as the intentional use of a lower stone layer to act as a capillary barrier, frost heave is not typically an issue in PP systems, even though the PP systems freezes prior to nearby soil (Roseen et al, 2012).

In this study, the values of the VMC in the cold months for the four probes were generally lower than those in warm months (Table 3). This is because some of the residual water held by the soil particles was frozen and was sensed by the probes as solids. However, the fluctuation of the moisture content during the precipitation events is evidence that the pore space in the soil was not completely occupied by frozen water, and that the soil still maintained opened pores capable of transmitting water. The latent heat of the infiltrating stormwater caused the temperature in the system to rapidly increase and melt some of the ice formed in the soil's pores during infiltration into the frozen filter media layer (Figure 7), therefore changing the VMC over the course of the storm. Although the air temperature was above freezing and the atmospheric conditions caused rainfall instead of snowfall, the temperature in the soil was still below freezing (Roseen et al, 2012). The VMC for storm events for which the temperature recorded in the PP system's filter layer were below-freezing were analyzed separately from above-freezing events and are presented in Table 3.

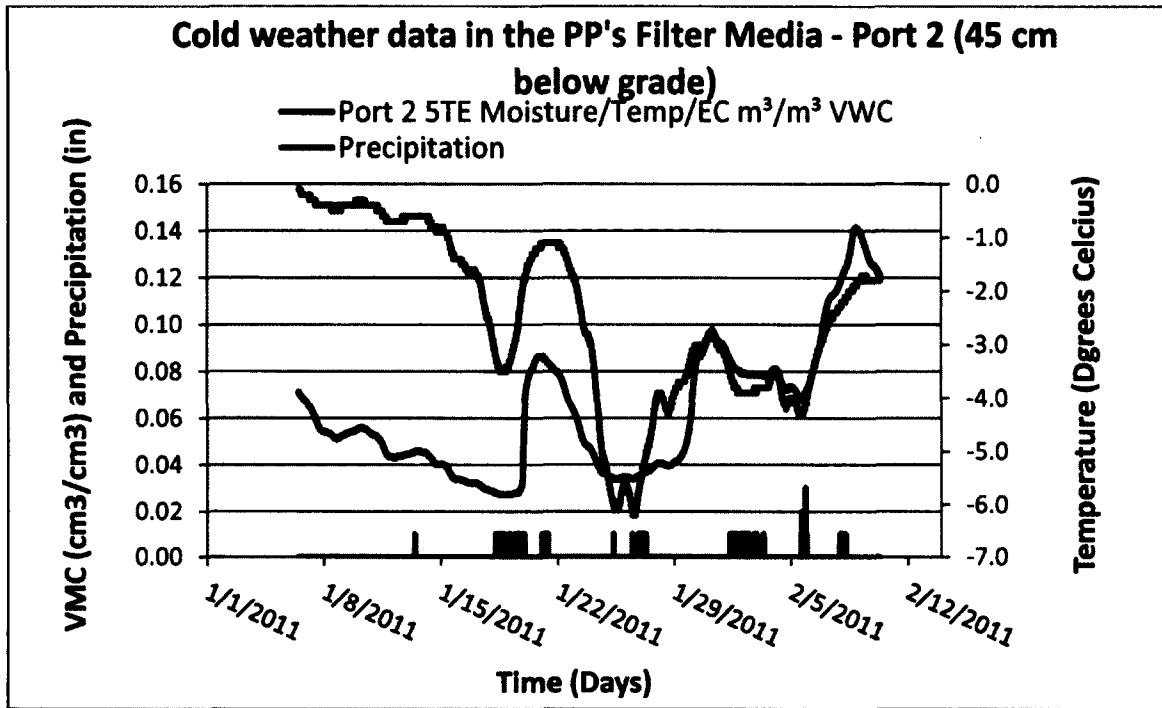


Figure 7 – The volumetric moisture content and temperature for Port 2 for below-freezing conditions. Saturation in this layer occurs at 29% VMC.

The temperatures at different levels in the PP sublayers are analyzed and summarized in Table 4. As expected, the temperature variation in response to air temperature fluctuation was smaller in the deeper layers of the system. The temperature in the lower layers was colder in the summer time and warmer in the winter time when compared to the temperature at the top of the system (Port 1). One noteworthy observation is that the top layers of the system – the pavement and choker layers – heat up above the air temperature during the summer months due to solar radiation and consequently transfer the heat to any infiltrating stormwater. The highest temperature in the system over the study period was 41.8 °C, recorded at Port 1, which is located 20 cm under the surface of the pavement. The maximum air temperature recorded for that period was only 37.6 °C.

Table 3 – Seasonal variation in volumetric moisture content in the PP system’s sublayers

	Above Freezing Temperatures				Below Freezing Temperatures			
	Port 1	Port 2	Port 3	Port4	Port 1	Port2	Port 3	Port 4
Min – VMC (%)	8.9	7.4	9.1	5.2	4.1	4.3	1.4	2.6
Max – VMC (%)	20.1	20.2	15.2	10.1	18.3	20.2	16.1	8.1
Range of VMC (%)	11.2	12.8	6.1	4.9	14.2	12.8	14.7	5.5

Table 4 – Temperature variation in the PP system sublayers

	Port 1	Port 2	Port 2	Port 4
Min – Temperature (°C)	-8.1	-6.2	-6.1	-2.7
Max – Temperature (°C)	41.8	37.8	30.9	28.0
Average – Temperature (°C)	13.2	13.4	8.8	8.5
Average – Summer Temperature (°C)	29.4	29.1	26.8	25.3
Average – Winter Temperature (°C)	-1.5	-0.7	-0.3	1.1

II.4.5 Volumetric moisture content range in the filter media

The PP system for this study does not receive run-on from surrounding impervious areas, which means that it has a 1:1 drainage area to filter area ratio. One of the main goals of this study was to investigate whether the filter media reaches saturation at any time. Two different tests performed on the filter media soil compacted at field conditions resulted in moisture content at saturation to be 29.3% and 28.29% respectively. The first measurement was part of an unsaturated hydraulic conductivity test, and the second measurement was taken during the inundation test performed when the soil specific equations were developed for the 5TE probes. Given the close agreement

of the two measurements, it is conservative to say that the saturation of the filter media soil at field compaction takes place at 28-29% VMC.

Probe 2 is considered to be most representative of the flow conditions in the filter media soil because its zone of investigation is entirely within the filter media. This probe is located in the middle of the filter media and it is unlikely that its signal reaches into the adjacent layers as is the case for probes 1 and 3. The values of the calibrated VMC data for the combined seasons in the middle of the filter media layer ranged from 4.3% to 20.2%. When compared to the computed porosity, effective porosity, and saturation moisture content (Table 5), it is apparent that the filter media was far from reaching saturation during the period of study. This is also supported by the comparison of the cumulative probability distribution for the VMC at this location to the VMC at saturation.

In below-freezing temperature, as some of the residual water in the soil freezes, the pore space is less than that of unfrozen soils. The 5TE probes sense the frozen water as solids, and their readings might not be an accurate measure of the actual VMC in the soil. The amount of solid water and that of the opened pore space fluctuates during a runoff event: as warmer stormwater infiltrates and increases the temperature in the PP system's sublayers. Although we could not obtain a measurement of the effective porosity of the frozen soils, we looked for any other signs of saturation. If, during a recharge event, the VMC reached the effective porosity, it would plateau at that maximum value until recharge slowed or ceased, and this was never observed at any point for below-freezing temperatures, or above-freezing temperatures for that matter.

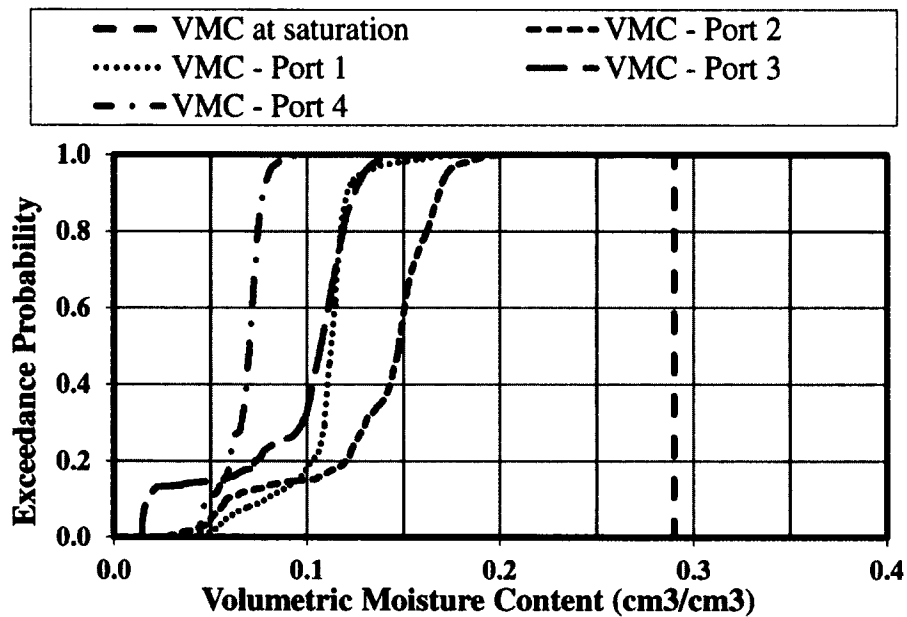


Figure 8 – Exceedance probability curves for the VMC monitored by the four ports and VMC at saturation in the filter media soil.

Generally, the coarse soils with uniform particle gradation like those used as the choker course and separation layer have higher permeability rates and hydraulic conductivities than the soil used as the filter media. Since probes 1 and 3 were likely receiving a mixed signal from coarser adjacent layers and the filter media, and probe 4 was placed in the separation layer itself, we assumed that the saturation at these three locations should be at least the same as for the filter media (but realistically most likely higher). The cumulative frequency distribution for the VMC for each of the four probes, as shown in Figure 8, suggests that saturation did not occur at any level in the sublayers of the system for the period of study. It is also apparent that the layers underlying the filter media do not reach saturation (based on VMC from Port 4), and this is most likely because the filter layer is throttling the flow through the system.

Table 5 – Comparison of the porosity of the filter media soil and the observed VMC

Effective Porosity range for gravels (%) (Fetter, 1988)	Computed Porosity (%) (Vukovic Eq.)	VMC at Saturation (%) (measured)	Max. VMC (%) (observed)	Min. VMC (%) (observed)
25 - 35	34	28 - 29	20.2	4.3

The moisture changes in the filter media in response to the largest (5/14/2011) and most intense (8/27/2011) precipitation events for the period of study were evaluated for any signs of saturation. The moisture profile in the PP system’s sub-base for these storms is presented in Figures 9 and 10.

The largest event (5/14/2011) registered 7.39 cm (2.89 in) of precipitation over a period of five days. The maximum VMC increase (6.6%) was recorded at the top of the filter media and corresponded to a maximum precipitation intensity of 0.7 cm/hour (0.27 in/hour). The maximum VMC was of 18.3%, which is well below the saturation VMC. The most intense event (8/27/2011) recorded rainfall intensities of a 1 year-12 hour storm, based on rainfall frequency data developed by the Northeast Regional Climate Forecasting Center with precipitation data recorded until 2010 (Appendix B). During this storm event, the maximum VMC increase (6.3%) was also recorded at the top of the filter media, and corresponded to a maximum precipitation intensity of 0.97 cm/hour (0.38 in/hour). The maximum VMC was recorded as 18.0%. No saturation was observed at any levels in the system even during the largest and the most intense storm events.

Averages of the initial and maximum VMC, and the average change in VMC for all other storm events are presented in Table 6, and a summary of the storm events characteristics are shown in Appendix A.

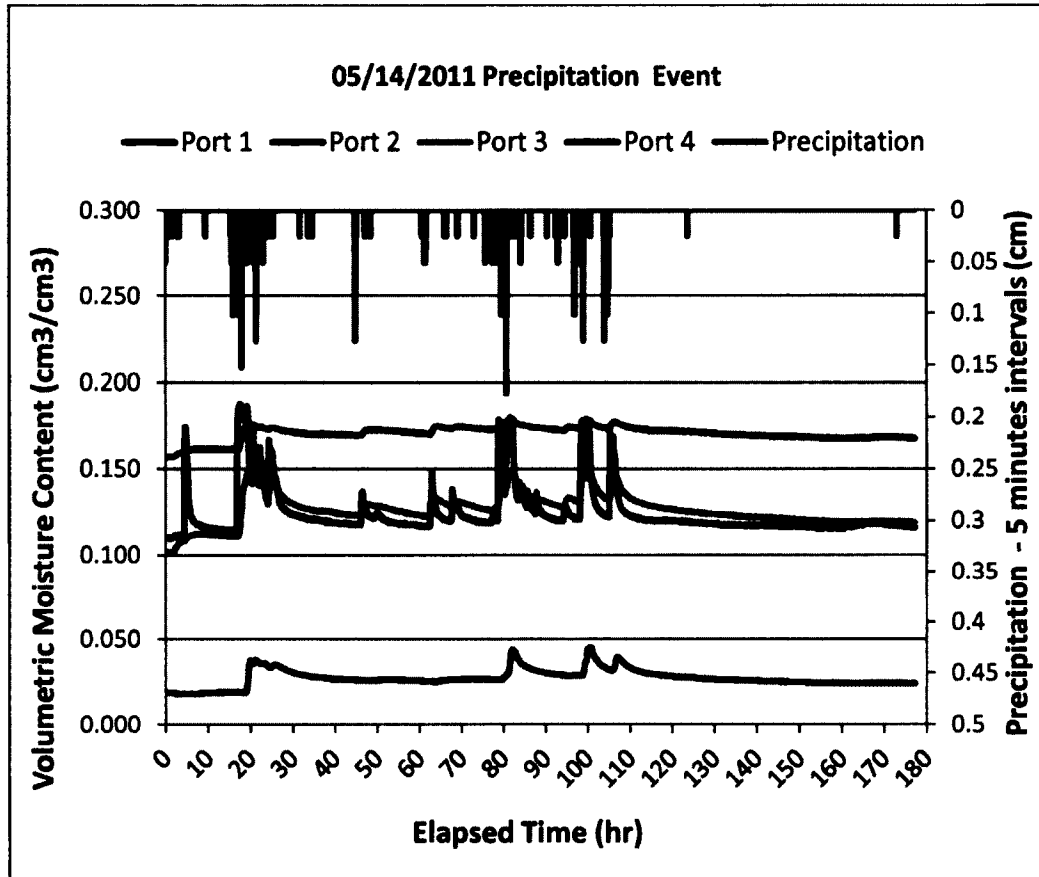


Figure 9 – The fluctuation of the VMC in the PP system’s sublayers during the largest storm. Saturation occurs at 29% VMC.

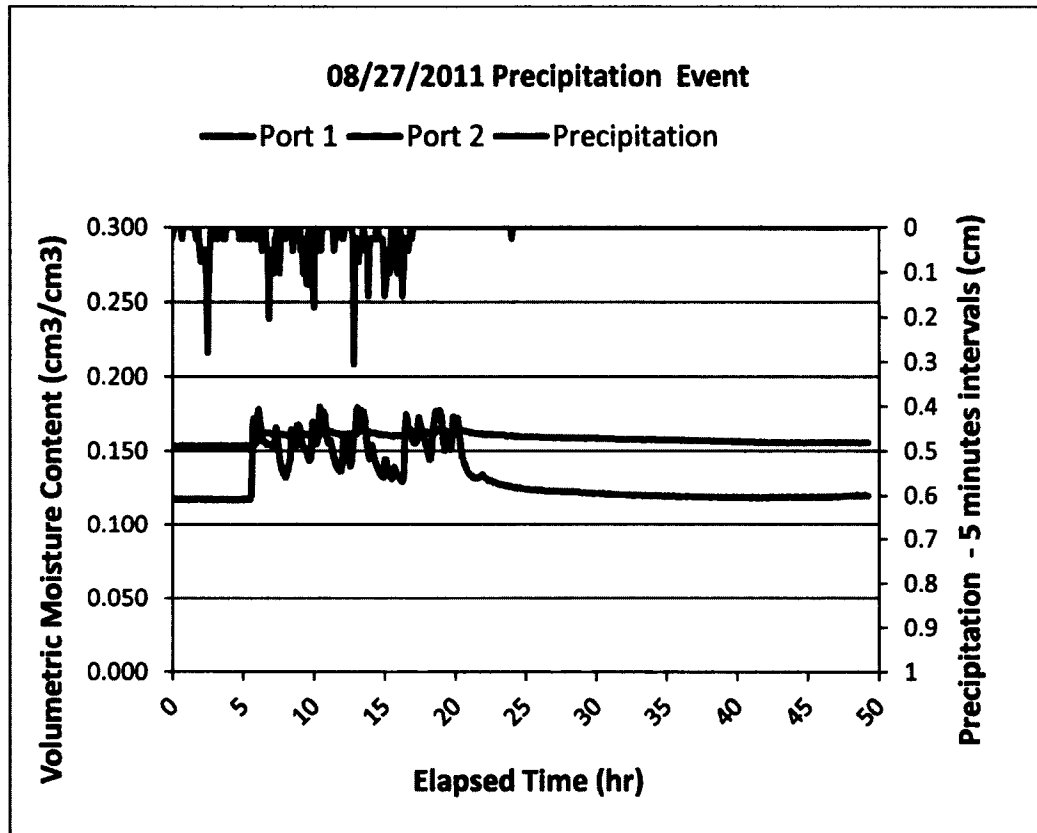


Figure 10 – The fluctuation of the VMC at the top (Port 1) and middle (Port 2) of the filter media during the most intense storm. Saturation occurs at 29% VMC. VMC data for probes 3 and 4 was not available for this precipitation event due to probe malfunctioning.

Table 6 – Average values of the initial, maximum and the change in the VMC during precipitation events

	Port 1	Port 2	Port3
Initial VMC (%)	11.1	13.0	9.2
Maximum VMC (%)	16.3	14.2	11.9
Change in VMC (%)	5.1	1.2	2.7

II.5 Conclusions

The main objective of this study was to investigate the nature of flow in PP systems in order to identify the most appropriate flow equations for modeling stormwater

routing through these systems. Special attention was given to the filter media, which is the most hydraulically restrictive material in the PP system, and which can control the flow through the entire system. The real time, continuous measurements of the VMC at four different levels in the PP system's sublayers showed that saturation did not occur at any level in the system over the period of study. In a similar monitoring study performed on bioretention systems, which typically are designed with a higher drainage area to filter media ratio (about 45:1), data showed that the bioretention soils did not reach saturation either (Carpenter, 2009). It appears that filtration stormwater management systems function predominantly under unsaturated conditions and consequently, unsaturated models such as Richard's Equation are more appropriate for hydrological simulation of these systems, rather than saturated flow equations such as Darcy's Law and Green-Ampt.

A disadvantage of representing the water flow through the filter media with saturated flow equations, as in current practice, is that the saturated hydraulic conductivity is much higher than the unsaturated hydraulic conductivity. Because of this, the saturated flow equations misrepresent the time to peak of the final system outflow hydrograph and the stormwater residence time in the system.

When PP systems are designed for extreme precipitation events or to receive runoff from adjacent impervious surfaces, the saturated flow modeling approach could lead to under sizing of the system with the result that the infiltrating water ponds above the filter media. Even when PP systems are designed based on unsaturated flow analysis, we recommend that proper consideration and design modifications are directed at sizing the storage provided above the filter media when the PP system is designed to receive run-

on. This is not a concern for PP systems designed to “treat” only the precipitation falling on the PP’s surface.

When PP systems are modeled as storage units, the incoming precipitation is, placed immediately at the bottom of the system (Jackson and Ragan, 1974) and theoretically, saturation occurs as moisture is added and the water level rises from the bottom to the top. In reality, the moisture travels with a piston-like movement through the permeable media layers, and saturation (or just an increase in moisture content in our study) occurs from the top down. Even if supposedly the entire pore space is available for storage, the availability of the pore space is restricted by the actual advancement of the wetting front. Only the pore space behind the wetting front is used for storage, while the pore space ahead of the wetting front (the bottom of the system) is temporarily unavailable until the wetting front actually reaches that level. Considering the volume of the pore space in the PP systems, the studied system could theoretically hold more than 20 cm (7.9 inches) of water, which for the study site is close to the 100-year, 24-hour rainfall. However, an unsaturated flow analysis should be performed to evaluate the actual storage available under precipitation loads of interest.

Based on the information presented in this study, we recommend that modeling of flow through the filter media of PP systems and other LID-SWM systems should be performed with unsaturated flow rather than saturated flow equations. Incorporation of unsaturated functions in commonly used design software for PP systems would allow for better hydrological performance assessment, as well as optimization of the system’s configuration for site specific hydrological requirements.

CHAPTER III

Unsaturated flow functions for filter media used in Low Impact Development - Stormwater Management Systems

Abstract

Moisture retention relationships for coarse, high infiltration soils are difficult to empirically determine and estimate. Present day software models for stormwater management (SWM) that are used as sizing and performance prediction tools for filtration Low Impact Development – Stormwater Management (LID-SWM) systems typically assume that these systems function under saturated flow conditions. This directly impacts prediction of system drainage and hydrographs, as well as the estimates from physically-based water quality improvement. Yet real time monitoring of these systems demonstrated that saturation of the filter media is rarely achieved. This article presents a framework for obtaining the moisture retention curves (MRC) and relative hydraulic conductivity $K_r(\theta)$ function for engineered filter media and other hydraulic control soils used in four LID-SWM systems: pervious pavement, sand filter, gravel wetland, and bioretention system. These functions needed in routing water through the filter media with unsaturated flow functions are developed from easily measurable soil properties like porosity and particle size distribution, and can be integrated in current available stormwater design software. The framework consists of a sequence of physically based equations: Arya-Paris for the $\theta(\psi)$ function, Bower for gravel content adjustments along with an extension of the $\theta(\psi)$ function proposed in this article, and

Mualem for the $K_r(\theta)$ function. This sequence is combined with Van-Genuchten fitting equation for soils with irregular particle size distributions.

III.1 Introduction

Increasing environmental problems caused by polluted stormwater runoff from urban development led to modifications of the Clean Water Act. As a result, standards for the quality of stormwater runoff allowed to be discharged into receiving waters were improved with the result being strict qualitative and quantitative restrictions for the stormwater runoff that can be discharged off-sites or to receiving waters. To meet these criteria, stormwater management and treatment infrastructure had to evolve over the last few decades from conventional systems (swales, detention and retention ponds) which controlled the peak flow of the discharged hydrograph but were ineffective for most water quality parameters (USEPA, 2013), to more advanced treatment systems which, in addition to controlling the peak flows, target removal of both solids and dissolved pollutants and replicate natural hydrology. These new systems are known as Low Impact Development-Stormwater Management (LID-SWM) or Green Infrastructure. A few examples of LID systems include: pervious pavements, bioretention systems, tree filters, ecoroofs, subsurface gravel wetlands, sand filters, and other variations and combinations of these systems (USEPA, 2000). The main difference between conventional and LID systems is that the latter uses engineered filter media or other permeable media layers and customized hydraulic controls in order to: increase the residence time of stormwater in the system, remove pollutants by filtration and possibly biological processes, and allow increased evapotranspiration. In some situations, infiltration is also an integral component of these systems. The subsurface gravel wetland (GW), bioretention system (BS), surface

sand filter (SF), and pervious pavement (PP) are four different, yet similar stormwater treatment systems that incorporate a range of elements which are commonly found in other LID systems (UNHSC, 2009).

The BS, SF, and GW systems are represented by excavations, which are typically only partially backfilled with engineered soil layers. Above the surface of these systems there is surface storage capacity for the inflowing, untreated runoff. These systems are designed to allow ponding on top of the system during more extreme precipitation events. The engineered soil mixes in the BS and SF act as a filter media that remove pollutants and hydraulically control the stormwater flow through the system. They are placed on top of a crushed stone reservoir that can temporarily store the treated stormwater, and allow for an extended time for recharge to groundwater if appropriate. In some cases, rather than allowing the filter media to control flow through the system, the hydraulic control is in the piping after the filter media. This hydraulic control is via an orifice or other hydraulically restrictive element that requires water to back up before a significant flow rate leaving the system can occur. The configuration of the GW system is different than most filtration systems in that the primary flow path is through a saturated coarse gravel layer, and the overlying lower conductivity soil's role is to support vegetation rather than filter pollutants or hydraulically control the system. The overlying soil layer along with the outlet flow control is used to create an anaerobic zone in the GW which is prolific for microbial processes in the underlying stone reservoir. The GW coarse gravel reservoir is maintained saturated in between precipitation events, in comparison to the unsaturated filter media condition in between runoff events for the other three LID systems. In comparison to the SF, BS, and GW systems, PP systems do not provide

above-ground system storage. A typical PP system is represented by a layer of pervious asphalt, concrete, geogrid, or interlocking blocks on top of a layered sub-base. The sub-base structure provides both structural and hydrological functions, and the configuration varies depending on the loading capacity needs and site conditions. A typical configuration for the sublayers is: a layer of crushed stone, then a layer of bank-run gravel serving as the filter media, and another layer of crushed stone which acts as a reservoir for the treated water. Underdrains may be placed in the stone layer at the base of the system if drainage control is needed.

The soils used as filter media or hydraulic controls in LID systems vary in texture from just one soil textural class (a uniform sand in the case of the SF) to media that incorporates a wide range of textures (loam, sand, gravel, wood chips, and compost in the BS) (Claytor and Schueler, 1996; UNHSC 2009). Typically, if the system needs to sustain vegetation, organic soils are added to the mix. For non-vegetated systems (for example PP, SF), mineral soils such as bank-run gravel that need little engineering are used. Technical specifications for some filter media compositions are not very well established and recommendations vary within different stormwater governmental jurisdictions (Carpenter et al, 2010). Standardized soil mix specifications are developed in order to obtain more consistent infiltration rates for filtration systems and to ensure appropriate drain down times of the system in between precipitation events (UNHSC, 2012). In addition, research progress has been made in customizing soil mixes to target specific pollutants, such as metals and phosphorus (Stone, 2013). This creates the potential for an even higher variability in the textures of soils for stormwater LID systems.

In engineering practice, the configuration design and hydrologic assessment of SWM systems is performed with the aid of computer simulation tools (ie SWMM, WINSLAM, HydroCAD, StormCAD, etc). These software packages were initially developed for conventional stormwater systems that were relatively simple to represent mathematically, and they do not have the capabilities of simulating more complex flow routing through the permeable layers of LID systems (Elliot and Trowsdale, 2006). The simplified methodologies for modeling flow through these layers either assume that the flow occurs under saturated conditions, or treat the entire system as a storage unit where the available storage is the pore space in the soil matrix (Dussailant, 2003; Jayasuriya, 2008; Aad, 2010). Recent data collection at two PP sites revealed that saturation in the filter media is not achieved under natural precipitation events (Barbu and Ballestero, 2013a). A similar study performed on the filter media of bioretention systems (Carpenter, 2010), suggests that saturation does not always occur in the filter media of BS either, although these systems are designed to function under ponded conditions during large runoff events. This implies that the use of saturated flow equations like Darcy's Law or Green-Ampt are not always appropriate for modeling flow through the permeable layers of LID systems. Unsaturated flow equations (for example, Richards' Equation) would lead to more accurate hydrological design of LID-SWM systems.

III.1.1 Unsaturated flow functions

The most common equation used to describe saturated flow in pervious media is Darcy's Law (Darcy, 1856). Solving this equation requires knowledge of the saturated hydraulic conductivity (K_{sat}), and the hydraulic head:

$$q = -K_{Sat} \left(\frac{dh}{dz} \right)$$

Equation 5

Where:

q = Darcian flow (L/T); K_{sat} = saturated hydraulic conductivity (L/T); dh = change in energy that drives the flow (L) across dz = the length of pervious media layer (L), z being the vertical direction.

Richards' Equation (Richards, 1931) is a non-linear partial differential equation that describes unsaturated flow conditions, and was derived by applying continuity to Darcy's Law. The moisture - based form of Richards' Equation is as follows:

$$\frac{\partial \theta}{\partial t} = \frac{\partial \left[D(\theta) \frac{\partial \theta}{\partial z} + K_r(\theta) \right]}{\partial z}$$

Equation 6

Where:

$\partial \theta$ = the change in volumetric moisture content (-); ∂t = the time interval for analysis (T);
 ∂z = the space interval/depth of layer (L); $\partial \psi$ = the change in matric potential (L^{-1}); $K_r(\theta)$
= hydraulic conductivity(L/T); and $D(\theta)$ = water diffusivity(L^2/T);

Solving Equation 6 is more computing intensive and requires more input information than saturated flow equations. This requires information on unsaturated hydraulic conductivity (K_r), matric potential (ψ), diffusivity (D), and volumetric moisture content (θ). D , K_r and ψ are dependent on θ and therefore change with the change in moisture content. In order to solve Richard's Equation, the moisture retention curves

(MRC), also known as the $\theta(\psi)$ function, and the unsaturated hydraulic conductivity functions $K_r(\psi)$ need to be first defined. These relationships are unique for each soil; however, for a given soil they are highly nonlinear, non-unique, and difficult to accurately represent with a single function for the entire range of values. They can be generalized either through a continuous function or in tabular form.

III.1.2 The moisture retention curves: $\theta(\psi)$

The measurement of the $\theta(\psi)$ function can be expensive and time consuming (Dane and Topp, 2002). Measurements could require 12-16 weeks and even longer for finer particle soils such as clays. The alternative is to predict the $\theta(\psi)$ with mathematical functions. This makes $\theta(\psi)$ a function of other variables which are easier to measure, such as soil texture, porosity, or density. These functions are known as Pedotransfer Functions.

Common approaches for mathematically obtaining the $\theta(\psi)$ curves include: regression models from statistical regression analysis (Gupta and Larson, 1981; Rawls and Brakensiek, 1982; Vereken et al., 1992; Fredlund et al., 2002), functional regression methods (Brooks and Corey, 1964; Vereken, 1989; Van-Genuchten, 1982); and physicoempirical models (Arya-Paris, 1981; Haverkamp-Paralange, 1986).

Regression models relate the matric potential to the soil textural class, organic carbon content, porosity, and bulk density through regression analysis of measured data for multiple soils. These models do not consider the shape of the retention curves, therefore some functions derive J-shaped or S-shaped curves. The functional regression models also employ regression analysis, but they first make an assumption of the curve's shape, and then adjust it with fitting parameters. In order to use these models, the

measurement or approximation of parameters like K_{sat} and the air entry matric potential (ψ_b) are needed. One disadvantage of these two types of models is that they were developed with statistical regression analysis taking into account several soil samples, and therefore cannot be fine-tuned or easily manipulated for engineered filter media. The fitting parameters in these models were developed for the major soil textural classes (clay, loam, silt, and sand) and not for coarse engineered soils like those used in LID-SWM systems.

The physicoempirical models (Arya-Paris, 1981; Haverkamp-Parlange, 1986) are based on the observation that the cumulative particle size distributions (PSD) and the $\theta(\psi)$ curves are very similar in shape. This implies that the pores-size distribution of the soil matrix, and therefore its water retention capacity, can be computed from PSD data and the degree of soil compaction. This hypothesis of shape similarity was confirmed later in 1998 by analyzing 660 soils from the GRIZZLY database (Haverkamp et al., 1998). While physicoempirical models rely on some parameter estimation to transition from an ideal pore to the natural pore characteristics corresponding to soil fractions, it is the most physically-based model developed for derivation of the $\theta(\psi)$ relationship, and allows for a more detailed representation of the soils' texture. Though both Arya-Paris and Haverkamp-Parlange have minimal input data requirements, Arya-Paris is especially preferred in practice as it is valid for more soil types, while the later model is valid only for pure sands with no organic matter (Dane and Topp, 2002).

III.1.3 The unsaturated hydraulic conductivity curves: $K_r(\theta)$

Unlike the $\theta(\psi)$ curve, the $K_r(\theta)$ or $K_r(\psi)$ curves are very difficult to measure, and even when performed, may have large errors (Dane and Topp, 2002). In practice, the K_r

curves are commonly derived with a selection of methods when the $\theta(\psi)$ curve is known: Baver et al, 1972; Childs and Collis-George, 1950; Burdine, 1953, Gardner, 1958; Marshall and Holmes, 1979; Brooks and Corey, 1966; Mualem, 1976, or Van Genuchten, 1980. Most of these mathematical models predict K_r based on the capillary tube theory which states that the pores are filled progressively from the smallest to the largest ones up to the point of saturation, and that the larger pores empty first. Mualem's model (Mualem, 1976) (Equation 7-8) is the most widely used model to predict the $K_r(\psi)$ function. The input data required for this model consists of the value of K_{sat} and the $\theta(\psi)$ function for a specific soil. If the $K_r(\psi)$ and $\theta(\psi)$ functions are known, $K_r(\theta)$ can be easily obtained.

$$K_r(\theta) = Se^n \left[\frac{\int_0^\theta \frac{d\theta}{\psi}}{\int_0^{\theta_{sat}} \frac{d\theta}{\psi}} \right]^2$$

Equation 7

$$Se = \frac{\theta - \theta_r}{\theta_s - \theta_r} \quad 0 \leq Se \leq 1$$

Equation 8

Where: θ_r = residual water content (L^3L^{-3}); θ_{sat} = water content at saturation (L^3L^{-3}); θ = actual water content (L^3L^{-3}); and Se = effective saturation (-).

The need for more detailed representation of the soil infiltration processes in LID systems is well recognized (Braga et al. 2007; Dussailant et al. 2004), but the intensive data input required for solving unsaturated functions is a hurdle for stormwater engineers

in using Richard's Equation. For this reason, saturated models are still preferred in practice for modeling LID systems. We believe that the development of predictive methods for MRCs and K_r functions, which require input data that is more accessible to designing engineers, would increase the likelihood that unsaturated flow modeling capabilities would be incorporated into SWM simulation software used for designing LID systems. In doing so, the design of these systems is more accurate. The development of a specifically adapted framework for obtaining the MRCs for soils used for flow control in LID-SWM systems from soil properties is further explored.

III.1.4 Applicability of traditional MRC models to SWM filter media

The challenge of obtaining the MRCs for SWM filter media with the previously cited models derives from the fact that filter media consists of disturbed and repacked engineered soils that contain appreciable amounts of particles larger than 2 millimeters and/or wood chips, while the traditional models were developed for agricultural and forest soils, based on undisturbed samples at field compaction. All reviewed models are valid for soils containing particles up to 2 millimeters. Because the ties of the methods to agricultural soil analyses, the prediction range of these models focuses on the dryer end of the MRC, as field capacity and wilting points were important concepts for crop management. In filter media design for stormwater treatment, fine particle content is limited in order to maintain appropriate drain-down of the system in between precipitation events and to minimize frost impacts in the cold seasons (Roseen et al, 2012). Therefore, the range of interest in employing these MRC and K_r models shifts to the wetter range of the MRC when evaluating LID-SWM filter media. This is where the coarser soil particles play an important role in the development of MRC's.

While gravel particles absorb a negligible amount of water and act as a dead volume in terms of water conductivity (Bouwer, 1984; Kahaleel and Relyea, 1997), dry wood chips can absorb considerable amounts of water at the beginning of the storm and retain it until the water around them is drained. Therefore, wood chips behave in a similar way to gravel when wet, as they contribute very little to water transport while there is still moisture in the soil around them, but behave as a sponge when dry. These factors are important when evaluating the MRCs for engineered filter media.

The most suitable models for LID-SWM filter media as they relate to fluid movement through the systems seem to be the physicoempirical models as they use for input the PSD, density, and porosity of a soil to derive the $\theta(\psi)$ relationships. These are the most common parameters that are reported when describing engineered soils and the most accessible data to practicing engineers. In addition, physicoempirical models generate data points for the entire range of moisture contents as opposed to other models that do not cover the wetter range. With the wide range of textural classes used in filter media for stormwater treatment (Figure 11), it would be useful for engineers to be able to derive the MRC's from easily measurable data for their specific soils instead of analyzing each soil mix in the laboratory.

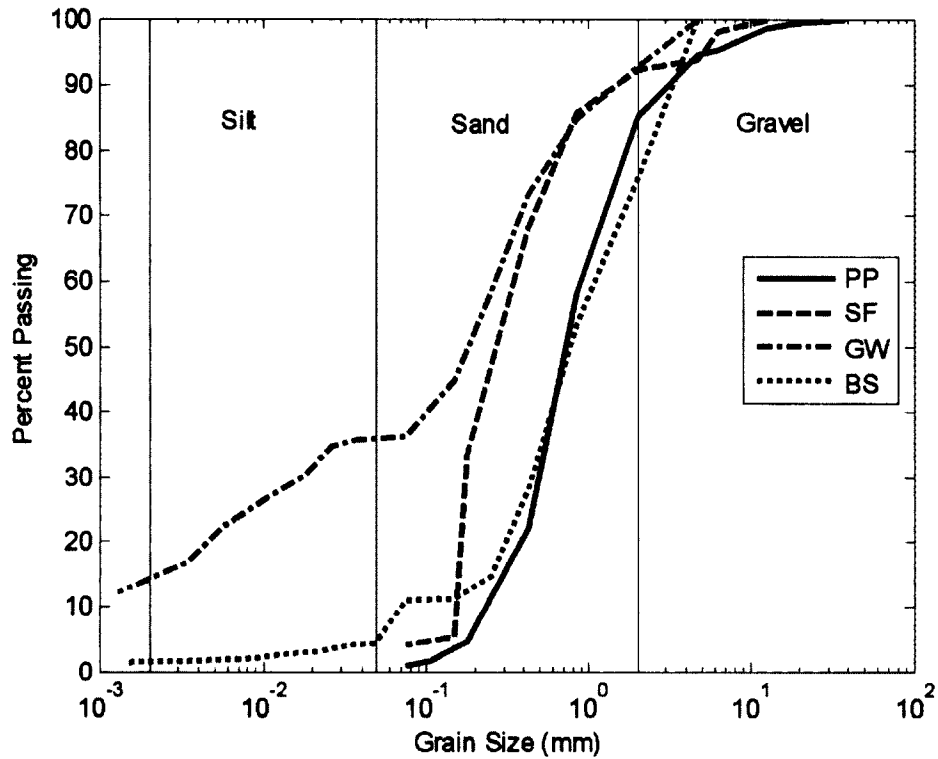


Figure 11 – Particle size distributions for the filter media in the PP, SF, GW and BS systems.

The effectiveness of using a series of available equations to derive the MRCs for typical LID-SWM filter media was tested: the Arya-Paris (A-P) model (Arya and Paris, 1981; Arya et al. 1999) was used to generate $\theta - \psi$ data points for the fine fraction of filter media soils; adjustments for large particles were made with the Bouwer Equation (Bouwer and Rice, 1984); spline interpolation (Arya et al. 1999) and Van-Genuchten (VG) Equation (Van Genuchten, 1980) were used to obtain the continuous $\theta(\psi)$ curve; and the $K_r(\theta)$ curve was generated with Mualem's Equation (Mualem, 1976). The performance of this sequence of equations to predict the MRCs for the original/bulk soil

was tested against laboratory measurements for four engineered soils used in actual SWM systems: PP, GW, BS and SF.

III.2 Materials and Methods

III.2.1 Particle size distributions

Soil samples used for the filter media in the four LID systems were gathered from the stockpiles used to build the actual systems and the PSD were developed conforming to ASTM D422-63, using standard engineering sieve sizes: # 4, 10, 20, 40, 60, 100 and 200 (Figure 11). Since the GW and BS samples contained a significant amount of fine particles, hydrometer tests were performed for the fraction that passed the # 200 sieve for these samples. The GW soil displayed significant aggregation, which made the PSD look more like a sandy-gravel after dry-sieve analysis. A wet-sieving analysis was performed for this soil in order to break down all the clusters of aggregated clay. Since the BS sample contained finer particle soils, wood chips, and organic matter, a sequence of dry-sieving, wet-sieving, and wood chips combustion were performed on this sample. PSDs were recorded after each step of the analysis on the BS mix as presented in Figure 19. The PSD obtained after combustion of the wood chips was used with the A-P model for this soil.

III.2.2 Arya – Paris Model

The final PSDs for the four soils (Figure 11) were used with the A-P model to develop a series of $\theta - \psi$ data points, following the detailed procedure presented in the Methods of Soil Analyses (Dane and Topp, 2002). The A-P model starts with the PSD

curve which is divided into soil fractions. A cubic closed-pack structure was assumed for uniform size particles, with a radius (R_i) equal to the average particle size for that fraction. Knowing the density of the particles (ρ_s), bulk density (ρ_b) and the void ratio (e), the number of soil particles (n_i) and the pore radius (r_i) was computed for each fraction. The pore space for each fraction was then successively summed to yield the total pore space in an ideal soil matrix with spherical particles. The total pore space represents the maximum moisture content that the soil can hold if the pore space is filled with water. To account for the non-uniform particle shapes and randomness of packing in a natural soil matrix, a scaling parameter (α) is computed for each soil fraction and applied to the pore radii.

The scaling parameter α was computed with the similarity method (Arya et al., 1999), using the sand values for a and b for the PP and SF samples, and loam values for GW and BS samples (Table 8). These values were selected based on the predominant soil fraction of each filter media soil:

$$\alpha_i = \log N_i / \log n_i$$

Equation 9

$$\log N_i = a + b \log(W_i / R_i^3)$$

Equation 10

Where: α_i = scaling parameter (-); R_i = average particle radius for soil fraction i , computed as the average radius of the upper and lower limits of the soil fraction i (L); N_i = the equivalent number of particles of radius R_i needed to trace the actual pore length (-);

n_i = the number of spherical particles in the fraction i (-); W_i = the fraction of solid mass (-); a, b = parameters for relating $\log(N_i)$ to $\log(W_i/R_i^3)$ (-);

Once corrected, the pore radii were converted to the matric potential corresponding to each fraction with the capillary equation:

$$h_i = \frac{2 \gamma (\cos\theta)}{\rho_w g r_i}$$

Equation 11

Where: h_i = capillary pressure head corresponding to fraction i (L); γ = air - water surface tension (MT^{-2}); θ = contact angle (degrees); ρ_w = the density of water (ML^{-3}); g = acceleration due to gravity (LT^{-2}); and r_i = pore radius for fraction i (L).

Since the pore space is equivalent to the moisture content that each soil fraction can hold, each pressure head – pore volume data point generated with the A-P model for each soil fraction used in the PSD curve represent one pair of $\theta - \psi$ values. The final number of data points corresponds to the number of soil fractions that were used to divide the initial PSD used in A-P model. Initially, the soil fractions used with A-P model were those corresponding to the standard engineering sieves that are commonly used in engineering practice. Additional runs were performed with the soil fraction intervals recommended by A-P.

In addition to the PSD, the A-P model requires knowledge of bulk density and the porosity of the soil. The bulk density was measured in the laboratory according to ASTM D7263 and porosity was computed with Vukovic Equation (Vukovic and Soro, 1992).

$$Porosity = 0.255 (1 + 0.83^\eta)$$

Equation 12

Where: η = the coefficient of uniformity of the soil (-) = D_{60}/D_{10} .

III.2.3 Correction for coarse particles

Since A-P is valid only for particles up to 2mm, the model was applied to the fine fraction of the soils which was normalized to 100%. In practice, mass- or volume-based equations (Peck and Watson, 1979; Brankensiek, 1986; Bouwer, 1984; Saxton and Rawls, 2006) are used to correct for the space occupied in the soil matrix by the gravel particles which do not contribute to water transport. The Bouwer Equation (Bouwer, 1984) was successfully used in similar studies to correct for gravel content (Bagarello and Iovino, 2007; Gribb et al, 2009), and was used for gravel adjustment for this application:

$$\theta_{bulk} = \theta_{fine} (1 - V_{gravel})$$

Equation 13

Where: θ_{bulk} = moisture content for the bulk soil (-); θ_{fine} = moisture content for the fine fraction of the soil (-); and V_{gravel} = volume fraction of gravel (-).

One shortcoming of this approach is that it does not account for the macropore formation due to coarser particles (Saxton and Rawls, 2006), which correspond to the saturation end of the $\theta(\psi)$ curve. The Bouwer Equation, or any of the other commonly used equations for this matter, (Peck and Watson, 1979; Brankensiek, 1986; Bouwer, 1984; Saxton and Rawls, 2006), adjusts the moisture content corresponding to each matric potential computed with A-P by subtracting the volume occupied by gravel

particles from the total pore space, but it does not extend the curve at the saturation end (Figure 12).

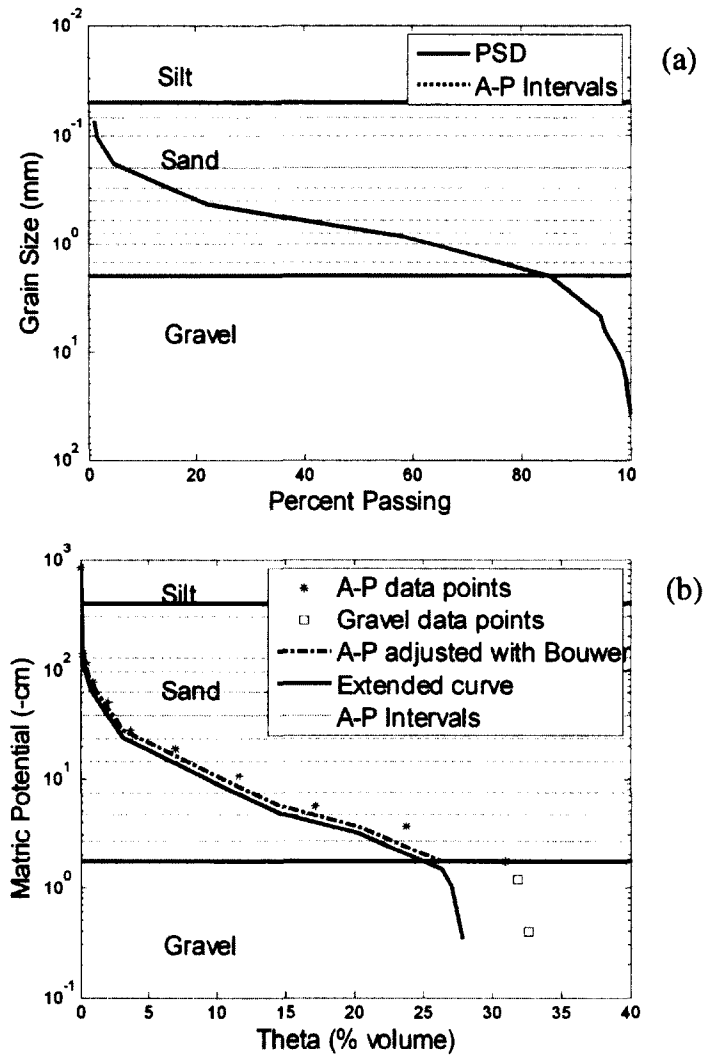


Figure 12 – Similarity principle: transition from a particle size distribution (a) to a moisture retention curve (b), adjustments for gravel content with Bouwer Equation (b), and extension of the MRC beyond Arya-Paris applicability range (b).

III.2.4 Curve fitting

The A-P model only generates paired data points of the moisture content and their corresponding matric potential. In order to obtain a continuous $\theta(\psi)$ curve, the A-P generated data points were connected with spline interpolation as in the original A-P model (Arya and Paris, 1981). A second approach for obtaining the complete $\theta - \psi$ curve was to fit the Van-Genuchten (VG) Equation (Van Genuchten, 1980) to the A-P generated data points. The VG Equation curve fitting was performed with the RETC program (Van Genuchten et al, 1991), which is public domain software.

$$\theta(\varphi) = \theta_r + \frac{\theta_s - \theta_r}{[1 + (\alpha * \varphi^n)]^{1-1/n}}$$

Equation 14

Where: $\theta(\psi)$ = moisture retention curve [L^3L^{-3}]; ψ = matric potential [L^{-1}]; θ_r = residual water content (L^3L^{-3}); θ_s = saturated water content (L^3L^{-3}); α = scaling parameter for the matric potential (L^{-1}); n = parameter that describes the pore size distribution (-).

The $\theta - \psi$ curves obtained this way were used in conjunction with Equation 7 to develop the second function needed to solve Richard's Equation: the $K_r(\theta)$ function.

III.2.5 Testing data

For testing purposes, the $\theta - \psi$ data points were measured in the laboratory on the initial wetting curves for each of the four filter media soils. A total of twelve data points were measured over the entire range of the $\theta(\psi)$ curves, with the following apparatus: hanging column (ASTM D2434), pressure plate (ASTM D6836), dew point potentiometer (ASTM D 6836), and relative humidity box (Karathensis and Hajeck, 1982).

Saturated hydraulic conductivity (K_{sat}) was measured with the constant head-rigid wall method (ASTM D2434). The continuous $\theta(\psi)$ curve was fitted with Van Genuchten and the $K_r(\theta)$ curve was derived with Mualem's Equation using the RETC code. Porosity at field compaction was also measured in the lab (ASTM D7263) and compared with the values computed with Vukovic Equation.

III.3 Results and Discussions

Engineered filter media tend to have more irregular PSD shapes than natural soils, as some soil fractions are left out for structural reasons. The percent of fines in SF and PP filter media for example is limited to 6% (UNHSC, 2009b) in order to avoid clogging of the media and allow for a quick drain down of the system. The BS mixes typically contain the most varied texture of soil and wood chips (which can be either shredded or chipped), but they do miss some intermediate particle sizes and this causes the PSD to have an irregular shape. Since the A-P model is based on the similarity principle, which states that the shape of the MRC is similar with that of the PSD curve, the irregularities in the PSD curves were carried over in the MRCs shape as well. In the original model (Arya and Paris, 1981), Arya obtained a continuous $\theta(\psi)$ curve by connecting the generated $\theta-\psi$ data points with spline interpolation. When interpolation was applied for the four filter media types, the irregular shape was more prominent in the BS, SF and GW soils and especially at the finer end of the PSD where certain soil fractions were missing (Figure 13 - 16). The PSD for the PP sample was a very smooth curve and the interpolation of the A-P generated data points for this sample resulted in a smooth curve as well (Figure 13).

In reality, the matric potential decreases as the moisture content increases so the $\theta(\psi)$ relationship should be described by a smooth curve. However, for the BS, SF, and GW samples, the interpolated curve displayed irregularities in the sections where corresponding soil fractions were missing from the PSD. These irregularities in the $\theta(\psi)$ shape would lead to computational errors when used to solve Richard's Equation. In practice, when $\theta - \psi$ data points are measured in the laboratory, the continuous $\theta(\psi)$ function is obtained by fitting the VG Equation to the measured data. Therefore, a second curve was fitted to the A-P generated data points using this method, with the fitting parameters presented in Table 7.

Table 7 – Van Genuchten fitting parameters

θ_r (%)	θ_{sat} (%)	VG – α (-)	n (-)	l (-)	Ksat (cm/min)
4.5	29.70	0.145	2.68	0.5	4.14
4.5	34.56	0.145	2.68	0.5	0.78
4.5	44.00	2.146	1.34	0.5	1.56
4.5	39.15	0.950	1.22	0.5	0.05

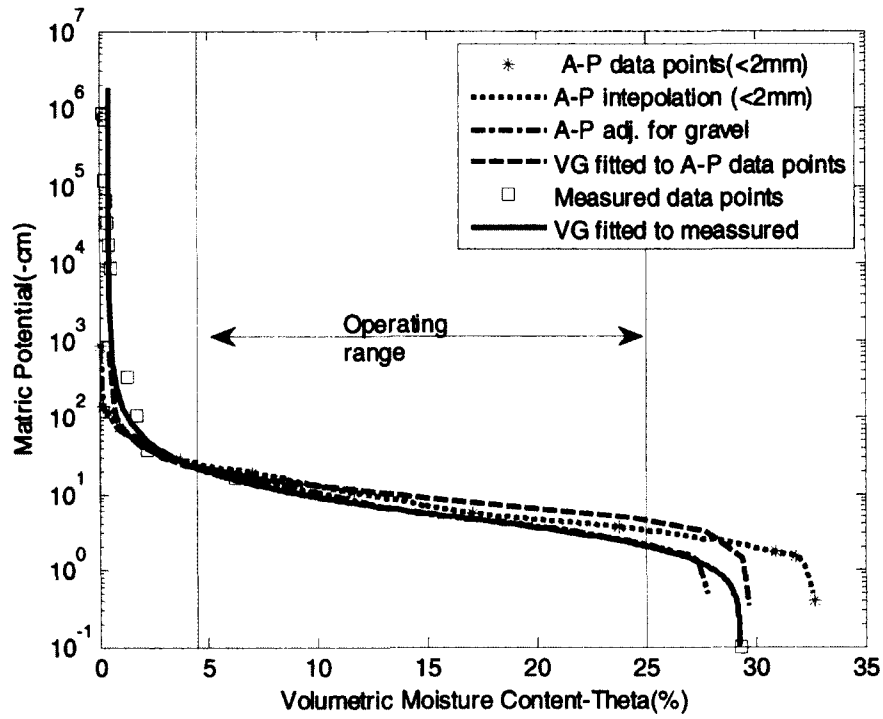


Figure 13 – The volumetric moisture content with respect to the matric potential for the PP filter media.

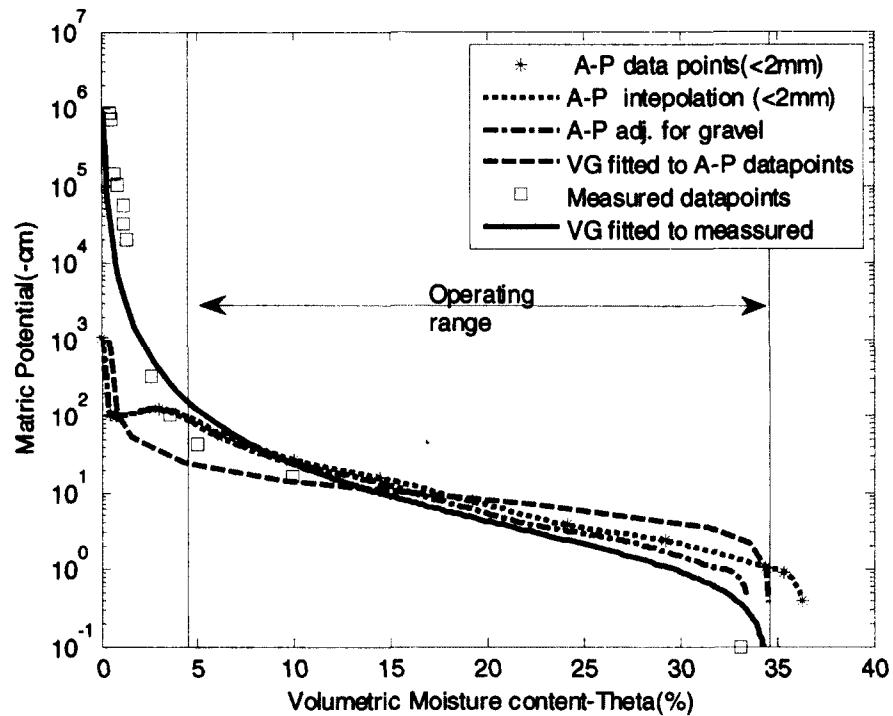


Figure 14 – The volumetric moisture content with respect to the matric potential for the SF filter media.

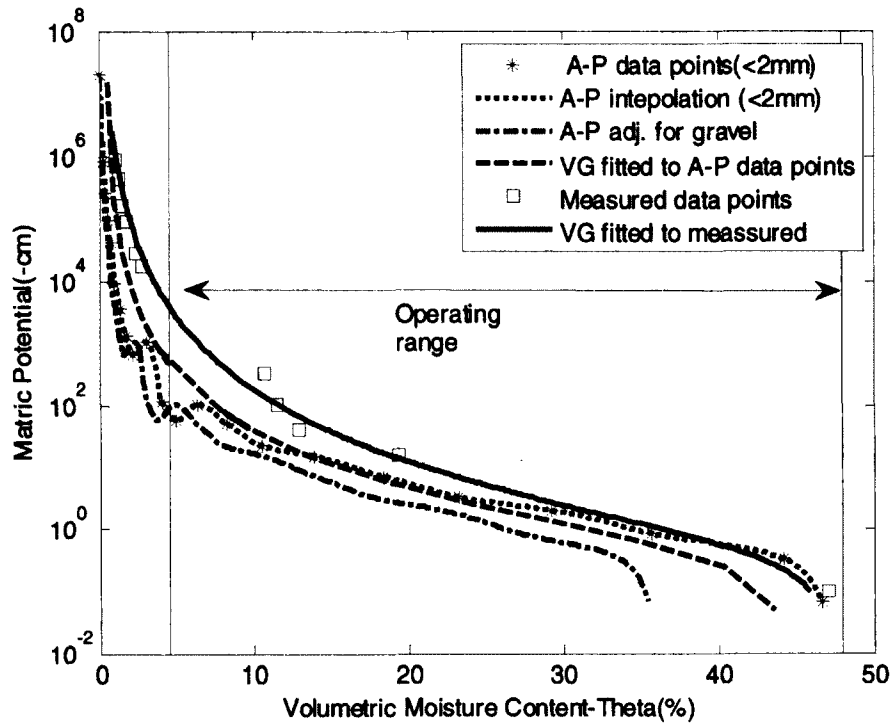


Figure 15 – The volumetric moisture content with respect to the matric potential for the GW filter media.

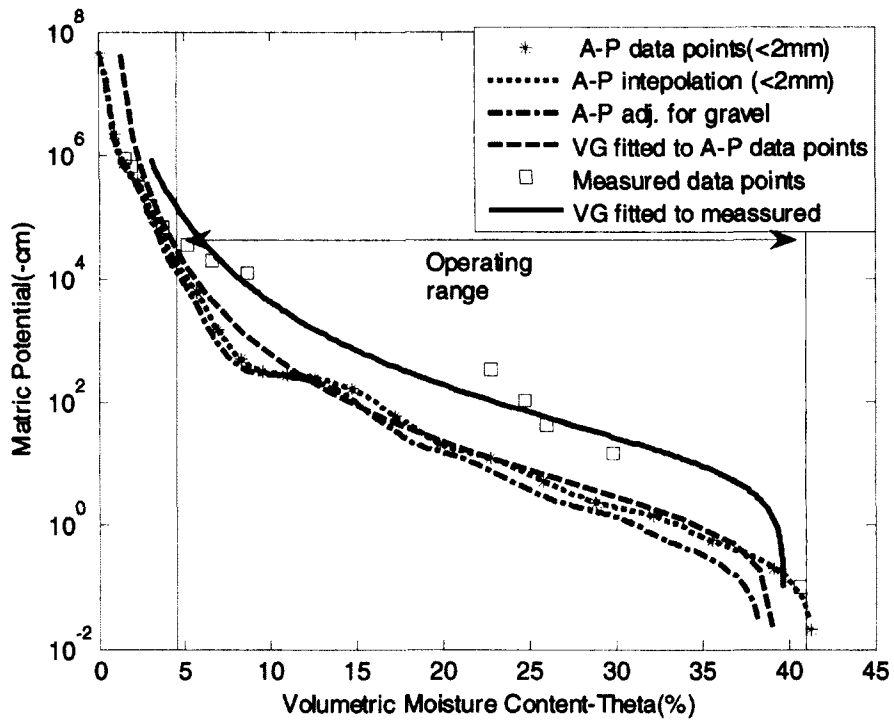


Figure 16 – The volumetric moisture content with respect to the matric potential for the BS filter media.

The comparison of the measured and A-P generated data points along with the spline interpolation and VG fitted curves for the four filter media types are presented in Figure 13 - 16. Accurate measurements in the wetter range of the $\theta(\psi)$ curve are difficult to obtain in the laboratory due to quick loss of water from the soil samples when the moisture is close to saturation. The measured data points are clustered mostly on the drier range of the curve, while the computed data points are more evenly distributed along the curve. For this reason, the comparison of the fitted curves is more relevant than comparison of the actual $\theta - \psi$ data points. The interpolated and VG fitted curves to the modeled $\theta - \psi$ data points were compared through statistical analyses to the VG curve fitted to the observed data for the operation range of each system (Table 8). While both interpolated and VG fitted curves had high coefficients of determination for most samples, the VG fitted curves are recommended when the PSD and its corresponding A-P generated $\theta(\psi)$ curves displays irregularities; this could potentially lead to computational problems when used with unsaturated flow equations.

Table 8 – The goodness of fit of the interpolated and Van Genuchten curves to the measured data: the coefficient of determination (r^2) and root mean square error (RMSE).

System	r^2 – Interpolated	r^2 – VG	RMSE- interpolated (cm)	RMSE- VG (cm)
PA	0.982	0.981	0.053	0.136
SF	0.959	0.761	0.348	0.804
GW	0.995	0.995	149.79	131.01
BS	0.583	0.982	17.53	15.41

Real time volumetric moisture content data collected for over one year in a PP system installed at the University of New Hampshire revealed that θ recorded at three different vertical locations within a 30 cm (12”) filter media layer ranged between 4.3%

and 20.2%. Since the filter media had a porosity of 34.4% and θ_{sat} of 29.3%, this implies that the filter media never achieved saturation under normal and even extreme precipitation which occurred over the monitoring period. Typical real time variation of the moisture content observed in the filter media of this system is presented in Figure 17.

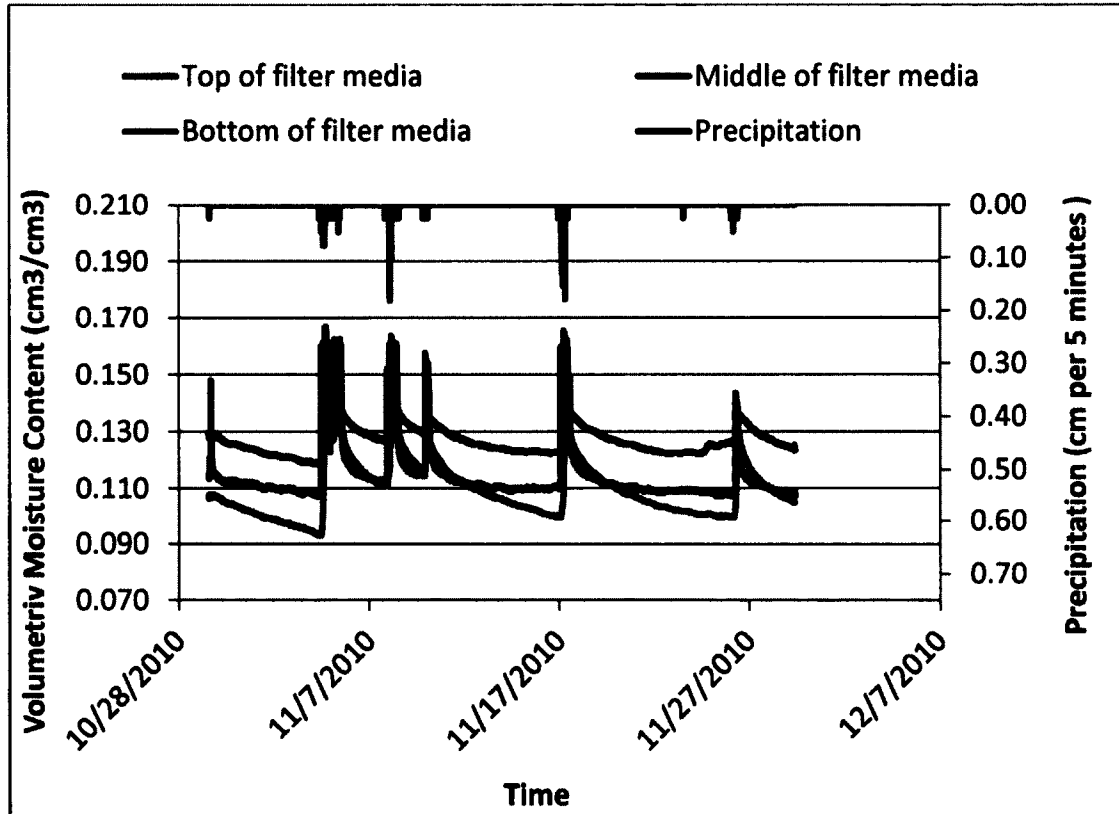


Figure 17 – The fluctuation of the volumetric moisture content (θ) measured at three levels within the filter media of a pervious pavement system under natural precipitation

The accuracy of the proposed sequence of equations for generating the $\theta(\psi)$ curve for the PP filter media was evaluated over a conservative moisture content operating range of 4.5% to 25%. This was based on observations of soil moisture profiles in the filter media of a PP system for over one year (Barbu and Ballesterro, 2013a). The other three systems (GW, SF, BS) are designed to function under ponded conditions during

larger design storms, and are likely to reach saturation several times a year, at least at the media surface where water is ponded. The operating range for which these three systems were evaluated was from residual moisture content (θ_r) to saturation moisture content (θ_{sat}). Similarly to the PP sample, the values for θ_r were selected at 4.5% for all three filter media, and θ_{sat} was based on laboratory measurements: 34% for the SF, 41% for the GW and 48% for the BS. The measured and model derived $\theta - \psi$ data points, along with the fitted curves for the four filter media soils are presented in Figure 13 - 16.

Based on the coefficient of determination (r^2) and root mean square error values (RMSE) presented in Table 8, the sequence of equations proposed in this study performed especially well for the mineral soils used as filter media in the PP and SF (Figures 13 - 14), but they underestimated the matric potentials for the GW and BS filter media that contained finer particles (Figure 15 - 16), especially at the low moisture content end of the curve. The RMSE were improved for these two soils if the fit was analyzed starting at a higher moisture content than 4.5%. Given that the finer particle soils are more hysteretic than coarser soils (Gallage and Uchimura, 2010), and that the laboratory measurements were taken on the wetting curve which has higher matric potential than the drying curve at the same moisture contents, the predicted curves are within the generally acceptable range of prediction. It is also important to consider that the test data for the statistical analyses is assumed to be error free, which is not necessarily true. The “observed” curves used to test for the accuracy of “predicted” curves were actually an estimated fit of VG Equation to measured $\theta - \psi$ data points.

III.3.1 The K_r function

The $K_r(\theta)$ curves developed with Mualem's model applied to the VG curve fitted to the measured and computed $\theta - \psi$ data points for the PP filter media were compared in Figure 18. Given that both data point series were fitted with VG, the shape of the two curves is very similar and that might be the reason for very good r^2 and RMSE values of 1.00, and 0.003 respectively, when evaluated for the operating range of moisture contents from 4.5 to 25%.

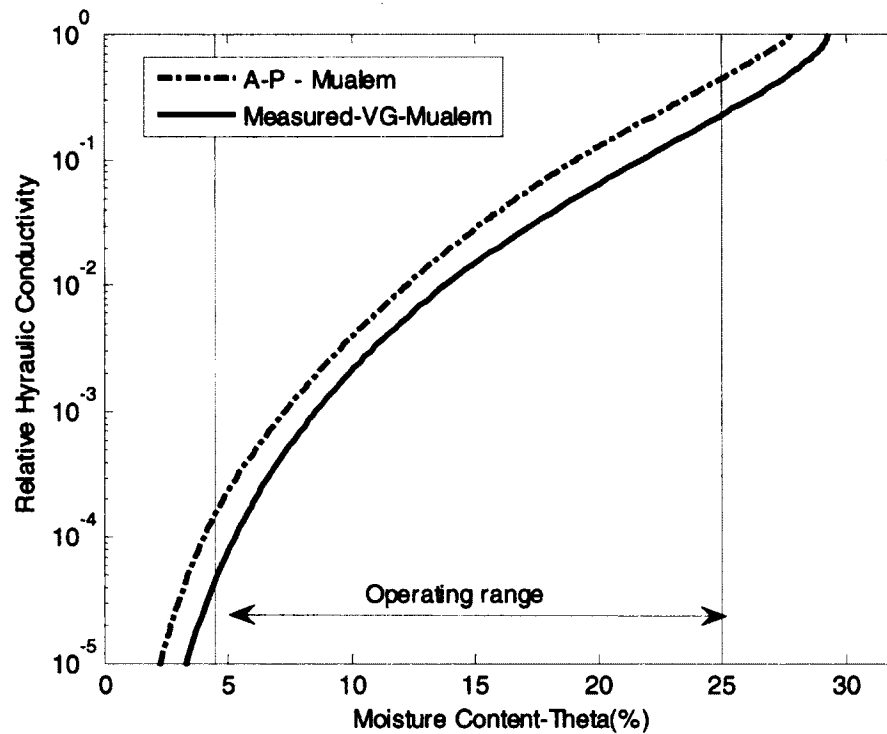


Figure 18 – Unsaturated hydraulic conductivity developed with Mualem's Equation as applied to the measured and computed volumetric moisture content – matric potential curves.

III.3.2 Gravel content compensation

Whether measured in the laboratory or developed with mathematical models, the $\theta - \psi$ data is customarily evaluated for the fine fraction of the soils, rather than bulk samples. There is some disagreement in the literature on whether the gravel adjustment of the measured data is necessary or not when developing the unsaturated functions for soils containing coarse particles (Khaleel and Relyea, 1997; Sauer and Logsdon, 2002). Other studies (Milczarek et al, 2006) found that the coarse particles can affect the hydrological properties of soils differently, depending on the ratio of the coarse particles to fine particles. Milczarek et al.(2006) found that there is a threshold of approximately 30% gravel content above which the gravel particles contributes to macropore formation and therefore increases the fluid transmission capacity of the soil matrix, while below this threshold, the finer particles become predominant in the soil matrix and fill the spaces between the gravel particles. In this case coarse particles act as a dead volume that increases the pore tortuosity and impede water transmission.

For the four filter media types, the gravel content ranged from 7.2 to 24% (Table 10), all below the 30% threshold. In this study, the $\theta(\psi)$ curves adjusted for gravel were in better agreement with the measured curves than the unadjusted curves. However, compensation only with the Bouwer Equation did not adequately represent the air entry section of the curve. This section of the curve is generally described by a steep increase in the matric potential with a small decrease in moisture content, as the air enters the larger pores when the soil begins to desaturate. This concept was not evident when adjustments were made only with the Bouwer Equation (Figure 12). Bouwer's assumption was that gravel particles do not contribute to fluid transport. He suggested

adjustment of the moisture content corresponding to each matric potential by subtracting the volume occupied by gravel particles from the total pore space. This approach only shifts the curve to the left (Figure 12), but does not extend it to the saturation end where the gravel particles are contributing to the macropore formation. With this approach, the largest alteration of the curve takes place at the saturation end, and decreases proportionally with the pore space towards the drier end of the curve. For this reason, correction for gravel content becomes especially important at the saturation end. In order to account for the macropore formation, the A-P generated $\theta - \psi$ data points were extended to the saturation end by adding data points corresponding to the soil fraction greater than 2mm which were outside the prediction range of the A-P model and were initially excluded from the PSD. To follow the same principle as in the A-P model, where each soil fraction generates a pair of $\theta - \psi$ points, two more data points were added initially for the fine gravel and coarse gravel soil fractions. Similarly as in the A-P model, the matric potential was represented by the capillary rise for each soil fraction, and the corresponding moisture contents were the volume of the pore space of that fraction. The capillary rise in fine and coarse gravel is typically in the range of 2 to 10 cm, and 0.5 to 2 cm, respectively (Lane and Washburn, 1946). The pore space occupied at saturation is generally in the range of 0.9 to 0.95% of the total porosity (Van Genuchten et al, 1991). Based on this information, the extension data points were initially set at matric potentials of -3.5 and -1 cm, and moisture content of 0.925 and 0.95% of the soil porosity, respectively. In order to account for the natural pore space and intermixing of different particle sizes, these values were then calibrated for each filter media type (Table 9), with measured data (Table 10). For the PP and SF samples which are coarser and have fewer

finer, two data points were needed to represent the saturation end of the curve, while for the GW and BS samples which have a larger amount of fine particles, only one extension data point was needed to meet the A-P generated data points.

Table 9 – Extended $\theta - \psi$ data points for the fine and coarse gravel soil fractions

System	θ_1	ψ_1	θ_2	ψ_2
	0.925*Porosity (%)	(cm)	0.95*Porosity (%)	(cm)
PP	31.82	1.5	32.68	0.4
SF	35.33	1.5	36.29	0.4
BS	N/A	N/A	41.33	1.2
GW	N/A	N/A	46.65	1.2

Table 10 – Soil properties for the four types of filter media

System	Gravel Content (%)	Porosity Measured (%)	Porosity Computed (%)	θ_{sat} (%)	Ksat (cm/min)
PP	14.8	34.4	33.97	29.3	4.14
SF	7.6	38.4	38.23	33.1	0.78
BS	24	49.1	23.43	47.1	1.56
GW	7.2	43.5	N/A	40.7	0.05

The combination of Bouwer Equation with the extension of the curve to saturation were in close agreement to the measured curves for the PP, SF and GW samples (Figure 13 - 15), but seemed to overcompensate for the coarse particles in the BS filter media (Figure 16). One thing that differentiates the BS soil from the other three samples is that it contains wood chips. Initially, the wood chips were considered in the A-P model as solids, and only the bulk density of the soil was changed to reflect the light weight of the soil mix. Since the PSD curves are typically developed on a weight basis, the dry wood chips content (approximately 10% by volume) contributes very little to the total mass of

the sample and is almost invisible in the PSD (Figure 19) which serves as input for the A-P model. In addition, the A-P model is developed for the fine fraction only and the wood chips are in the coarse particle fraction of the soil. If the wood chips were to be wet while performing the PSD analysis, as they would be at field condition, then the weight of the coarse fraction would be higher. Therefore, wood chips could be considered to behave in a similar way to gravel particles, as they initially absorb water but do not contribute to the moisture flux during precipitation events while there is still moisture in the pore space. However, wet wood chips increase the overall moisture content of the soil, and cause the θ values to be higher than for the soil without wood chips for the same matric potentials. We suggest that the adjustment of the $\theta(\psi)$ curve for wood chips content may be performed in a similar way to the gravel adjustments, though corrections for wood chips would shift the curve in the opposite way from that of gravel corrections. Based on the assumption that wood chips would offset the gravel particle effect on the MRC, when the volume of gravel and wood chips present in the soil is approximately the same, the gravel adjustment would not be necessary. If the volumes are different, the adjustment would be done proportionally on volumetric bases. The overcompensation for the BS soil at the saturation end was approximately 12%, while the wood chips content was 10%. The concept for wood chips content adjustment on the $\theta(\psi)$ curve seems to hold true for the BS soil in this study, although further investigation and testing of this theory is warranted.

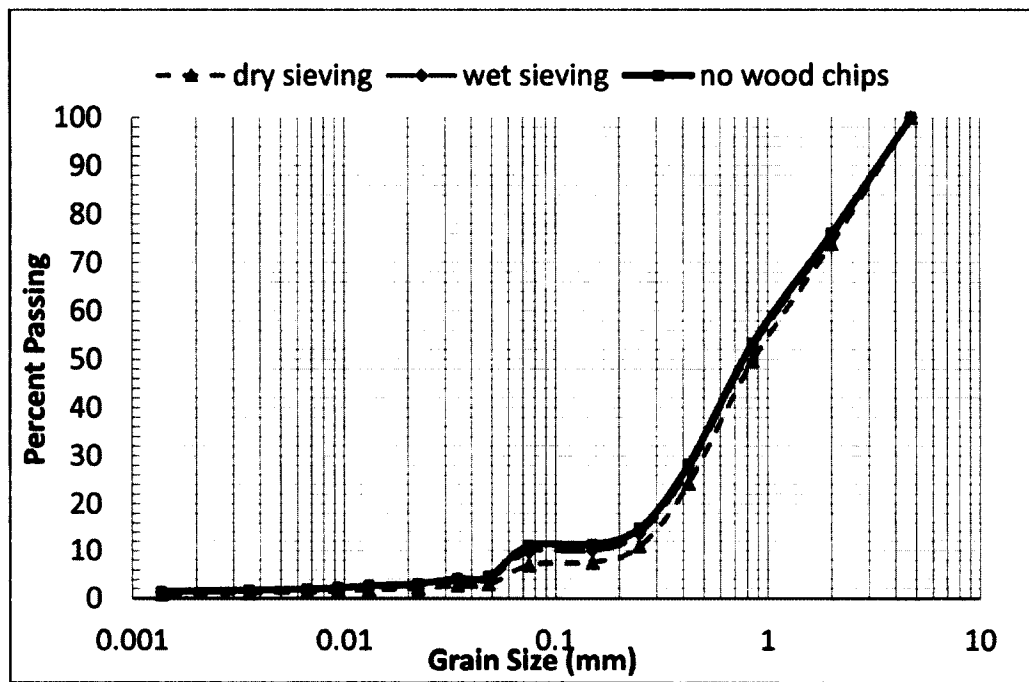


Figure 19 – The particle size distribution for the BS filter media, developed after dry- and wet-sieving, and combustion of wood chips.

III.3.3 A-P Model sensitivity with respect to number of intervals and a computation

The number of soil fractions for the PSD division recommended by Arya was set to twenty (Dane and Topp, 2002), but it is known that the A-P model is sensitive to the number of intervals used to subdivide the PSD. The θ (ψ) curve sensitivity to the number of intervals was analyzed in order to understand whether a different number of fractions would yield a better fit to measured data for coarser engineered soils. For this analysis, the number of intervals selected initially was that corresponding to the soil fractions obtained with standard engineering sieves. Then a series of analyses were performed with logarithmically, evenly distributed intervals of the PSD curve (Figure 20), varying from 8 to 40 intervals. Special attention was given to the range of values for the scaling parameter α . The typical range for α is between 0.95 and 2.5 (Arya et al., 1999), but

values even higher were reported for coarse soil fractions (Dane and Topp, 2002). We concluded that the best fit for the measured data for these soils was developed with twenty soil intervals, as recommended by Arya-Paris. A smaller number of intervals resulted in a narrow range of α values, clustered at the upper end of the normal range (1.343 to 1.399), while an increased number of intervals caused α to become very small and even negative (Table 11). When the original soil fractions were used for the four filter media soils, α was within the expected range of values (Table 12).

Table 11 – Arya-Paris model sensitivity analysis with respect to the number of intervals

Number of intervals	α range
8	1.343 – 1.379
13	1.287 – 1.373
20	1.115 – 1.364
26	0.887 – 1.362
30	0.254 – 1.361
40	-0.350 – 1.361

Table 12 – Arya-Paris model scaling parameters

System	A-P fitting parameters		
	a	b	α range
PP	-2.478	1.49	1.0194 - 1.3200
SF	-2.478	1.49	0.7290 - 1.3345
BS	-3.398	1.773	0.9615 - 1.6313
GW	-3.398	1.773	0.6301 - 1.6415

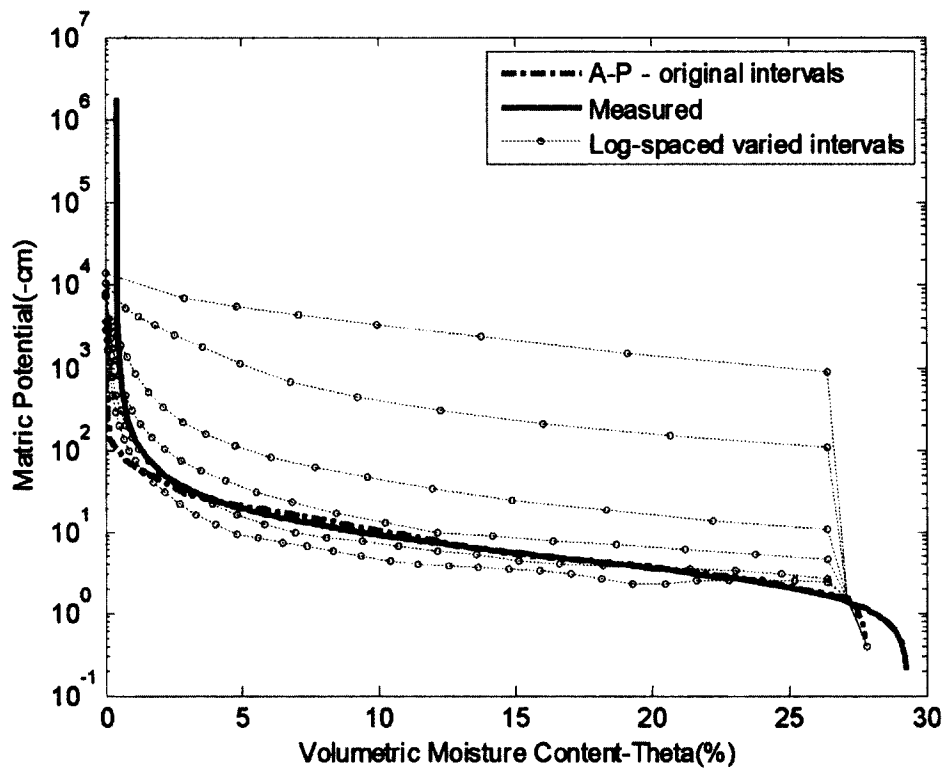


Figure 20 – The sensitivity analysis of the Arya-Paris model with respect to the number of intervals used for the particle size distribution data

III.3.4 Model limitations and error

The framework limitations derive from the limitations of the main equations proposed in this methodology. The A-P fitting parameters used to derive α for each of the four engineered soils were chosen to the closest of the five soils textural classes for which fitting parameters were developed by A-P (Arya et al, 1999). Specific fitting parameters for computing the value of α for SWM filter media soils might lead to a better fit. A second limitation is that the more non-uniform soil gradation of the engineered soil the more irregularly shaped the $\theta(\psi)$ curve when it is obtained by interpolation of the A-P model generated data points, and this could lead to computational errors when used with Richards' Equation. This shortcoming can be overcome by applying the VG fitting

function to the derived A-P data points instead of interpolation. Another weakness comes from the fact that the A-P model does not account for hysteresis and this could affect the accuracy of continuous long term simulations that includes multiple wetting and drying cycles of the filter media under natural precipitation events.

The correction for the coarse particles as presented here is assumed to be valid for soils with coarse particle content up to 30%, this being the threshold above which the coarse particles becomes predominant and enhance the soil's hydraulic properties. Future work should include a more refined methodology for adjusting the wood chips effects on the MRCs.

Possible model error could be introduced by the fact that the $\theta(\psi)$ curves were measured on the wetting curves only, and the $K_r(\theta)$ curve used for the testing of the proposed framework was computed with Mulaem's Equation using the $\theta(\psi)$ curves, rather than being measured. Given that coarse soils used as filter media in LID systems are less hysteretic, the error in estimating moisture transport through these soils is minimized.

III.4 Conclusion

This article presented a methodology for obtaining the hydraulic characteristics of engineered soils. These characteristics are used to aid in the modeling of unsaturated flow through engineered soils typical of stormwater management systems. The proposed model performed well for the four soil types studied and it is based primarily on physically-based equations that require data input easily accessible to stormwater system design practitioners. A summary of the methodology is as follows:

- Develop the PSD for the soil (filter) media
- Determine the mass percentage of the particles $> 2\text{mm}$, then normalize the PSD of the fine fraction ($< 2\text{mm}$) of the soil to 100%
- Interpolate the coordinates of the normalized PSD of the fine soil fraction with the twenty intervals recommended by A-P
- Apply the A-P model and compute the $\theta - \psi$ data points for each soil fraction
- Evaluate whether coarse particles/wood chips adjustments are needed
- Adjust the θ values corresponding to ψ for the effect of coarse particles with the Bouwer Equation: if wood chips are present, subtract the volume of wood chips from the volume of coarse particles, then convert volume to a mass and apply the Bouwer Equation (Equation 13).
- Extend the data set at saturation to account for the effects of fine and coarse gravel soil fractions in the macropore formation
- Develop the continuous $\theta(\psi)$ function by fitting VG (Equation 14), or spline interpolation if the PSD is smooth
- Obtain the $K_r(\theta)$ function with Mualem model (Equation 7-8).

This sequence of equations does not require extensive computational time and can be easily integrated in existing hydrological software used for SWM system design. When coupled with watershed models, this framework could be especially valuable in long term continuous simulation analyses and planning of LID-SWM strategies. Integrated in system scale models, this framework would allow for the prediction of

system performance, as well as optimization of the filter media composition in order to attain targeted discharge hydrographs.

CHAPTER IV

A physical model for stormwater flow simulation through a pervious pavement system: relating the design parameters to the outflow hydrographs

Abstract

Permeable Pavements (PP) are a valuable Low Impact Development (LID) technology that can serve both as stormwater management and transportation infrastructure. PP systems are typically designed for load capacity, hydrologic modification and frost depth criteria. However, the hydraulic design of the system is not specifically addressed in design criteria. Existing stormwater management modeling software possesses the capabilities to represent outflow hydrographs for PP systems, but cannot simulate stormwater routing through the permeable sublayers of the systems. Due to the lack of modeling tools to accurately predict the hydraulic behavior of these systems, engineers, regulators, planners, and industry have some challenges with the implementation and recognition of PP systems as functional stormwater management strategies. This article discusses the flow components of PP systems, presents equations for each segment of flow through the system, and relates the system's design parameters to the final outflow hydrographs. A set of physically-based equations for representing flow through PP systems is tested against real time data monitored for two PP systems. The equations used to model flow through the layered PP system include: the Kuang Equation for flow routing through the PP layer, Richards' Equation for unsaturated flow through the filter media, and Glover's and Manning's Equations for outflow from the

system's underdrains. Special attention is given to the routing of stormwater through the filter media layers in unsaturated conditions. Lag times of the hydrograph peak resulting from the routing through the filter media soils were found to increase with the increase of the layer thickness, following a power function rather than being linear. Similarly, the hydrograph lag time decreases with an increase of the hydraulic conductivity of the soil and also follows a power function.

IV.1 Introduction

Permeable pavement systems are one of the LID technologies that were found to effectively minimize the impacts of urbanization on the water quality of surface water bodies (Boving, 2006; UNHSC, 2012). These systems also serve as transportation infrastructure (Schwartz, 2010). However, the acceptance of PP systems as a functional stormwater management technology continues to face challenges (Houle et al, 2013). This is due in part to: the lack of familiarity with this technology by some reviewing agencies responsible for approval of stormwater management plans for construction projects (Houle et al, 2013); concerns that the pavement's surface might clog over time and prevent rainfall from entering the system; concerns regarding proper system installation; lack of familiarity with maintenance requirements; and the lack of accurate, scientifically-derived modeling tools to predict the hydrologic behavior of PP systems, especially as it relates to changes in design variables.

Correct design and sizing of LID technologies ensures that the cumulative effects of large scale implementation of the technology over time will result in water quality improvement and flood reduction rather than further contribute to environmental

problems. Generally, long-term policy development and implementation strategies of new stormwater management technologies at the watershed level are based on studies which demonstrate that alternatives are superior to existing technology and the fact that conventional strategies are not helping to meet water quality goals. Because demonstration at the watershed scale is expensive, includes many causative variables, and requires long term studies, watershed scale assessments are typically performed with computer simulations that employ urban hydrology software. However, currently available watershed models do not include capabilities to predict hydrologic consequences resulting from individual LID systems such as PP systems. Moreover, accurate modeling at the watershed scale first requires in-depth understanding of the technology's functionality at the system level, and this has not yet been given sufficient attention. The relationship between design variables (layer thickness, media particle size distribution, under drains, etc.) and the system's outcome (outflow hydrograph) has not yet been empirically developed for PP systems (Elliot, 2006). This lack of physically-based modeling of PP systems served as the impetus for this study: the hydraulic modeling of PP systems.

At the moment, there is little available information about how design variables affect the hydraulic performance of the PP systems. Several monitoring studies were performed on built PP systems where the hydrological outcomes were summarized and reported (Dempsey and Swisher, 2003; Boving et al, 2004; Roseen et al, 2006), but there are only a few studies that looked at developing methodologies to empirically model these systems (Jackson and Ragan, 1974; Ladd, 2004; Barbu et al, 2009; Schwartz, 2010). These proposed models are simplified tools that disregard the water routing

through the hydraulically restrictive soil layers in the system, and make the assumption that the system functions under saturated conditions.

IV.1.1 Pervious pavement types and configurations

PP systems are very similar to conventional pavements. However in stark contrast, the PP system is designed to allow stormwater to infiltrate and easily pass into the sublayer materials. PP surface layers can be made of different materials: porous asphalt, pervious concrete, interlocking blocks, or geo-cells filled with gravel or grass (Ferguson, 2005). The pavement layer is typically set on a support layer that can support both its construction and traffic loads. Below the support layer may be multiple sublayers, each serving a different purpose. A common configuration might include: the permeable surface layer, the support layer (a structural layer – in some applications referred to as the choker course, and typically composed of crushed stone) below the permeable surface layer; then a layer of coarse sand/fine gravel (bank run gravel) which serves as a filter media to remove pollutants and slow down the stormwater; and below that another layer of crushed stone which acts as a reservoir to hold water, prevent moisture from moving upwards (frost heave inhibition), allow it to move to underdrains, and/or hold it to allow for infiltration into the native soil in between storms. An example of a PP system configuration is shown in Figure 21. A simpler configuration in high permeability soils might only include the pavement layer and a setting bed consisting of crushed stone. Underdrains are placed in the stone layer at the base of the system if drainage control is needed in low permeability native soils or where infiltration is undesirable. At sites with very high permeability soils, the lower stone layer and drainage piping may be absent. Some designs might exclude the filter media layer, instead opting

for only a crushed stone reservoir. Generally, the configuration of the system is designed to meet site specific objectives, constraints, and needs. However, irrespective of the design configuration, water movement takes place primarily in the vertical direction through these systems until it reaches the native soil or underdrains if present.

From an engineering point of view, a good hydrological simulation model should: assess the effects of each of the sublayer characteristics on the outflow hydrograph from the system; allow the designers to evaluate the contribution of each of the design variables (ie. system geometry, filter media type and depth, drain spacing and diameter or the lack of drains) to the outflow hydrograph (provided that underdrains are present); and require easily accessible data input.

To optimize design parameters and system configuration for targeted outflow hydrographs, simulation tools need to explicitly relate the water flow to the design parameters of interest through empirical equations. This can only be done with physico-empirical equations that explicitly model the flow through each component in the system rather than lumped or regression equations. Existing models (EPASWMM5, PCSWMM , XPSWMM, HydroCAD and other urban hydrology models) do have some capabilities to model the hydraulics and geometry of PP systems, but are missing the capability to route water through the hydraulically restrictive sublayers of the system (Elliot, 2006; Dietz, 2007, Schwartz, 2010) or link design variables to the outflow hydrograph.

IV.1.2 Segments of flow and corresponding equations

Due to limitations of the existing urban hydrology software, PP systems are currently modeled either as storage units with reduced storage space which account only for the pore space in the soils, as black box systems (for example using a lag time or

fictitious curve number to represent the system), or as simple soils. They are modeled with the assumption that water flows under saturated conditions (Ladd, 2004; Barbu et al, 2009; Schwartz, 2010), or that water freely flows to the bottom of the systems and then saturation occurs from the bottom to the top, as moisture is added in the system (Jackson and Ragan, 1974). According to a recent study which monitored the moisture profile in the sub-base of a PP system installed on the University of New Hampshire campus (Alumni lot), (Figure 21), saturation did not occur at any level in the system's sub-base at any time during the study period of a little over one year (Barbu and Ballestero, 2013a). This system did not have any run-on from surrounding impervious areas, the only stormwater received being direct precipitation falling on the surface of the pavement. In this study, the volumetric moisture content (VMC) was measured at 5 minute intervals at different depths in the system's sublayers. The cumulative frequency distribution of the VMC in reference to the VMC at saturation for the four probes installed at different levels in the PP system's sub-base are presented in Figure 22. This demonstrates that the moisture content was well below the saturation point throughout the period of study.

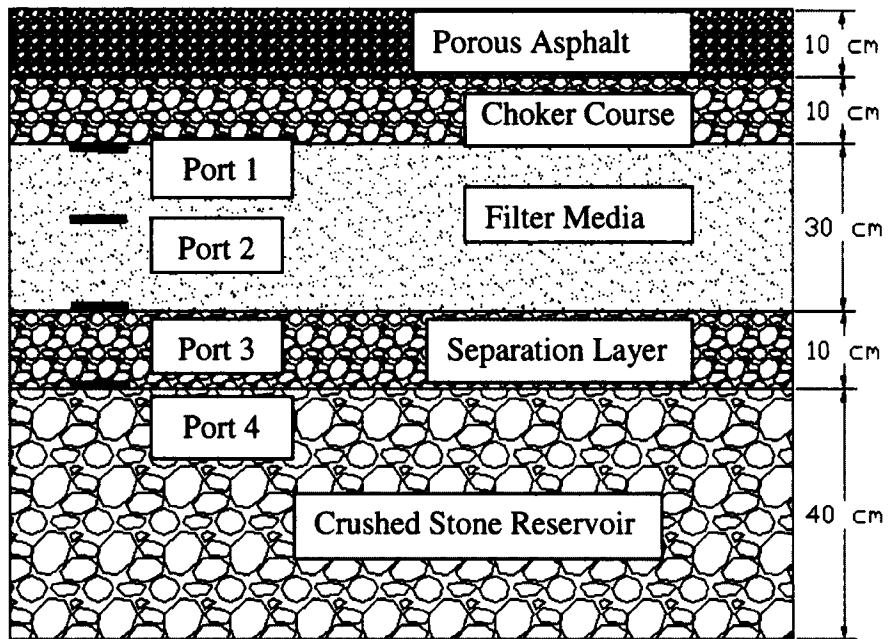


Figure 21 – Cross section of the Alumni lot PP system and location of volumetric moisture content (VMC) sensors

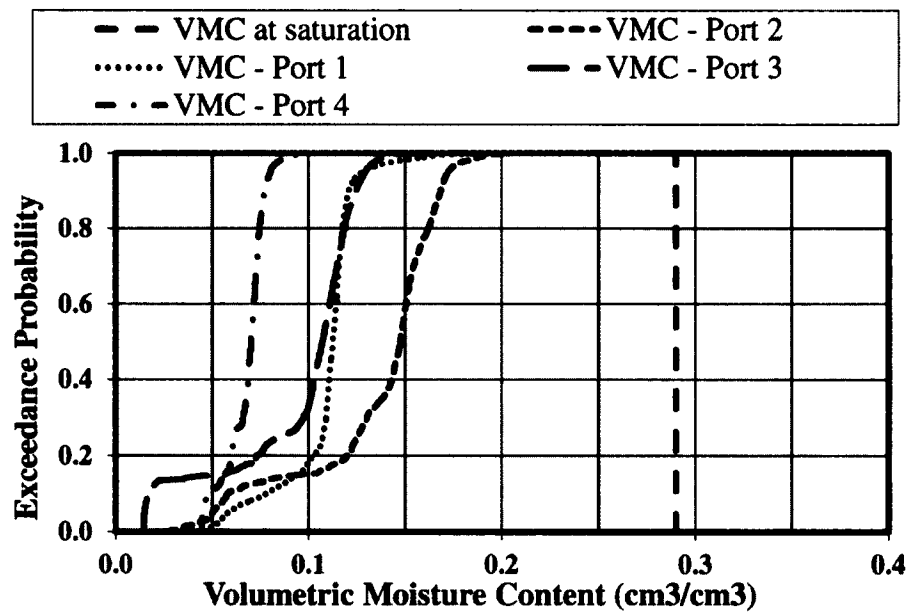


Figure 22 – The cumulative frequency of the VMC at the top (Port 1), middle (Port 2) and bottom (Port 3) of the filter media layer, and at the top of the stone reservoir (Port 4) for one year of monitoring, compared to the measured VMC at saturation in the filter media soil.

When modeling PP hydrology, unsaturated flow conditions are more difficult to mathematically represent than saturated flow and require more data input regarding the soil hydraulic properties, which is not readily available to designing engineers. For any given soil, unsaturated hydraulic conductivities are typically much lower than saturated hydraulic conductivity.

Against this background, the equations selection for modeling flow through the PP system is herein discussed. Modeling decisions to be made regarding the following flow components in the system include: surface infiltration, routing through the permeable layers { surface layer (here porous asphalt), choker, filter media and stone }, infiltration in the native soils, and flow through the underdrains.

Infiltration at the pavement surface: The infiltration capacity of the permeable asphalt layer ranges anywhere from 1,250 to 10,000 cm per hour (UNHSC, 2012) as measured with double ring infiltrometers, a method that creates saturated conditions of the pore space at least at the surface of the asphalt layer. Even in areas where the pavement's surface is partially clogged, the asphalt maintains infiltration rates higher than naturally occurring precipitation rates, and the pavement does not generate runoff, the entire precipitation event being absorbed by the system.

Kuang et al. (2011) measured the hydraulic conductivity of 19 samples of pervious concrete with different porosities. Based on this data, they developed the following power form equation that predicts the saturated hydraulic conductivity of the pervious concrete (K_{sat}) as a function of the total porosity of the permeable asphalt:

$$K_{sat} = 0.0286 * (\phi_t)^{2.0721}$$

Equation 15

Where:

K_{sat} = saturated hydraulic conductivity (cm/min); ϕ_t = total porosity of the pervious concrete (%).

Equation 15 is valid for permeable pavements with porosities up to 20%. The pervious asphalt in the present study had porosities of approximately 18%. Based on Equation 15 the saturated hydraulic conductivity of this pavement is 46 cm per hour, which is vastly different than infiltration capacities measured in the field with the double-ring infiltrometer (UNHSC, 2012).

Barbu and Ballestero (2013a) found that the average time for precipitation to percolate through the permeable pavement and the choker course layers of the PP system in Figure 21 (the lag time from the beginning of precipitation to when a moisture content change was detected at Port 1) was on average 2.45 hours. This time most likely includes the initial abstractions of precipitation on the asphalt surface. Nevertheless, it is a reflection of lag times at field conditions under natural precipitation. Based on this study, the average hydraulic conductivity through the combined pervious asphalt and choker layers is approximately 8.2 cm per hour. In spite of the very high potential infiltration capacities of both PP layer and the 1.8 cm (3/4") crushed stone choker course, the actual infiltration is much lower. This is most likely due to the fact that water moves slower under unsaturated condition (field condition) than at saturation (inundation tests).

Choker course: Due to the high potential infiltration capacity of uniformly graded crushed rock materials, even in unsaturated conditions the water moves very fast through

this layer under gravitational forces. However, the water flow through this layer is restricted by the flow through the PP layer above. In unsaturated conditions, the travel time through this layer is comparable to that through the PP layer, and can be simulated by a delay of the precipitation with observed lag-times (Barbu and Ballestero, 2013a). In the case of saturated conditions created by water building up above the filter media layer, the choker course could be represented as storage, with the outflow being limited to the infiltration capacity of the underlying soil layer.

Filter media: Filter media in PP systems consist of mineral soils in the sand and gravel textural classes. Proposed equations for modeling filter media for PP systems or other LID filtration systems include: Darcy's Law (Lucas, 2010), the original Green-Ampt Equation (Dussailant, 2003; Jayasuriya, 2008; Aad, 2010), the modified Green-Ampt solution (Lee, 2011), and Richards' Equation (Dussailant, 2004; Browne, 2008). These equations, with the exception of Richards', are valid only for saturated flow. Based on the findings of Barbu and Ballestero (2013a), which recognized that flow through a PP filter media layer takes place under unsaturated conditions, it is suggested that Richards' Equation should be used instead of saturated flow equations. Richards' Equation (Richards, 1931) can be derived with the moisture content (θ) or matric potential (ψ) as the dependent variable, or in a mixed form that depends on both θ and ψ . The equation in its moisture based form is:

$$\frac{\partial \theta}{\partial t} = \frac{\partial \left[D(\theta) \frac{\partial \theta}{\partial z} + K_r(\theta) \right]}{\partial z}$$

Equation 16

Where:

$\delta\theta$ = the change in volumetric moisture content (-); δt = the time interval for analysis (T);
 δz = the space interval/depth of layer (L); $\delta\psi$ = the change in matric potential (L^{-1}); K_r =
hydraulic conductivity(L/T); and D = water diffusivity(L^2/T);

Solving Equation 16 requires first knowing the moisture characteristic curves, $\theta(\psi)$, and the relative hydraulic conductivity function, $K_r(\theta)$, which are unique for each soil. Generally, the $\theta(\psi)$ curve is measured in the laboratory or estimated with Van Genuchten fitting equations (Van Genuchten, 1980), and the $K_r(\theta)$ function is commonly derived with Mualem's Equation (Mualem, 1976). Measurements of the $\theta(\psi)$ relationship in the laboratory can take 12 to 14 weeks and even longer for fine particle soils (Dane and Topp, 2002).

Stone reservoir and underdrains: These are commonly modeled with storage indication methods and the Manning Equation, or the orifice equation for systems that function under outlet control (Ferguson, 1998, pp. 127-133). Other alternatives for the flow through the drains include the Dupuit formula, (Krebs and Walker, 1971), Glover's parallel drain equation (Glover, 1974), or the Hooghoudt drainage equation (Hooghoudt, 1940).

Infiltration in the native soils: This is typically modeled with Darcy's Equation (Darcy, 1856), under the assumption that water accumulates above the native soil surface, however this could also subscribe to Richard's Equation.

The development of a physically-based model that explicitly models each flow component of the system and relates the final outflow hydrograph to the system design parameters – particularly those related to the filter media soil – is further explored. Real

time precipitation, moisture profiles in the system's sublayers, and outflow collected at two PP sites on the University of New Hampshire's campus are used for the calibration and validation of the model.

IV.2 Materials and Methods

IV.2.1 Site description

The main PP testing site at the University of New Hampshire Stormwater Center (UNHSC) is the West Edge lot, which was built in 2006 as part of the University of New Hampshire Stormwater Center field research facility. This 483 m² (5200 ft²) PP site is located adjacent to the West Edge Commuter Parking lot. Although this PP site is hydrologically disconnected from the rest of the parking lot, it does receive minimal runoff from the 37 m² dense mix asphalt curb on the perimeter of the actual permeable asphalt surface during rainfall events. Also, in the winter time, a considerable amount of snowmelt from the snow banks surrounding the site can enter the sublayers of the PP systems through the crushed stone shoulder surrounding its perimeter. For this reason, only summer data was used for the model calibration and verification in this study. The native soils under the PP site consist of a silt clay with a low infiltration rate of approximately 0.5 cm/hour. The system configuration and layout are shown in Figure 23.

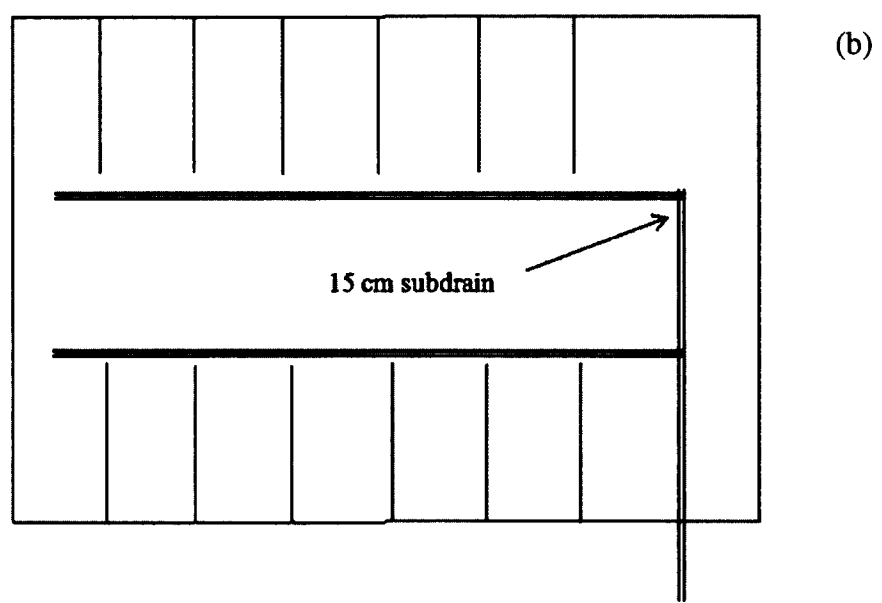
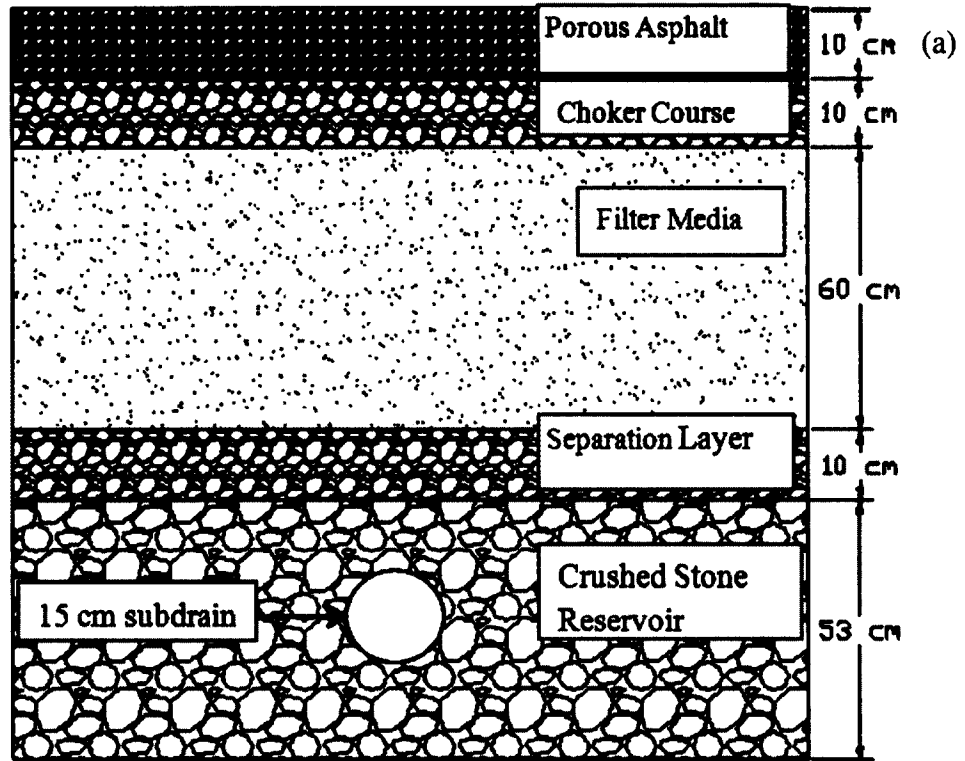


Figure 23 – The cross section (a) and plan view (b) of the PP system at West Edge parking lot. The outflow hydrograph is measured at the end of the subdrain.

The Alumni lot system (Figure 21) is the second UNHSC testing facility. This system is designed similarly to the main testing site, except that this system was designed with a shallower filter media depth (30 cm instead of 60 cm) and stone reservoir (40 cm instead of 53 cm). The bank-run gravel soil used as the filter media in the Alumni lot originated from the same source as that used in the West Edge lot. The difference is that the former has less gravel content (soil particles greater than 2mm). The particle size distribution comparison of the two soils is presented in Figure 24 . Since the Alumni lot system does not have subdrains, no outflow data is available from this site. Only precipitation and moisture profiles in the PP system sublayers were collected for this lot. A modeling module for flow routing through the filter media was first developed and calibrated for the Alumni system. This was then incorporated into the complete PP system model developed for the West Edge system which possessed outflow hydrographs from its subdrains. Precipitation and outflow data were collected continuously from 2005 to 2009 at the West Edge parking lot.

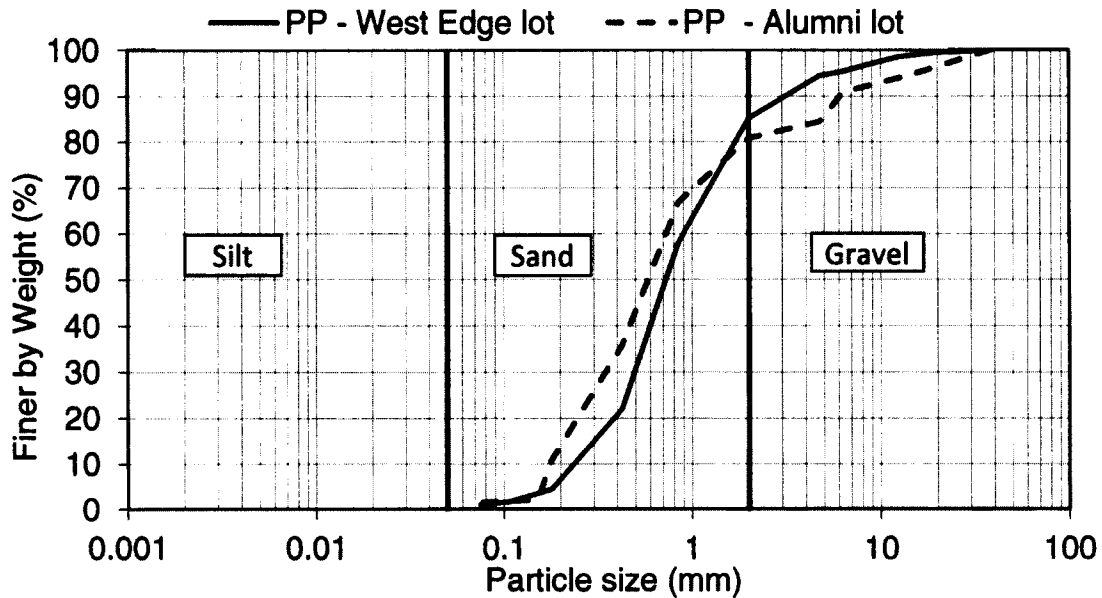


Figure 24 – Particle size distribution of the soils used as filter media in the West Edge and Alumni PP systems

IV.2.2 Monitoring and data calibration

Concurrent, real time precipitation and outflow data at the West Edge lot was collected at 5 minutes intervals. Precipitation data was collected with a NOAA rain gage located 0.5 km (0.3 miles) away from the location of the main testing site. Flow measurements were taken continuously at the end of the subdrain with a water stage recorder (ISCO bubbler) coupled with a Thelmar compound weir. The accuracy of the automatic flow measurements was verified with a “bucket and stop watch” method. The comparison of the two flow measurements is presented in Figure 25. Based on the close agreement of the two types of measurements ($r^2 = 0.967$), calibration was not needed for the automated flow measurements. Therefore, the original data was further used for the model calibration and verification. After data underwent quality control by checking for

any instrumentation error, eight independent storm events were selected for model calibration and verification (Appendix H).

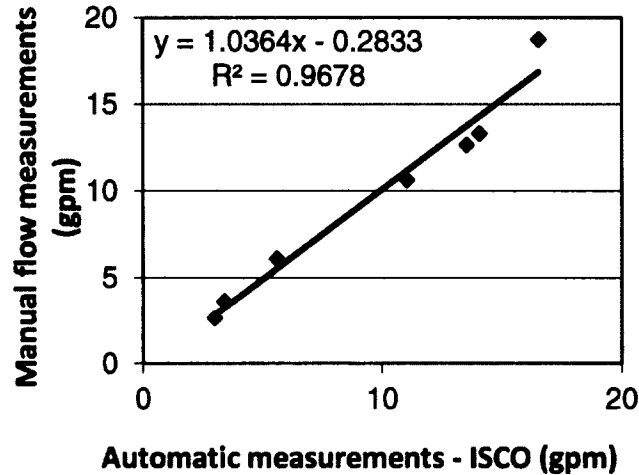


Figure 25 – Comparison of the “bucket and stop watch” flow measurements and automated flow measurements recorded by ISCO bubblers coupled with a Thelmar weir and manufacturer’s rating curve

Real time VMC data was measured at 5 minute intervals at the top, middle, and bottom of the filter media layer of the Alumni lot for 14 months. This data was used for the calibration of the unsaturated flow module developed for the filter media component.

IV.2.3 Model development

The one dimensional moisture transport model was developed in Matlab, 2009a. The precipitation is carried through the system as units of depth until it reaches the native soil at the base where it is allowed to back up in the basal stone layer or the groundwater table, wherever that may reside. Once it reaches the stone reservoir, the water depth is converted to a volume and then the outflow hydrograph is generated with Glover’s parallel drain equation. The segments of flow identified in the system, recommended

equations for modeling these flow components, and data input needs are presented in Table 13.

Surface infiltration and flow through the PP layer and choker course: The infiltration capacities were measured (double-ring infiltrometer or other inundation test) periodically at the West Edge site for over 8 years and were in the range of thousands of centimeters per hour (UNHSC, 2012). Surface runoff was never observed at this site. Thus, it was assumed for the purposes of modeling that surface runoff generation does not occur and that the total amount of precipitation enters the PP system. The flow through the PP layer and choker course was modeled with Kuang's Equation (Equation 15), as it produces lag-times closer to the observed data at the Alumni lot (Barbu and Ballesterro, 2013a).

Table 13 – Segments of flow identified in the PP system, recommended equations and data input needed

Flow component	Equation	Data input / Design parameters being related to the outflow hydrograph
Precipitation	N/A	Real time rainfall data, or design storms
Permeable pavement layer	Kuang Equation	Total porosity of the asphalt layer
Choker layer	Not explicitly modeled; reservoir equation if storage is needed in this layer	N/A; Geometric dimensions
Filter media layer	Barbu framework for the $\theta(\psi)$ and $K_r(\theta)$ relationships (Barbu and Ballester, 2013b), and Richards' Equation (Richards, 1931)	Particle size distribution, porosity, density, saturated hydraulic conductivity
Stone reservoir and drains	Reservoir coupled with Orifice Equation or Manning's Equation, or Glover (Glover, 1974) combined with mass conservation conditions	Geometric dimensions of the storage and pore space available; and subdrains diameter, length, and spacing
Infiltration of the native soils	Darcy (Darcy, 1856)	Saturated hydraulic conductivity

Flow through the filter media was represented with the moisture based form of Richard's Equation (Equation 16), which was solved using a finite difference scheme as described by Tuteja (Tuteja et al, 2004). The soil profile was discretized in M layers with a thickness $\Delta z = \text{depth of filter media} / M$. The change in moisture content (θ) was tracked through the soil profile, as computed with Equation 17 – 19. The θ matrix representation is described in Figure 26, where $j, j-1,$ and $j+1$ indicate the position in the finite difference mesh, and $t, t-1,$ and $t+1$ indicate the time steps of the iteration. The soil profile was discretized with a $dz = 2.5$ cm (1 inch), and the time step was selected as $\Delta t = 1$ minute, as recommended in a similar study by Browne (Browne et al, 2008).

Solving Richards' Equation at the saturation end where there are steep matric potentials can create mathematical errors (convergence problems). To address this, the derivative interpolation of the moisture content was first performed for the entire range of values and was used in conjunction with Richards' Equation.

The flow at the bottom of the filter media was computed with Equation 20. Given that the crushed stone underneath the filter media layer is an opened pore layer that drains freely, the flux from the lower boundary of the filter media is controlled only by the hydraulic conductivity of the filter media soil and is not restricted by the underlying layers.

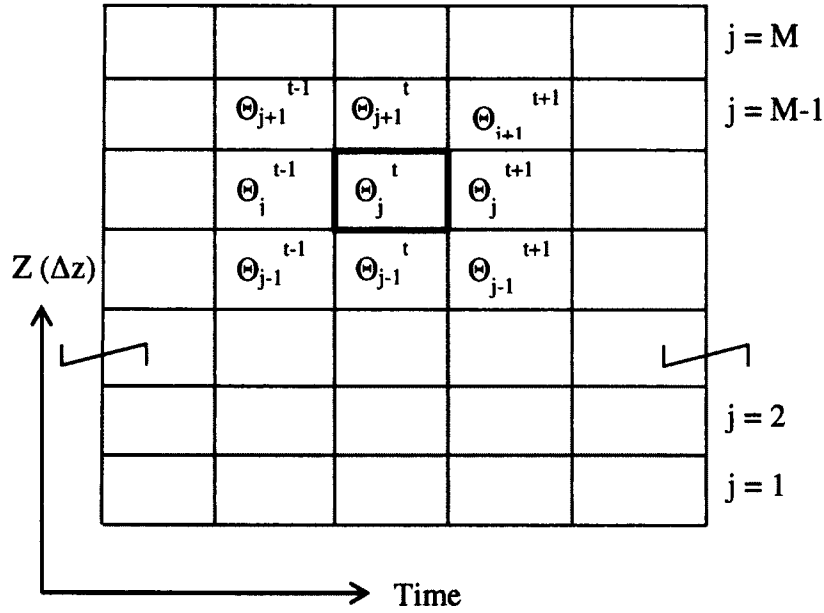


Figure 26 – Representation of θ through the filter media layer in space and time

$$\theta_M^{t+1} = \theta_M^t + \frac{I^t}{\Delta z} + \left(-\sqrt{D(\theta_{M-1}^t) * D(\theta_M^t)} * \left(\frac{\theta_M^t - \theta_{M-1}^t}{(\Delta z)^2} \right) - \sqrt{\frac{K(\theta_M^t) * K(\theta_{M-1}^t)}{\Delta z}} \right) * \Delta t$$

Equation 17 – Top Layer

$$\theta_j^{t+1} = \theta_j^t + \left(\sqrt{D(\theta_{j+1}^t) * D(\theta_j^t)} * \left(\frac{\theta_{j+1}^t - \theta_j^t}{(\Delta z)^2} \right) + \sqrt{\frac{K(\theta_{j+1}^t) * K(\theta_j^t)}{\Delta z}} - \sqrt{D(\theta_j^t) * D(\theta_{j-1}^t)} * \left(\frac{\theta_{Mj}^t - \theta_{j-1}^t}{(\Delta z)^2} \right) - \sqrt{\frac{K(\theta_j^t) * K(\theta_{j-1}^t)}{\Delta z}} \right) * \Delta t$$

Equation 18 – Middle Layers

$$\theta_1^{t+1} = \theta_1^t + \left(\sqrt{D(\theta_2^t) * D(\theta_1^t)} * \left(\frac{\theta_2^t - \theta_1^t}{(\Delta z)^2} \right) + \sqrt{\frac{K(\theta_2^t) * K(\theta_1^t)}{\Delta z}} - \left(\frac{K(\theta_1^t)}{\Delta z} \right) \right) * \Delta t$$

Equation 19 – Bottom layer

$$Flow_j^t = \left(\frac{K(\theta_j^t)}{\Delta z} \right) * \Delta t$$

Equation 20

Where:

Δz = depth of the discrete soil layer (L); Δt = time interval for moisture redistribution (T);

j = space iteration (-); t = time iteration; I' = precipitation rate, or inflow from the layers

above (L/T); θ_j^t = moisture content for layer j at time t (-); $D(\theta_j^t)$ = diffusivity for layer j

at time t (L²/T); $K(\theta_j^t)$ = relative hydraulic conductivity of layer j at time t (L/T); $Flow_j^t$ =

flow at the bottom of the filter media (L/T).

The θ (ψ) and K_r (θ) relationships needed to solve the unsaturated flow function (Equation 16) are typically measured in the laboratory or developed with Van Genuchten (1980) and Mualem (1976) equations. Since the filter media soil is a coarse engineered soil disturbed and repacked at recommended compaction degrees, typical equations used to derive the moisture characteristic curves do not apply to this type of soil (Gribb et al, 2009). The θ (ψ) and K_r (θ) relationships for the filter media soil function were obtained with the framework developed in Barbu and Ballestero, (2013b). This framework starts with data input easily available to design engineers (such as porosity and PSD) and derives a complete curve from residual moisture content to saturation, which allows for the simulation of stormwater routing through the restrictive layers of PP systems. This sequence of equations adds little computational time to the total analysis time for water

flow simulation through the system. The main equations included in this framework include the Arya-Paris model (Arya and Paris, 1981) for the development of the $\theta(\psi)$ relationship, the Bouwer Equation (Bouwer, 1984) for gravel content adjustment along with an extension to the saturation portion of the curve (Barbu and Ballestero, 2013b), and the Mualem model (Mualem, 1976) for the development of the $K_r(\theta)$ function. The PSD of the filter media bank-run gravel in the West Edge system and its corresponding $\theta(\psi)$ and $K_r(\theta)$ curves derived with this framework are presented in Figure 27.

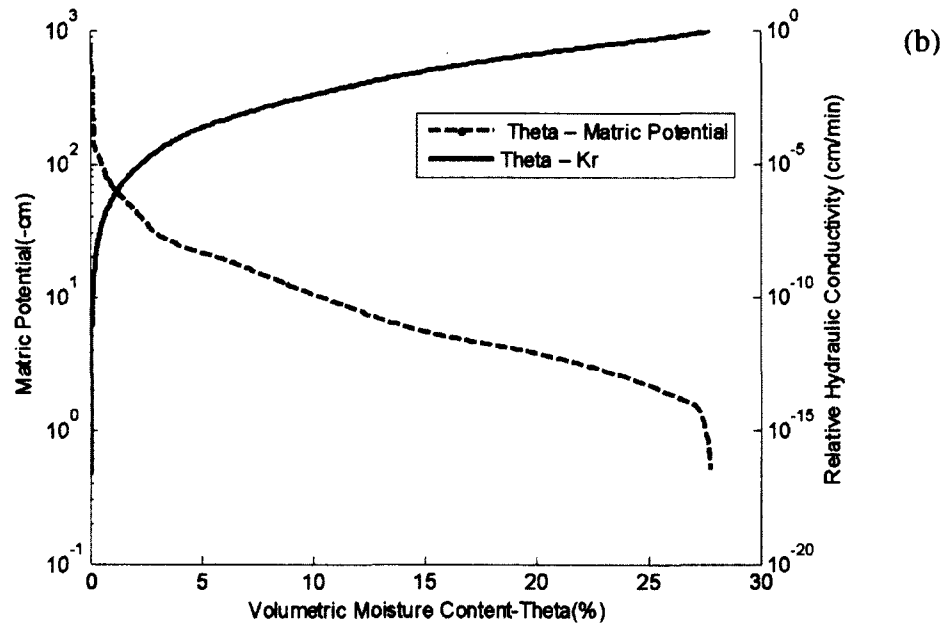
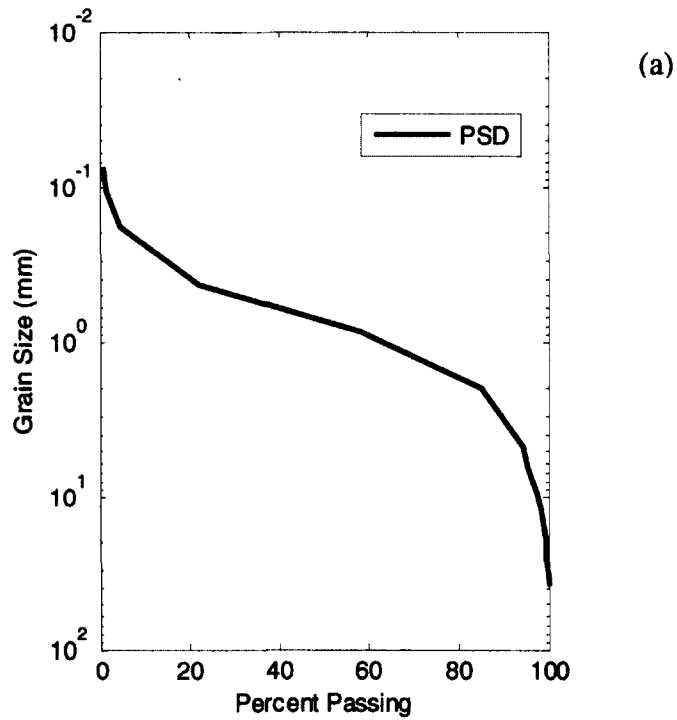


Figure 27 – The particle size distribution (a) of the filter media soil in the West Edge lot and the resulting $\theta(\psi)$ and $K_r(\theta)$ curves (b) as derived after Barbu and Ballestero, 2013b.

Flow through the underdrains: was modeled with the parallel drain equation developed by Glover for transient water flow in soils (Glover, 1974) (Equation 21), and the Manning Equation (Manning et al, 1890)(Equation 22):

$$q = \frac{8iL}{\pi^2} * \sum_{n=1,3,5\dots}^{\infty} \frac{1}{n^2} - \frac{8iL}{\pi^2} * \sum_{n=1,3,5\dots}^{\infty} \frac{e^{-n^2 \pi^2 \left(\frac{\alpha t}{L^2}\right)}}{n^2}$$

Equation 21

Where:

i = recharge rate (L/T); q = flow from one side of a drain (L³/T); D = depth of water in the soil (L); α = aquifer constant (-); ϕ = soil porosity (-); L = distance between parallel drains (L); t = time interval for the analysis (T), K = hydraulic conductivity of the soil (L/T).

$$Q = \frac{1}{n} * A * R^{2/3} * S^{1/2}$$

Equation 22

Where:

Q = Flow through the pipes (L³/T); n = Manning's roughness coefficient; A = Cross sectional area of the pipe (L²); R = the hydraulic radius (L); S = the slope of the water surface (L/L).

IV.3 Results and Discussions

IV.3.1 Derivation of the θ - ψ - K_r functions for the Alumni lot

The framework described in Barbu and Ballesterro (2013b) for deriving the complete θ - ψ - K_r curves was applied to the bank run gravel used as filter media in the

Alumni system. The effectiveness of this framework in conjunction with Richards' Equation for modeling flow routing through the filter media was verified with the monitored real time VMC data recorded at three different levels in the filter layer.

The PSD curve for the Alumni lot filter media displayed significant irregularities (Figure 28a) This was also reflected in the $\theta(\psi)$ curve generated with the original Arya-Paris (A-P) model (Figure 28b). The Van Genuchten (VG) Equation was fitted to the A-P generated data points, and this curve was further used for the flow routing routine. The VG fitting parameters for this soil are as follows: $\theta_s = 0.26$; $\theta_r = 0.025$; $\alpha = 0.175$; and $n = 1.97$. The $\theta-\psi-K_r$ relationships developed for this soil are shown in Figure 29.

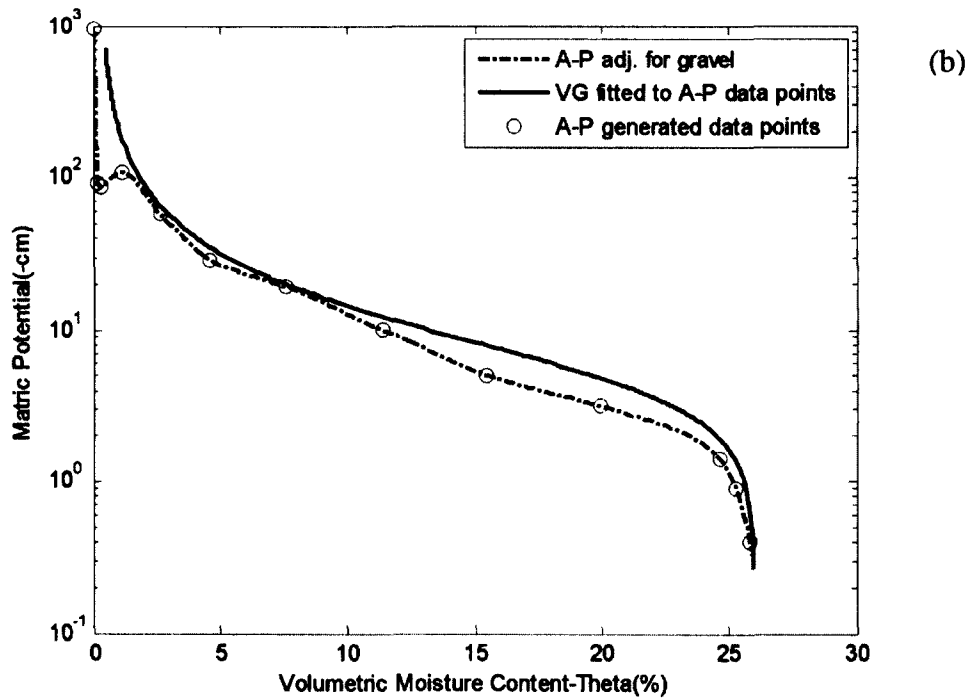
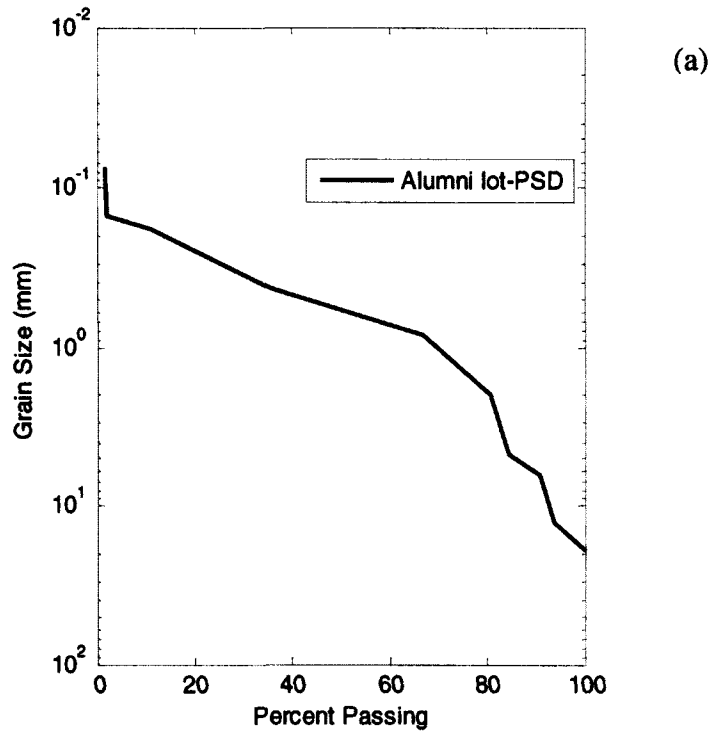


Figure 28 – The particle size distribution of the filter media soil in the Alumni lot (a), and the θ (ψ) curve obtained by interpolation and fitted with VG Equation to the A-P generated data points (b)

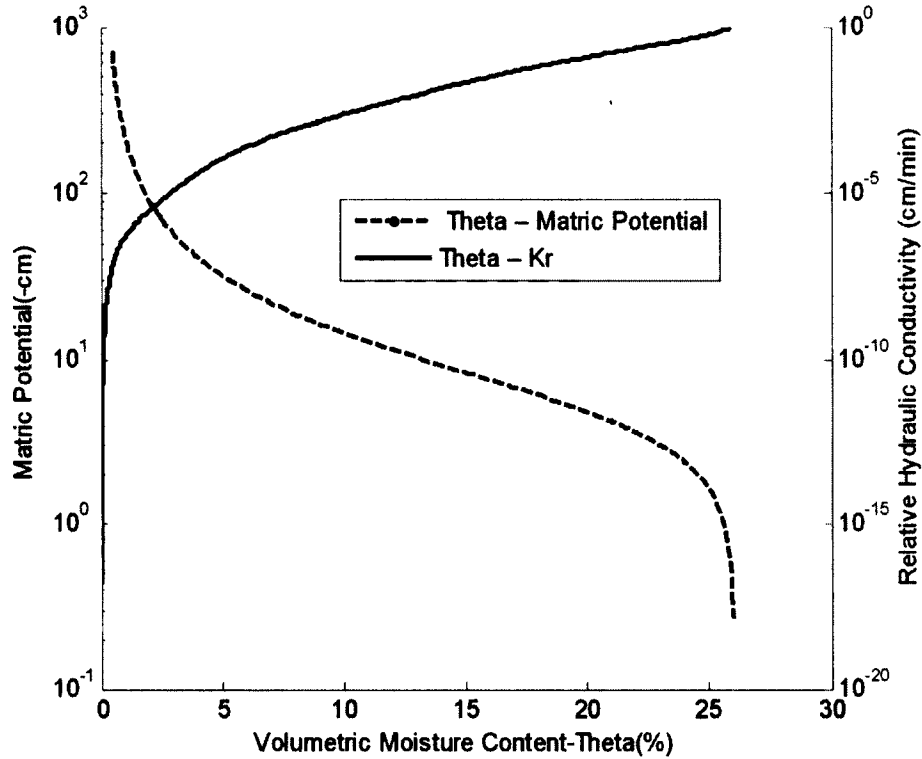


Figure 29 – The θ (ψ) and K_r (θ) curves for the Alumni lot filter media as derived with Barbu methodology (Barbu and Ballesterio, 2013b)

IV.3.2 Water routing through the filter media – Alumni lot

The obtained θ - ψ - K_r curves were then used to solve the unsaturated flow equation to route precipitation through the filter media of the Alumni lot. Since the effectiveness of the proposed framework for the θ - ψ - K_r curves development was verified with laboratory measurements for this soil (Barbu and Ballesterio, 2013b), none of the parameters that are involved in this method were changed during calibration of the flow routing module. The only parameters that were used for calibration were K_{sat} , and the initial θ in the soil profile. Real time VMC data observed in this system showed that the moisture content throughout the profile is not uniform and varies at each depth in the

layer. As the moisture content of the soil at the beginning of each storm for the Alumni lot was known, the actual values were used for θ initialization. However, it was found that the initial θ is not very important as the model converges after a short number of time step iterations. Shorter convergence time was observed when θ initial was set from 5 to 10% VMC.

Three storms with precipitation depths over 2.5 cm (1") were used for calibration of the K_{sat} values and three other storms were used for verification (Appendix I). Although the system functions under unsaturated conditions, K_{sat} plays an important role in the flow routine, as this value is used to scale the K_r curve (Figure 29) used in Richard's Equation. K_{sat} was varied from 0.21 cm/min to 1.27 cm/min, which is the equivalent of 3 to 18.3 meters/day (10 to 30 ft/day) – the range recommended by filter media design standards (UNHSC, 2009). The best fit for the moisture content at the top, middle, and bottom of the filter media, the three levels at which the VMC was monitored in the Alumni lot, was obtained for a K_{sat} of 0.25 cm/min. As an example, the modeled and measured VMC at the three depths in the filter media layer during the 11/04/2010 precipitation event are shown in Figure 30. Additional storm events used for calibration and verification of the flow routine are shown in Appendix J.

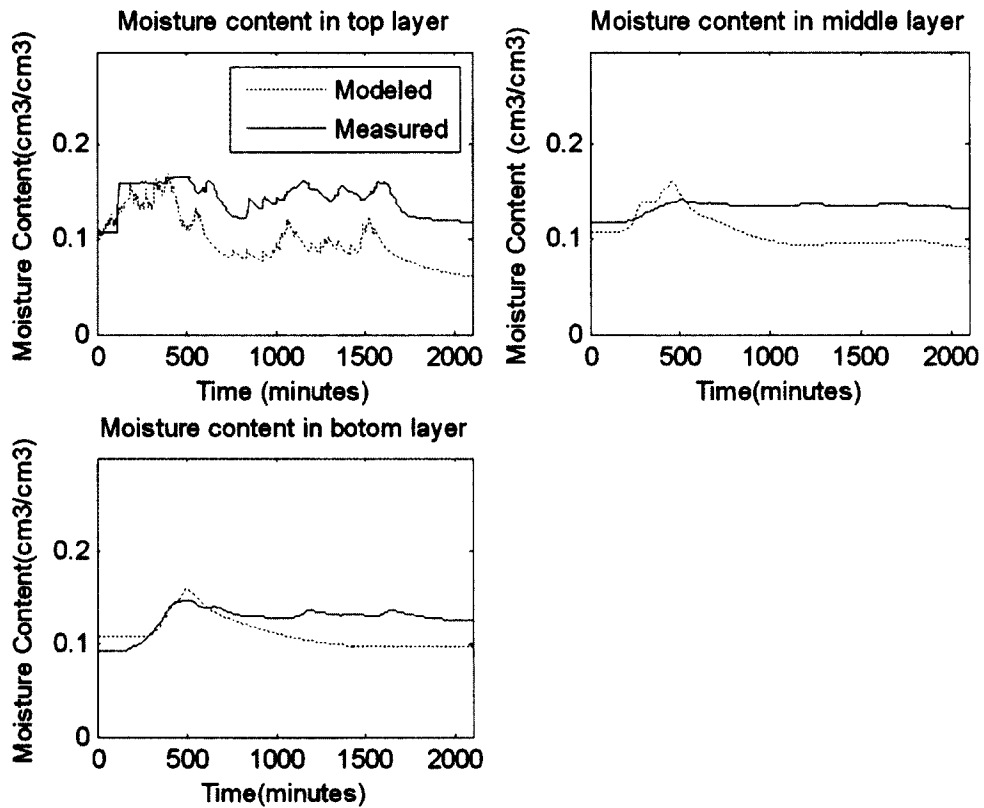


Figure 30 – The VMC in the filter media soil profile in response to the 11/04/2010 precipitation event (total depth of 3 cm). $K_{sat} = 0.75$ cm/min. θ initial was set to observed VMC values at each level

When solving Richards' Equation, the change in moisture content, θ , is computed in each layer with Equation 17 through 19, and is updated after each time step for moisture inputs and outputs through diffusivity and conductivity. The corresponding matric potential and K_r are then updated for the new θ , based on the θ - ψ - K_r relationships in Figure 29. Generally, the changes in the moisture content in response to precipitation are larger at the surface of the filter media, and become more moderate as the water diffuses to greater depths. This phenomenon was represented well by the model (Figure

30), although the changes in modeled VMC were more prominent than the changes in the measured data.

The water moves through the soil profile driven by gravity and the moisture gradient (the difference in moisture content over two consecutive layers), $(\theta_j - \theta_{j-1})/\Delta z$, and therefore the correct representation of the moisture gradient becomes equally important to that of the actual moisture content in the soil. The computed and observed moisture gradient in the top half and the bottom half of the filter media soil for the 11/04/2010 precipitation event are presented in Figure 31a. It is apparent that the values of the modeled VMC vary more than the observed values, the model slightly overreacting to the change in moisture content. When the moisture gradient becomes larger, the water moves faster through the soil profile. However, Figure 31 a and b show that the model overestimates the higher VMC and underestimates the lower VMC almost in equal measure, and balances out over the time of the analysis.

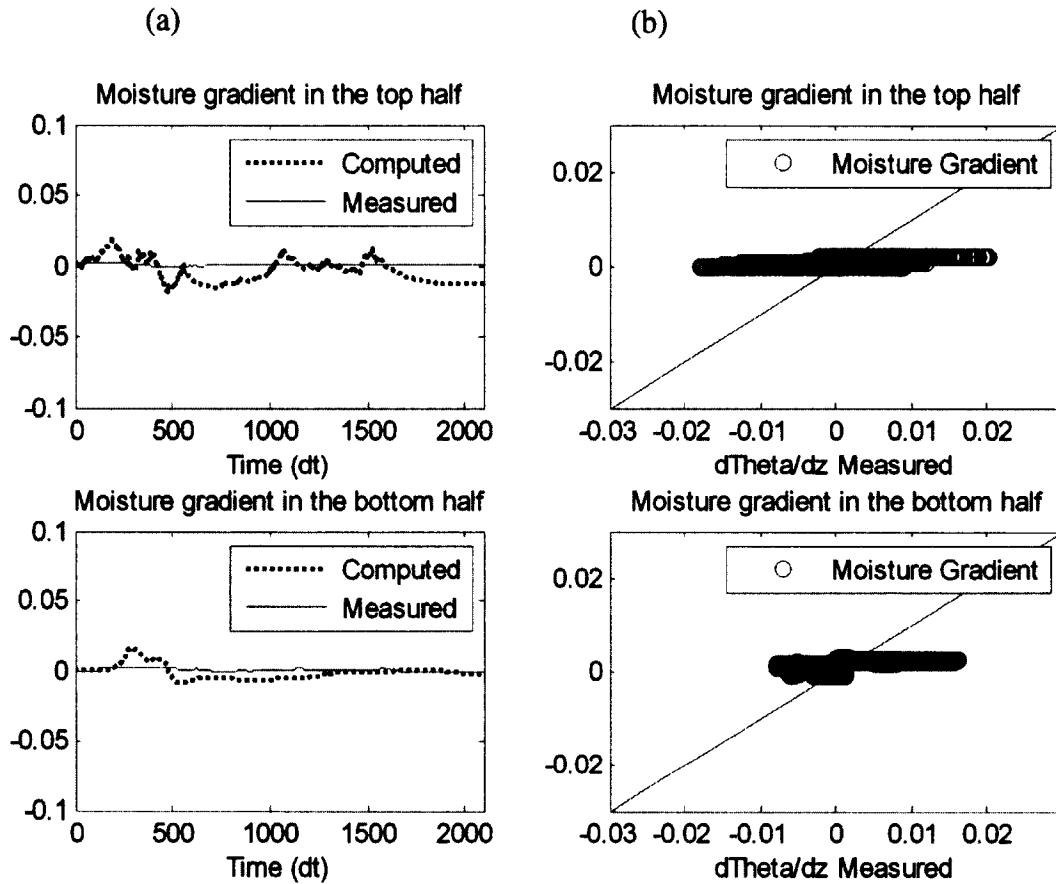


Figure 31 – The moisture gradient in the top half and bottom half of the filter media, computed as the difference between the VMC at the upper and lower boundaries of the two halves of the filter media

According to Legates and McCabe (1999), the goodness of fit of hydrological models should include both statistics of relative error measures and absolute error measures. Therefore, the fit of the modeled VMC to the observed data was tested with the index of agreement (d) developed by Willmott (1981) for the first category and the root mean square error (RMSE) and mean absolute error (MAE) for the second category. The index of agreement (d) is proposed as an alternative to the coefficient of determination (r^2) for hydrological studies (Legates and McCabe, 1999). Similarly to r^2 , the index of

agreement is dimensionless and can vary from 0 to 1, with 1 being perfect agreement.

The MAE and RMSE have the units of the parameter evaluated. Lower values indicate a better fit.

When comparing the computed to measured VMC at the three levels in the filter media, both MAE and RMSE indicators had relatively low values and were mostly positive, signifying that the model performed well, but is generally overestimating the VMC (Table 14). High d values show an overall good performance of the flow routine simulating water movement through the filter media. The good fit indicated by high values of the index of agreement for Port 3 (at the bottom of the filter media) is especially important (Table 14), as this is the location where the outflow hydrograph for the filter media layer is generated.

Table 14 – The “goodness of fit” analysis for routing stormwater through the filter media of the Alumni lot with Richard’s Equation and Barbu framework for obtaining the θ - ψ - K_r curves (Barbu and Ballestero, 2013b), and the initialization parameters.

	Storm Event	K_{sat} (cm/min)	θ_{in} (% VMC)	RMSE (% VMC)			MAE (% VMC)			d (-)		
				Port1	Port2	Port3	Port1	Port2	Port3	Port1	Port2	Port3
Calibration Storms	11/04/2010	0.25	10.7	0.10	0.07	0.05	4.0	2.5	1.6	0.484	0.407	0.730
	11/07/2010	0.25	11.3	0.11	0.07	0.04	3.3	1.8	0.8	0.617	0.588	0.898
	11/16/2010	0.25	11.0	0.13	0.08	0.05	3.2	1.0	-0.3	0.717	0.876	0.989
Verification Storms	11/26/2010	0.25	10.8	0.12	0.08	0.03	2.7	2.3	0.4	0.548	0.264	0.948
	04/10/2011	0.25	10.9	0.12	0.09	0.04	2.7	2.7	-0.6	0.600	0.305	0.821
	04/13/2011	0.25	11.0	0.09	0.13	0.03	3.2	5.1	-0.6	0.661	0.305	0.858

IV.3.3 The complete PP system model – West Edge lot

Once calibrated and knowing its weaknesses, the flow routing routine through the filter media developed for the Alumni lot was integrated into the complete PP system hydraulic model for the West Edge lot. Since the soil used in the filter media for both systems came from the same source, the PSDs were very similar (Figure 24). The difference is that the Alumni lot filter media had a gravel content of 19%, which is slightly higher than the one for the West Edge lot at 15%. This most likely affects the hydraulic conductivity of the two soils. Gravel particles in finer soils were found to impede water flow (Barbu and Ballesterro, 2013b). The appropriate PSD and gravel content were updated for the West Edge soil in the $\theta-\psi-K_r$ routine. Based on the calibration of the model for the Alumni lot filter material, the K_{sat} for the West Edge soil was initially set to 0.25 cm/min and was subject to later calibration. The VMC was initialized as constant throughout the soil profile and ranged from 5 to 10% VMC for individual storm events.

The effectiveness of the filter media flow routine along with Kuang, and Glover Equations to replicate observed hydrographs for this system was then evaluated for eight independent storm events (Appendix H). K_{sat} for the filter media in the West Edge lot was calibrated at 0.75 cm/min. The Manning Equation was also tested as an alternative to the Glover Equation. The “goodness of fit” of the generated hydrographs to the measured hydrographs was tested with the index of agreement (d), the root mean square error (RMSE), and mean absolute error (MAE). The statistical analysis was performed for the hydrographs generated at the bottom of the filter media layer and the hydrograph at the

end of the pipe generated with Glover and Manning Equations, as compared with observed hydrographs for the system.

Table 15 – The “goodness of fit” analysis for the flow modeled with Glover Equation, Manning Equation, and flow at the bottom of the filter media layer, compared with the observed flow at the end of the subdrain

Storm event	RMSE (liters)			MAE(liters)			Index of Agreement, d (-)		
	Observed vs Glover Eq.	Observed vs Manning Eq.	Observed vs Filter Media output	Observed vs Glover Eq.	Observed vs Manning Eq.	Observed vs Filter Media output	Observed vs Glover Eq.	Observed vs Manning Eq.	Observed vs Filter Media output
06/11/2009	0.027	0.039	0.031	-1.093	-1.139	-1.481	0.928	0.916	0.881
06/18/2009	0.023	0.023	0.021	1.568	1.368	1.348	0.896	0.915	0.917
07/02/2009	0.034	0.043	0.029	1.873	1.884	1.496	0.839	0.821	0.899
07/07/2009	0.017	0.014	0.014	1.133	0.789	0.787	0.818	0.904	0.904
07/23/2009	0.182	0.216	0.170	1.749	1.079	0.974	0.986	0.995	0.996
08/21/2009	0.020	0.022	0.023	-0.642	-0.033	-1.289	0.928	0.995	0.786
08/28/2009	0.053	0.053	0.062	-1.909	-0.589	-2.567	0.900	0.991	0.842
09/11/2009	0.035	0.029	0.046	-1.592	-1.635	-2.145	0.626	0.611	0.475

An example of the modeled filter media moisture conditions of the West Edge lot during the 07/23/2009 storm event is presented in Figure 32 and demonstrates that saturation of the filter media did not occur during this precipitation event with a total depth of 4.5 cm. The close agreement of the peak time of the modeled hydrograph at the bottom of the filter media, the modeled hydrograph at the end of the subdrain (Glover and Manning Equations) and the observed hydrograph at the end of the pipe (Figure 33) suggests that there was no storage available under the drains for this event at the time that the water passed through the filter media; therefore, water was directly drained out of the system. This also suggests that the Glover Equation effectively represented the drainage once water reached the drain's invert. Since the system is built in a silt clay native soil with very low infiltration rates and there was known to be a high water table during wetter times of the year, the water level in the system was set at the base of the drain and was further analyzed for individual storms. The comparison of the modeled and observed hydrographs for seven other storm events is shown in Appendix K. An important observation is that the timing of the modeled peak flow at the bottom of the filter media and the timing of the observed peak of the hydrograph to the end of the subdrain pipe coincides for most of the storms analyzed. This also suggests that the storage in the stone reservoir below the subdrain invert was not available at the beginning of the storms and that the drains were very efficient at draining the new precipitation after it was routed through the filter media layer.

Hydrograph peak flow

The final outflow hydrograph was generated with both Glover and Manning Equations, which are two different types of flow generating approaches. With the Manning Equation, the flow through the drain is controlled by the drain diameter. The flow can be modeled with the aid of a rating curve that relates the flow to the water depth in the stone reservoir. With Glover, the flow through the pipes is controlled by the hydraulic conductivity of the soil surrounding the drains, rather than the diameter of the pipe. Originally, the Glover Equation was developed for agricultural soils: finer particle soils than the crushed stone used for the PP basal reservoir. In order to match the observed hydrographs, the hydraulic conductivity of the crushed stone used in the Glover equation was calibrated at 122,000 m/day (400,000 ft/day), which is one order of magnitude higher than K_{sat} commonly used for crushed stone. Due to these high hydraulic conductivities, the parallel drain equation did not significantly delay the hydrograph after it passed through the filter media, and the hydrograph passed through the subdrains almost as soon as it reached them. However, both the Glover Equation and the Manning Equation replicated well the timing of the observed peak flows for most of the storms. We suggest that the Glover Equation might be more appropriate if the drains are placed in finer soils rather than crushed stone or for systems with drains that are farther apart. For systems where the subdrains are placed in very high conductivity materials such as crushed stone, a storage indication method coupled with an appropriate subdrain rating curve (Manning's Equation) might be sufficient for representing this

segment of flow. Manning's Equation also offers more flexibility in estimating the change in flow for small changes in water depth in the system.

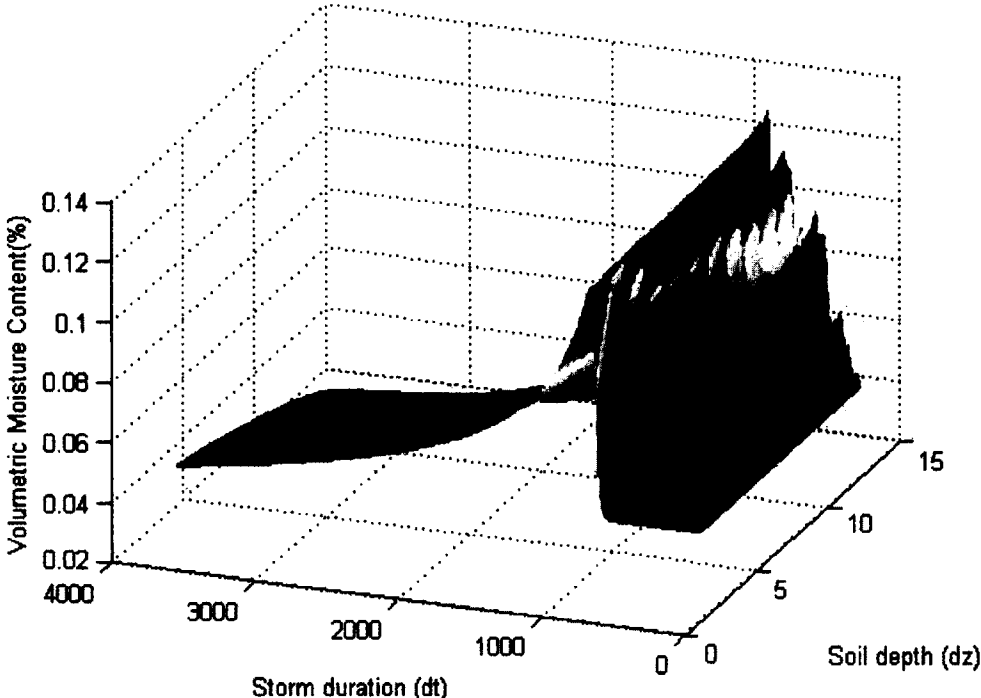


Figure 32 – Moisture content fluctuation in the filter media in response to the 07/23/2009 storm event (dt = 1 min, dz = 2.5 cm (1")). Saturation occurs at 27%.

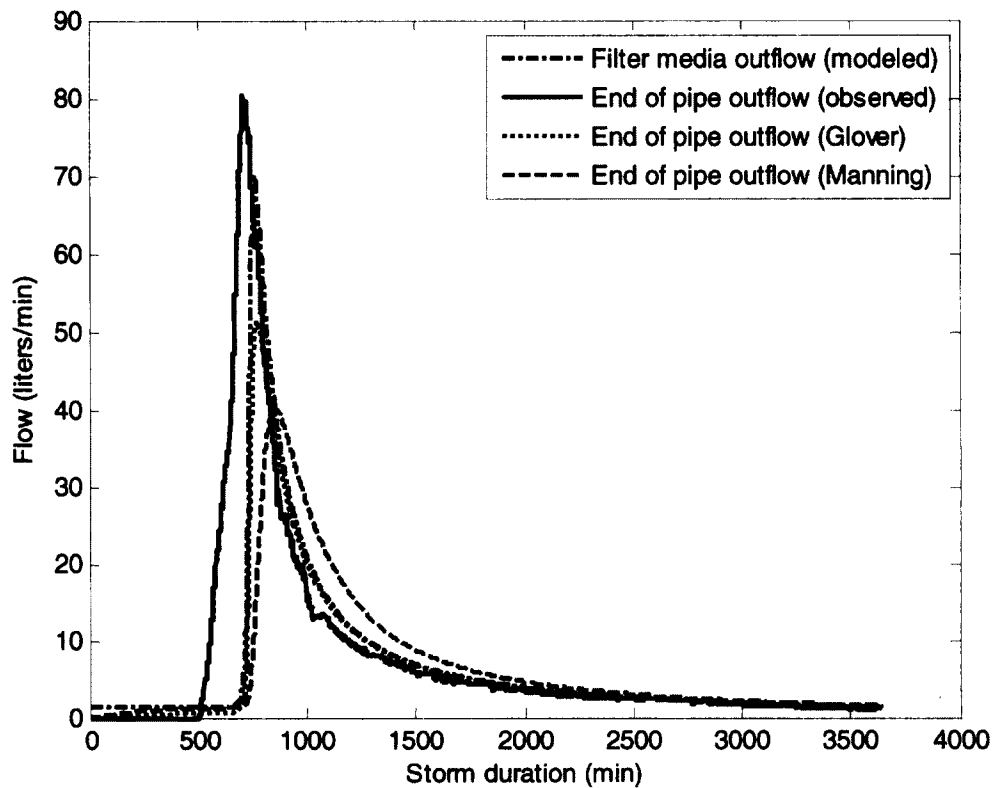


Figure 33 – Observed outflow hydrograph as compared to the modeled outflow for the West Edge system computed with Glover and Manning Equations for subdrains, and with Richards’ Equation as draining at the bottom of the filter media

Hydrograph’s volume

A closer look at the total storm volumes (Table 16) shows that for the storms in June and July 2009, the observed outflow volume is higher than the total amount of precipitation fallen on the surface of the pavement. This suggests that groundwater was entering the base of the system during the storm events and draining through the system’s sub drains. For other storms, the outflow volumes were lower than the total volume of precipitation, suggesting that the water level in the system was slightly below

the drain's invert, reduction in the overall volumes of "run-off" taking place in the system. Due to the imprecision of the monitored outflow volumes, the prediction ability of the overall volume of this model could not be verified. However, when the predicted volumes with Glover and Manning Equations were compared with the precipitation volume, the agreement was considerably closer (Table 16), which verifies that overall the model conserves the mass while routing precipitation through the system.

Although generally the modeled outflow volume was under predicted both with Manning and Glover equations, the opposite was true for the 08/21/2009, 08/28/2009 and 09/11/2009 events: the modeled hydrograph volumes were larger than the observed volumes. This suggests that there was some storage available below the drains at the beginning of these storms. The rating curve for the drains developed with Manning Equation was adjusted to account for storage, and it was found that the systems had 2.5, 2, and 2.75 cm, respectively of available storage under the drain's invert at the beginning of the three storm events. Figures of the generated hydrographs for these storms are presented in Appendix K, and storm volumes are shown in Table 16.

Table 16 – Total stormwater volumes computed as the cumulative area under hydrographs generated at the bottom of the filter media, and at the end of the pipe (Glover Equation). These are compared with the total volume observed at the end of the subdrain, and total precipitation fallen on the pavement surface.

Storm event	Modeled	Modeled	Modeled	Observed	Observed	Observed
	- end of the pipe (Glover) (liters)	- end of the pipe (Manning) (liters)	- filter media outflow (liters)	- end of the pipe (liters)	- Rainfall volume (liters)	- Rainfall depth (cm)
06/11/2009	25,145	25,481	27,979	17,170	26,152	5.03
06/18/2009	22,820	25,469	25,646	43,530	22,454	4.32
07/02/2009	17,080	17,000	13,119	30,937	16,246	1.78
07/07/2009	10,059	12,659	12,675	18,616	9,245	3.12
07/23/2009	21,902	24,340	24,725	28,270	23,642	4.55
08/21/2009	8,612	4,129	11,156	6,085	10,434	2.01
08/28/2009	19,457	13,836	22,267	11,326	22,982	4.42
09/11/2009	12,472	12,680	15,172	4,703	12,416	2.39

IV.3.4 Design variables effects on lag time through the filter media

It is generally recognized that runoff volumes can be reduced by infiltration losses and evapotranspiration; equations and modeling techniques for these losses are available and can be integrated in urban hydrology software.

The main way that hydrographs are transformed by routing through the filter media of PP systems is the attenuation of the peak flows through diffusion in the soils via unsaturated flow, as only minor losses can take place as the water evaporates or is retained in that layer after the precipitation ceases. The effect of the filter media on the lag time of the hydrographs is further analyzed.

Filter media thickness effects on lag time

The lag time contribution by different filter media thicknesses and permeability rates were further analyzed in response to a 2.5 cm Type II – SCS design storm. The lag times through the filter media were computed as the time difference between when the peak intensity of the precipitation event and the peak moisture content value recorded at the bottom of the filter media layer occurred. Several scenarios were analyzed by varying the thickness of the filter media from 15 cm (6”) to 61 cm (24”), as presented in Figure 34. The result of these simulations indicated that the lag time of the peak flow values in the filter media increase as the filter media thickness increases and follows a power relationship (Figure 35):

$$\text{Lag time} = 0.1061 * D^{1.9527}$$

Equation 23

Where:

Lag Time = the time difference between the precipitation peak intensity and peak flow occurring at the bottom of the filter media (minutes); *D* = the thickness of the filter media (cm).

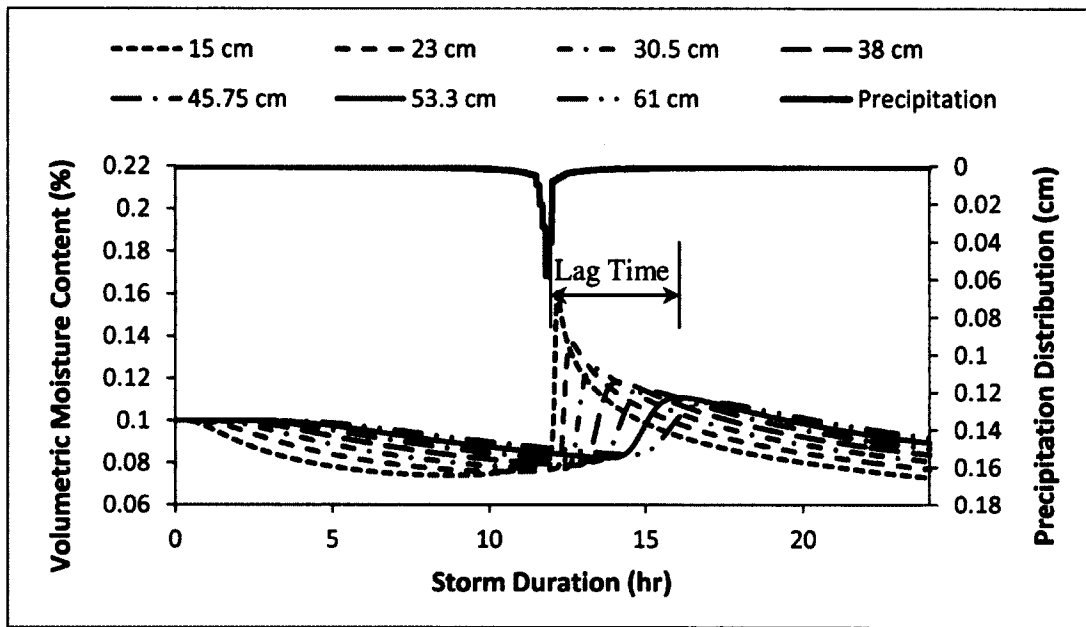


Figure 34 – The peak moisture content at the bottom of the filter media layer for various thicknesses, in response to a 2.5 cm Type II – SCS design storm

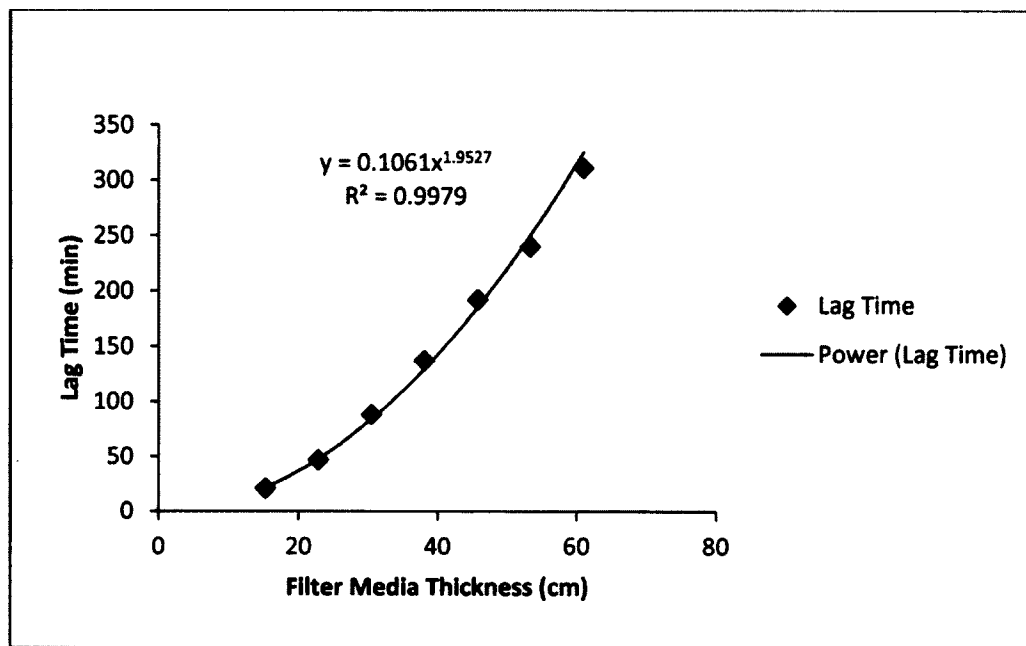


Figure 35 – Peak flow lag times of as a function of the filter media thicknesses

Filter media's K_{sat} effects on lag time

Although the flow in the filter media takes place under unsaturated conditions and the analysis is performed with unsaturated flow functions, the relative hydraulic conductivity function, $K_r(\theta)$, is scaled by the magnitude of K_{sat} . The effect of filter media's K_{sat} on the lag time through a 30 cm (12") filter media layer was analyzed under a 2.5 cm SCS-Type II design storm. The fluctuation of the VMC is presented in Figure 36. The relationship between the lag time and K_{sat} also followed a power function (Equation 24), the lag time decreasing as K_{sat} increases (Figure 37):

$$Lag\ time = 103.33 * K_{sat}^{-0.29}$$

Equation 24

Where:

Lag Time = the time difference between the precipitation peak intensity and peak flow occurring at the bottom of the filter media (minutes); K_{sat} = hydraulic conductivity at saturation (cm/min)

By combining the two sets of analysis, a family of curves was developed for estimating the lag times of peak flows caused by routing stormwater through filter media with various thicknesses and hydraulic conductivities (Figure 38). The coefficients for the general power functions describing each curve are presented in Table 17:

$$Lag\ time = a * K_{sat}^b$$

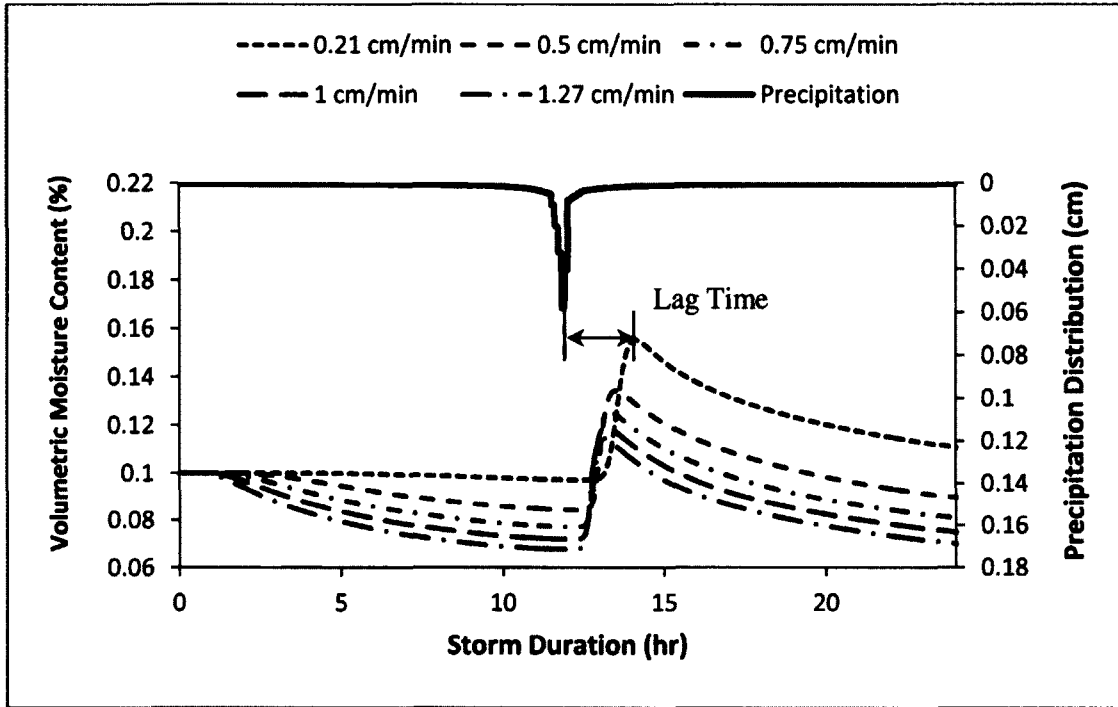


Figure 36 – The peak moisture content at the bottom of a 30 cm filter media layer for various filter media saturated hydraulic conductivities, in response to a 2.5 cm Type II – SCS design storm

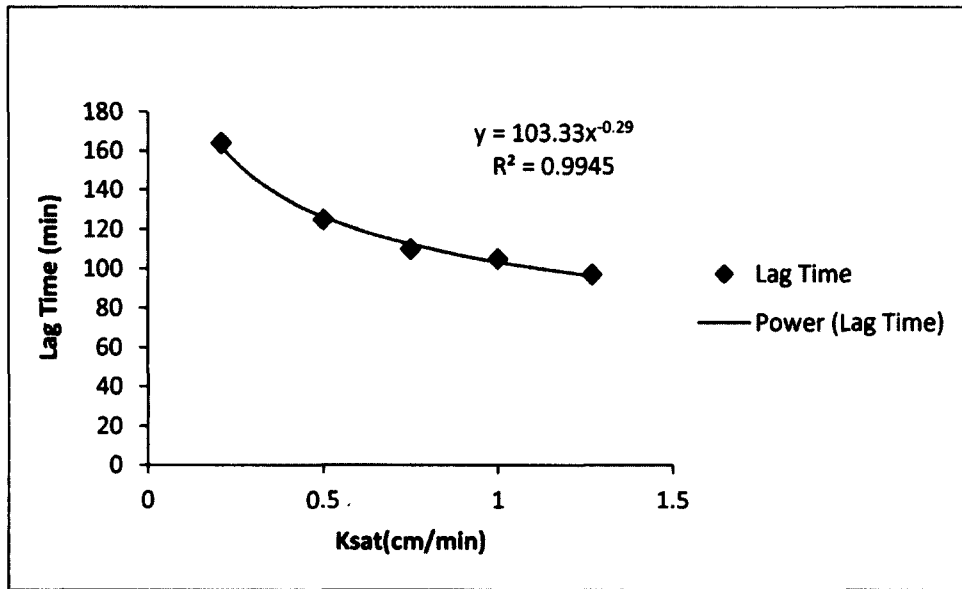


Figure 37 – Peak flow lag times for varying filter media K_{sat} in response to a 2.5 cm Type II – SCS design storm

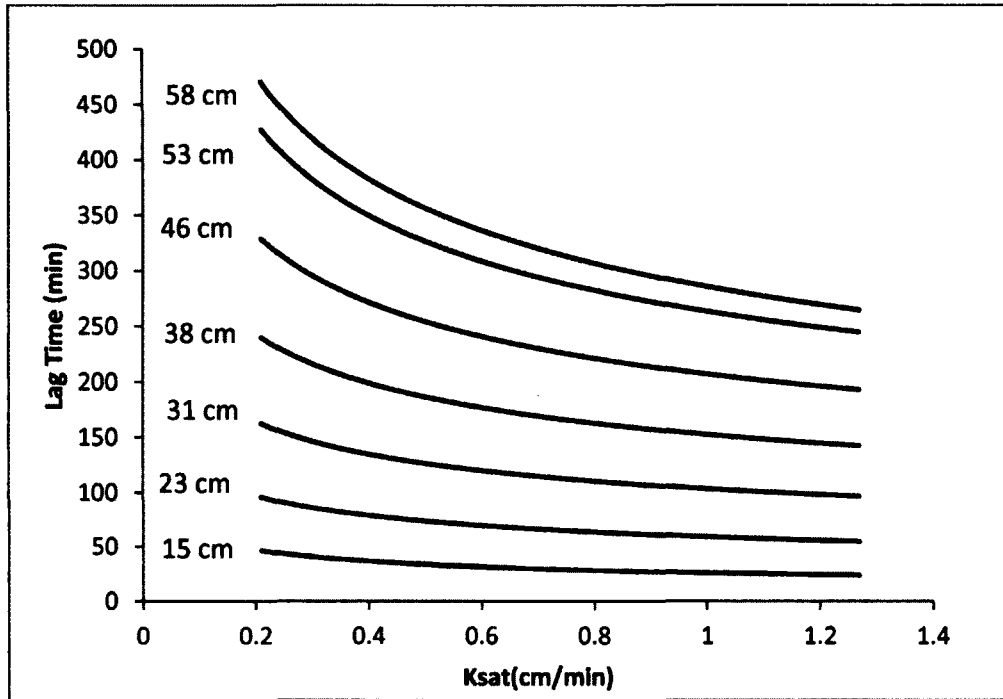


Figure 38 – Lag time through the filter media for permeable pavement systems with various thicknesses and hydraulic conductivities

Table 17 – The power function coefficients for the family of curves presented in Figure 38.

Filter media thickness (cm)	a (-)	b (-)	r ² (-)
15	26.01	-0.373	0.998
23	58.89	-0.312	0.994
31	103.33	-0.290	0.995
38	152.49	-0.290	0.997
46	207.00	-0.297	0.993
53	263.48	-0.310	0.992
59	285.69	-0.320	0.986

IV.4 Conclusions

This article presents a detailed, physically-based mathematical model for evaluating the hydrological behavior of PP systems. The proposed empirical equations relate the various design parameters of the system to the final outflow hydrograph of the system underdrains. Since most hydrologic software packages have good hydraulic capabilities to represent the drainage and geometry of the system, central attention was given to the testing of a framework for developing the $\theta-\psi-K_r$ relationship needed to solve Richards' Equation for the soils used as the filter media in PP systems. This framework started with easily accessible soil properties information. The water routing through the filter media module performed with good results when tested on two different PP systems.

CHAPTER V

Summary and Conclusions

The focus of this dissertation was the physical modeling of filtration LID-SWM systems. Simulating flow through these systems requires that models incorporate both hydraulic and hydrologic modeling capabilities in the same modeling module. Existing software packages used for sizing and designing of stormwater treatment systems do not have adequate capabilities to physically simulate the flow through the permeable layers of LID-SWM systems. However, they do have good capabilities of representing basic hydraulics of the systems (such as storage and piping networks; some continuous simulation models can also represent losses through evapotranspiration and infiltration). This dissertation focused on developing physically based models for simulating flow routing through filter media of LID systems that can be incorporated in both continuous simulation and design-storm approach software packages.

Chapter 2 presented a monitoring study of the moisture profile in the filter media of a permeable pavement system which revealed that this soil layer does not reach saturation. Based on this monitoring study, unsaturated flow equations are recommended for simulating flow through the filter media layer of permeable pavement systems. Although other filtration LID- SWM systems such as gravel wetlands, subsurface sand filters, and bioretention systems are designed to function under ponding conditions, which suggest saturation of the soils at least for extreme storm events. These systems transition from saturated to unsaturated flow between storm events and may function

under unsaturated conditions for small storms. Continuous simulation models for these systems would require capabilities to represent both saturated and unsaturated flow conditions, and the ability to switch from one to another as needed.

Since equations describing saturated flow conditions are well known and easily accessible, this study further addressed the modeling of unsaturated flow conditions for engineered LID-SWM systems filter media. In Chapter 3, a framework for obtaining the moisture retention curves and unsaturated hydraulic conductivity curves needed to solve unsaturated flow equations was developed. The goal of this framework was to compute these relationships starting with readily accessible soil data such as porosity and particle size distribution. This framework was developed for the filter media typically used in four common LID systems: permeable pavement, sand filter, bioretention, and subsurface gravel wetland. This framework performed well when tested against laboratory measurements of these relationships. Since it was developed with physical equations that took into account the detailed particle size distributions of the soils and engineered permeable media, this methodology is applicable to other mix variations of filter media soils.

The ability of the moisture retention curves and relative hydraulic conductivity characteristics developed with the framework described in Chapter 3 used in conjunction with Richards' Equation to replicate the moisture profiles in the filter media of the permeable pavement monitored in Chapter 2 were tested with good results. This sequence of equations used for simulating flow through the filter media was integrated and tested in a full permeable pavement system model, along with other physically-based equations,

as detailed in Chapter 4. For this model, simulated hydrographs at the end of the system's subdrains were compared with real time monitored flow data.

This dissertation presented a detailed methodology on modeling flow through a complex permeable pavement system using a series of physically-based equations. The routing through the filter media modeling routine described in Chapters 3 and 4 was developed to be integrated in continuous simulation models. Combining this flow routine with the basic hydraulic modeling capabilities of most stormwater system design software (such as storage and outlet structures hydraulics) would create a full physically-based model for simulating flow through permeable pavement systems. Such a model relates the physical properties of the filter media soils and the system's geometry to the final outflow hydrograph and would allow for easy optimization of the system's configuration to obtain targeted hydrographs. The simplified equations that relate the thickness and hydraulic conductivity of the filter media to the lag time of stormwater passing through this layer detailed in Chapter 4 were developed to be used with design-storm approach software packages. Routing through the restrictive soil layers of LID systems only affects the lag time and the overall water residence time in the system; this does not directly affect the total volume of the storm. Volume reduction takes place through losses such as evapotranspiration and infiltration in the native soils. Accurate representation of the lag time and residence time in the system would consequently lead to more accurate representation of volume reduction caused by routing stormwater through permeable pavement systems.

The unsaturated flow function framework presented in Chapter 3 and the physically-based methodology for the permeable pavement system presented in Chapter 4 could be further developed to accommodate other LID SWM systems that are designed to function temporarily under saturated conditions (subsurface gravel wetland, sand filter, bioretention system, and other variations of these systems). This can be accomplished by allowing the unsaturated flow model to switch to a saturated flow routine as needed. Simplified equations that relate the lag time to the thickness of the filter media and hydraulic conductivities for these systems can then be developed.

References

Aad, M. P. A., Suidan, M. T., & Shuster, W. D. (2009). Modeling techniques of best management practices: rain barrels and rain gardens using EPA SWMM-5. *Journal of Hydrologic Engineering*, 15(6), 434-443.

American Concrete Institute (ACI) (2006). *Pervious Concrete*. ACI 522R-06, Detroit.

Arya, L. M., & Paris, J. F. (1981). A physicoempirical model to predict the soil moisture characteristic from particle-size distribution and bulk density data. *Soil Science Society of America Journal*, 45(6), 1023-1030.

Arya, L. M., Leij, F. J., van Genuchten, M. T., & Shouse, P. J. (1999). Scaling parameter to predict the soil water characteristic from particle-size distribution data. *Soil Science Society of America Journal*, 63(3), 510-519.

ASTM D2434, (2006). *Standard Test Method for Permeability of Granular Soils (Constant Head)*. Annual Book of ASTM Standard, Vol. 04.09, ASTM International, West Conshohocken, PA.

ASTM D422-63, (2007). *Standard Test Method for Particle-Size Analysis of Soils*. Annual Book of ASTM Standard, Vol. 04.08, ASTM International, West Conshohocken, PA.

ASTM D6836 (2008). *Standard Test Methods for Determination of the Soil Water Characteristic Curve for Desorption Using a Hanging Column, Pressure Head Extractor, Chilled Mirror Hygrometer, and/or Centrifuge*. Annual Book of ASTM Standard, Vol. 04.09, ASTM International, West Conshohocken, PA.

ASTM D7263 (2009). *Standard Test Method for Laboratory Determination of Density (unit Weight) of Soil Specimens*. Annual Book of ASTM Standard, Vol. 04.09, ASTM International, West Conshohocken, PA.

Bagarello, V., & Iovino, M. (2007). Comments on “Predicting the effect of rock fragments on saturated soil hydraulic conductivity”. *Soil Science Society of America Journal*, 71(5), 1584-1584.

Barbu I., Ballesterro T., Roseen R. (2009): Hydrological Response of SWM-LID Practices and Their Abilities of Mitigating Climate Change Impacts, ASCE Conf. Proc.

Barbu, I.A., Ballesterro, T.P., (2013a). The investigation of the nature of flow in a permeable pavement system. To be submitted to ASCE J. Hydraulics: May, 2013.

Barbu, I.A., Ballesterro, T.P., (2013b). Unsaturated Flow Functions for Filter Media used in Low Impact Development - Stormwater Management Systems. To be submitted to Soil Science Society America Journal: April, 2013.

Baver, L.D., Gardner, W.H., and Gardner, W.R. (1972). *Soil Physics*. New York: John Wiley & Sons.

Braga, A., Horst, M., and Traver, R.G. (2007). Temperature effects on the infiltration rate through an infiltration basin BMP. *J. Irrig. Drain. Eng.*, 133(6), 593-601.

Brakensiek, D. L., Rawls, W. J., & Stephenson, G. R. (1986). Determining the saturated hydraulic conductivity of a soil containing rock fragments. *Soil Science Society of America Journal*, 50(3), 834-835.

Boving, T., M. Stolt, and J. Augenstern, (2006). Investigation of the University of Rhode Island, Kingston, RI, porous pavement parking lot and its impact on subsurface water quality. University of Rhode Island. Kingston, University of Rhode Island.

Bouwer, H., & Rice, R. C. (1984). Hydraulic Properties of Stony Vadose Zones. *Groundwater*, 22(6).

Brooks, R.H., and Corey, A.T., 1966. Properties of porous media affecting fluid flow. *J. Irrig. Drain. Div. Am. Soc. Civil. Eng.* 92, 61-88.

Browne, D., Deletic, A., Mudd, G. M., & Fletcher, T. D. (2008). A new saturated/unsaturated model for stormwater infiltration systems. *Hydrological Processes*, 22(25), 4838-4849.

Burdine, N. T. (1953). Relative permeability calculations from pore size distribution data. *Journal of Petroleum Technology*, 5(3), 71-78.

Carpenter, D. D., & Hallam, L. (2009). Influence of planting soil mix characteristics on bioretention cell design and performance. *Journal of Hydrologic Engineering*, 15(6), 404-416.

Childs, E.C. and Collis-George, N. 1950. The permeability of porous materials. *Proc. R. Soc. London A201*: 392-405.

Claytor, R. A., Schueler, T. R. (1996). Design of stormwater filtering systems. Chesapeake Research Consortium.

Dane, J.H., and Topp, G.C. 2002. *Methods of Soil Analysis. Part 4. Physical Methods.* SSSA Book Ser. 5 SSSA, Madison, WI.

Darcy, H. P. G. (1856). Dètermination des lois d'écoulement de l'eau à travers le sable.

Decagon Devices, (2011). Calibration Equations for the ECH2O EC-5, ECH2O-TE and 5TE Sensors. Retrieved on August 9, 2012 from <http://www.decagon.com>.

Dempsey, B. A., and D.M. Swisher (2003). Evaluation of porous pavement and infiltration in Centre County, PA. World Water & Environmental Resources Congress 2003 and Related Symposia.

Dietz, M. (2007). Low Impact Development Practices: A Review of Current Research and Recommendations for Future Directions. *Water, Air, and Soil Pollution* (2007) 186:351–363.

Dussaillant, A., Cozzetto, K., Brander, K., & Potter, K. (2003). Green-Ampt model of a rain garden and comparison to Richards equation model. *SUSTAINABLE PLANNING & DEVELOPMENT.*, 891-900.

Dussaillant, A. R., Wu, C. H., & Potter, K. W. (2004). Richards equation model of a rain garden. *Journal of Hydrologic Engineering*, 9(3), 219-225.

Elliott A.H., and Trowsdale S.A. (2006). A review of models for low impact urban stormwater drainage. *Environmental Modeling & Software* 22, 394-405.

Ferguson, B. (2005). *Porous Pavements, Integrative studies in Water Management and Land Development.*

Ferguson, B. K. (1998). *Introduction to stormwater: concept, purpose, design.* John Wiley & Sons.

Fetter, C. W. (1988). *Applied Hydrogeology.* Merrill Publishing Co., Columbus Ohio. 1988. 592.

Fredlund, M. D., Wilson, G. W., & Fredlund, D. G. (2002). Use of the grain-size distribution for estimation of the soil-water characteristic curve. *Canadian Geotechnical Journal*, 39(5), 1103-1117.

Gallage, C., & Uchimura, T. (2010). Effects of dry density and grain size distribution on soil-water characteristic curves of sandy soils. *Soils and Foundations*, 50(1), 161-172.

Gardner, W. R. (1958). Some steady-state solutions of the unsaturated moisture flow equation with application to evaporation from a water table. *Soil science*, 85(4), 228-232.

Gribb, M. M., Forkutsa, I., Hansen, A., Chandler, D. G., & McNamara, J. P. (2009). The effect of various soil hydraulic property estimates on soil moisture simulations. *Vadose Zone Journal*, 8(2), 321-331.

Glover, R. E. (1974). *Transient ground water hydraulics*. Department of Civil Engineering, College of Engineering, Colorado State University.

Haverkamp, R., Zammit, C., Boubkraoui, F., Rajkai, K., Arrúe, J. L., & Heckmann, N. (1997). GRIZZLY, Grenoble Soil Catalogue: Soil survey of field data and description of particle size, soil water retention and hydraulic conductivity functions. Laboratoire d'Etude des Transferts en Hydrologie et Environnement (LTHE), Grenoble Cedex, 9.

Hooghoudt, S. B. (1940). "Bijdrage tot de kennis van eenige natuurkundige grootheden van den grond No. 7." *Algemeene beschouwingen van het probleem van de detailontwatering en de infiltratie door middel van parallel loopende drains, greppels, slooten en kanalen*, Departement van landbouw en visscherij, directie van de landbouw, Algemeene Staatsdrukkerij, The Hague, The Netherlands, Verslagen van Landbouwkundige Onderzoekingen, 46(14), 515-707 (in Dutch).

Houle, K. M. (2008). *Winter performance assessment of permeable pavements*. MS Thesis, University of New Hampshire, Durham, NH.

Houle, J., Roseen, R., Ballesterro, T., Puls, T., and Sherrard, J.(2013). A Comparison of Maintenance Cost, Labor Demands, and System Performance for LID and Conventional Stormwater Management. *J. Environ. Eng.*

Jackson, T. J., & Ragan, R. M. (1974). Hydrology of porous pavement parking lots. *Journal of the Hydraulics Division*, 100(12), 1739-1752.

Jayasuriya, N., & Kadurupokune, N. (2008). *Impact of Pervious Pavements on Drainage Infrastructure*. Proceedings of 11th ICUD, Melbourne, 31st of August to the 5th of September.

Karathanasis, A. D., & Hajek, B. F. (1982). Quantitative evaluation of water adsorption on soil clays. *Soil Science Society of America Journal*, 46(6), 1321-1325.

Khaleel, R., & Relyea, J. F. (1997). Correcting laboratory-measured moisture retention data for gravels. *Water resources research*, 33(8), 1875-1878.

Krebs, R. D., & Walker, R. D. (1971). *Highway materials*. McGraw-Hill.

Kuang, X., Sansalone, J., Ying, G., & Ranieri, V. (2011). Pore-structure models of hydraulic conductivity for permeable pavement. *Journal of Hydrology*, 399(3), 148-157.

Ladd, T. C. (2004). *Water quantity study of a porous concrete infiltration basin best management practice*. PhD Thesis, Villanova University, Villanova, PA.

Lane, K. S., Washburn, D. E., & Krynine, D. P. (1947). Capillarity tests by capillarimeter and by soil filled tubes. In *Highway Research Board Proceedings (Vol. 27)*.

Lee, R. S. (2011). *Modeling infiltration in a stormwater control measure using modified Greem and Ampt*. MS Thesis, Villanova University, Villanova, PA.

Leming, M. L., Malcom, H. R., & Tennis, P. D. (2007). *Hydrologic design of pervious concrete*. Portland Cement Association and National Ready Mixed Concrete Association, Silver Spring, MD.

Lucas, W. C. (2009). Design of integrated bioinfiltration-detention urban retrofits with design storm and continuous simulation methods. *Journal of Hydrologic Engineering*, 15(6), 486-498.

Manning, R., Griffith, J. P., Pigot, T. F., & Vernon-Harcourt, L. F. (1890). *On the flow of water in open channels and pipes*.

Marshall, T.J., and Holmes, J.W. (1979). *Soil Physics*. New York: Cambridge Univ. Press.

Milczarek, M. A., Zyl, D., Peng, S., & Rice, R. C. (2006, March). Saturated and Unsaturated Hydraulic Properties Characterization at Mine Facilities: Are We Doing it Right?. In *Int. Conf. on Acid Rock Drainage, 7th*, St. Louis, MO (pp. 26-30).

Mualem, Y. (1976). A New Model for Predicting the Hydraulic Conductivity of Unsaturated Porous Media. *Water Resources Research*, 12(3).

NOAA (2012). *Climate Information Library – National Weather Service Forecast Portland Grey Maine*. Retrieved December 14, 2012 from: http://www.erh.noaa.gov/er/gyx/climate_f6.shtml

Peck, A. J., & Watson, J. D. (1979,). Hydraulic conductivity and flow in non-uniform soil. In *Workshop on soil physics and field heterogeneity*. CSIRO Division of Environmental Mechanics, Canberra, Australia.

Richards, L.A. (1931). "Capillary conduction of liquids through porous mediums". *Physics 1* (5): 318–333.

Roseen, R.M., Ballesterro, T.P., Houle, J.J., Avelleneda, P., Wildey, R., & Briggs, J. (2006). Storm water low-impact development, conventional, structural, and manufactured treatment strategies for parking lot runoff: Performance evaluations under varied mass loading conditions. *Transportation Research Record: Journal of the Transportation Research Board*. No. 1984: 135-147.

Roseen, R.M., Ballesterro, T. P., Houle, J.J., Briggs, J. F., Houle, K. M. (2012). Water Quality and Hydrologic Performance of a Porous Asphalt Pavement as a Storm-Water Treatment Strategy in a Cold Climate. *J. of Environmental Engineering*, 138(1), 81-89.

Rosenbaum, U., Huisman, J.A., Weuthen, A., Vereecken, H., Bogaen, H.R., (2010). Sensor-to-Sensor Variability of the ECHO EC-5, TE, and 5TE Sensors in Dielectric Liquids, *Vadose Zone Journal*, (9): 181–186.

Sansalone, J., Kuang, X., & Ranieri, V. (2008). Permeable pavement as a hydraulic and filtration interface for urban drainage. *Journal of irrigation and drainage engineering*, 134(5), 666-674.

Sauer, T. J., Logsdon, S. D. (2002). Hydraulic and physical properties of stony soils in a small watershed. *Soil Science Society of America Journal*, 66(6), 1947-1956.

Schwartz, S. S. (2010). Effective Curve Number and Hydrologic Design of Pervious Concrete Storm-Water Systems. *Journal of Hydrologic Engineering*, 15(6), 465-474.

Stone, R. (2013). Evaluation and optimization of the effectiveness of stormwater control measures for nitrogen and phosphorus removal. MS Thesis, University of New Hampshire, Durham, NH.

Topp, G. C., Davis, J. L., and Annan, A. P. (1980). Electromagnetic determination of soil water content: measurements in coaxial transmission lines, *Water Resources Research*, 16(3): 574-582.

Tuteja, N. K., Vaze, J., Murphy, B., & Beale, G. (2004). CLASS: Catchment scale multiple -landuse atmosphere soil water and solute transport model. CRC for Catchment Hydrology.

USEPA (2000). Low Impact Development (LID) – A literature review. Washington, DC. EPA-841-B-00-005

USEPA, (2013). Detention/retention ponds – fact sheet. Retrieved from web March 2013): <http://cfpub.epa.gov/npdes/stormwater/menuofbmps/index.cfm>

University of New Hampshire Stormwater Center (UNHSC). (2009a). "UNHSC design specifications for porous asphalt pavement and infiltration beds." http://www.unh.edu/erg/cstev/pubs_specs_info.htm.

University of New Hampshire Stormwater Center (UNHSC), (2009b). Bi-annual Report - 2009. University of New Hampshire, Durham, NH.

University of New Hampshire Stormwater Center (UNHSC), (2012). Bi-annual Report - 2012. University of New Hampshire, Durham, NH.

Van Genuchten, M. T. (1980). A closed-form equation for predicting the hydraulic conductivity of unsaturated soils. *Soil Science Society of America Journal*, 44(5), 892-898.

Van Genuchten, M. T., Leij, F. J., & Yates, S. R. (1991). The RETC code for quantifying the hydraulic functions of unsaturated soils (pp. 2-91). EPA.

Vucovik, M., & Soro, A. (1992). Determination of hydraulic conductivity of porous media from grain-size composition. *Water Resources Publications*, Littleton, Colorado.

Weibull, W., (1939). The Phenomenon of Rupture in Solids: *Ingeniors Vetenskaps Akademien Handlinga* 153, Stockholm, p. 17.

Appendix A: Storm events inventory analyzed for the Alumni Lot study (Chapter II)

Rank	Storm date	Total Precipitation	Precipitation Duration	Residence time	Lag time Port1	Initial VMC- Port 2	Maximum VMC Port 2
	(-)	(cm)	(hr)	(days)	(hr)	(%)	(%)
1	11/04/10	3.10	25.83	2.94	2.00	11.9	14.2
2	11/07/10	2.54	17.42	1.29	1.92	12.7	14.3
3	11/16/10	3.25	12.00	3.13	2.42	12.3	14.4
4	11/26/10	0.89	8.25	3.01	3.25	12.7	13.6
5	12/01/10	1.60	3.92	1.42	0.25	12.2	13.7
6	12/11/10	4.67	43.75	5.68	0.58	11.1	13.1
7	12/07/10	1.19	32.08	3.89	2.67	10.9	10.9
9	01/21/11	0.81	8.50	N/A*	N/A*	4.7	4.7
10	01/26/11	0.66	7.83	1.33	1.50	4.4	4.4
11	02/01/11	1.55	37.50	2.72	3.42	4.4	4.4
12	02/05/11	1.17	7.50	3.64	0.42	4.4	4.5
13	02/25/11	2.34	13.08	1.09	0.50	5.7	5.8
14	02/28/11	1.42	4.08	N/A*	2.33	5.8	5.9
15	03/06/11	3.84	14.50	0.76	0.58	7.1	8.5
16	03/10/11	1.68	18.08	3.96	0.75	18.5	20.2
17	04/10/11	1.27	5.50	1.99	0.50	13.0	14.4
18	04/13/11	2.39	24.08	3.04	1.00	14.2	17.0
19	04/16/11	3.28	25.00	3.45	1.58	16.6	18.1
20	04/23/11	1.80	18.08	3.95	1.25	16.4	17.8
21	05/04/11	1.55	19.67	7.52	2.08	16.1	17.7
22	05/14/11	7.39	123.83	N/A*	1.92	15.7	17.1

23	06/11/11	2.82	21.42	2.88	4.08	16.5	17.8
24	06/22/11	4.01	65.58	6.88	5.67	16.1	17.6
25	07/13/11	0.51	25.50	4.60	9.83	14.3	15.9
26	07/28/11	0.66	5.50	3.48	1.33	14.1	15.6
27	07/29/11	4.60	75.75	4.07	6.42	14.1	16.2
28	08/15/11	4.98	31.42	6.00	5.42	14.5	16.0
29	08/25/11	0.66	10.92	1.71	4.00	15.0	16.0
30	08/27/11	6.17	24.00	2.31	5.58	15.3	16.6
31	09/06/11	4.22	53.67	2.97	4.83	14.7	16.3
32	09/22/11	0.99	23.50	1.57	2.00	14.5	15.8
33	09/23/11	1.78	12.42	2.30	1.50	15.3	16.1
34	09/29/11	1.30	15.58	3.02	2.25	14.6	16.2
35	10/02/11	5.21	60.42	3.88	0.33	15.0	16.2
36	10/13/11	3.10	39.75	5.17	2.50	14.6	16.1
37	10/19/11	3.18	25.58	3.76	2.25	14.9	16.5
38	10/24/11	2.44	31.50	N/A*	N/A*	15.0	15.0
39	10/27/11	1.65	23.33	0.52	N/A*	15.6	15.9
40	11/10/11	2.54	8.67	1.54	1.92	14.5	16.2
41	11/16/11	0.53	11.42	2.44	4.17	14.0	14.9
42	11/22/11	3.25	9.33	5.02	2.58	13.9	15.5
43	11/29/11	1.60	3.92	2.05	1.67	14.7	16.0
44	12/07/11	4.34	20.17	1.69	2.00	15.3	16.0
45	12/23/11	0.99	7.33	0.39	1.25	15.1	15.6
46	12/27/11	0.81	6.58	1.98	0.33	12.4	13.9

* - Data not available for this storm due to probe malfunctioning.

Appendix B: Design Precipitation – Durham, NH

Extreme Precipitation Estimates – Jan 2013, Northeast Regional Climate Forecasting Center (NERCC): <http://precip.eas.cornell.edu/>

	5min	10min	15min	30min	60min	120min	1hr	2hr	3hr	6hr	12hr	24hr	48hr	1day	2day	4day	7day	10day
1yr	0.26	0.40	0.50	0.65	0.81	1.03	0.70	0.98	1.20	1.55	2.00	2.61	2.84	2.31	2.73	3.13	3.85	4.43
2yr	0.32	0.49	0.61	0.81	1.01	1.29	0.88	1.17	1.50	1.91	2.44	3.13	3.47	2.77	3.34	3.84	4.57	5.20
5yr	0.37	0.57	0.72	0.96	1.23	1.58	1.06	1.44	1.85	2.38	3.07	3.97	4.45	3.51	4.28	4.89	5.78	6.54
10yr	0.40	0.63	0.80	1.09	1.42	1.84	1.22	1.69	2.18	2.82	3.66	4.74	5.37	4.20	5.17	5.88	6.91	7.78
25yr	0.46	0.74	0.94	1.29	1.72	2.27	1.48	2.09	2.69	3.52	4.61	6.01	6.90	5.32	6.63	7.51	8.75	9.80
50yr	0.51	0.83	1.06	1.48	1.99	2.66	1.72	2.46	3.17	4.18	5.49	7.19	8.34	6.37	8.02	9.04	10.47	11.68
100yr	0.58	0.93	1.20	1.70	2.31	3.12	2.00	2.89	3.74	4.96	6.54	8.62	10.08	7.62	9.69	10.88	12.54	13.92
200yr	0.64	1.04	1.35	1.94	2.69	3.66	2.32	3.40	4.42	5.89	7.81	10.32	12.19	9.13	11.72	13.10	15.02	16.60
500yr	0.75	1.24	1.61	2.34	3.28	4.52	2.83	4.21	5.48	7.38	9.86	13.11	15.67	11.60	15.07	16.75	19.07	20.97

Appendix C: The Matlab code for obtaining the $\theta - \psi$ - Kr curves for the PP filter media

```

%%%%%%%%%%%%%%%%%%%%%%%%%%%%%%%%%%%%%%%%%%%%%%%%%%%%%%%%%%%%%%%%%%%%%%%%
% Arya-Paris-Mualem mathematical model for the PA filter media
%%%%%%%%%%%%%%%%%%%%%%%%%%%%%%%%%%%%%%%%%%%%%%%%%%%%%%%%%%%%%%%%%%%%%%%%

%-----
% PURPOSE:
% Derive the MRC - the Theta(psi) function
% This function is adjusted for gravel content (anything >2mm),
% then is used to derive the Kr(psi) with Mualem model
%-----

%% Standard sieves fractions:
%[pan, #200 #100 #80 #40 #20 #10 #4 1/4in 3/8in 1/2in 3/4in 1in 1.5in]
sieves_size=[0 0.075 0.15 0.18 0.425 0.85 2 4.75 6.35 9.53 12.7 19
25.4...
38.1]; %mm

%Complete soil fractions as used by Arya-Paris model plus the soil
%particles greater then 2mm, minus fractions up to 0.075mm

all_fraction_size=[0 0.075 0.100 0.150 0.200 0.300 0.400 0.600
0.800...
1.000 1.500 2.000 4.75 6.35 9.53 12.7 19 25.4 38.1];
all_fraction_mass =[0 0.01 0.028 0.046 0.22 0.582 0.852 0.945
0.954...
0.973 0.985 0.994 0.996 1]; %percentile

%soil fractions interpolated over intervals of size x:
x=0.05;
x_fraction_sizes= logspace(-1.1249,1.5809);
x_fraction_sizes_mass =interp1( sieves_size, all_fraction_mass,...
x_fraction_sizes, 'pchip');

%Following data is read directly from the Particle Size Distribution
%report(PSD)for each soil fraction

up_frac_mass=all_fraction_mass(2:length(all_fraction_mass));
low_frac_mass=all_fraction_mass(1:length(all_fraction_mass)-1);
frac_mass=up_frac_mass -low_frac_mass;

% fraction mass Interpolation over the 18 intervals of Arya-Paris
new_up_frac_mass=interp1( sieves_size(2:14), up_frac_mass,...
all_fraction_size(2:19), 'pchip');% this is mass
new_low_frac_mass=interp1(sieves_size(1:13), low_frac_mass,...
all_fraction_size(1:18), 'pchip');% this is mass
new_frac_mass=new_up_frac_mass-new_low_frac_mass;

% fraction mass interpolated over intervals of size x:

```

```

x_up_frac_mass=x_fraction_sizes_mass(2:length(x_fraction_sizes_mass));
x_low_frac_mass=x_fraction_sizes_mass(1:length...
(x_fraction_sizes_mass)-1);
x_frac_mass=x_up_frac_mass - x_low_frac_mass;

%%Verify that the total mass = 1
total_mass=sum(frac_mass);
new_total_mass=sum(new_frac_mass);
x_total_mass=sum(x_frac_mass);

%%
%-----
% Arya-Paris model normalized to 2 mm (particles greater than 2mm are
not
% considered
%-----

% For this model only soil fractions smaller than 2mm(#10 sieve) are
used
up_mass_finesand=up_frac_mass(1:6);
low_mass_finesand=up_frac_mass(1:6);
% AP Interpolated soil fractions:
new_up_mass_finesand=new_up_frac_mass(1:11);
new_low_mass_finesand=new_low_frac_mass(1:11);
% 'm' Interpolated soil fractions:
x_up_mass_finesand=x_up_frac_mass(1:(2/x));
x_low_mass_finesand=x_low_frac_mass(1:(2/x));

% gravel content (%-ile):
gravel=up_frac_mass(13)-up_frac_mass(6); %Percent gravel
%New Gravel content(%-ile). Note: it should be the same value as
above,
%but calculated as:
new_gravel=new_up_frac_mass(18)-new_up_frac_mass(11); %Percent
gravel
x_gravel=new_gravel;

% 1) Di= Mean particle diameter for each soil fraction (cm):
up_bound_diam=sieves_size(2:7); %mm
low_bound_diam=sieves_size(1:6); %mm
Di=(up_bound_diam+low_bound_diam)/(2*10); %cm
% New Di:
new_up_bound_diam=all_fraction_size(2:12);
new_low_bound_diam=all_fraction_size(1:11);
new_Di=(new_up_bound_diam+new_low_bound_diam)/(2*10); %cm
% x Di:
x_up_bound_diam=x_fraction_sizes_mass(2:(2/x)+1); %mm
x_low_bound_diam=x_fraction_sizes_mass(1:(2/x)); %mm
x_Di=(x_up_bound_diam+x_low_bound_diam)/(2*10); %cm

% 2) Cummulative Mass for all soil fractions:
cumm_mass_frac=up_mass_finesand;
%New Cummulative Mass for AP soil fractions
new_cumm_mass_frac=new_up_mass_finesand;

```

```

%New Cummulative Mass for AP soil fractions
x_cumm_mass_frac=x_up_mass_finesand;

% 3) Ri= Mean particle radius for each soil fractions (cm):
Ri=Di/2;
%New Ri= Mean particle radius for interpolated soil fractions (cm):
new_Ri=new_Di/2;
%x_Ri= Mean particle radius for interpolated soil fractions over
%intervals of size 'x' (cm):
x_Ri=x_Di/2;

% 4) Wi= solid mass/unit sample in (g/g)...normalized
Wi_cumm=[(cumm_mass_frac(1)*1)/cumm_mass_frac(6)...
(cumm_mass_frac(2)*1)/cumm_mass_frac(6)...
(cumm_mass_frac(3)*1)/cumm_mass_frac(6)...
(cumm_mass_frac(4)*1)/cumm_mass_frac(6)...
(cumm_mass_frac(5)*1)/cumm_mass_frac(6) 1];

%new Wi= solid mass/unit sample in (g/g)...normalized
new_Wi_cumm=[(new_cumm_mass_frac(1)*1)/new_cumm_mass_frac(11)...
(new_cumm_mass_frac(2)*1)/new_cumm_mass_frac(11)...
(new_cumm_mass_frac(3)*1)/new_cumm_mass_frac(11)...
(new_cumm_mass_frac(4)*1)/new_cumm_mass_frac(11)...
(new_cumm_mass_frac(5)*1)/new_cumm_mass_frac(11)...
(new_cumm_mass_frac(6)*1)/new_cumm_mass_frac(11)...
(new_cumm_mass_frac(7)*1)/new_cumm_mass_frac(11)...
(new_cumm_mass_frac(8)*1)/new_cumm_mass_frac(11)...
(new_cumm_mass_frac(9)*1)/new_cumm_mass_frac(11)...
(new_cumm_mass_frac(10)*1)/new_cumm_mass_frac(11) 1];

%x_Wi= solid mass/unit sample in (g/g)...normalized
x_Wi_cumm=zeros(1,length(x_cumm_mass_frac));
for i=1:1:length(x_cumm_mass_frac)
    x_Wi_cumm(i)=x_cumm_mass_frac(i)/x_cumm_mass_frac...
        (length(x_cumm_mass_frac));
end

Wi=zeros(1,length(Wi_cumm));
for n=2:1:length(Wi_cumm)
    Wi(1)=Wi_cumm(1);
    Wi(n)=Wi_cumm(n)-Wi_cumm(n-1);
end

new_Wi=zeros(1,length(new_Wi_cumm));
for n=2:1:length(new_Wi_cumm)
    new_Wi(1)=new_Wi_cumm(1);
    new_Wi(n)=new_Wi_cumm(n)-new_Wi_cumm(n-1);
end

x_Wi=zeros(1,length(x_Wi_cumm));
for n=2:1:length(x_Wi_cumm)
    x_Wi(1)=x_Wi_cumm(1);
    x_Wi(n)=x_Wi_cumm(n)-x_Wi_cumm(n-1);
end

```

```

% 5) ni=number of spherical particles for each fraction:
ro_s=2.82; %particle density (grams/cm3)

ni=zeros(1,length(Ri));
for n=1:1:length(Ri)
    ni(n)=(3*Wi(n))/(4*pi*ro_s*(Ri(n))^3);
end
    new_ni=zeros(1,length(new_Ri));
    for n=1:1:length(new_Ri)
        new_ni(n)=(3*new_Wi(n))/(4*pi*ro_s*(new_Ri(n))^3);
    end

    x_ni=zeros(1,length(x_Ri));
    for n=1:1:length(x_Ri)
        x_ni(n)=(3*x_Wi(n))/(4*pi*ro_s*(x_Ri(n))^3);
    end

% 6) Theta_i= volumetric water content coresponding to each fraction.
This
    % iscomputed by dividing the effective pore volume to the bulk
volume
    % for each fraction.

% Compute porosity from Particle Size Distribution data with Vukovic
eq.,
% OR imput directly if it is known:

d60=interp1(cumm_mass_frac, Di, 0.6, 'pchip');
d10=interp1(cumm_mass_frac, Di, 0.1, 'pchip');

    new_d60=interp1(new_cumm_mass_frac, new_Di, 0.6, 'pchip');
    new_d10=interp1(new_cumm_mass_frac, new_Di, 0.1, 'pchip');

    x_d60=interp1(x_cumm_mass_frac, x_Di, 0.6, 'pchip');
    x_d10=interp1(x_cumm_mass_frac, x_Di, 0.1, 'pchip');

u=d60/d10;%uniformity coefficient
    new_u=new_d60/new_d10;
    x_u=x_d60/x_d10;

% porosity=0.225*(1+0.83^u)*100;%Vukovic equation
%     new_porosity=0.225*(1+0.83^new_u)*100;%Vukovic equation
%     x_porosity=0.225*(1+0.83^x_u)*100;%Vukovic equation

porosity=34.4;
    new_porosity=34.4;
    x_porosity=34.4;
Sw=0.90; %maximum water content to prosity (can be determined
    %from theta(head)-curve at head=1cm)

Theta_i=zeros(1, length(Wi_cumm));
partsum_Wi_cumm=zeros(1, length(Wi_cumm));
for n=2:1:length(Wi_cumm)

```



```

partsum_Wi_cumm(1)=Wi_cumm(1);
partsum_Wi_cumm(n)=partsum_Wi_cumm(n-1)+Wi_cumm(n);
Theta_i(n)=porosity*Sw*(partsum_Wi_cumm(n)/sum(Wi_cumm));
end
Theta_i_ext= [Theta_i 0.925*porosity 0.95*porosity];%curve extended to
%include two more data points coresponding to fine gravel(2-11mm) and
%coarse gravel(<11mm)

new_Theta_i=zeros(1, length(new_Wi_cumm));
new_partsum_Wi_cumm=zeros(1, length(new_Wi_cumm));
for n=2:1:length(new_Wi_cumm)
    new_partsum_Wi_cumm(1)=new_Wi_cumm(1);
    new_partsum_Wi_cumm(n)=new_partsum_Wi_cumm(n-
1)+new_Wi_cumm(n);
    new_Theta_i(n)=new_porosity*Sw*(new_partsum_Wi_cumm(n)/...
sum(new_Wi_cumm));
end
new_Theta_i_ext= [new_Theta_i 0.925*new_porosity
0.95*new_porosity];
%curve extended to include two more data points coresponding to
% fine gravel (2-11mm) and coarse gravel(<11mm)

x_Theta_i=zeros(1, length(x_Wi_cumm));
x_partsum_Wi_cumm=zeros(1, length(x_Wi_cumm));
for n=2:1:length(x_Wi_cumm)
    x_partsum_Wi_cumm(1)=x_Wi_cumm(1);
    x_partsum_Wi_cumm(n)=x_partsum_Wi_cumm(n-1)+x_Wi_cumm(n);
x_Theta_i(n)=x_porosity*Sw*(x_partsum_Wi_cumm(n)/sum(x_Wi_cumm));
end
x_Theta_i_ext= [x_Theta_i 0.925*x_porosity 0.95*x_porosity];
%curve extended to include
%two more data points coresponding to fine gravel(2-11mm) and
%coarse gravel(<11mm)
%%
%-----
% From here on, Method 2(Similarity principle) is followed from Arya
et
% al. (1999a) for finding alpha scaling factor for a sandy soil.
%-----

% 12) LogNi= a+b*log(Wi/Ri^3); with a=-2.478 and b=1.490 for SAND
logNi=zeros(1, length(Wi));
for n=1:1:length(Wi)
    a=-2.478;
    b=1.490;
    logNi(n)=a+b*log10(Wi(n)/((Ri(n))^3));
end
    new_logNi=zeros(1, length(new_Wi));
    for n=1:1:length(new_Wi)
        a=-2.478;
        b=1.490;
        new_logNi(n)=a+b*log10(new_Wi(n)/((new_Ri(n))^3));
    end

x_logNi=zeros(1, length(x_Wi));

```

```

    for n=1:1:length(x_Wi)
        a=-2.478;
        b=1.490;
        x_logNi(n)=a+b*log10(x_Wi(n)/((x_Ri(n))^3));
    end

% 13) alpha_i=log(Ni)/log(ni) scaling parameter for pore length:
alpha_i=zeros(1,length(ni));
for n=1:1:length(ni)
    alpha_i(n)=logNi(n)/log10(ni(n));
end

    new_alpha_i=zeros(1,length(new_ni));
    for n=1:1:length(new_ni)
        new_alpha_i(n)=new_logNi(n)/log10(new_ni(n));
    end

    x_alpha_i=zeros(1,length(x_ni));
    for n=1:1:length(x_ni)
        x_alpha_i(n)=x_logNi(n)/log10(x_ni(n));
    end

% 14) ri=pore radii;
bulk_dens=1.75; % bulk density (grams/cm^3)
part_dens=2.82; % particle density (gr/cm^3)
e=(part_dens-bulk_dens)/bulk_dens; % void ratio (dimensionless)

% compute e_comp knowing relative COMPACTION, e_min and e_max:
RC=95;
e_min=0.2;%From Rowle
e_max=0.95;%From Rowle
e_comp=e_max-(((RC-80)*(e_max-e_min))/0.2)/100;

ri=zeros(1,length(Ri));
for n=1:1:length(Ri)
    ri(n)=Ri(n)*sqrt((4*e*(ni(n))^(1-alpha_i(n)))/6);
end
    new_ri=zeros(1,length(new_Ri));
    for n=1:1:length(new_Ri)
        new_ri(n)=new_Ri(n)*sqrt((4*e*(new_ni(n))^(1-
new_alpha_i(n)))/6);
    end

    x_ri=zeros(1,length(x_Ri));
    for n=1:1:length(x_Ri)
        x_ri(n)=x_Ri(n)*sqrt((4*e*(x_ni(n))^(1-x_alpha_i(n)))/6);
    end

% 15) Capillary head hc=(2*water surface tension* cos(water angle))/
% (gravity*water density*pore radius); for water angle=0, H2O
% density=1gr/cm^3-> the equation reduces to h=0.149/pore
radius;
hc=zeros(1, length(ri));
for n=1:1:length(ri)
    hc(n)=0.149/ri(n);

```

```

end

if min(hc)<1.5
    z=min(hc) - (min(hc) -0.4)*0.2;
else z=1.5;
end
hc_complete=[hc z 0.4];% hc (cm)

    new_hc=zeros(1, length(new_ri));
    for n=1:1:length(new_ri)
        new_hc(n)=0.149/new_ri(n);
    end
    if min(hc)<1.5
        y=min(new_hc) - (min(new_hc) -0.4)*0.2;
    else y=1.5;
    end
    new_hc_complete=[new_hc y 0.4];

    x_hc=zeros(1, length(x_ri));
    for n=1:1:length(x_ri)
        x_hc(n)=0.149/x_ri(n);
    end

    if min(x_hc)<1.5
        x_y=min(x_hc) - (min(x_hc) -0.4)*0.2;
    else x_y=1.5;
    end
    x_hc_complete=[x_hc x_y 0.4];

% Get values on curve with shape-preserving piecewise cubic
interpolation:
final_Theta_i=0.01:0.2:(0.95*porosity);
final_hc=interp1(Theta_i_ext, hc_complete, final_Theta_i, 'pchip');
%plot(Theta_i, hc,'o', new_Theta_i, new_hc, '-');

    new_final_Theta_i_1=logspace(-2,
log(0.94*new_porosity)/log(10),200);
    %logscaled interpolated data
    new_final_Theta_i_2=0.02:0.2:(0.95*new_porosity);
    %initial data
    new_final_Theta_i=sort([new_final_Theta_i_1,new_final_Theta_i_2]);
    % this puts together the two datasets and then put them in order
    new_final_hc=interp1(new_Theta_i_ext, new_hc_complete,...
        new_final_Theta_i, 'pchip');

    x_final_Theta_i_1=logspace(-2, log(0.94*x_porosity)/log(10),200);
    %logscaled interpolated data
    x_final_Theta_i_2=0.02:0.2:(0.95*x_porosity);
    %initial data
    x_final_Theta_i=sort([x_final_Theta_i_1,x_final_Theta_i_2]);
    % this puts together the two datasets and then put them in order
    x_final_hc=interp1(x_Theta_i_ext, x_hc_complete,...
        x_final_Theta_i, 'pchip');

%-----

```

```

% Following, correction for gravel content for the Theta-matric
potential
% is applied, according to (Bouwer and Rice 1984)and (Mehuys et al.
1974:
% Theta-matric potential curves are multiplied by(1-gravel content)
%-----
%-----
% After correcting the Theta-matric potential curves for gravel
content
% with Bower and Rice, The curves are extended at the lower matric
% potential for the gravel fraction
%-----
Theta_gravel=final_Theta_i *(1-gravel);
new_Theta_gravel=new_final_Theta_i *(1-new_gravel);
x_Theta_gravel=x_final_Theta_i *(1-x_gravel);

*****
% VG applied to the computed AP data points compensated for gravel
content
*****

%Datapoints used: "new_Theta_i_ext", and "new_hc_complete*(1-gravel)"
Theta_AP_VG = new_Theta_gravel;
hc_AP_VG = new_final_hc*(1-new_gravel);

AP_Theta_s=29.7;
AP_Theta_r=0.45;
AP_Alpha_vg=0.145;
AP_N=2.68;
AP_m=1-(1/AP_N);

AP_water_content_VG = ones(1,length(hc_AP_VG));
for n=1:length(hc_AP_VG)
    AP_water_content_VG(n)=AP_Theta_r+((AP_Theta_s-AP_Theta_r)/((1+...
        (AP_Alpha_vg * hc_AP_VG(n))^AP_N)^AP_m));
end

%%
*****
% Mualem model applied to the Arya-Paris curves
*****

%-----
% PURPOSE:
%Using the Theta(psi)function developed with
%Arya-Paris model, develop the unsaturated hydraulic conductivity curve
%Kr(psi)
%-----

%-----
%NOTE: from here on I use the 11 intervals curve adjusted for gravel
%content from the Arya-Paris model
%-----

%Step 1: Define Th_r=residual water content and Th_s=saturation water

```

```

%content, then compute Se for the entire range of moisture:

Th_r=min((new_Theta_gravel)/100);
Th_s=max((new_Theta_gravel)/100);

Se=zeros(1,length( new_Theta_gravel));
for n=1:1:length( new_Theta_gravel);
    Se(n)=(new_Theta_gravel(n)/100-Th_r)/(Th_s-Th_r);
end

%Step 2: Relate the matric potential to Se and then fit an equation
%which will be the integrand for the Mualem Eq.

SeContinv=@(x) interp1(Se,1./new_final_hc,x,'spline');
%continuous Se interpolated as a function
Q1=@(v) quad(SeContinv,0,v);%the top integral of Mualem
FI=quad(SeContinv,0,1);% the bottom integral of Mualem
Sevec=zeros(1,length(Se));

for j=1:length(Se)
    Sevec(j)=Q1(Se(j))/FI;
end
Sevec;

%Step 3: Compute the integrals for Mualem eq:
Kr=zeros(1,length(Sevec));
for n=1:1:length(Sevec)
    Kr(n)=((Se(n))^0.5)*Sevec(n)^2;
end

Ksat=1.75;% as calibrated for the Alumni lot
Theta_range=new_Theta_gravel/100;% dimensionless
Phi_range=(new_final_hc); % centimeters
K_range=Kr*Ksat;%cm/min (the units of Ksat)

%%%%%%%%%%%%%%%%%%%%%%%%%%%%%%%%%%%%%%%%%%%%%%%%%%%%%%%%%%%%%%%%%%%%%%%%
% Mualem model applied to the Arya-Paris curves over 'x' intervals
%%%%%%%%%%%%%%%%%%%%%%%%%%%%%%%%%%%%%%%%%%%%%%%%%%%%%%%%%%%%%%%%%%%%%%%%
%-----
%NOTE: from here on I use the x size intervals curve adjusted for
gravel
%content from the Arya-Paris model
%-----

x_Th_r=min((x_Theta_gravel)/100);
x_Th_s=max((x_Theta_gravel)/100);%max(new_Theta_gravel);

x_Se=zeros(1,length( x_Theta_gravel));
for n=1:1:length( x_Theta_gravel);
    x_Se(n)=(x_Theta_gravel(n)/100-x_Th_r)/(x_Th_s-x_Th_r);
end

%Step 2: Relate the matric potential to Se and then fit an equation
%which will be the integrand for the Mualem Eq.

```

```

x_SeContinv=@(x) interp1(x_Se,1./x_final_hc,x,'spline');%continuous Se
interpolated as a function
x_Q1=@(v) quad(x_SeContinv,0,v);%the top integral of Mualem
x_FI=quad(x_SeContinv,0,1);% the bottom integral of Mualem
x_Sevec=zeros(1,length(x_Se));

for j=1:length(x_Se)
    x_Sevec(j)=x_Q1(x_Se(j))/x_FI;
end
x_Sevec;

%Step 3: Compute the integrals for Mualem eq:
x_Kr=zeros(1,length(x_Sevec));
for n=1:length(x_Sevec)
    x_Kr(n)=((x_Se(n))^0.5)*x_Sevec(n)^2;
end

Ksat=4.14; % 3.6cm/min (from Lab report)
x_Theta_range=x_Theta_gravel/100;% dimensionless
x_Phi_range=(x_final_hc); % centimeters
x_K_range=x_Kr*Ksat;%cm/min (the units of Ksat)

%%
%Lab results:
head_1=[0.1 16 38    105 337 8566 17745 33347 62820 120438 711412
858458];
water_content_1=[29.3  6.2356 2.2158    1.7067 1.3183 0.5563 0.4511 ...
0.3533 0.3082  0.2706  0.2105  0.1869];

water_content_2=0.02:0.2:water_content_1(1);
head_2=interp1(water_content_1, head_1, water_content_2, 'pchip');

Theta_s=29.3;
Theta_r=0.4438;
Alpha_vg=0.2996;
N=2.0327;
m=1-(1/N);

water_content_VG = ones(1,length(head_2));
for n=1:length(head_2)
    water_content_VG(n)=Theta_r+((Theta_s-Theta_r)/((1+(Alpha_vg *
head_2(n))^N)^m));
end

%%%%%%%%%%%%%%%%%%%%%%%%%%%%%%%%%%%%%%%%%%%%%%%%%%%%%%%%%%%%%%%%%%%%%%%%
%Mualem model applied to measured data + fitted VG curves
%%%%%%%%%%%%%%%%%%%%%%%%%%%%%%%%%%%%%%%%%%%%%%%%%%%%%%%%%%%%%%%%%%%%%%%%

% Step 1:
Th_r_VG=min((water_content_VG)/100);
Th_s_VG=max((water_content_VG)/100);

Se_VG=zeros(1,length( water_content_VG));

```

```

for n=1:1:length( water_content_VG);
    Se_VG(n)=(water_content_VG(n)/100-Th_r_VG)/(Th_s_VG-Th_r_VG);
end

%Step 2:Relate the matric potential to Se and then fit an equation
%which will be the integrand for the Mualem Eq.

rmin=0.0;
rmax=1.0;
xi=[rmin:(rmax-rmin)/1000:rmax];
yi = interp1( Se_VG,head_2,xi,'spline');

SeContinv_VG=@(x) interp1(Se_VG,1./head_2,x,'spline');%continuous Se
interpolated as a function
Q1_VG=@(v) quad(SeContinv_VG,0,v);%the top integral of Mualem
FI_VG=quad(SeContinv_VG,0,1);% the bottom integral of Mualem
Sevec_VG=zeros(1,length(Se_VG));

for j=1:length(Se_VG)
    Sevec_VG(j)=Q1_VG(Se_VG(j))/FI_VG;
end
Sevec_VG;

%Step 3: Compute the integrals for Mualem eq:

Kr_VG=zeros(1,length(Sevec_VG));
for n=1:1:length(Sevec_VG)
    Kr_VG(n)=((Se_VG(n))^0.5)*Sevec_VG(n)^2;
end

theta_lower=[4.5 4.5];
theta_upper=[25 25];
hc_limits=[10^-1 10^7];

figure(1)
h=semilogy(new_Theta_i_ext, new_hc_complete,'*k',
new_final_Theta_i,...
    new_final_hc, ':k',new_Theta_gravel, new_final_hc, '-.k',...
    AP_water_content_VG,hc_AP_VG,'--k',...
    water_content_1, head_1,'squarek',...
    water_content_VG,head_2,'-k', theta_lower,hc_limits,'-k',...
    theta_upper,hc_limits,'-k'),
    %title ('PP - Arya-Paris Model - Comparison of Moisture Retention
Curves'),
    xlabel('Volumetric Moisture Content-Theta(%)'), ylabel...
    ('Matric Potential(-cm)'), legend...
    (' A-P data points (<2mm)',...
    'A-P interpolation (<2mm)',...
    'A-P adj. for gravel',...
    'VG fitted to A-P data points',...
    'Measured data points',...
    'VG fitted to measured'),...
    set(h(2),'linewidth',2);...
    set(h(3),'linewidth',2);...
    set(h(4),'linewidth',2);...

```

```

set(h(6), 'linewidth', 2);...
annotation('doublearrow', [0.2429 0.6797], [0.5228 0.5219]),...
annotation('textbox', [0.3643 0.5267 0.1152 0.04375]),...
'String', {'Operating range'},...
'LineStyle', 'none');

k_limits=[10^0 10^-5];

figure(2)
h=semilogy(new_Theta_gravel, Kr, '-.k', water_content_VG, Kr_VG, '-k',...
theta_lower, k_limits, '-k', theta_upper, k_limits, '-k');
%title('PP Unsaturated Hydraulic Conductivity Curves'),
xlabel('Moisture Content-Theta(%)'), ylabel...
('Relative Hyraulic Conductivity'), axis([0,32,10^-5,1]);
legend('A-P - Mualem', 'Measured-VG-Mualem'),...
set(legend, 'Position', [0.1756 0.7937 0.3357 0.1]);...
set(h(1), 'linewidth', 2);...
set(h(2), 'linewidth', 2);...
annotation('doublearrow', [0.2518 0.7393], [0.1728 0.1714]),...
annotation('textbox', [0.3714 0.181 0.2803 0.0514]),...
'String', {'Operating range'},...
'FitBoxToText', 'off',...
'LineStyle', 'none');

%%
%-----
%-----
% Model Performance
%-----
%-----

theta=4:1:25;
h_AP_interp=interp1(new_Theta_gravel, new_final_hc, theta, 'pchip');
h_AP_VG =interp1(AP_water_content_VG, hc_AP_VG, theta, 'pchip');
h_measured_VG = interp1(water_content_VG, head_2, theta, 'pchip');

P1=h_AP_interp;
P2=h_AP_VG;
O=h_measured_VG;

%for RMSE:
P1mO=P1-O;
P2mO=P2-O;
RMSE1= sqrt((1/length(theta))*(sum((P1mO).^2))/length(P1));
% root mean square error (cm of metric potential);
RMSE2= sqrt((1/length(theta))*(sum((P2mO).^2))/length(P2));
% root mean square error (cm of metric potential);

% for MAE, Mean absolute error:
OmP1=O-P1;
OmP2=O-P2;
Obar=mean(O);
MAE1=sum(OmP1)*(1/length(P1));
MAE2=sum(OmP2)*(1/length(P2));

% for R^2:
P1bar=mean(P1);

```



```
P2bar=mean(P2);  
Rsqr1=(sum((O-Obar).*(P1-P1bar))/((sum((O-Obar).^2)^0.5)*...  
    (sum((P1-P1bar).^2)^0.5)))^2;  
Rsqr2=(sum((O-Obar).*(P2-P2bar))/((sum((O-Obar).^2)^0.5)*...  
    (sum((P2-P2bar).^2)^0.5)))^2;
```

Appendix D: The Matlab code for obtaining the $\theta - \psi$ - Kr curves for the SF filter media

```

*****
% Arya-Paris Mathematical model for the Sand Filter - filter media
*****

%-----
% PURPOSE:
% Derive the MRC - the Theta(psi) function
% This function will adjusted for gravel content (anything >2mm),
% then is used to derive the Kr(psi) with Mualem model
%-----

%% Standard sieves fractions:
%[pan, #200 #100 #80 #40 #20 #10 #4 ]
sieves_size=[0 0.075 0.15 0.18 0.425 0.85 2 4.75 6.35 12.7 ]; %mm

%Complete soil fractions as used by Arya-Paris model plus the soil
%particles greater then 2mm, minus fractions up to 0.075mm

all_fraction_size=[0 0.075 0.100 0.150 0.200 0.300 0.400 0.600
0.800...
1.000 1.500 2.000 4.75 6.35 9.53 12.7];

%The following data is read directly from the Particle Size
Distribution
%report (PSD) for each soil fraction
up_frac_mass=[0.0407 0.0546 0.3354 0.6828 0.8579 0.9237 0.9393 0.9809
1];
low_frac_mass=[0 0.0407 0.0546 0.3354 0.6828 0.8579 0.9237 0.9393
0.9809];
frac_mass=up_frac_mass -low_frac_mass;

%Interpolation of the fraction mass over the 18 intervals
new_up_frac_mass=interp1( sieves_size(2:10), up_frac_mass,...
all_fraction_size(2:16), 'pchip');% this is mass
new_low_frac_mass=interp1(sieves_size(1:9), low_frac_mass,...
all_fraction_size(1:15), 'pchip');% this is mass
new_frac_mass=new_up_frac_mass-new_low_frac_mass;

%%Verify that the total mass = 1
total_mass=sum(frac_mass);
new_total_mass=sum(new_frac_mass);

%%
%-----
% Arya-Paris model normalized to 2 mm (particles greater then 2mm are
not
% considered
%-----

```

```

% For this model only soil fractions smaller than 2mm(#10 sieve) are
used
up_mass_finesand=up_frac_mass(1:6);
low_mass_finesand=up_frac_mass(1:6);
% All Interpolated soil fractions:
new_up_mass_finesand=new_up_frac_mass(1:11);
new_low_mass_finesand=new_low_frac_mass(1:11);

% gravel content (%-ile):
gravel=up_frac_mass(9)-up_frac_mass(6); %Percent gravel
new_gravel=new_up_frac_mass(15)-new_up_frac_mass(11); %Percent
gravel

% 1) Di= Mean particle diameter for each soil fraction (cm):
up_bound_diam=sieves_size(2:7);%mm
low_bound_diam=sieves_size(1:6);%mm
Di=(up_bound_diam+low_bound_diam)/(2*10); %cm
% New Di:
new_up_bound_diam=all_fraction_size(2:12);
new_low_bound_diam=all_fraction_size(1:11);
new_Di=(new_up_bound_diam+new_low_bound_diam)/(2*10); %cm

% 2) Cumulative Mass for all soil fractions:
cumm_mass_frac=up_mass_finesand;
%New Cumulative Mass for interpolated soil fractions
new_cumm_mass_frac=new_up_mass_finesand;

% 3) Ri= Mean particle radius for each soil fractions (cm):
Ri=Di/2;
%New_Ri= Mean particle radius for interpolated soil fractions (cm):
new_Ri=new_Di/2;

% 4) Wi= solid mass/unit sample in (g/g)...normalized
Wi_cumm=[(cumm_mass_frac(1)*1)/cumm_mass_frac(6)...
(cumm_mass_frac(2)*1)/cumm_mass_frac(6)...
(cumm_mass_frac(3)*1)/cumm_mass_frac(6)...
(cumm_mass_frac(4)*1)/cumm_mass_frac(6)...
(cumm_mass_frac(5)*1)/cumm_mass_frac(6) 1];

%new_Wi= solid mass/unit sample in (g/g)...normalized
new_Wi_cumm=[(new_cumm_mass_frac(1)*1)/new_cumm_mass_frac(11)...
(new_cumm_mass_frac(2)*1)/new_cumm_mass_frac(11)...
(new_cumm_mass_frac(3)*1)/new_cumm_mass_frac(11)...
(new_cumm_mass_frac(4)*1)/new_cumm_mass_frac(11)...
(new_cumm_mass_frac(5)*1)/new_cumm_mass_frac(11)...
(new_cumm_mass_frac(6)*1)/new_cumm_mass_frac(11)...
(new_cumm_mass_frac(7)*1)/new_cumm_mass_frac(11)...
(new_cumm_mass_frac(8)*1)/new_cumm_mass_frac(11)...
(new_cumm_mass_frac(9)*1)/new_cumm_mass_frac(11)...
(new_cumm_mass_frac(10)*1)/new_cumm_mass_frac(11) 1];

Wi=zeros(1,length(Wi_cumm));
for n=2:1:length(Wi_cumm)
Wi(1)=Wi_cumm(1);

```

```

    Wi(n)=Wi_cumm(n)-Wi_cumm(n-1);
end
    new_Wi=zeros(1,length(new_Wi_cumm));
    for n=2:1:length(new_Wi_cumm)
        new_Wi(1)=new_Wi_cumm(1);
        new_Wi(n)=new_Wi_cumm(n)-new_Wi_cumm(n-1);
    end

% 5) ni=number of spherical particles for each fraction:
ro_s=2.75; %particle density (grams/cm3)
ni=zeros(1,length(Ri));
for n=1:1:length(Ri)
    ni(n)=(3*Wi(n))/(4*pi*ro_s*(Ri(n))^3);
end
    new_ni=zeros(1,length(new_Ri));
    for n=1:1:length(new_Ri)
        new_ni(n)=(3*new_Wi(n))/(4*pi*ro_s*(new_Ri(n))^3);
    end

% 6) Theta_i= volumetric water content corresponding to each fraction.
This
    % is computed by dividing the effective pore volume to the bulk
volume
    % for each fraction.

%Or, compute porosity from Particle Size Distribution data with Vukovic
eq:
d60=interp1(cumm_mass_frac, Di, 0.6, 'pchip');
d10=interp1(cumm_mass_frac, Di, 0.1, 'pchip');

    new_d60=interp1(new_cumm_mass_frac, new_Di, 0.6, 'pchip');
    new_d10=interp1(new_cumm_mass_frac, new_Di, 0.1, 'pchip');

u=d60/d10;%uniformity coefficient
    new_u=new_d60/new_d10;

porosity=0.225*(1+0.83^u)*100;
    new_porosity=0.225*(1+0.83^new_u)*100;

Sw=0.9; %maximum water content to porosity

Theta_i=zeros(1, length(Wi_cumm));
partsum_Wi_cumm=zeros(1, length(Wi_cumm));
for n=2:1:length(Wi_cumm)
    partsum_Wi_cumm(1)=Wi_cumm(1);
    partsum_Wi_cumm(n)=partsum_Wi_cumm(n-1)+Wi_cumm(n);
    Theta_i(n)=porosity*Sw*(partsum_Wi_cumm(n)/sum(Wi_cumm));
end
Theta_i_ext= [Theta_i 0.925*porosity 0.95*porosity];%curve extended to
%include two more data points corresponding to fine gravel (2-11mm)
%and coarse gravel (<11mm)

    new_Theta_i=zeros(1, length(new_Wi_cumm));
    new_partsum_Wi_cumm=zeros(1, length(new_Wi_cumm));
    for n=2:1:length(new_Wi_cumm)

```

```

        new_partsum_Wi_cumm(1)=new_Wi_cumm(1);
        new_partsum_Wi_cumm(n)=new_partsum_Wi_cumm(n-
1)+new_Wi_cumm(n);
        new_Theta_i(n)=new_porosity*Sw*(new_partsum_Wi_cumm(n)/...
            sum(new_Wi_cumm));
    end
    new_Theta_i_ext= [new_Theta_i 0.925*new_porosity...
        0.95*new_porosity];%curve extended to include
    %two more data points corresponding to fine gravel(2-11mm)
    %and coarse gravel (<11mm)
    %%

%-----
% From here on, Method 2(Similarity principle) is followed from Arya
et
% al. (1999) for finding alpha scaling factor for a sandy soil.
%-----

% 12) LogNi= a+b*log(Wi/Ri^3); with a=-2.478 and b=1.490 for SAND
logNi=zeros(1, length(Wi));
for n=1:1:length(Wi)
    a=-2.478;
    b=1.490;
    logNi(n)=a+b*log10(Wi(n)/((Ri(n))^3));
end
    new_logNi=zeros(1, length(new_Wi));
    for n=1:1:length(new_Wi)
        a=-2.478;
        b=1.490;
        new_logNi(n)=a+b*log10(new_Wi(n)/((new_Ri(n))^3));
    end

% 13) alpha_i=log(Ni)/log(ni) scaling parameter for pore length:
alpha_i=zeros(1,length(ni));
for n=1:1:length(ni)
    alpha_i(n)=logNi(n)/log10(ni(n));
end
    new_alpha_i=zeros(1,length(new_ni));
    for n=1:1:length(new_ni)
        new_alpha_i(n)=new_logNi(n)/log10(new_ni(n));
    end

% 14) ri=pore radii;
bulk_dens=1.63; % bulk density (grams/cm^3)
part_dens=2.75; % particle density (gr/cm^3)
e=(part_dens-bulk_dens)/bulk_dens; % void ratio (dimensionless)

% compute e_comp knowing relative compaction, e_min and e_max:
RC=95;
e_min=0.2;%From Rowle
e_max=0.95;%From Rowle
e_comp=e_max-(((RC-80)*(e_max-e_min))/0.2)/100;

ri=zeros(1,length(Ri));

```

```

for n=1:1:length(Ri)
    ri(n)=Ri(n)*sqrt((4*e*(ni(n))^(1-alpha_i(n)))/6);
end
    new_ri=zeros(1,length(new_Ri));
    for n=1:1:length(new_Ri)
        new_ri(n)=new_Ri(n)*sqrt((4*e*(new_ni(n))^(1-
new_alpha_i(n)))/6);
    end

% 15) Capillary head hc=(2*water surface tension* cos(water angle))/
% (gravity*water density*pore radius); for water angle=0, H2O
% density=1gr/cm^3-> the equation reduces to h=0.149/pore
radius;
hc=zeros(1, length(ri));
for n=1:1:length(ri)
    hc(n)=0.149/ri(n);
end

if min(hc)<1.5
z=min(hc) - (min(hc) - 0.4)*0.2;
else z=1.5;
end
hc_complete=[hc z 0.4];% hc (cm)

    new_hc=zeros(1, length(new_ri));
    for n=1:1:length(new_ri)
        new_hc(n)=0.149/new_ri(n);
    end

    if min(new_hc)<1.5
y=min(new_hc) - (min(new_hc) - 0.4)*0.2;
else y=1.5;
end
    new_hc_complete=[new_hc y 0.4];% hc (cm)

%
*****
% Get values on curve with shape-preserving piecewise cubic
interpolation:
final_Theta_i=0.01:0.2:(0.95*porosity);
final_hc=interp1(Theta_i_ext, hc_complete, final_Theta_i, 'pchip');
%plot(Theta_i, hc,'o', new_Theta_i, new_hc, '-');
    new_final_Theta_i_1=logspace(-2,
log(0.94*new_porosity)/log(10),200);
    %logscaled interpolated data
    new_final_Theta_i_2=0.02:0.2:(0.95*new_porosity);
    %initial data
    new_final_Theta_i=sort([new_final_Theta_i_1,new_final_Theta_i_2]);
% this puts together the two datasets and then put them in order
new_final_hc=interp1(new_Theta_i_ext, new_hc_complete,...
    new_final_Theta_i, 'pchip');

%-----
% Following, correction for gravel content for the Theta-matric
potential

```

```

% is applied, according to (Bouwer and Rice 1984) and (Mehuys et al.
1974:
% Theta-matric potential curves are multiplied by(1-gravel content)
%-----
%-----
% After correcting the Theta-matric potential curves for gravel
content
% with Bower and Rice, the curves are extended at the lower matric
% potential for gravel effect
%-----
Theta_gravel=final_Theta_i *(1-gravel);
new_Theta_gravel=new_final_Theta_i *(1-new_gravel);

*****
% VG applied to the computed AP data points compensated for gravel
content
*****

%Datapoints used: "new_Theta_i_ext", and "new_hc_complete*(1-gravel)"
Theta_AP_VG = new_Theta_i_ext;
hc_AP_VG = new_hc_complete*(1-new_gravel);

AP_Theta_s=34.56;
AP_Theta_r=0.45;
AP_Alpha_vg=0.145;
AP_N=2.68;
AP_m=1-(1/AP_N);

AP_water_content_VG = ones(1,length(hc_AP_VG));
for n=1:length(hc_AP_VG)
    AP_water_content_VG(n)=AP_Theta_r+((AP_Theta_s-AP_Theta_r)/((1+...
        (AP_Alpha_vg * hc_AP_VG(n))^AP_N)^AP_m));
end

%%

*****
% Mualem model
*****

%-----
% PURPOSE:
%Using the Theta(psi)function developed with
%Arya-Paris model, develop the unsaturated hydraulic conductivity curve
%Kr(psi)
%-----

%-----
%NOTE: from here on I use the 11 intervals curve adjusted for gravel
%content from the Arya-Paris model
%-----

%Step 1: Define Th_r=residual water content and Th_s=saturation water

```

```

%content, then compute Se for the entire range of moisture:

Th_r=min((new_Theta_gravel)/100);
Th_s=max((new_Theta_gravel)/100);

Se=zeros(1,length( new_Theta_gravel));
for n=1:1:length( new_Theta_gravel);
    Se(n)=(new_Theta_gravel(n)/100-Th_r)/(Th_s-Th_r);
end

%Step 2: Relate the matric potential to Se and then fit an equation
%which will be the integrand for the Mualem Eq.

SeContinv=@(x) interp1(Se,1./new_final_hc,x,'spline');%continuous Se
%interpolated as a function
Q1=@(v) quad(SeContinv,0,v);%the top integral of Mualem
FI=quad(SeContinv,0,1);% the bottom integral of Mualem
Sevec=zeros(1,length(Se));

for j=1:length(Se)
    Sevec(j)=Q1(Se(j))/FI;
end
Sevec;

%Step 3: Compute the integrals for Mualem eq:
Kr=zeros(1,length(Sevec));
for n=1:1:length(Sevec)
    Kr(n)=((Se(n))^0.5)*Sevec(n)^2;
end

Ksat=0.2733; % inches/min or 16.4 in/hour;!NOTE: to be calibrated
Theta_range=new_Theta_gravel/100;
Phi_range=(new_final_hc)/2.54; % inches
K_range=Kr/Ksat;
%%
%Lab results:
head_1=[0.1 16 44 104 337 20192 31512 55069 104122 143834 710495
858458];
water_content_1=[33.1 9.9 5.0 3.5 2.6 1.3 1.14 1.12 0.8 0.7 0.5 0.4];

water_content_2=0.1:0.2:water_content_1(1);
head_2=interp1(water_content_1, head_1, water_content_2, 'pchip');

Theta_s=34.56;
Theta_r=0.001;
Alpha_vg=0.753;
N=1.4283;
m=1-(1/N);

water_content_VG = ones(1,length(head_2));
for n=1:1:length(head_2)
    water_content_VG(n)=Theta_r+((Theta_s-Theta_r)/...
((1+(Alpha_vg * head_2(n))^N)^m));

```



```

end

*****
%Mualem model applied to measured data + fitted VG curves
*****

% Step 1:
Th_r_VG=min((water_content_VG)/100);%
Th_s_VG=max((water_content_VG)/100);%max(new_Theta_gravel);

Se_VG=zeros(1,length( water_content_VG));
for n=1:1:length( water_content_VG);
    Se_VG(n)=(water_content_VG(n)/100-Th_r_VG)/(Th_s_VG-Th_r_VG);
end

%Step 2:Relate the matric potential to Se and then fit an equation
%which will be the integrand for the Mualem Eq.

rmin=0.0;
rmax=1.0;
xi=[rmin:(rmax-rmin)/1000:rmax];
yi = interp1( Se_VG,head_2,xi,'spline');

SeContinv_VG=@(x) interp1(Se_VG,1./head_2,x,'spline');%continuous Se
%interpolated as a function
Q1_VG=@(v) quad(SeContinv_VG,0,v);%the top integral of Mualem
FI_VG=quad(SeContinv_VG,0,1);% the bottom integral of Mualem
Sevec_VG=zeros(1,length(Se_VG));

for j=1:length(Se_VG)
    Sevec_VG(j)=Q1_VG(Se_VG(j))/FI_VG;
end
Sevec_VG;

%Step 3: Compute the integrals for Mualem eq:

Kr_VG=zeros(1,length(Sevec_VG));
for n=1:1:length(Sevec_VG)
    Kr_VG(n)=((Se_VG(n))^0.5)*Sevec_VG(n)^2;
end

theta_lower=[4.5 4.5];
theta_upper=[34.6 34.6];
hc_limits=[10^-1 10^7];

figure(1)
h=semilogy(new_Theta_i_ext, new_hc_complete,'*k',
new_final_Theta_i,...
    new_final_hc, ':k',new_Theta_gravel, new_final_hc, '-.k',...
    AP_water_content_VG,hc_AP_VG,'--k',...
    water_content_1, head_1,'squarek',...
    water_content_VG,head_2,'-k', theta_lower,hc_limits,'-k',...
    theta_upper,hc_limits,'-k'),

```

```

    %title('SF-Arya-Paris Model-Comparison of Moisture Retention
Curves'),
    xlabel('Volumetric Moisture content-Theta(%)'), ylabel...
    ('Matric Potential(-cm)'), legend...
    (' A-P data points(<2mm)',...
    'A-P intepolation (<2mm)',...
    'A-P adj. for gravel',...
    'VG fitted to A-P datapoints',...
    'Measured datapoints',...
    'VG fitted to measured'),...
    set(h(2),'linewidth',2);...
    set(h(3),'linewidth',2);...
    set(h(4),'linewidth',2);...
    set(h(6),'linewidth',2);...
    annotation('doublearrow',[0.2295 0.7969],[0.5631 0.5625]),...
    annotation('textbox',[0.4448 0.5661 0.1152 0.04375]),...
    'String',{'Operating range'},...
    'LineStyle','none');

```

```

k_limits=[10^0 10^-5];

```

```

figure(2)
h=semilogy(new_Theta_gravel, Kr, '-.k',water_content_VG,Kr_VG, '-k',...
    theta_lower,k_limits,'-k', theta_upper,k_limits,'-k');
%title('SF - Unsaturated Hydraulic Conductivity Curves'),
xlabel('Moisture Content-Theta(%)'), ylabel...
('Relative Hyraulic Conductivity'), axis([0,40,10^-5,1]);
legend('A-P - Mualem', 'Measured-VG-Mualem'),...
set(legend,'Position',[0.1756 0.7937 0.3357 0.1]);...
set(h(1),'linewidth',2);...
set(h(2),'linewidth',2);...
annotation('doublearrow',[0.225 0.7946],[0.1728 0.1714]),...
annotation('textbox',[0.3714 0.181 0.2803 0.0514]),...
'String',{'Operating range'},...
'FitBoxToText','off',...
'LineStyle','none');

```

Appendix E: The Matlab code for obtaining the $\theta - \psi - K_r$ curves for the GW filter media

```

*****
% Arya-Paris Mathematical model for the Gravel Wetland topsoil (with
% PSD from wet sieve analysis)
*****

%-----
% PURPOSE:
% Derive the MRC - the Theta(psi) function
% This function will adjusted for gravel content(anything >2mm),
% then is used to derive the Kr(psi) with Mualem model
%-----

%% Standard sieves fractions:
%[pan(various diameters based on the hydrometer test), #200 #100 #80
#40 #20 #10 #4 ]
sieves_size=[0 0.0013 0.0034 0.0056 0.0077 0.0107 0.0177 0.0263
0.0364...
0.075 0.15 0.18 0.425 0.85 2 4.75]; %mm
all_fraction_mass =[0 0.123 0.168 0.224 0.246 0.268 0.302 0.347
0.358...
0.363 0.449 0.584 0.733 0.846 0.928 1];
%Complete soil fractions as used by Arya-Paris model plus the soil
%particles greater then 2mm (22 fractions)

all_fraction_size=[0 0.001 0.002 0.003 0.005 0.010 0.020 0.030
0.040...
0.050 0.075 0.100 0.150 0.200 0.300 0.400 0.600 0.800...
1.000 1.500 2.000 4.75];
%soil fractions interpolated over intervals of size x:
x=0.15;
x_fraction_sizes= logspace(-3,0.6767,75);
x_fraction_sizes_mass =interp1( sieves_size, all_fraction_mass,...
x_fraction_sizes, 'pchip');

%Following data is read directly from the Particle Size Distribution
%report(PSD)for each soil fraction
up_frac_mass=all_fraction_mass(2:length(all_fraction_mass));
low_frac_mass=all_fraction_mass(1:length(all_fraction_mass)-1);
frac_mass=up_frac_mass -low_frac_mass;

%Interpolation of the fraction mass over the 18 intervals
new_up_frac_mass=interp1( sieves_size(2:16), up_frac_mass,...
all_fraction_size(2:22), 'pchip');% this is mass
new_low_frac_mass=interp1(sieves_size(1:15), low_frac_mass,...
all_fraction_size(1:21), 'pchip');% this is mass
new_frac_mass=new_up_frac_mass-new_low_frac_mass;
% fraction mass interpolated over intervals of size x:

```

```

x_up_frac_mass=x_fraction_sizes_mass(2:length(x_fraction_sizes_mass));
x_low_frac_mass=x_fraction_sizes_mass...
(1:length(x_fraction_sizes_mass)-1);
x_frac_mass=x_up_frac_mass - x_low_frac_mass;

%%Verify that the total mass = 1
total_mass=sum(frac_mass);
new_total_mass=sum(new_frac_mass);
x_total_mass=sum(x_frac_mass);
%%

%-----
% Arya-Paris model normalized to 2 mm (particles greater then 2mm are
not
% considered
%-----

% For this model only soil fractions smaller then 2mm(#10 sieve) are
used
up_mass_finesand=up_frac_mass(1:14);
low_mass_finesand=up_frac_mass(1:14);
% All Interpolated soil fractions:
new_up_mass_finesand=new_up_frac_mass(1:21);
new_low_mass_finesand=new_low_frac_mass(1:21);
% 'm' Interpolated soil fractions:
x_up_mass_finesand=x_up_frac_mass(1:(2/x));
x_low_mass_finesand=x_low_frac_mass(1:(2/x));

% gravel content (%-ile):
gravel=up_frac_mass(15)-up_frac_mass(14); %Percent gravel
%New Gravel content(%-ile). Note: it should be the same value as
above,
%but calculated as:
new_gravel=new_up_frac_mass(21)-new_up_frac_mass(20); %Percent
gravel
x_gravel=0.11; %Percent gravel

% 1) Di= Mean particle diameter for each soil fraction (cm):
up_bound_diam=sieves_size(2:15);%mm
low_bound_diam=sieves_size(1:14);%mm
Di=(up_bound_diam+low_bound_diam)/(2*10); %cm
% New Di:
new_up_bound_diam=all_fraction_size(2:22);
new_low_bound_diam=all_fraction_size(1:21);
new_Di=(new_up_bound_diam+new_low_bound_diam)/(2*10); %cm
% x_Di:
x_up_bound_diam=x_fraction_sizes_mass(2:(2/x)+1);%mm
x_low_bound_diam=x_fraction_sizes_mass(1:(2/x));%mm
x_Di=(x_up_bound_diam+x_low_bound_diam)/(2*10); %cm

% 2) Cumulative Mass for all soil fractions:
cumm_mass_frac=up_mass_finesand;
%New Cummulative Mass for interpolated soil fractions

```

```

new_cumm_mass_frac=new_up_mass_finesand;
%New Cummmulative Mass for AP soil fractions
x_cumm_mass_frac=x_up_mass_finesand;

% 3) Ri= Mean particle radius for each soil fractions (cm):
Ri=Di/2;
    %New_Ri= Mean particle radius for interpolated soil fractions (cm):
    new_Ri=new_Di/2;
    %x_Ri= Mean particle radius for interpolated soil fractions over
    %intervals of size 'x' (cm):
    x_Ri=x_Di/2;

% 4) Wi= solid mass/unit sample in (g/g)...normalized
Wi_cumm=[(cumm_mass_frac(1)*1)/cumm_mass_frac(14)...
(cumm_mass_frac(2)*1)/cumm_mass_frac(14)...
(cumm_mass_frac(3)*1)/cumm_mass_frac(14)...
(cumm_mass_frac(4)*1)/cumm_mass_frac(14)...
(cumm_mass_frac(5)*1)/cumm_mass_frac(14)...
(cumm_mass_frac(6)*1)/cumm_mass_frac(14)...
(cumm_mass_frac(7)*1)/cumm_mass_frac(14)...
(cumm_mass_frac(8)*1)/cumm_mass_frac(14)...
(cumm_mass_frac(9)*1)/cumm_mass_frac(14)...
(cumm_mass_frac(10)*1)/cumm_mass_frac(14)...
(cumm_mass_frac(11)*1)/cumm_mass_frac(14)...
(cumm_mass_frac(12)*1)/cumm_mass_frac(14)...
(cumm_mass_frac(13)*1)/cumm_mass_frac(14)  1];

%new_Wi= solid mass/unit sample in (g/g)...normalized
new_Wi_cumm=[(new_cumm_mass_frac(1)*1)/new_cumm_mass_frac(21)...
(new_cumm_mass_frac(2)*1)/new_cumm_mass_frac(21)...
(new_cumm_mass_frac(3)*1)/new_cumm_mass_frac(21)...
(new_cumm_mass_frac(4)*1)/new_cumm_mass_frac(21)...
(new_cumm_mass_frac(5)*1)/new_cumm_mass_frac(21)...
(new_cumm_mass_frac(6)*1)/new_cumm_mass_frac(21)...
(new_cumm_mass_frac(7)*1)/new_cumm_mass_frac(21)...
(new_cumm_mass_frac(8)*1)/new_cumm_mass_frac(21)...
(new_cumm_mass_frac(9)*1)/new_cumm_mass_frac(21)...
(new_cumm_mass_frac(10)*1)/new_cumm_mass_frac(21)...
(new_cumm_mass_frac(11)*1)/new_cumm_mass_frac(21)...
(new_cumm_mass_frac(12)*1)/new_cumm_mass_frac(21)...
(new_cumm_mass_frac(13)*1)/new_cumm_mass_frac(21)...
(new_cumm_mass_frac(14)*1)/new_cumm_mass_frac(21)...
(new_cumm_mass_frac(15)*1)/new_cumm_mass_frac(21)...
(new_cumm_mass_frac(16)*1)/new_cumm_mass_frac(21)...
(new_cumm_mass_frac(17)*1)/new_cumm_mass_frac(21)...
(new_cumm_mass_frac(18)*1)/new_cumm_mass_frac(21)...
(new_cumm_mass_frac(19)*1)/new_cumm_mass_frac(21)...
(new_cumm_mass_frac(20)*1)/new_cumm_mass_frac(21)  1];

%x_Wi= solid mass/unit sample in (g/g)...normalized
x_Wi_cumm=zeros(1,length(x_cumm_mass_frac));
for i=1:1:length(x_cumm_mass_frac)
    x_Wi_cumm(i)=x_cumm_mass_frac(i)/x_cumm_mass_frac...
        (length(x_cumm_mass_frac));
end

```

```

Wi=zeros(1,length(Wi_cumm));
for n=2:1:length(Wi_cumm)
    Wi(1)=Wi_cumm(1);
    Wi(n)=Wi_cumm(n)-Wi_cumm(n-1);
end
    new_Wi=zeros(1,length(new_Wi_cumm));
for n=2:1:length(new_Wi_cumm)
    new_Wi(1)=new_Wi_cumm(1);
    new_Wi(n)=new_Wi_cumm(n)-new_Wi_cumm(n-1);
end

    x_Wi=zeros(1,length(x_Wi_cumm));
for n=2:1:length(x_Wi_cumm)
    x_Wi(1)=x_Wi_cumm(1);
    x_Wi(n)=x_Wi_cumm(n)-x_Wi_cumm(n-1);
end

% 5) ni=number of spherical particles for each fraction:
ro_s=2.75; %particle density (grams/cm3)
ni=zeros(1,length(Ri));
for n=1:1:length(Ri)
    ni(n)=(3*Wi(n))/(4*pi*ro_s*(Ri(n))^3);
end
    new_ni=zeros(1,length(new_Ri));
for n=1:1:length(new_Ri)
    new_ni(n)=(3*new_Wi(n))/(4*pi*ro_s*(new_Ri(n))^3);
end

    x_ni=zeros(1,length(x_Ri));
for n=1:1:length(x_Ri)
    x_ni(n)=(3*x_Wi(n))/(4*pi*ro_s*(x_Ri(n))^3);
end

% 6) Theta_i= volumetric water content corresponding to each fraction.
% This is computed by dividing the effective pore volume to the
%bulk volume for each fraction.
%Or, compute porosity from Particle Size Distribution data with Vukovic
eq:
d60=interp1(cumm_mass_frac, Di, 0.6, 'pchip');
d10=interp1(cumm_mass_frac, Di, 0.1, 'pchip');

    new_d60=interp1(new_cumm_mass_frac, new_Di, 0.6, 'pchip');
    new_d10=interp1(new_cumm_mass_frac, new_Di, 0.1, 'pchip');

    x_d60=interp1(x_cumm_mass_frac, x_Di, 0.6, 'pchip');
    x_d10=interp1(x_cumm_mass_frac, x_Di, 0.1, 'pchip');

u=d60/d10;%uniformity coefficient
new_u=new_d60/new_d10;
x_u=x_d60/x_d10;

porosity=43.5;%0.225*(1+0.83^u)*100;
new_porosity=43.5;%0.225*(1+0.83^new_u)*100;
x_porosity=43.5;%0.225*(1+0.83^x_u)*100;

```

```

Sw=0.90;

Theta_i=zeros(1, length(Wi_cumm));
partsum_Wi_cumm=zeros(1, length(Wi_cumm));
for n=2:1:length(Wi_cumm)
    partsum_Wi_cumm(1)=Wi_cumm(1);
    partsum_Wi_cumm(n)=partsum_Wi_cumm(n-1)+Wi_cumm(n);
    Theta_i(n)=porosity*Sw*(partsum_Wi_cumm(n)/sum(Wi_cumm));
end
Theta_i_ext= [Theta_i 0.95*porosity];%curve extended to include
%two more data points corresponding to fine gravel (2-11mm) and coarse
%gravel (<11mm)

    new_Theta_i=zeros(1, length(new_Wi_cumm));
    new_partsum_Wi_cumm=zeros(1, length(new_Wi_cumm));
    for n=2:1:length(new_Wi_cumm)
        new_partsum_Wi_cumm(1)=new_Wi_cumm(1);
        new_partsum_Wi_cumm(n)=new_partsum_Wi_cumm(n-
1)+new_Wi_cumm(n);
        new_Theta_i(n)=new_porosity*Sw*(new_partsum_Wi_cumm(n)/...
sum(new_Wi_cumm));
    end
    new_Theta_i_ext= [new_Theta_i 0.95*new_porosity];%curve
extended
    %to include two more data points corresponding to fine
    %gravel (2-11mm) and coarse gravel (<11mm)

x_Theta_i=zeros(1, length(x_Wi_cumm));
x_partsum_Wi_cumm=zeros(1, length(x_Wi_cumm));
for n=2:1:length(x_Wi_cumm)
    x_partsum_Wi_cumm(1)=x_Wi_cumm(1);
    x_partsum_Wi_cumm(n)=x_partsum_Wi_cumm(n-1)+x_Wi_cumm(n);
    x_Theta_i(n)=x_porosity*Sw*...
(x_partsum_Wi_cumm(n)/sum(x_Wi_cumm));
end
x_Theta_i_ext= [x_Theta_i 0.95*x_porosity];%curve extended
%to include two more data points corresponding to fine
%gravel(2-11mm) and coarse gravel(<11mm)

%%
%-----
% From here on, Method 2 (Similarity principle) is followed from Arya
et
% al. (1999a) for finding alpha scaling factor for a sandy soil.
%-----

% 12) LogNi= a+b*log(Wi/Ri^3); with a=-2.478 and b=1.490 for SAND
logNi=zeros(1, length(Wi));
for n=1:1:length(Wi)
    a=-3.398;
    b=1.773;
    logNi(n)=a+b*log10(Wi(n)/((Ri(n))^3));
end
    new_logNi=zeros(1, length(new_Wi));
    for n=1:1:length(new_Wi)

```

```

        a=-3.398;
        b=1.773;
        new_logNi(n)=a+b*log10(new_Wi(n)/((new_Ri(n))^3));
    end

        x_logNi=zeros(1,length(x_Wi));
    for n=1:1:length(x_Wi)
        a=-3.398;
        b=1.773;
        x_logNi(n)=a+b*log10(x_Wi(n)/((x_Ri(n))^3));
    end

% 13) alpha_i=log(Ni)/log(ni) scaling parameter for pore length:
alpha_i=zeros(1,length(ni));
for n=1:1:length(ni)
    alpha_i(n)=logNi(n)/log10(ni(n));
end

    new_alpha_i=zeros(1,length(new_ni));
    for n=1:1:length(new_ni)
        new_alpha_i(n)=new_logNi(n)/log10(new_ni(n));
    end

    x_alpha_i=zeros(1,length(x_ni));
    for n=1:1:length(x_ni)
        x_alpha_i(n)=x_logNi(n)/log10(x_ni(n));
    end

% 14) ri=pore radii;
bulk_dens=1.35; % bulk density(grams/cm^3)
part_dens=2.75; % particle density (gr/cm^3)
e=(part_dens-bulk_dens)/bulk_dens; % void ratio (dimensionless)

% compute e_comp knowing relative compaction, e_min and e_max:
RC=95;
e_min=0.2;%From Rowle
e_max=0.95;%From Rowle
e_comp=e_max-(((RC-80)*(e_max-e_min))/0.2)/100;

ri=zeros(1,length(Ri));
for n=1:1:length(Ri)
    ri(n)=Ri(n)*sqrt((4*e*(ni(n))^(1-alpha_i(n)))/6);
end

    new_ri=zeros(1,length(new_Ri));
    for n=1:1:length(new_Ri)
        new_ri(n)=new_Ri(n)*sqrt((4*e*(new_ni(n))^(1-
new_alpha_i(n)))/6);
    end

    x_ri=zeros(1,length(x_Ri));
    for n=1:1:length(x_Ri)
        x_ri(n)=x_Ri(n)*sqrt((4*e*(x_ni(n))^(1-x_alpha_i(n)))/6);
    end

% 15) Capillary head hc=(2*water surface tension* cos(water angle))/
% (gravity*water density*pore radius); for water angle=0, H2O
% density=1gr/cm^3-> the equation reduces to h=0.149/pore
radius;

```



```

hc=zeros(1, length(ri));
for n=1:1:length(ri)
    hc(n)=0.149/ri(n);
end

if min(hc)<1.2
    z=min(hc)*0.1;
else z=1.2;
end
hc_complete=[hc z];% hc (cm)

new_hc=zeros(1, length(new_ri));
for n=1:1:length(new_ri)
    new_hc(n)=0.149/new_ri(n);
end

if min(new_hc)<1.2
    y=min(new_hc)*0.1;
else y=1.2;
end

new_hc_complete=[new_hc y];% hc (cm)

x_hc=zeros(1, length(x_ri));
for n=1:1:length(x_ri)
    x_hc(n)=0.149/x_ri(n);
end

if min(x_hc)<1.2
    x_y=min(x_hc)*0.1;
else x_y=1.2;
end

x_hc_complete=[x_hc x_y];% hc (cm)

%
*****
% Get values on curve with shape-preserving piecewise cubic
interpolation:
final_Theta_i=0.01:0.2:(0.95*porosity);
final_hc=interp1(Theta_i_ext, hc_complete, final_Theta_i, 'pchip');
%plot(Theta_i, hc,'o', new_Theta_i, new_hc, '-');
new_final_Theta_i_1=logspace(-2,
log(0.94*new_porosity)/log(10),200);
%logscaled interpolated data
new_final_Theta_i_2=0.02:0.2:(0.95*new_porosity);
%initial data
new_final_Theta_i=sort([new_final_Theta_i_1,new_final_Theta_i_2]);
% this puts together the two datasets and then put them in order
new_final_hc=interp1(new_Theta_i_ext, new_hc_complete,...
    new_final_Theta_i, 'pchip');

x_final_Theta_i_1=logspace(-2, log(0.94*x_porosity)/log(10),200);

```

```

%logscaled interpolated data
x_final_Theta_i_2=0.02:0.2:(0.95*x_porosity);
%initial data
x_final_Theta_i=sort([x_final_Theta_i_1,x_final_Theta_i_2]);
% this puts together the two datasets and then put them in order
x_final_hc=interp1(x_Theta_i_ext, x_hc_complete,...
    x_final_Theta_i, 'pchip');

%-----
% Following, correction for gravel content for the Theta-matric
potential
% is applied, according to (Bouwer and Rice 1984)and (Mehuys et al.
1974:
% Theta-matric potential curves are multiplied by(1-gravel content)
%-----
%-----
% After correcting the Theta-matric potential curves for gravel
content
% with Bower and Rice, The curves are extended at the lower matric
% potential for the gravel content
%-----
Theta_gravel=final_Theta_i *(1-gravel);
new_Theta_gravel=new_final_Theta_i *(1-new_gravel);
x_Theta_gravel=x_final_Theta_i *(1-x_gravel);

*****
% VG applied to the computed AP data points compensated for gravel
content
*****

%Datapoints used: "new_Theta_i_ext", and "new_hc_complete*(1-gravel)"
Theta_AP_VG = new_Theta_i_ext;
hc_AP_VG = new_hc_complete*(1-new_gravel);

AP_Theta_s=39.15;
AP_Theta_r=0.45;
AP_Alpha_vg=0.95;
AP_N=1.22;
AP_m=1-(1/AP_N);

AP_water_content_VG = ones(1,length(hc_AP_VG));
for n=1:1:length(hc_AP_VG)
    AP_water_content_VG(n)=AP_Theta_r+((AP_Theta_s-AP_Theta_r)/((1+...
        (AP_Alpha_vg * hc_AP_VG(n)) ^AP_N) ^AP_m));
end

%%
*****
% Mualem model
*****
%-----
% PURPOSE:
%Using the Theta(psi)function developed with
%Arya-Paris model, develop the unsaturated hydraulic conductivity curve

```

```

%Kr(psi)
%-----

%-----
%NOTE: from here on I use the 11 intervals curve adjusted for gravel
%content from the Arya-Paris model
%-----

%Step 1: Define Th_r=residual water content and Th_s=saturation water
%content, then compute Se for the entire range of moisture:

Th_r=min((new_Theta_gravel)/100);
Th_s=max((new_Theta_gravel)/100);

Se=zeros(1,length( new_Theta_gravel));
for n=1:length( new_Theta_gravel);
    Se(n)=(new_Theta_gravel(n)/100-Th_r)/(Th_s-Th_r);
end

%Step 2: Relate the matric potential to Se and then fit an equation
%which will be the integrand for the Mualem Eq.

SeContinv=@(x) interp1(Se,1./new_final_hc,x,'spline');
%continuous Se interpolated as a function
Q1=@(v) quad(SeContinv,0,v);%the top integral of Mualem
FI=quad(SeContinv,0,1);% the bottom integral of Mualem
Sevec=zeros(1,length(Se));

for j=1:length(Se)
    Sevec(j)=Q1(Se(j))/FI;
end
Sevec;

%Step 3: Compute the integrals for Mualem eq:
Kr=zeros(1,length(Sevec));
for n=1:length(Sevec)
    Kr(n)=((Se(n))^0.5)*Sevec(n)^2;
end

Ksat=0.2733; % cm/min
Theta_range=new_Theta_gravel/100;
Phi_range=(new_final_hc)/2.54; % inches
K_range=Kr/Ksat;

*****
% Mualem model applied to the Arya-Paris curves over 'x' intervals
*****

%-----
%NOTE: from here on I use the x size intervals curve adjusted for
%gravel content from the Arya-Paris model
%-----

```

```

x_Th_r=min((x_Theta_gravel)/100);
x_Th_s=max((x_Theta_gravel)/100);

x_Se=zeros(1,length( x_Theta_gravel));
for n=1:1:length( x_Theta_gravel);
    x_Se(n)=(x_Theta_gravel(n)/100-x_Th_r)/(x_Th_s-x_Th_r);
end

%Step 2: Relate the matric potential to Se and then fit an equation
%which will be the integrand for the Mualem Eq.

x_SeContinv=@(x) interp1(x_Se,1./x_final_hc,x,'spline');
%continuous Se interpolated as a function
x_Q1=@(v) quad(x_SeContinv,0,v);%the top integral of Mualem
x_FI=quad(x_SeContinv,0,1);% the bottom integral of Mualem
x_Sevec=zeros(1,length(x_Se));

for j=1:length(x_Se)
    x_Sevec(j)=x_Q1(x_Se(j))/x_FI;
end
x_Sevec;

%Step 3: Compute the integrals for Mualem eq:
x_Kr=zeros(1,length(x_Sevec));
for n=1:1:length(x_Sevec)
    x_Kr(n)=((x_Se(n))^0.5)*x_Sevec(n)^2;
end

Ksat=0.2733; % cm/min
x_Theta_range=x_Theta_gravel/100;% dimensionless
x_Phi_range=(x_final_hc); % centimeters
x_K_range=x_Kr*Ksat;%cm/min (the units of Ksat)

%%
%Lab results:
head_1=[0.1 15 43 104 337 12748 20090 36203 68531 148789 665521
858458];
water_content_1=[40.7 29.8 26 24.7 22.8 8.6 6.6 5.1 3.7 3 1.9 1.6];

water_content_2=1.6:0.2:water_content_1(1);
head_2=interp1(water_content_1, head_1, water_content_2, 'pchip');

Theta_s=39.73;
Theta_r=0.01;
Alpha_vg=0.1077;
N=1.2248;
m=1-(1/N);

water_content_VG = ones(1,length(head_2));
for n=1:1:length(head_2)
    water_content_VG(n)=Theta_r+((Theta_s-Theta_r)/((1+(Alpha_vg *...
    head_2(n))^N)^m));
end

```

```

*****
%Mualem model applied to measured data + fitted VG curves
*****

% Step 1:
Th_r_VG=min((water_content_VG)/100);%
Th_s_VG=max((water_content_VG)/100);%max(new_Theta_gravel);

Se_VG=zeros(1,length( water_content_VG));
for n=1:length( water_content_VG);
    Se_VG(n)=(water_content_VG(n)/100-Th_r_VG)/(Th_s_VG-Th_r_VG);
end

%Step 2:Relate the matric potential to Se and then fit an equation
%which will be the integrand for the Mualem Eq.

rmin=0.0;
rmax=1.0;
xi=[rmin:(rmax-rmin)/1000:rmax];
yi = interp1( Se_VG,head_2,xi,'spline');

SeContinv_VG=@(x) interp1(Se_VG,1./head_2,x,'spline');
%continuous Se interpolated as a function
Q1_VG=@(v) quad(SeContinv_VG,0,v);%the top integral of Mualem
FI_VG=quad(SeContinv_VG,0,1);% the bottom integral of Mualem
Sevec_VG=zeros(1,length(Se_VG));

for j=1:length(Se_VG)
    Sevec_VG(j)=Q1_VG(Se_VG(j))/FI_VG;
end
Sevec_VG;

%Step 3: Compute the integrals for Mualem eq:

Kr_VG=zeros(1,length(Sevec_VG));
for n=1:length(Sevec_VG)
    Kr_VG(n)=((Se_VG(n))^0.5)*Sevec_VG(n)^2;
end

theta_lower=[4.5 4.5];
theta_upper=[41 41];
hc_limits=[10^-2 10^8];

figure(1)
h=semilogy(new_Theta_i_ext, new_hc_complete,'*k',
new_final_Theta_i,...
    new_final_hc, ':k',new_Theta_gravel, new_final_hc, '-.k',...
    AP_water_content_VG,hc_AP_VG,'--k',...
    water_content_1, head_1,'squarek',...
    water_content_VG,head_2,'-k', theta_lower,hc_limits,'-k',...
    theta_upper,hc_limits,'-k'),
    %title('GW-Arya-Paris Mode -Comparison of Moisture Retention
Curves'),
    xlabel('Volumetric Moisture Content-Theta(%)'), ylabel...

```

```

('Matric Potential(-cm)'), legend...
(' A-P data points(<2mm)',...
 'A-P intepolation (<2mm)',...
 'A-P adj. for gravel',...
 'VG fitted to A-P data points',...
 'Measured data points',...
 'VG fitted to meassured'),...
set(h(2),'linewidth',2);...
set(h(3),'linewidth',2);...
set(h(4),'linewidth',2);...
set(h(6),'linewidth',2);...
annotation('doublearrow',[0.2217 0.834],[0.685 0.6844]),...
annotation('textbox',[0.4438 0.6427 0.1152 0.04375]),...
 'String',{'Operating range'},...
 'LineStyle','none');

k_limits=[10^0 10^-13];

figure(2)
h=semilogy(new_Theta_gravel, Kr, '-.k',...
 water_content_VG,Kr_VG, '-k',...
 theta_lower,k_limits,'-k', theta_upper,k_limits,'-k');
 %title ('GW - Unsaturated Hydraulic Conductivity Curves'),
 xlabel ('Volumetric Moisture Content-Theta(%)'), ylabel...
 ('Relative Hyraulic Conductivity'), axis([0,42,10^-13,1]);
 legend ('A-P - Mualem', 'Measured-VG-Mualem'),...
 set(legend,'Position',[0.1756 0.7937 0.3357 0.1]);...
set(h(1),'linewidth',2);...
set(h(2),'linewidth',2);...
annotation('doublearrow',[0.225 0.8875],[0.1728 0.1714]),...
annotation('textbox',[0.3714 0.181 0.2803 0.0514]),...
 'String',{'Operating range'},...
 'FitBoxToText','off',...
 'LineStyle','none');

```

Appendix F: The Matlab code for obtaining the $\theta - \psi$ - Kr curves for the BS filter media

```

%%%%%%%%%%%%%%%%%%%%%%%%%%%%%%%%%%%%%%%%%%%%%%%%%%%%%%%%%%%%%%%%%%%%%%%%
% Arya-Paris Mathematical model for the Bioretention soil (with PSD
% from wet sieve analysis and combustion of the wood chips)
%%%%%%%%%%%%%%%%%%%%%%%%%%%%%%%%%%%%%%%%%%%%%%%%%%%%%%%%%%%%%%%%%%%%%%%%
%-----
% PURPOSE:
% Derive the MRC - the Theta (psi) function
% This function is adjusted for gravel content (anything >2mm),
% then is used to derive the Kr(psi) with Mualem model
%-----

%% Standard sieves fractions:
%[pan(various diameters based on the hydrometer test), #200 #100 #80
#40
%#20 #10 #4 ]
sieves_size=[0 0.0014 0.0036 0.0067 0.0093 0.0131 0.0224 0.0343
0.0482...
0.075 0.15 0.18 0.425 0.85 2 4.75 ]; %mm
all_fraction_mass =[0 0.014 0.017 0.019 0.023 0.026 0.031 0.042
0.045...
0.110 0.113...
0.148 0.281 0.533 0.760 1];
%Complete soil fractions as used by Arya-Paris model plus the soil
%particles greater then 2mm (22 fractions)

all_fraction_size=[0 0.001 0.002 0.003 0.005 0.010 0.020 0.030
0.040...
0.050 0.075 0.100 0.150 0.200 0.300 0.400 0.600 0.800...
1.000 1.500 2.000 4.75];
%soil fractions interpolated over intervals of size x:
x=0.1;
x_fraction_sizes= logspace(log10(0.001),log10(4.75),75);
x_fraction_sizes_mass =interp1( sieves_size, all_fraction_mass,...
x_fraction_sizes, 'pchip');

%Following data is read directly from the Particle Size Distribution
%report (PSD)for each soil fraction
up_frac_mass=all_fraction_mass(2:length(all_fraction_mass));
low_frac_mass=all_fraction_mass(1:length(all_fraction_mass)-1);
frac_mass=up_frac_mass -low_frac_mass;

%Interpolation of the fraction mass over the 18 intervals
new_up_frac_mass=interp1( sieves_size(2:16), up_frac_mass,...
all_fraction_size(2:22), 'pchip');% this is mass
new_low_frac_mass=interp1(sieves_size(1:15), low_frac_mass,...
all_fraction_size(1:21), 'pchip');% this is mass
new_frac_mass=new_up_frac_mass-new_low_frac_mass;
% fraction mass interpolated over intervals of size x:

```

```

x_up_frac_mass=x_fraction_sizes_mass(2:length(x_fraction_sizes_mass));
x_low_frac_mass=x_fraction_sizes_mass(1:length...
(x_fraction_sizes_mass)-1);
x_frac_mass=x_up_frac_mass - x_low_frac_mass;

%%Verify that the total mass = 1
total_mass=sum(frac_mass);
new_total_mass=sum(new_frac_mass);
x_total_mass=sum(x_frac_mass);
%%

%-----
% Arya-Paris model normalized to 2 mm (particles greater then 2mm are
not
% considered
%-----

% For this model only soil fractions smaller then 2mm(#10 sieve) are
used
up_mass_finesand=up_frac_mass(1:14);
low_mass_finesand=up_frac_mass(1:14);
% All Interpolated soil fractions:
new_up_mass_finesand=new_up_frac_mass(1:21);
new_low_mass_finesand=new_low_frac_mass(1:21);
% 'm' Interpolated soil fractions:
x_up_mass_finesand=x_up_frac_mass(1:(2/x));
x_low_mass_finesand=x_low_frac_mass(1:(2/x));

% gravel content (%-ile):
gravel=up_frac_mass(15)-up_frac_mass(14); %Percent gravel
%New Gravel content (%-ile). Note: it should be the same value as
above,
%but calculated as:
new_gravel=new_up_frac_mass(21)-new_up_frac_mass(20); %Percent
gravel
x_gravel=0.11;

% 1) Di= Mean particle diameter for each soil fraction (cm):
up_bound_diam=sieves_size(2:15);%mm
low_bound_diam=sieves_size(1:14);%mm
Di=(up_bound_diam+low_bound_diam)/(2*10); %cm
% New Di:
new_up_bound_diam=all_fraction_size(2:22);
new_low_bound_diam=all_fraction_size(1:21);
new_Di=(new_up_bound_diam+new_low_bound_diam)/(2*10); %cm
% x_Di:
x_up_bound_diam=x_fraction_sizes_mass(2:(2/x)+1);%mm
x_low_bound_diam=x_fraction_sizes_mass(1:(2/x));%mm
x_Di=(x_up_bound_diam+x_low_bound_diam)/(2*10); %cm

% 2) Cummulative Mass for all soil fractions:
cumm_mass_frac=up_mass_finesand;
%New Cumulative Mass for interpolated soil fractions

```



```

new_cumm_mass_frac=new_up_mass_finesand;
%New Cummulative Mass for AP soil fractions
x_cumm_mass_frac=x_up_mass_finesand;

% 3) Ri= Mean particle radius for each soil fractions (cm):
Ri=Di/2;
    %New_Ri= Mean particle radius for interpolated soil fractions (cm):
    new_Ri=new_Di/2;
    %x_Ri= Mean particle radius for interpolated soil fractions over
    %intervals of size 'x' (cm):
    x_Ri=x_Di/2;

% 4) Wi= solid mass/unit sample in (g/g)...normalized
Wi_cumm=[(cumm_mass_frac(1)*1)/cumm_mass_frac(14)...
(cumm_mass_frac(2)*1)/cumm_mass_frac(14)...
(cumm_mass_frac(3)*1)/cumm_mass_frac(14)...
(cumm_mass_frac(4)*1)/cumm_mass_frac(14)...
(cumm_mass_frac(5)*1)/cumm_mass_frac(14)...
(cumm_mass_frac(6)*1)/cumm_mass_frac(14)...
(cumm_mass_frac(7)*1)/cumm_mass_frac(14)...
(cumm_mass_frac(8)*1)/cumm_mass_frac(14)...
(cumm_mass_frac(9)*1)/cumm_mass_frac(14)...
(cumm_mass_frac(10)*1)/cumm_mass_frac(14)...
(cumm_mass_frac(11)*1)/cumm_mass_frac(14)...
(cumm_mass_frac(12)*1)/cumm_mass_frac(14)...
(cumm_mass_frac(13)*1)/cumm_mass_frac(14) 1];

%new_Wi= solid mass/unit sample in (g/g)...normalized
new_Wi_cumm=[(new_cumm_mass_frac(1)*1)/new_cumm_mass_frac(21)...
(new_cumm_mass_frac(2)*1)/new_cumm_mass_frac(21)...
(new_cumm_mass_frac(3)*1)/new_cumm_mass_frac(21)...
(new_cumm_mass_frac(4)*1)/new_cumm_mass_frac(21)...
(new_cumm_mass_frac(5)*1)/new_cumm_mass_frac(21)...
(new_cumm_mass_frac(6)*1)/new_cumm_mass_frac(21)...
(new_cumm_mass_frac(7)*1)/new_cumm_mass_frac(21)...
(new_cumm_mass_frac(8)*1)/new_cumm_mass_frac(21)...
(new_cumm_mass_frac(9)*1)/new_cumm_mass_frac(21)...
(new_cumm_mass_frac(10)*1)/new_cumm_mass_frac(21)...
(new_cumm_mass_frac(11)*1)/new_cumm_mass_frac(21)...
(new_cumm_mass_frac(12)*1)/new_cumm_mass_frac(21)...
(new_cumm_mass_frac(13)*1)/new_cumm_mass_frac(21)...
(new_cumm_mass_frac(14)*1)/new_cumm_mass_frac(21)...
(new_cumm_mass_frac(15)*1)/new_cumm_mass_frac(21)...
(new_cumm_mass_frac(16)*1)/new_cumm_mass_frac(21)...
(new_cumm_mass_frac(17)*1)/new_cumm_mass_frac(21)...
(new_cumm_mass_frac(18)*1)/new_cumm_mass_frac(21)...
(new_cumm_mass_frac(19)*1)/new_cumm_mass_frac(21)...
(new_cumm_mass_frac(20)*1)/new_cumm_mass_frac(21) 1];

%x_Wi= solid mass/unit sample in (g/g)...normalized
x_Wi_cumm=zeros(1,length(x_cumm_mass_frac));
for i=1:length(x_cumm_mass_frac)
    x_Wi_cumm(i)=x_cumm_mass_frac(i)/x_cumm_mass_frac...
        (length(x_cumm_mass_frac));
end

```

```

Wi=zeros(1,length(Wi_cumm));
for n=2:1:length(Wi_cumm)
    Wi(1)=Wi_cumm(1);
    Wi(n)=Wi_cumm(n)-Wi_cumm(n-1);
end
    new_Wi=zeros(1,length(new_Wi_cumm));
for n=2:1:length(new_Wi_cumm)
    new_Wi(1)=new_Wi_cumm(1);
    new_Wi(n)=new_Wi_cumm(n)-new_Wi_cumm(n-1);
end

    x_Wi=zeros(1,length(x_Wi_cumm));
for n=2:1:length(x_Wi_cumm)
    x_Wi(1)=x_Wi_cumm(1);
    x_Wi(n)=x_Wi_cumm(n)-x_Wi_cumm(n-1);
end

% 5) ni=number of spherical particles for each fraction:
ro_s=2.82; %particle density (grams/cm3)
ni=zeros(1,length(Ri));
for n=1:1:length(Ri)
    ni(n)=(3*Wi(n))/(4*pi*ro_s*(Ri(n))^3);
end
    new_ni=zeros(1,length(new_Ri));
for n=1:1:length(new_Ri)
    new_ni(n)=(3*new_Wi(n))/(4*pi*ro_s*(new_Ri(n))^3);
end

    x_ni=zeros(1,length(x_Ri));
for n=1:1:length(x_Ri)
    x_ni(n)=(3*x_Wi(n))/(4*pi*ro_s*(x_Ri(n))^3);
end

% 6) Theta_i= volumetric water content corresponding to each fraction.
% This is computed by dividing the effective pore volume to the
bulk
% volume for each fraction.
%Or, compute porosity from Particle Size Distribution data with Vukovic
eq.:
d60=interp1(cumm_mass_frac, Di, 0.6, 'pchip');
d10=interp1(cumm_mass_frac, Di, 0.1, 'pchip');

    new_d60=interp1(new_cumm_mass_frac, new_Di, 0.6, 'pchip');
    new_d10=interp1(new_cumm_mass_frac, new_Di, 0.1, 'pchip');

    x_d60=interp1(x_cumm_mass_frac, x_Di, 0.6, 'pchip');
    x_d10=interp1(x_cumm_mass_frac, x_Di, 0.1, 'pchip');

u=d60/d10;%uniformity coefficient
new_u=new_d60/new_d10;
x_u=x_d60/x_d10;

porosity=49.1;%0.225*(1+0.83^u)*100;
new_porosity=49.1;%0.225*(1+0.83^new_u)*100;

```

```

x_porosity=49.1;%0.225*(1+0.83^x_u)*100;

Sw=0.90;

Theta_i=zeros(1, length(Wi_cumm));
partsum_Wi_cumm=zeros(1, length(Wi_cumm));
for n=2:1:length(Wi_cumm)
    partsum_Wi_cumm(1)=Wi_cumm(1);
    partsum_Wi_cumm(n)=partsum_Wi_cumm(n-1)+Wi_cumm(n);
    Theta_i(n)=porosity*Sw*(partsum_Wi_cumm(n)/sum(Wi_cumm));
end
Theta_i_ext= [Theta_i 0.95*porosity];%curve extended to include
%two more data points corresponding to fine gravel (2-11mm) and coarse
%gravel (<11mm)

    new_Theta_i=zeros(1, length(new_Wi_cumm));
    new_partsum_Wi_cumm=zeros(1, length(new_Wi_cumm));
    for n=2:1:length(new_Wi_cumm)
        new_partsum_Wi_cumm(1)=new_Wi_cumm(1);
        new_partsum_Wi_cumm(n)=new_partsum_Wi_cumm(n-
1)+new_Wi_cumm(n);
        new_Theta_i(n)=new_porosity*Sw*(new_partsum_Wi_cumm(n)/...
sum(new_Wi_cumm));
    end
    new_Theta_i_ext= [new_Theta_i 0.95*new_porosity];%curve
extended
%to include two more data points corresponding to fine gravel
%(2-11mm) and coarse gravel (<11mm)

x_Theta_i=zeros(1, length(x_Wi_cumm));
x_partsum_Wi_cumm=zeros(1, length(x_Wi_cumm));
for n=2:1:length(x_Wi_cumm)
    x_partsum_Wi_cumm(1)=x_Wi_cumm(1);
    x_partsum_Wi_cumm(n)=x_partsum_Wi_cumm(n-1)+x_Wi_cumm(n);
    x_Theta_i(n)=x_porosity*Sw*(x_partsum_Wi_cumm(n)/...
sum(x_Wi_cumm));
end
x_Theta_i_ext= [x_Theta_i 0.95*x_porosity];%curve extended to
%include two more data points corresponding to fine gravel (2^
%11mm) and coarse gravel (<11mm)

%%
%-----
% From here on, Method 2 (Similarity principle) is followed from Arya
% et al. (1999a) for finding alpha scaling factor for a sandy soil.
%-----

% 12) LogNi= a+b*log(Wi/Ri^3); with a=-2.478 and b=1.490 for SAND
logNi=zeros(1, length(Wi));
for n=1:1:length(Wi)
    a=-3.398;
    b=1.773;
    logNi(n)=a+b*log10(Wi(n)/((Ri(n))^3));
end
    new_logNi=zeros(1, length(new_Wi));

```

```

for n=1:1:length(new_Wi)
    a=-3.398;
    b=1.773;
    new_logNi(n)=a+b*log10(new_Wi(n)/((new_Ri(n))^3));
end

    x_logNi=zeros(1, length(x_Wi));
for n=1:1:length(x_Wi)
    a=-3.398;
    b=1.773;
    x_logNi(n)=a+b*log10(x_Wi(n)/((x_Ri(n))^3));
end

% 13) alpha_i=log(Ni)/log(ni) scaling parameter for pore length:
alpha_i=zeros(1, length(ni));
for n=1:1:length(ni)
    alpha_i(n)=logNi(n)/log10(ni(n));
end
    new_alpha_i=zeros(1, length(new_ni));
for n=1:1:length(new_ni)
    new_alpha_i(n)=new_logNi(n)/log10(new_ni(n));
end

    x_alpha_i=zeros(1, length(x_ni));
for n=1:1:length(x_ni)
    x_alpha_i(n)=x_logNi(n)/log10(x_ni(n));
end

% 14) ri=pore radii;
bulk_dens=1.35; % bulk density(grams/cm^3)
part_dens=2.75; % particle density (gr/cm^3)
e=(part_dens-bulk_dens)/bulk_dens; % void ratio (dimensionless)

% compute e_comp knowing relative compaction, e_min and e_max:
RC=95;
e_min=0.2;%From Rowle
e_max=0.95;%From Rowle
e_comp=e_max-(((RC-80)*(e_max-e_min))/0.2)/100;

ri=zeros(1, length(Ri));
for n=1:1:length(Ri)
    ri(n)=Ri(n)*sqrt((4*e*(ni(n))^(1-alpha_i(n)))/6);
end
    new_ri=zeros(1, length(new_Ri));
for n=1:1:length(new_Ri)
    new_ri(n)=new_Ri(n)*sqrt((4*e*(new_ni(n))^(1-
new_alpha_i(n)))/6);
end
    x_ri=zeros(1, length(x_Ri));
for n=1:1:length(x_Ri)
    x_ri(n)=x_Ri(n)*sqrt((4*e*(x_ni(n))^(1-x_alpha_i(n)))/6);
end

% 15) Capillary head hc=(2*water surface tension* cos(water angle))/
% (gravity*water density*pore radius); for water angle=0, H2O

```

```

        %density=1gr/cm^3-> the equation reduces to h=0.149/pore
radius;
hc=zeros(1, length(ri));
for n=1:1:length(ri)
    hc(n)=0.149/ri(n);
end

if min(hc)<1.2
    z=min(hc)*0.2;
else z=1.2;
end
hc_complete=[hc z];% hc (cm)

    new_hc=zeros(1, length(new_ri));
    for n=1:1:length(new_ri)
        new_hc(n)=0.149/new_ri(n);
    end

        if min(new_hc)<1.2
            y=min(new_hc)*0.2;
        else y=1.2;
        end

new_hc_complete=[new_hc y];% hc (cm)%NOTE:1.5 in place for
%2.5 used in the original model

x_hc=zeros(1, length(x_ri));
for n=1:1:length(x_ri)
    x_hc(n)=0.149/x_ri(n);
end

        if min(x_hc)<1.2
            x_y=min(x_hc)*0.2;
        else x_y=1.2;
        end
x_hc_complete=[x_hc x_y];% hc (cm)%NOTE:1.5 in place for
%2.5 used in the original model

%
*****
% Get values on curve with shape-preserving piecewise cubic
interpolation:
final_Theta_i=0.01:0.2:(0.95*porosity);
final_hc=interp1(Theta_i_ext, hc_complete, final_Theta_i, 'pchip');
%plot(Theta_i, hc,'o', new_Theta_i, new_hc, '-');
    new_final_Theta_i_1=logspace(-2,
log(0.94*new_porosity)/log(10),200);
        %logscaled interpolated data
    new_final_Theta_i_2=0.02:0.2:(0.95*new_porosity);
        %initial data
new_final_Theta_i=sort([new_final_Theta_i_1,new_final_Theta_i_2]);
% this puts together the two datasets and then put them in order
new_final_hc=interp1(new_Theta_i_ext, new_hc_complete,...
    new_final_Theta_i, 'pchip');

```

```

x_final_Theta_i_1=logspace(-2, log(0.94*x_porosity)/log(10),200);
    %logscaled interpolated data
x_final_Theta_i_2=0.02:0.2:(0.95*x_porosity);
    %initial data
x_final_Theta_i=sort([x_final_Theta_i_1,x_final_Theta_i_2]);
    % this puts together the two datasets and then put them in order
x_final_hc=interp1(x_Theta_i_ext, x_hc_complete,...
    x_final_Theta_i, 'pchip');

%-----
% Following, correction for gravel content for the Theta-matric
potential
% is applied, according to (Bouwer and Rice 1984)and (Mehuys et al.
1974:
% Theta-matric potential curves are multiplied by(1-gravel content)
%-----
%-----
% After correcting the Theta-matric potential curves for gravel
content
% with Bower and Rice, The curves are extended at the lower matric
% potential for the gravel content
%-----
Theta_gravel=final_Theta_i *(1-gravel);
    new_Theta_gravel=new_final_Theta_i *(1-new_gravel);
    x_Theta_gravel=x_final_Theta_i *(1-x_gravel);

*****
% VG applied to the computed AP data points compensated for gravel
content
*****

%Datapoints used: "new_Theta_i_ext", and "new_hc_complete*(1-gravel)"
Theta_AP_VG = new_Theta_i_ext;
hc_AP_VG = new_hc_complete*(1-new_gravel);

AP_Theta_s=44.15;
AP_Theta_r=0.45;
AP_Alpha_vg=2.146;
AP_N=1.34;
AP_m=1- (1/AP_N);

AP_water_content_VG = ones(1,length(hc_AP_VG));
for n=1:length(hc_AP_VG)
    AP_water_content_VG(n)=AP_Theta_r+((AP_Theta_s-AP_Theta_r)/((1+...
        (AP_Alpha_vg * hc_AP_VG(n))^AP_N)^AP_m));
end

%%
*****
% Mualem model
*****

%-----
% PURPOSE:
%Using the Theta(psi)function developed with

```

```

%Arya-Paris model, develop the unsaturated hydraulic conductivity curve
%Kr(psi)
%-----

%-----
%NOTE: from here on I use the 11 intervals curve adjusted for gravel
%content from the Arya-Paris model
%-----

%Step 1: Define Th_r=residual water content and Th_s=saturation water
%content, then compute Se for the entire range of moisture:

Th_r=min((new_Theta_gravel)/100);
Th_s=max((new_Theta_gravel)/100);

Se=zeros(1,length( new_Theta_gravel));
for n=1:1:length( new_Theta_gravel);
    Se(n)=(new_Theta_gravel(n)/100-Th_r)/(Th_s-Th_r);
end

%Step 2: Relate the matric potential to Se and then fit an equations
%which will be the integrand for the Mualem Eq.

SeContinv=@(x) interp1(Se,1./new_final_hc,x,'spline');
%continuous Se interpolated as a function
Q1=@(v) quad(SeContinv,0,v);%the top integral of Mualem
FI=quad(SeContinv,0,1);% the bottom integral of Mualem
Sevec=zeros(1,length(Se));

for j=1:length(Se)
    Sevec(j)=Q1(Se(j))/FI;
end
Sevec;

%Step 3: Compute the integrals for Mualem eq:
Kr=zeros(1,length(Sevec));
for n=1:1:length(Sevec)
    Kr(n)=((Se(n))^0.5)*Sevec(n)^2;
end

Ksat=0.2733;
Theta_range=new_Theta_gravel/100;
Phi_range=(new_final_hc)/2.54; % inches
K_range=Kr/Ksat;

%%
%Lab results:
head_1=[0.1 17 43 106 337 17745 27841 90048 162658 423013 858458];
water_content_1=[47.1 19.3 12.9 11.5 10.7 2.7 2.3 1.7 1.4 1.2 1];

water_content_2=0.1:0.2:water_content_1(1);
head_2=interp1(water_content_1, head_1, water_content_2, 'pchip');

Theta_s=47.14;

```

```

Theta_r=0.01;
Alpha_vg=2.0716;
N=1.2602;
m=1-(1/N);

water_content_VG = ones(1,length(head_2));
for n=1:1:length(head_2)
    water_content_VG(n)=Theta_r+((Theta_s-Theta_r)/...
        ((1+(Alpha_vg * head_2(n))^N)^m));
end

%%%%%%%%%%%%%%%%%%%%%%%%%%%%%%%%%%%%%%%%%%%%%%%%%%%%%%%%%%%%%%%%%%%%%%%%
%Muallem model applied to measured data + fitted VG curves
%%%%%%%%%%%%%%%%%%%%%%%%%%%%%%%%%%%%%%%%%%%%%%%%%%%%%%%%%%%%%%%%%%%%%%%%

% Step 1:
Th_r_VG=min((water_content_VG)/100);%
Th_s_VG=max((water_content_VG)/100);%max(new_Theta_gravel);

Se_VG=zeros(1,length( water_content_VG));
for n=1:1:length( water_content_VG);
    Se_VG(n)=(water_content_VG(n)/100-Th_r_VG)/(Th_s_VG-Th_r_VG);
end

%Step 2:Relate the matric potential to Se and then fit an equation
%which will be the integrand for the Muallem Eq.

rmin=0.0;
rmax=1.0;
xi=[rmin:(rmax-rmin)/1000:rmax];
yi = interp1( Se_VG,head_2,xi,'spline');

SeContinv_VG=@(x) interp1(Se_VG,1./head_2,x,'spline');
%continuous Se interpolated as a function
Q1_VG=@(v) quad(SeContinv_VG,0,v);%the top integral of Muallem
FI_VG=quad(SeContinv_VG,0,1);% the bottom integral of Muallem
Sevec_VG=zeros(1,length(Se_VG));

for j=1:length(Se_VG)
    Sevec_VG(j)=Q1_VG(Se_VG(j))/FI_VG;
end
Sevec_VG;

%Step 3: Compute the integrals for Muallem eq:

Kr_VG=zeros(1,length(Sevec_VG));
for n=1:1:length(Sevec_VG)
    Kr_VG(n)=((Se_VG(n))^0.5)*Sevec_VG(n)^2;
end

theta_lower=[4.5 4.5];
theta_upper=[48 48];
hc_limits=[10^-2 10^8];

```



```

figure(1)
h=semilogy(new_Theta_i_ext, new_hc_complete, '*k',
new_final_Theta_i,...
new_final_hc, ':k',new_Theta_gravel, new_final_hc, '-.k',...
AP_water_content_VG,hc_AP_VG,'--k',...
water_content_1, head_1,'squarek',...
water_content_VG,head_2,'-k', theta_lower,hc_limits,'-k',...
theta_upper,hc_limits,'-k'),
%title('BS- Arya-Paris Model-Comparison of Moisture Retention
Curves'),
xlabel ('Volumetric Moisture Content-Theta(%)'), ylabel...
('Matric Potential(-cm)'), legend...
(' A-P data points(<2mm)',...
'A-P interpolation (<2mm)',...
'A-P adj. for gravel',...
'VG fitted to A-P data points',...
'Measured data points',...
'VG fitted to measured'),...
set(h(2),'linewidth',2);...
set(h(3),'linewidth',2);...
set(h(4),'linewidth',2);...
set(h(6),'linewidth',2);...
annotation('doublearrow',[0.2143 0.8714],[0.5881 0.5857]),...
annotation('textbox',[0.4134 0.5405 0.1919 0.04835]),...
'String',{'Operating range'},...
'LineStyle','none');

```

```

k_limits=[10^0 10^-15];

```

```

figure(2)
h=semilogy(new_Theta_gravel, Kr, '-.k',water_content_VG,Kr_VG, '-k',...
theta_lower,k_limits,'-k', theta_upper,k_limits,'-k');
%title ('BS - Unsaturated Hydraulic Conductivity Curves'),
xlabel ('Moisture Content-Theta(%)'), ylabel...
('Relative Hydraulic Conductivity'), axis([0,49,10^-15,1]);
legend ('Arya-Paris-Mualem', 'Measured-VG-Mualem'),...
set(legend, 'Position',[0.1756 0.7937 0.3357 0.1]);...
set(h(1),'linewidth',2);...
set(h(2),'linewidth',2);...
annotation('doublearrow',[0.2232 0.8875],[0.1714 0.1714]),...
annotation('textbox',[0.4535 0.1786 0.2803 0.0514]),...
'String',{'Operating range'},...
'FitBoxToText','off',...
'LineStyle','none');

```

Appendix G: The Matlab code for the PP system for the West Edge lot

```

*****
% Mathematical model for the hydrology of a POROUS PAVEMENT system
*****
%-----
% PURPOSE:
% Create a mathematical model that would
% simulate flow through each segment of the system
%-----
% MODEL INPUT:
% System geometry and design parameters
% Precipitation data - time series
%-----
% MODEL OUTPUT:
% Outflow hydrographs - time series
%-----
%%
tic
% This section of code will read precipitation, outflow and water level
%in the system
X= importdata('9_11_2009.txt');
A=X.data;

% This section of code will convert 5 minutes data into 1 min data:
B = A(:)';
Z=5;
C = B(ones(1,Z),:);
C1 = C(:)';
C2 = reshape(C1,length(A)*5,3);
C3=C2(:,1)*2.54/5;%cm
C4=[ C3 C2(:,2)*12 C2(:,3)];
Data=C4;

% This section of code will convert 1 minute data to dt intervals
data:

MediaThickness=60.96;%60.96;%(cm)==24in
dt=1;
N=1/dt;

D = C4(:)';
C5 = D(ones(1,N),:);
C6 = C5(:)';
C7 = reshape(C6,length(C3)*1/dt,3);
C8=C7(:,1)./N;%precip datain cm/per dt interval
C9=[ C8 C7(:,2)*12 C7(:,3)*3.7854];%Precip in cm/dt;
%well water level in cm/dt; outflow in liters/dt
toc
%%
% Storm summary:
precip=Data(:,1);
total_precip=sum(precip);%depth of precipitation (cm)
Precip_volume=total_precip*5200000/1000;%liters

```

```

total_volume=sum(Data(:, 3));% gallons
%%
% This section of code will run the precipitation data through the PA
% layers

Theta_range;
Phi_range;
K_range;

%for filter media layer

M=12; %M=inches of filtering media
T=length(C8);
dz=MediaThickness/M; %inches

%Initial conditions and preallocating values

Theta=ones(T,M)*0.05;
Phi=interp1(Theta_range, Phi_range, Theta, 'pchip');
K=interp1(Theta_range, K_range, Theta, 'pchip');
Kloss=zeros(T,M);
Djplj=ones(T,M)*0.33;
Djjm1=ones(T,M)*0.33;
Flow=zeros(T,M);

%%
%step1: initialize D(difusivity) and define boundary conditions
X=zeros(T,M);
Y=zeros(T,M);

tic
for t=1:1:T

    % Boundary conditions:
    Theta_tzero=0.05;
    Theta_tMp1=0.05;
    Theta_tMp2=0.05;
    K_tzero=interp1(Theta_range, K_range, Theta_tzero, 'pchip');
    K_tMp1=interp1(Theta_range, K_range, Theta_tMp1, 'pchip');
    Phi_tzero=interp1(Theta_range, Phi_range, Theta_tzero, 'pchip');
    Phi_tMp1=interp1(Theta_range, Phi_range, Theta_tMp1, 'pchip');
    Phi_tMp2=interp1(Theta_range, Phi_range, Theta_tMp2, 'pchip');

    Djjm1(t,1)=sqrt(K(t,1)*K_tzero*interp1(TD_Deriv,PD_Deriv,...
        Theta(t,1))*interp1(TD_Deriv,PD_Deriv,Theta_tzero));
    Djjm1(t,M)=sqrt(K(t,M)*K(t,M-1)*interp1(TD_Deriv,PD_Deriv,...
        Theta(t,M))*interp1(TD_Deriv,PD_Deriv,Theta(t,M-1)));

    Djplj(t,1)=sqrt(K(t,2)*K(t,1)*interp1(TD_Deriv,PD_Deriv,...
        Theta(t,2))*interp1(TD_Deriv,PD_Deriv,Theta(t,1)));
    Djplj(t,M)=sqrt(K_tMp1*K(t,M)*interp1(TD_Deriv,PD_Deriv,...
        Theta_tMp1)*interp1(TD_Deriv,PD_Deriv,Theta(t,M)));

    for j=M-1:-1:2

```

```

Djplj(t,j)=sqrt(K(t,j+1)*K(t,j)*interp1(TD_Deriv,PD_Deriv,...
Theta(t,j+1))*interp1(TD_Deriv,PD_Deriv,Theta(t,j)));

Djjml(t,j)=sqrt(K(t,j)*K(t,j-1)*interp1(TD_Deriv,PD_Deriv,...
Theta(t,j))*interp1(TD_Deriv,PD_Deriv,Theta(t,j-1)));
end

Theta(t+1,M)=Theta(t,M)+ C8(t)/dz+(-(Djjml(t,M))*(Theta(t,M)-...
Theta(t,M-1))/dz^2-sqrt(K(t,M)*K(t,M-1))/dz)*dt;
Theta(t+1,1)=Theta(t,1)+((Djplj(t,1))*(Theta(t,2)-
Theta(t,1))/dz^2+...
sqrt(K(t,2)*K(t,1))/dz -K(t,1)/dz)*dt;

for j=M-1:-1:2
Theta(t+1,j)=Theta(t,j)+((Djplj(t,j))*(Theta(t,j+1)-
Theta(t,j))/...
dz^2+sqrt(K(t,j+1)*K(t,j))/dz-(Djjml(t,j))*(Theta(t,j)-...
Theta(t,j-1))/dz^2-sqrt(K(t,j)*K(t,j-1))/dz)*dt;
end

for j=M:-1:1
if Theta(t+1,j)<min(Theta_range)
Theta(t+1,j)=min(Theta_range);
end

if Theta(t+1,j)>max(Theta_range)
Theta(t+1,j)=max(Theta_range);
end

K(t+1,j)=interp1(Theta_range, K_range, Theta(t+1,j), 'pchip');
Phi(t+1,j)=interp1(Theta_range, Phi_range, Theta(t+1,j),
'pchip');

end

x=1:1:T+1;%needed to plot Theta at different levels
y=1:1:T;%needed to plot Theta at different levels
w=1:1:T-1;
end

toc
%%
tic
%-----
% PARALLEL DRAIN MODEL
%-----

% parameters:
% L = underdrain spacing(cm); 26 ft=793 cm
% v=voids in the crushed stone layer= 40% for stone reservoir
% according to ASTM for #57 stone
% K= hydraulic conductivity at saturation for the crushed
% stone(40000ft/day)= 4233cm/5 minutes

```

```

%LofPipe=199"=6065cm

L=793;%cm distance between pipes
v= 0.4;% dimensionless
Kstone=(400000*12*2.54/(24*60*N)); %cm/dt
LofPipe=6065;%cm

% variables:
%w =recharge rate;
%D= water depth at half distance between underdrains;

alph=zeros(T,1);
D1=zeros(T,1);
sum1=0;
sum2=zeros(T,1);
Q=zeros(T,1);
q1=zeros(T,1);
q1_depth=zeros(T,1);
Q2=zeros(T,1);

for t=2:1:T
    alph(t)=(Kstone*D1(t))/v;
    for j=1:2:1111
        sum1=(pi^2)/8;
        Exp(t)=(exp(-(j^2)*(pi^2)*alph(t)*dt/L^2))/j^2;
        sum2(t)=sum2(t)+Exp(t);
    end

    q1(t)=(K(t,1)*L)*(1-(8/pi^2)*(sum2(t))); % (cm^2/dt) per cm of
pipe,
%from one side
Q(t)=q1(t)*LofPipe*2;%*0.0026417; %cm^3/dt converted to
gallons/dt
q1_depth(t) = Q(t)/(4830958*v); %cm
Q2(t)=Q(t)/1000;% liters/ dt
D1(t+1) = D1(t) + K(t,1)/v- (q1_depth(t));%
end

toc
%%
%-----
% Mannings Equation (rating curve for a 6 inch pipe)
% and storage indication methods
%-----
tic
h_Eng=[0 0.5 1 1.5 2 2.5 3 3.5 4 4.5 5 5.5 6];%inches
h_SI=h_Eng*2.54;%cm
flow_Mann_Eng=[0 0.01 0.03 0.08 0.14 0.21 0.29 0.37 0.45 0.52 0.58...
0.61 0.57];%cfs
flow_Mann_SI=1699.01*[0 0.01 0.03 0.08 0.14 0.21 0.29 0.37 0.45 0.52...
0.58 0.61 0.57];%liters/minute

H=zeros(1,T);
FlowwithMann=zeros(1,T);

for t=1:1:T-1

```

```

H(1)=0;
FlowwithMann(t+1)=interp1(h_SI, flow_Mann_SI, H(t), 'pchip');
H(t+1)= H(t)+(K(t,1)/v - FlowwithMann(t)*1000/(4830958*v) -
0*1000/...
(4830958*v));
H(T)=H(T-1)+(K(T-1,1)/v - FlowwithMann(T-1)*1000/(4830958*v));

FlowwithMann(T)=interp1(h_SI, flow_Mann_SI, FlowwithMann(T),
'pchip');
end
FlowwithMann(FlowwithMann<0)=0;
toc
%%

figure(1)
h=plot(x',K(:,1)*4830958*0.001,'-.',y, C9(1:1:T,3),'-
',y,Q2(1:1:T),...
':',w, FlowwithMann(1:1:T-1),'--');
xlabel('Storm duration (min)'), ylabel...
(' Flow (liters/min)'), legend...
('Filter media outflow (modeled) ',...
'End of pipe outflow (observed)',...
'End of pipe outflow (Glover)',...
'End of pipe outflow (Manning)');
set(h(1), 'linewidth', 2);...
set(h(2), 'linewidth', 2);...
set(h(3), 'linewidth', 2);...
set(h(4), 'linewidth', 2);

figure (2)
mesh(Theta); figure(gcf);
xlabel('Soil depth (dz)'), ylabel...
('Storm duration (min)'), zlabel('Volumetric Moisture
Content (cm3/cm3)');
set(gca, 'YDir', 'Reverse')

figure(3)
h=plot( y',C9(1:1:T,1), '-blue');xlabel('Time (min)'), legend...
('Precipitation (cm/5 min)');
set(gca, 'YDir', 'Reverse');
set(h(1), 'linewidth', 2);
set(legend, 'Location', 'SouthEast');

```

**Appendix H: Storms used for the model calibration of the West Edge
PP system**

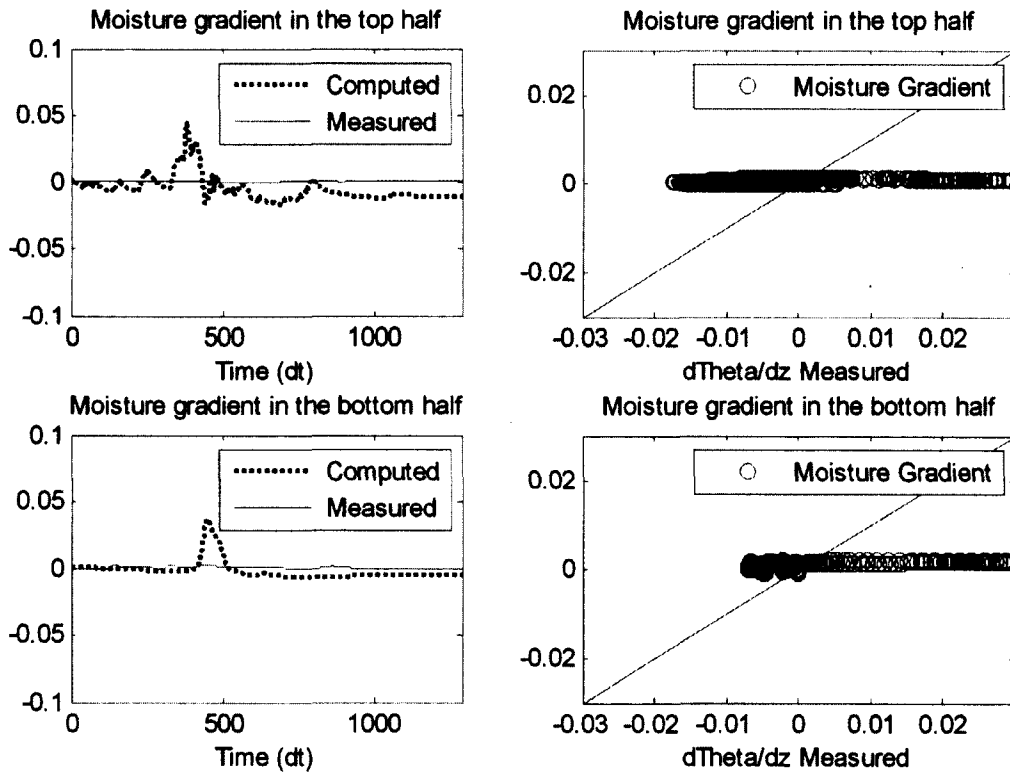
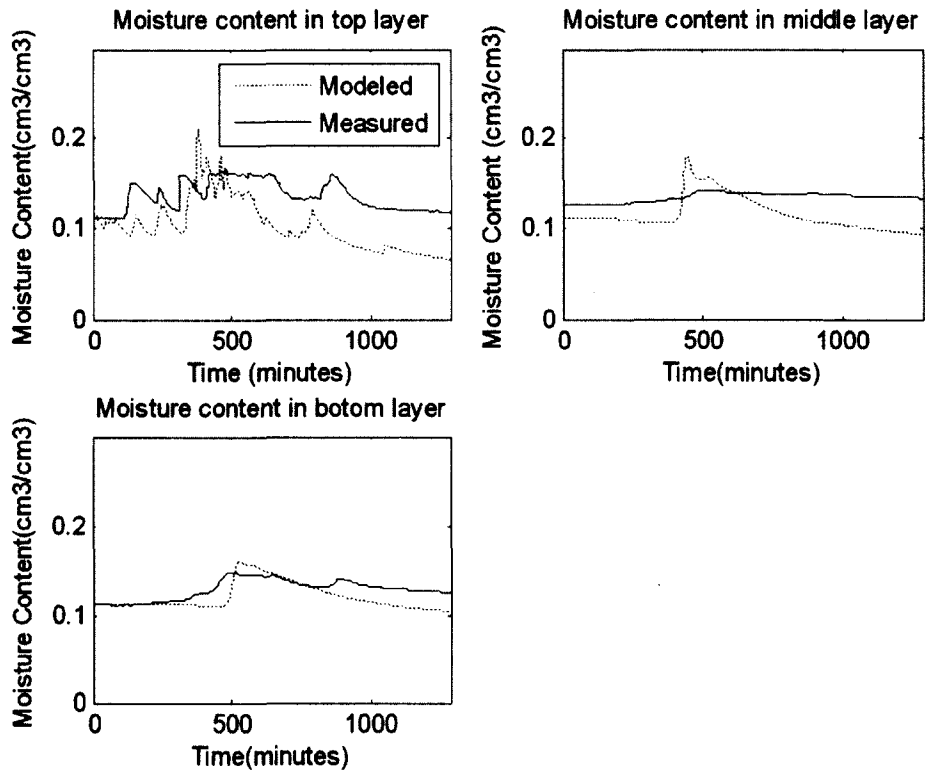
Storm Date	Precipitation (in)	Precipitation (cm)
06/11/2009	1.98	5.03
06/18/2009	1.7	4.32
07/02/2009	1.77	3.12
07/07/2009	0.7	1.78
07/23/2009	1.79	4.55
08/21/2009	0.79	2.01
08/28/2009	1.74	4.42
09/11/2009	0.94	2.39

Appendix I: Storms used for the calibration of the Alumni Lot - filter media model

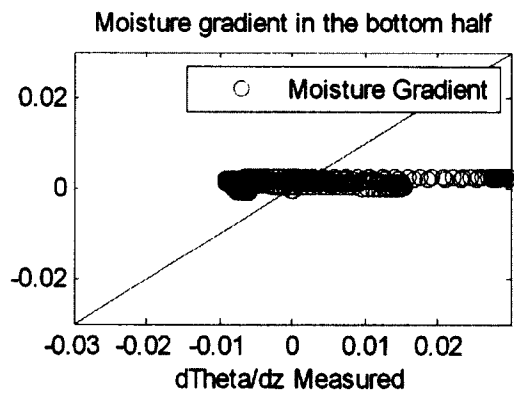
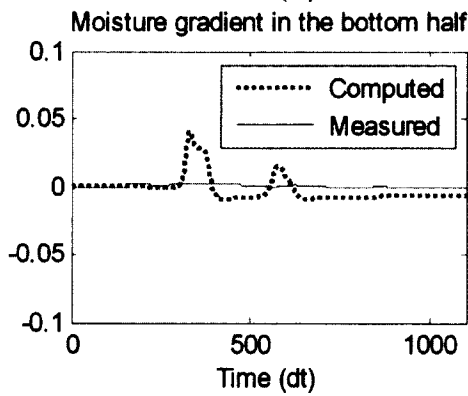
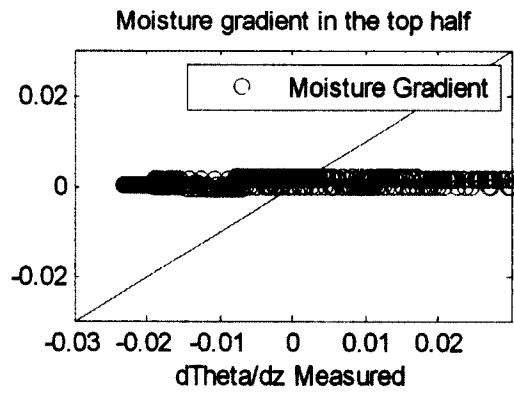
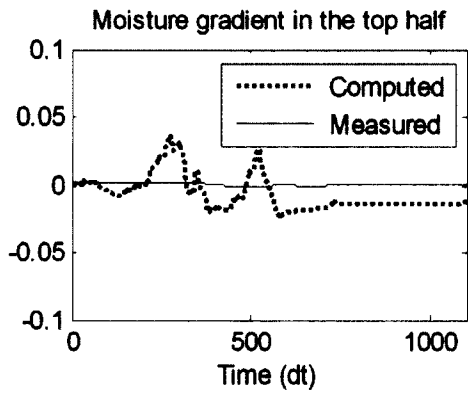
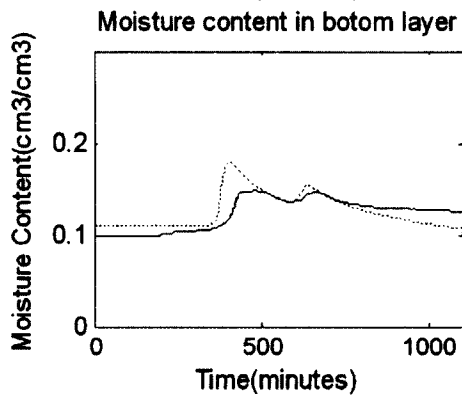
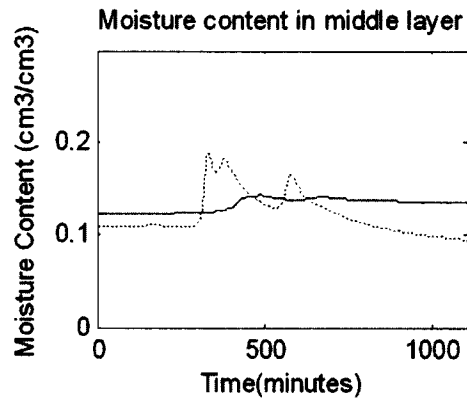
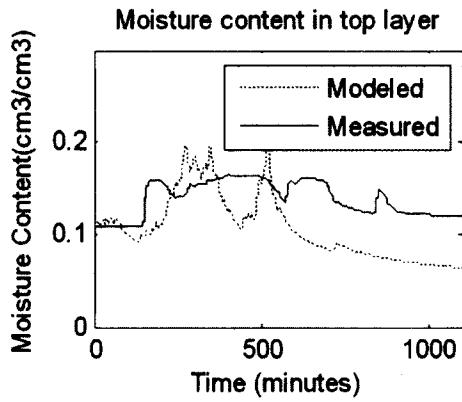
	Storm Date	Precipitation (in)	Precipitation (cm)
Calibration	11/04/2010	1.22	3.10
Storms	11/07/2010	1.00	2.54
	11/16/2010	1.28	3.25
Verification	11/26/2010	0.35	0.89
Storms	04/10/2011	0.50	1.27
	04/13/2011	0.94	2.38

Appendix J: Calibration storms for the filter media of the Alumni Lot

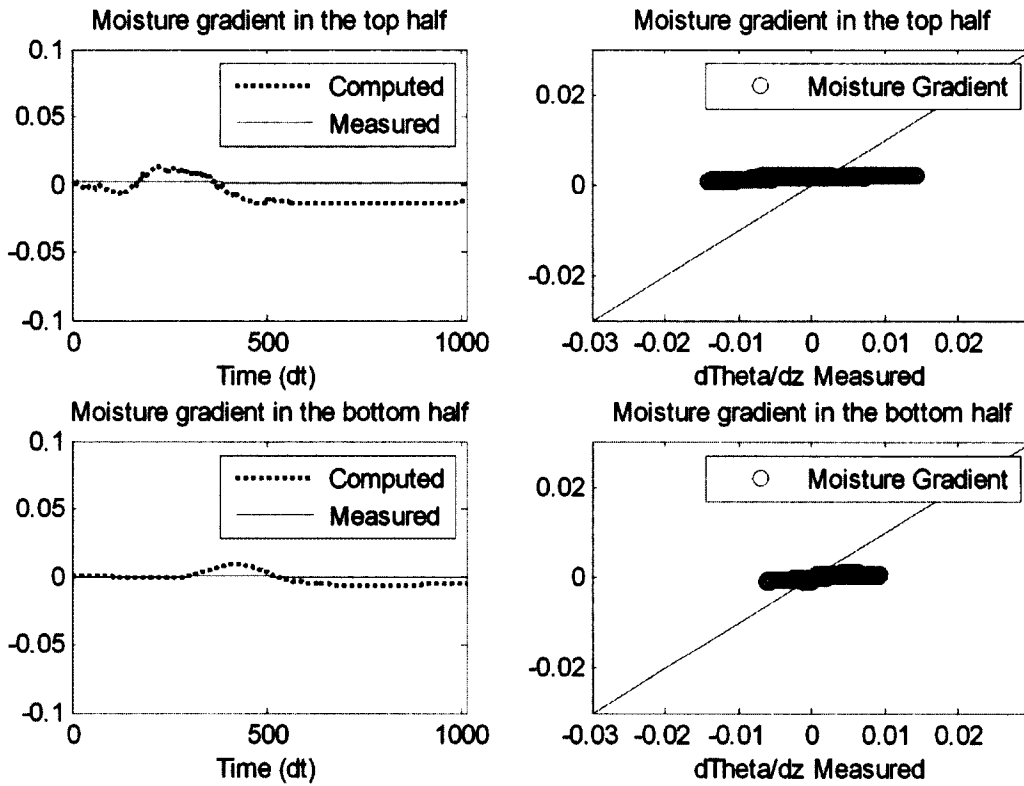
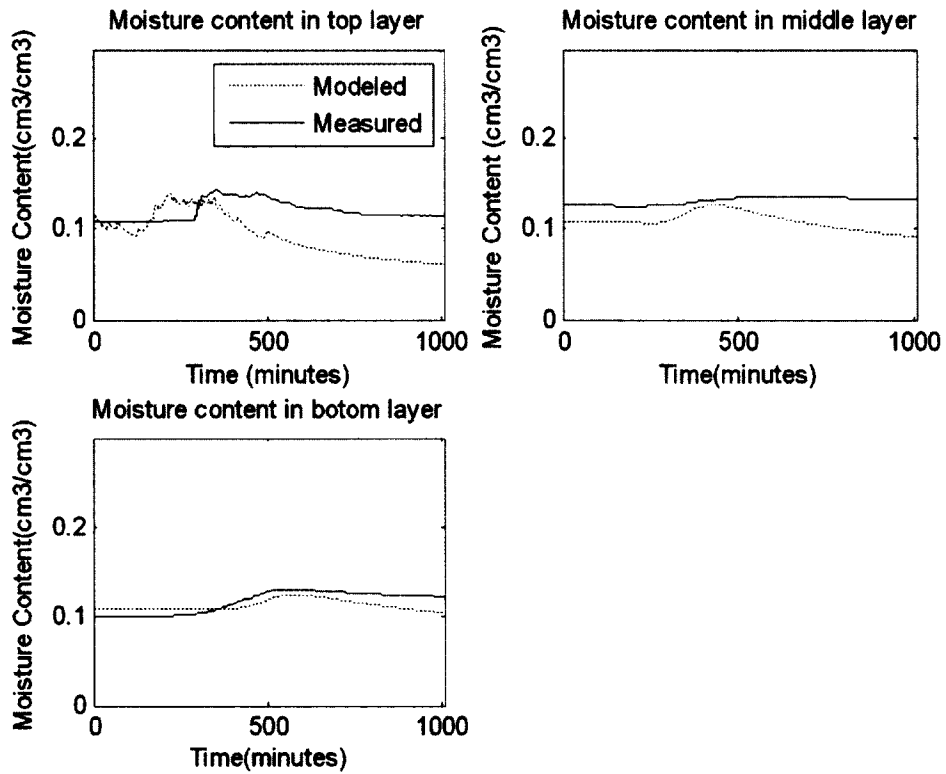
11/07/2010 Storm Event



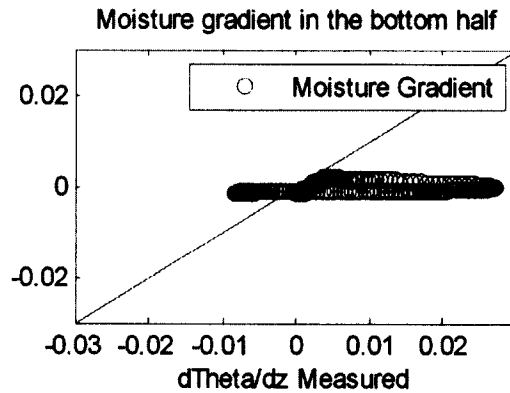
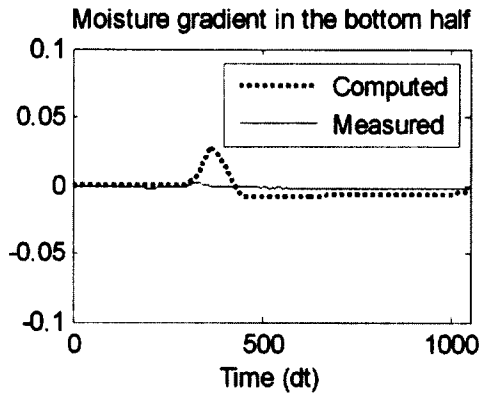
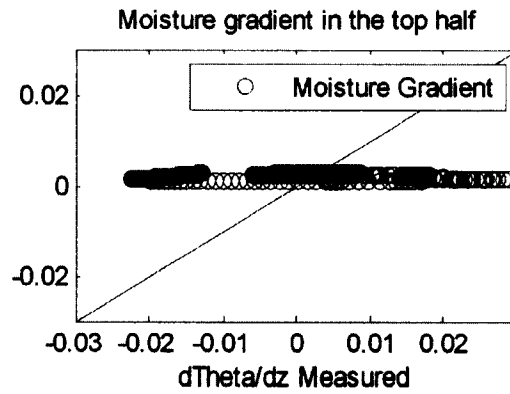
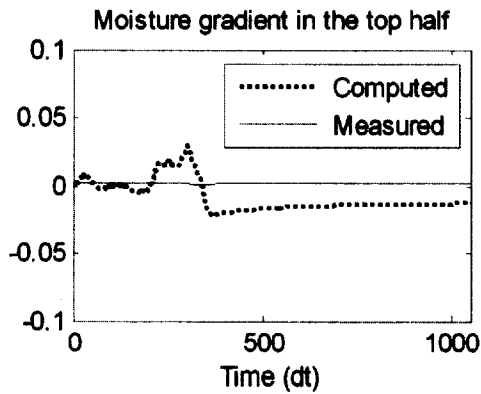
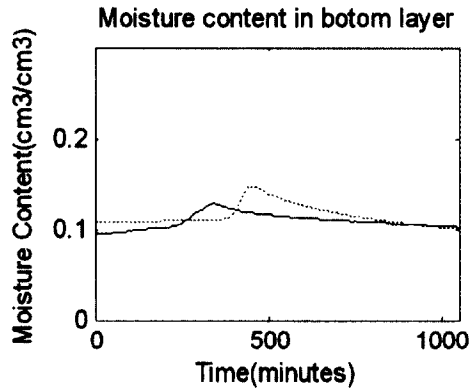
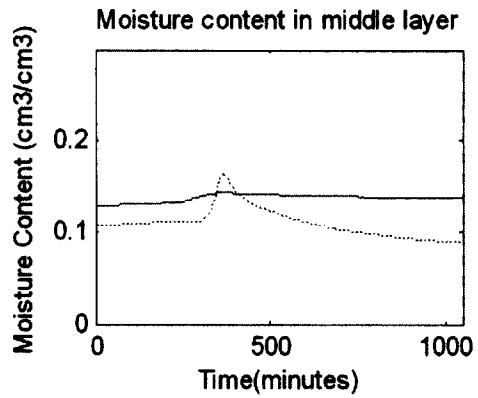
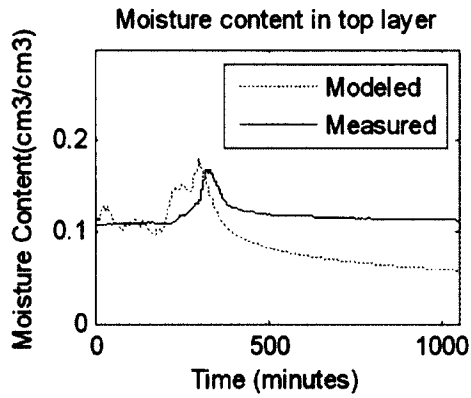
11/16/2010 Storm Event



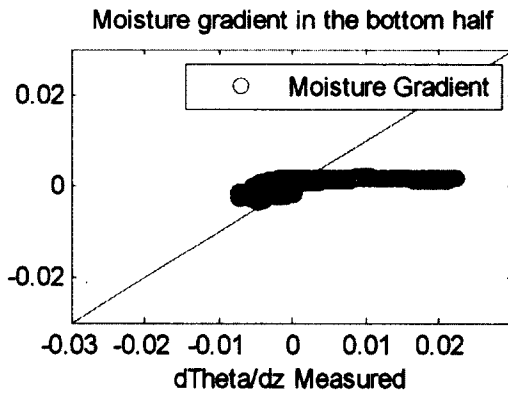
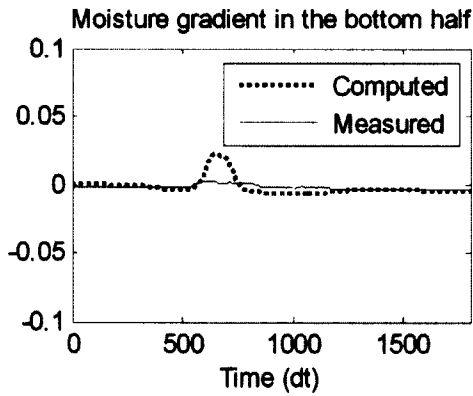
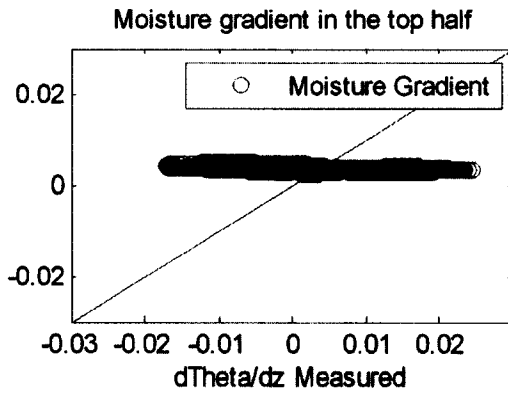
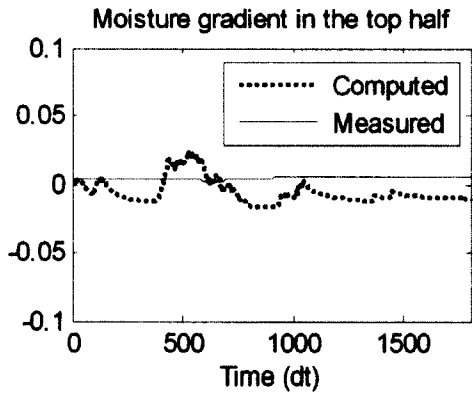
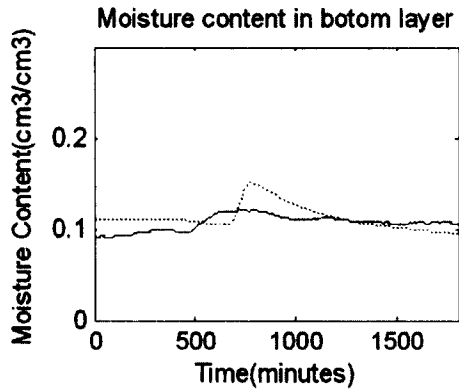
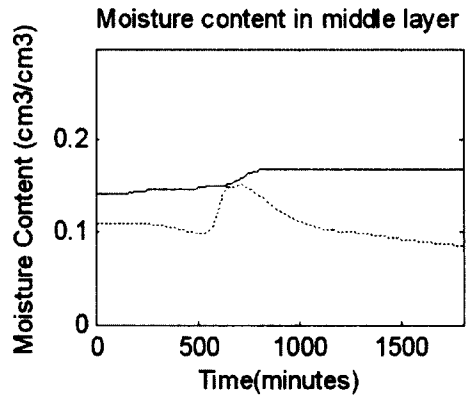
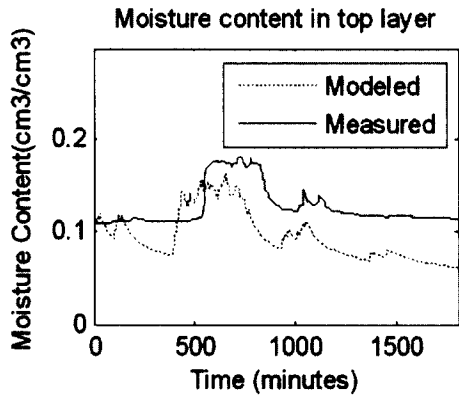
11/26/2010 Storm Event



04/10/2011 Storm Event

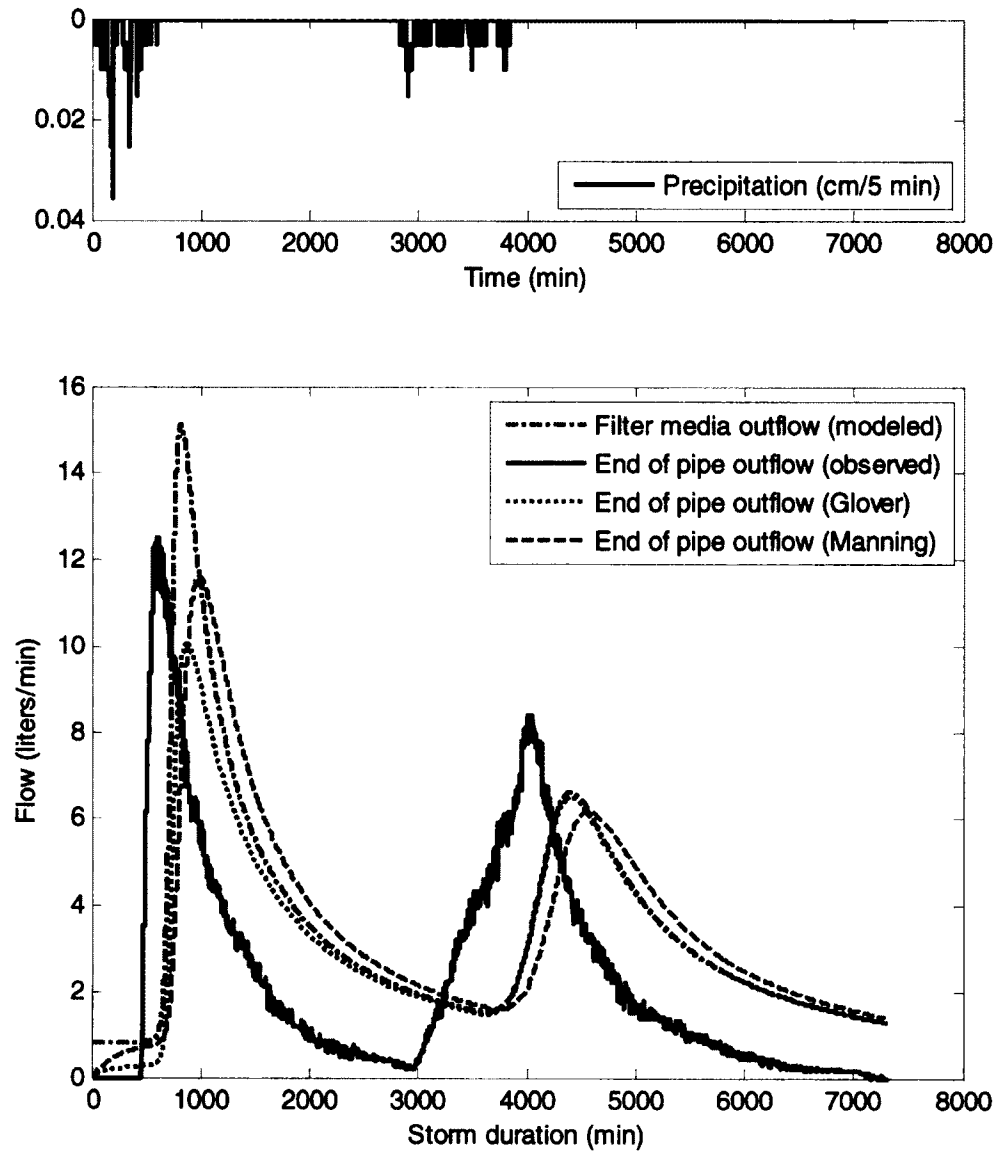


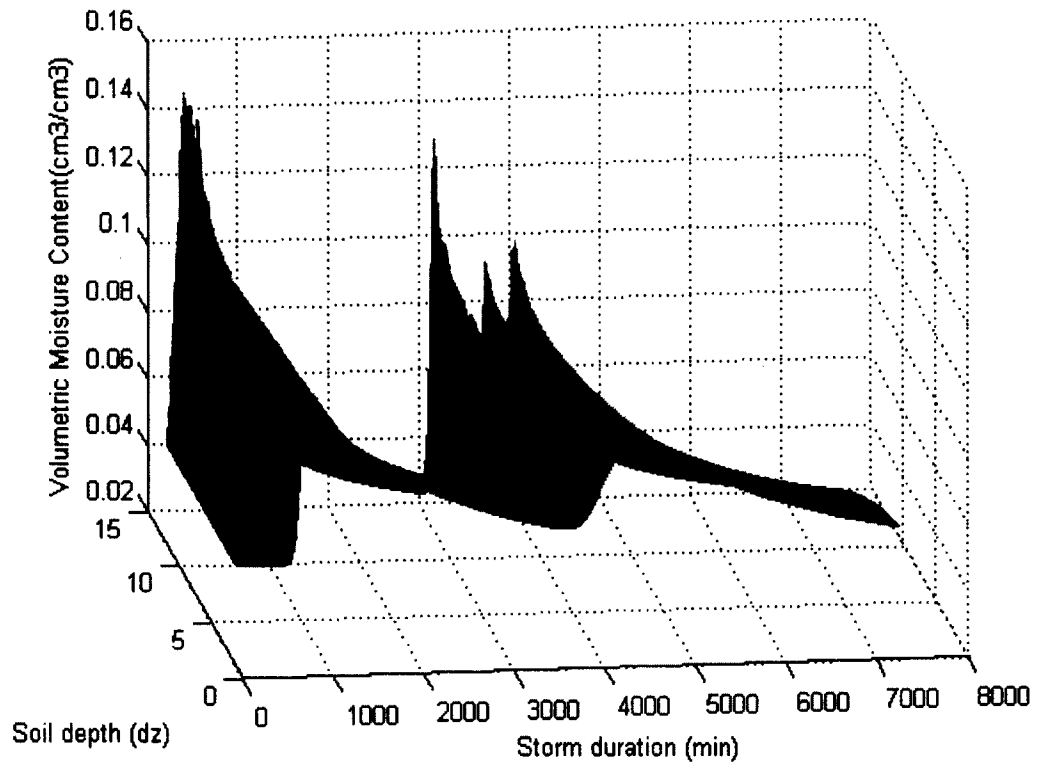
04/13/2011 Storm Event



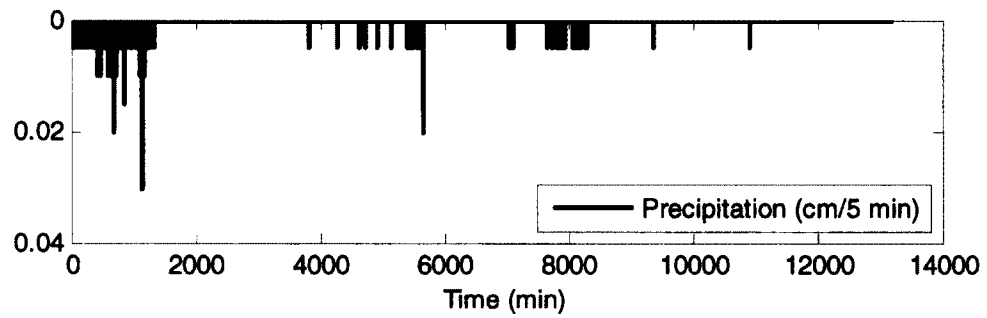
Appendix K: Testing storms for the West Edge PP model

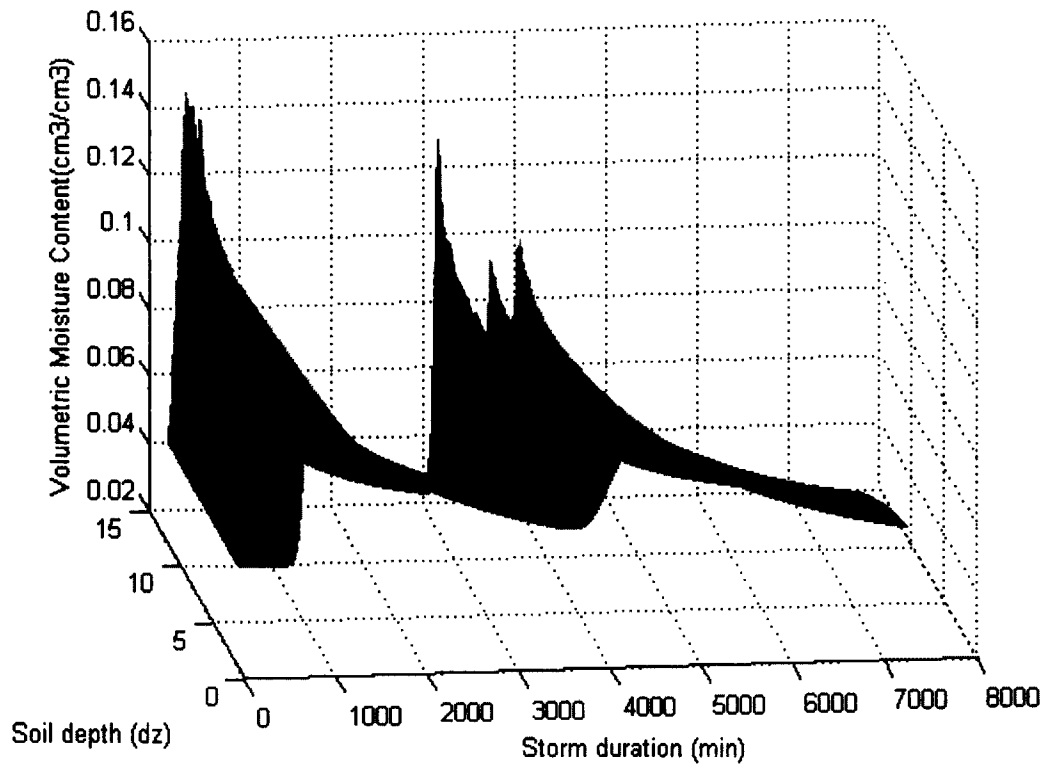
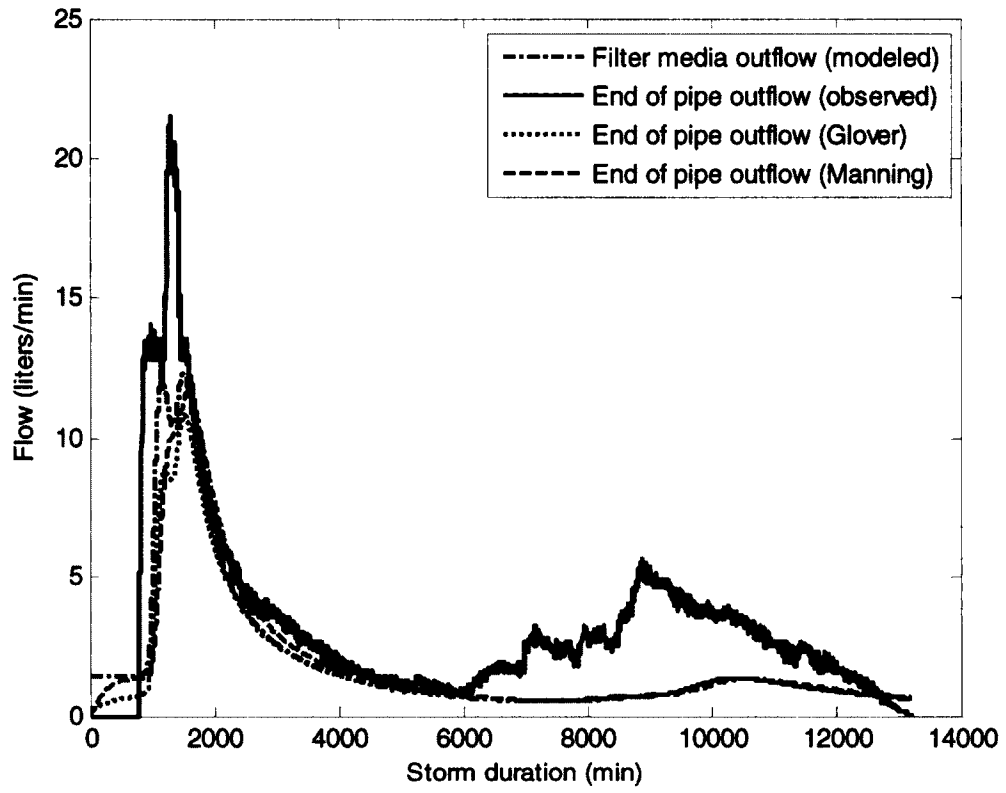
06/11/2009 Storm Event



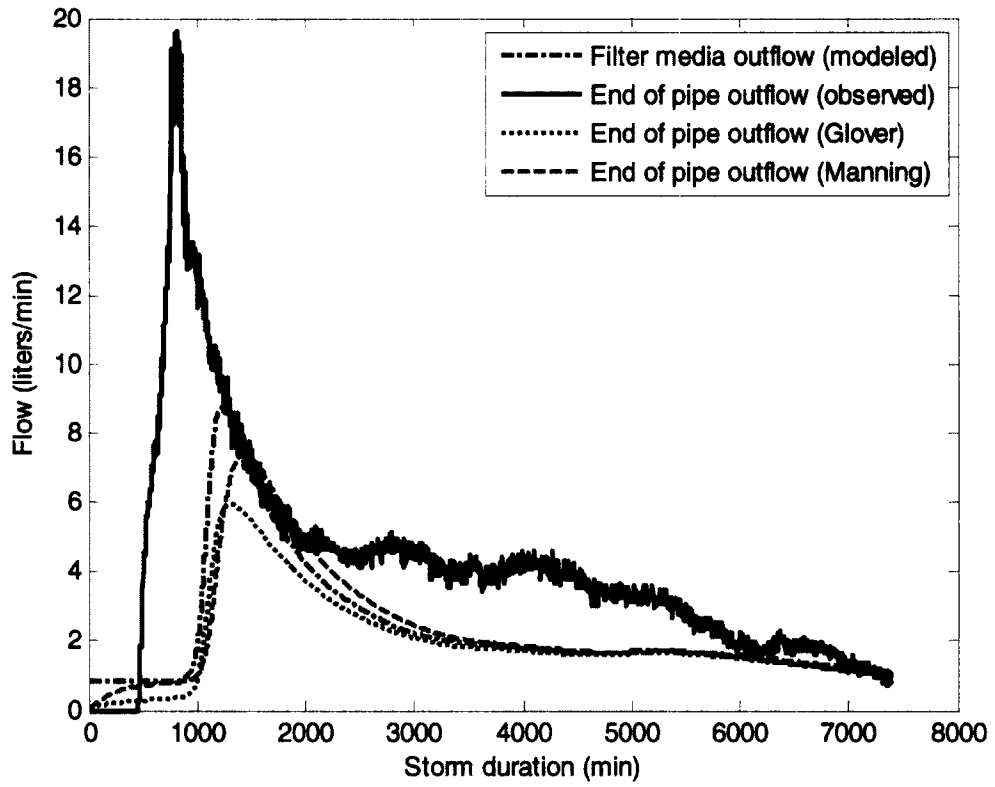
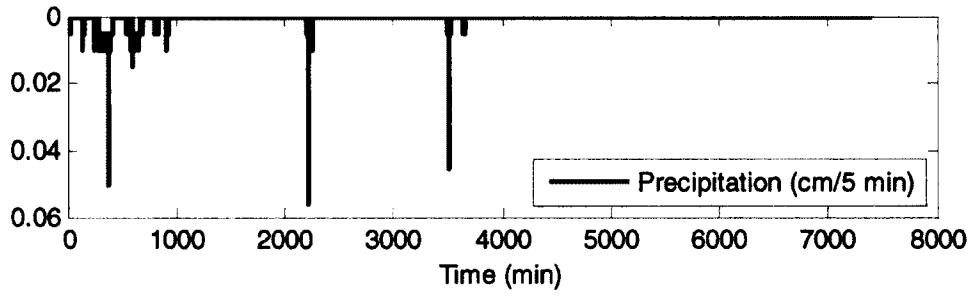


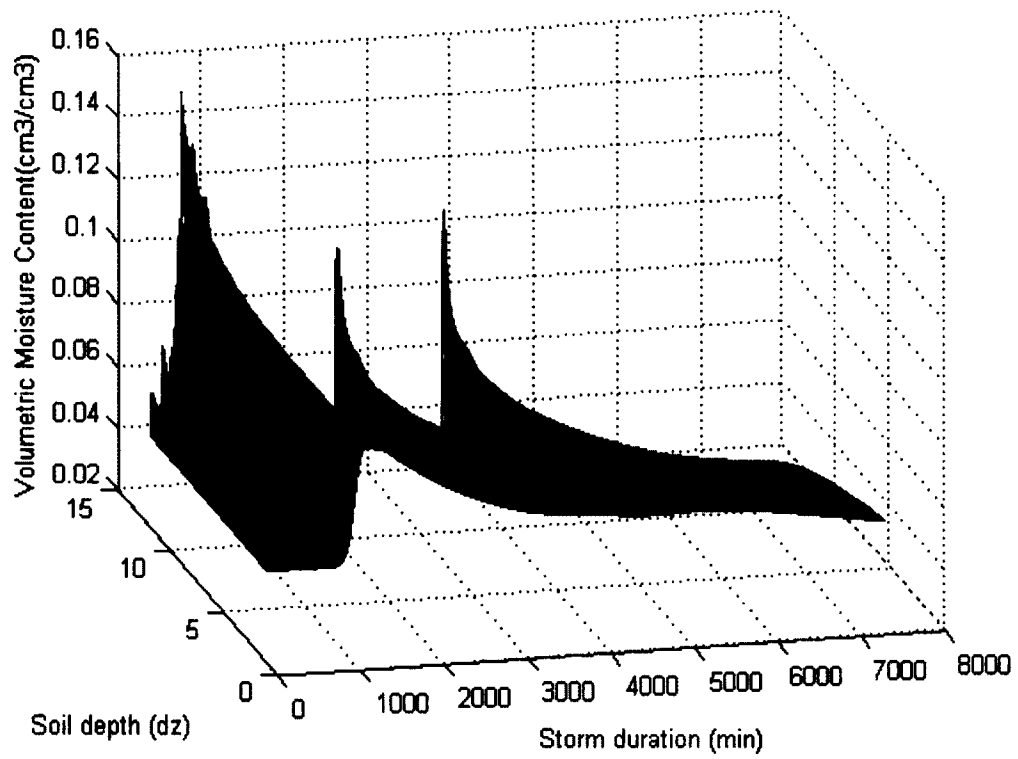
06/18/2009 Storm Event



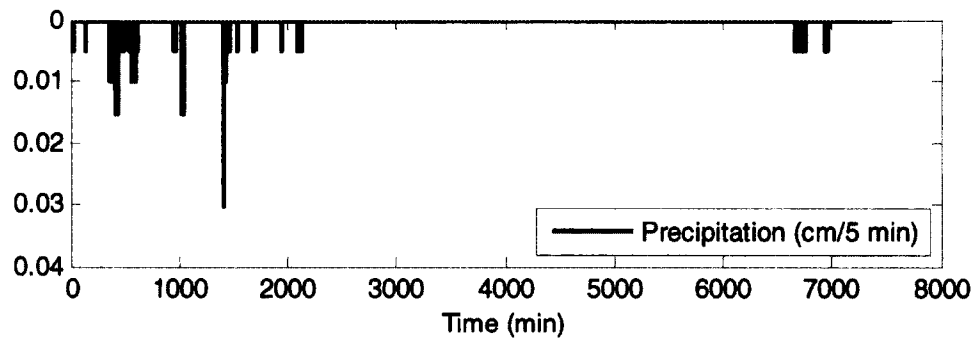


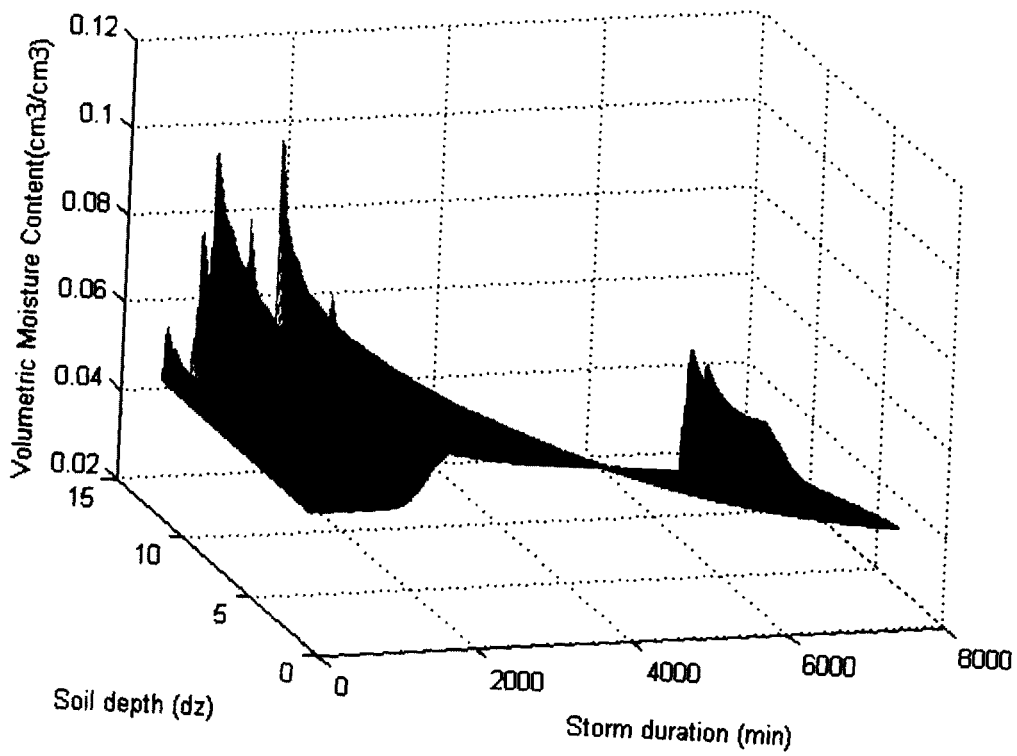
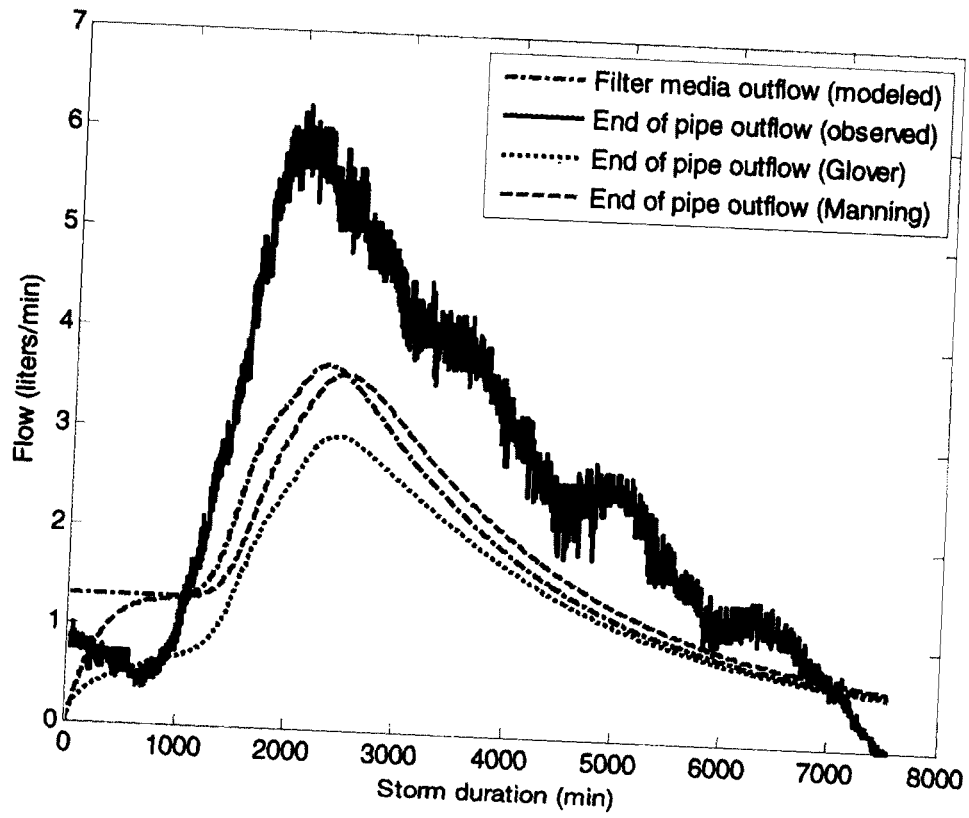
07/02/2009 Storm Event



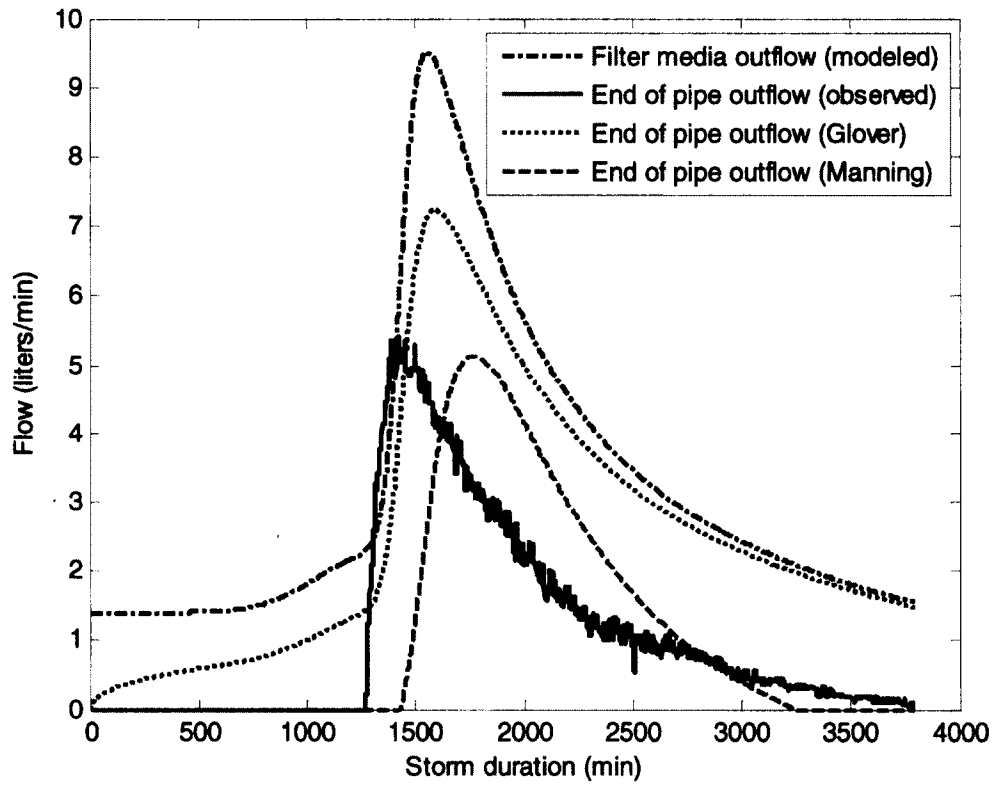
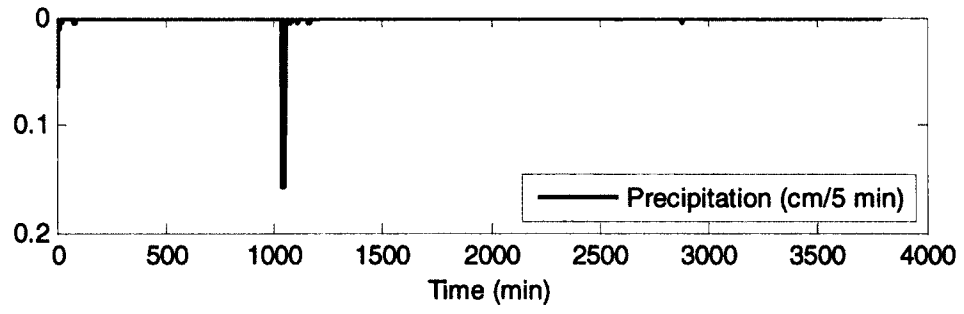


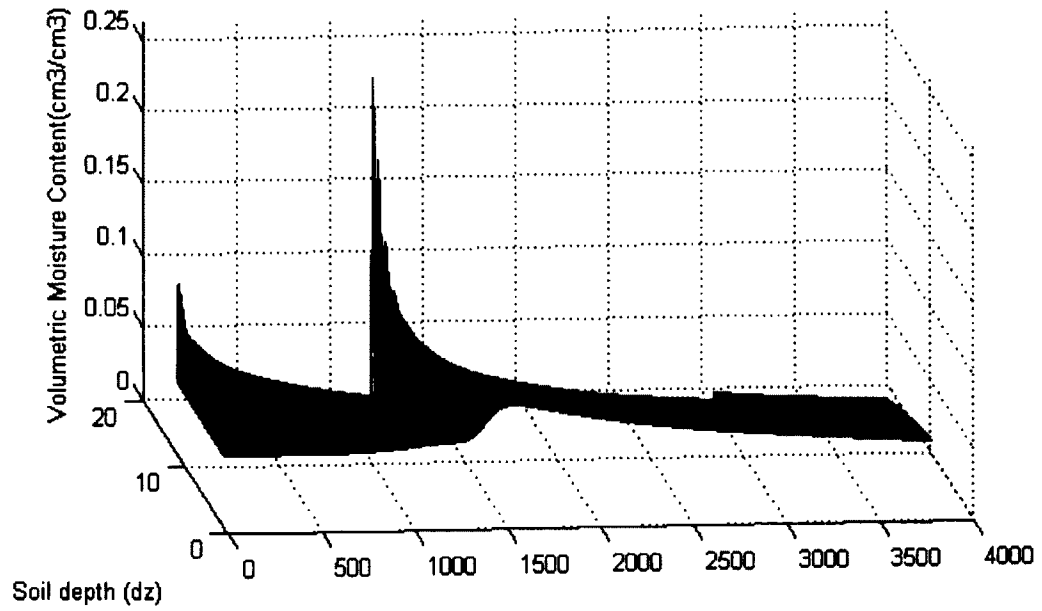
07/07/2009 Storm Event



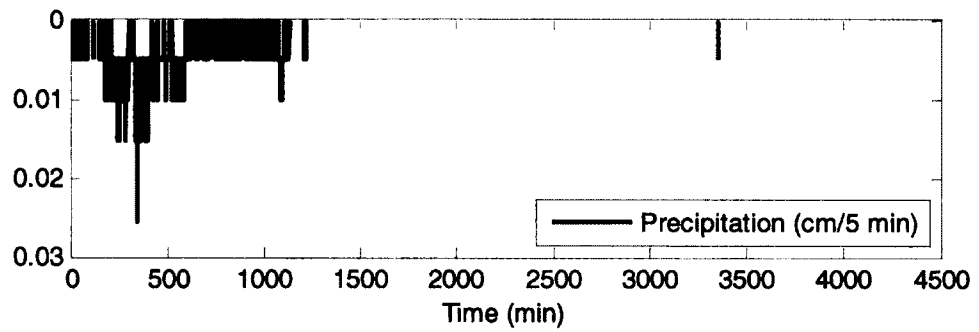


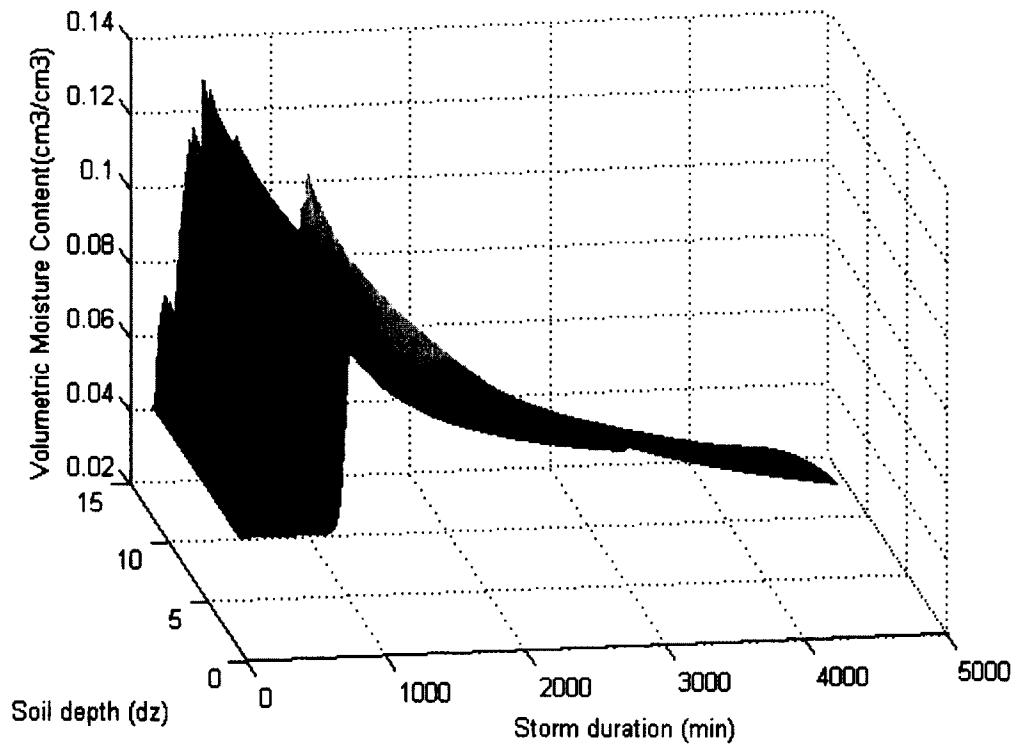
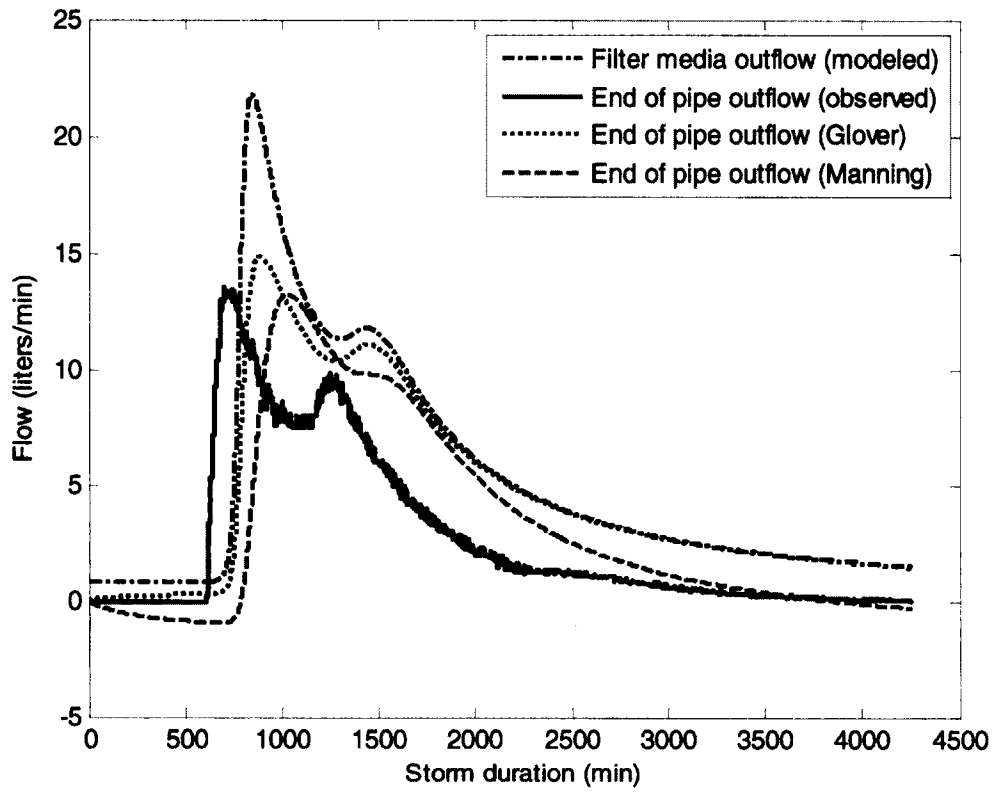
08/21/2009 Storm Event





08/28/2009 Storm Event





09/11/2009 Storm Event

